INVESTIGATION OF MERCURY CYANIDE AS A BUILDING BLOCK IN THE FORMATION OF SUPRAMOLECULAR COORDINATION COMPOUNDS

by

Neil D. Draper

B.Sc., Simon Fraser University, 2001

THESIS
SUBMITTED IN PARTIAL FULFILLMENT OF THE
REQUIREMENTS FOR THE DEGREE OF

MASTER OF SCIENCE

In the Department
of
Chemistry

© Neil D. Draper 2004
SIMON FRASER UNIVERSITY
July 2004

All rights reserved. This work may not be
reproduced in whole or in part, by photocopy
or other means, without permission of the author

APPROVAL

Name: **Neil D. Draper**

Degree: **Master of Science**

Title of Thesis: **Investigation of Mercury Cyanide as a Building Block in the Formation of Supramolecular Coordination Compounds**

Examining Committee:

Chair: Dr. R.H. Hill, Professor

Dr. D.B. Leznoff, Assistant Professor, Senior Supervisor

Dr. V.E. Williams, Assistant Professor, Supervisory Committee Member

Dr. Z.-G. Ye, Professor, Supervisory Committee Member

Dr. J.A. Clyburne, Associate Professor, Internal Examiner

Date Approved: July 22, 2004

SIMON FRASER UNIVERSITY

Partial Copyright Licence

The author, whose copyright is declared on the title page of this work, has granted to Simon Fraser University the right to lend this thesis, project or extended essay to users of the Simon Fraser University Library, and to make partial or single copies only for such users or in response to a request from the library of any other university, or other educational institution, on its own behalf or for one of its users.

The author has further agreed that permission for multiple copying of this work for scholarly purposes may be granted by either the author or the Dean of Graduate Studies.

It is understood that copying or publication of this work for financial gain shall not be allowed without the author's written permission.

The original Partial Copyright Licence attesting to these terms, and signed by this author, may be found in the original bound copy of this work, retained in the Simon Fraser University Archive.

Bennett Library
Simon Fraser University
Burnaby, BC, Canada

ABSTRACT

Several coordination polymers using neutral $Hg(CN)_2$ as a building block have been prepared. The Lewis-acidic, linear $Hg(CN)_2$ moieties accept chloride ligands *in situ* from coordinately saturated metal-ligand complex chlorides or organic chloride salts, forming mercury cyanide / chloride double salt anions that in several cases increase the structural dimensionality of the polymer formed. The structures of $[Cat][Hg(CN)_2Cl]$ (Cat = organic cation), $[Ni(terpy)_2][Hg(CN)_2Cl]_2$ (terpy = 2,2':6',6"-terpyridine), $[Cu(en)_2][Hg(CN)_2Cl]_2$ (en = ethylenediamine), $[Co(en)_3][Hg(CN)_2Cl_2]\{[Hg(CN)_2]_2Cl\}$, and $[Co(NH_3)_6]_2[Hg(CN)_2]_5Cl_6 \cdot 2\ H_2O$ range from molecular units to two dimensional layered structures. The presence (or absence), number, and profile of hydrogen bond donor sites of the transition metal amine ligands were observed to strongly influence the structural motif and dimensionality adopted by the anionic double salt coordination polymers, while cation shape and cation charge had little effect.

When unsaturated transition metal complexes are employed, competition occurs between halide and *N*-cyano coordination of the double salt mercurate units. The structures of $[ML_2(\mu\text{-}Cl)_2Hg(CN)_2]$ (M = Mn(II), Ni(II); L = 2,2'-bipyridine (bipy), 1,10-phenanthroline (phen)), $[Cu(terpy)Cl_2(\mu\text{-}Hg(CN)_2)]$, $\{[Cu(phen)_2Cl]_2Hg(CN)_2[Hg(CN)_2Cl]_2\}$, $[Cu(dien)Cl][Hg(CN)_2Cl]$ (dien = diethylethylenetriamine), $[Cu(tren)Hg(CN)_2Cl][Hg(CN)_xCl_y]$; tren = tris(2-aminoethyl)amine), $\{[Ni(en)_2][Hg(CN)_2]_3Cl_2\}_2$, and $\{[Ni(tren)]_4[Hg(CN)_2]_8Cl_6\}HgCl_4$ range from molecular units to three dimensional extended structures. Ligand basicity was observed to have a significant impact influencing the type of structure observed with higher dimensionality typically achieved with *N*-cyano coordination.

A non-centrosymmetric two dimensional layered structure, $\{(tmeda)Cu[Hg(CN)_2]_2\}HgCl_4$ (tmeda = *N,N,N',N'*-tetramethylethylenediamine), showed strong optical birefringence and a high dielectric constant due to its anisotropic crystal structure and highly polarizable Hg(II) ions. A series of these 2-D coordination polymers were formed upon changing the halides (Br or I for Cl) and/or M(II) centre (Ni for Cu).

Although the synthesis of bipy analogues of the 2-D layer structure proved unsuccessful, four new structures, $[Cu(bipy)_2(\mu\text{-}Cl)_2Hg(CN)_2]$, $[Cu(bipy)_2Hg_2Cl_6]_2$, $\{[Cu(bipy)Hg(CN)_2Cl_2]_2Hg(CN)_2\}$, and $\{[Cu(bipy)(OH)(Cl)]_2Hg(CN)_2\} \cdot 2\ H_2O$ were isolated and characterized. The latter two compounds illustrate that significant magnetic interactions can be propagated by Hg(II) centres.

DEDICATION

To all of my family

A crystal is an atomic tessellation, a tridimensional
jigsaw puzzle in which every piece is the same shape.

A crystal is nothing more
than a breeze blowing sand
into the form of a castle
or a film played backwards
of a window being smashed.

An archaeologist without any mineralogical
experience
might easily mistake a crystal
for the artificial product of a precision
technology.

A word is a bit of crystal in formation.

Christian Bök

ACKNOWLEDGEMENTS

I cannot begin to express enough thanks to my senior supervisor Dr. Daniel B. Leznoff for all of his encouragement, support and patience. His incredible enthusiasm for chemistry inspired me to pursue my graduate studies.

I like to extend thanks to all the past and present members of the Leznoff group who made for an exciting and enjoyable working environment. Thank you to Michael Katz and Graham Taylor, two exceptional undergraduate students that I had the opportunity and pleasure to work with.

I would also like to express my deep gratitude and appreciation to Dr. Ray Batchelor and Dr. Fred Einstein for spending many long hours teaching me X-ray crystallography and how to solve acquired diffraction data sets and to Dr. Zuo-Guang Ye for his time spent interpreting the birefringence, and dielectric constant results. Mr. Bryan Sih is also gratefully appreciated for teaching me how to polish crystals and to measure their birefringence, Mr. Wenzhi Chen for completing the dielectric constant measurements, and Mr. Miki Yang for completing all the C, H, N analyses.

Finally a special thank you goes out to all of my family whose love, support, and encouragement was essential during my studies.

TABLE OF CONTENTS

LIST OF FIGURES

LIST OF TABLES

LIST OF ABBREVIATIONS

Å	Angstrom
AF	antiferromagnetic
Anal	analysis
bipy	2,2'-bipyridine
Bu	butyl
C	Curie constant
C	Celsius
C	compensator constant
C_o	capacitance as measured in a vacuum
C_d	capacitance as measured through a dielectric
Calcd	calculated
cm	centimetre
cyclam	1,4,8,11-tetraazacyclotetradecane
D	zero-field splitting parameter
d	crystal thickness
dien	diethylenetriamine
dmeda	*N,N*-dimethylethylenediamine

EA	elemental analysis
en	ethylenediamine
Et	ethyl
F	ferromagnetic
g	Landé g factor
g	gram
$\hat{H}$	Hamiltonian
H	magnetic field
Hz	Hertz
IR	infrared
J	magnetic coupling parameter
K	Kelvin
k	Boltzmann constant
kHz	kilohertz
L	ligand
m	medium
mL	millilitre
mm	millimeter
mmol	millimole
mol	mole
M	metal

M	magnetization
N	Avogadro's number
n	index of refraction
ORTEP	Oak Ridge Thermal Ellipsoid Plot Program
P	paramagnetic impurity factor
phen	1,10-phenanthroline
[PPN]Cl	bis(triphenylphosphoranylidene)ammonium chloride
S	total spin quantum number
s	strong
SHG	second harmonic generation
SQUID	superconducting quantum interference device
T	temperature
T_C	Curie Temperature
T_N	Néel Temperature
TM	transition metal
terpy	2,2':6',6"-terpyridine
tmeda	*N,N,N',N'*-tetramethylethylenediamine
tren	tris(2-aminoethyl)amine
vs	very strong
vw	very weak
w	weak

zJ'	molecular field parameter
1-D	one dimensional
2-D	two dimensional
3-D	three dimensional
°	degree
α	alternation parameter
β	Bohr magneton
Δn	birefringence
ε'	dielectric constant
Γ	optical retardation
θ	Weiss constant
θ	mean value of the compensator angle measurements
μ_{eff}	effective magnetic moment
μ_B	Bohr magneton
τ	tau parameter
ν_{CN}	cyanide infrared stretching frequency
χ_M	molar magnetic susceptibility
χ'_M	corrected molar magnetic susceptibility

CHAPTER 1
INTRODUCTION

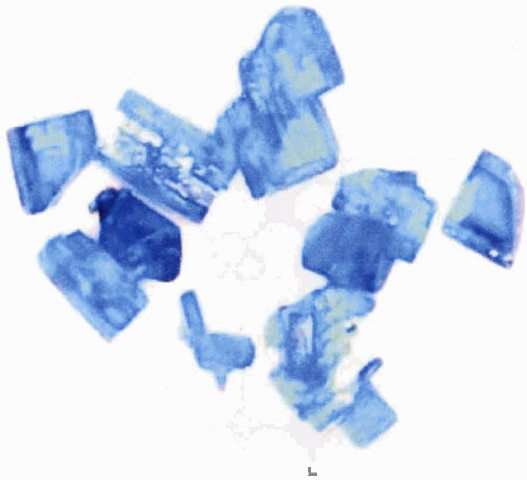

1.1 CRYSTAL ENGINEERING: CYANOMETALLATE COORDINATION POLYMERS

Research into the chemistry of supramolecular coordination polymers has rapidly grown in recent years due to an increased demand for functional materials with tunable properties such as catalytic, conductive, luminescent, magnetic, non-linear optical effects or the formation of porous materials.[1-20] The self-assembly of simple molecular building blocks containing organic ligands and inorganic metal ions provides an efficient and reliable approach for the design and synthesis of such organic / inorganic hybrid materials.[8,9,21-23] The metal atoms in coordination polymers can be imagined as templating and assembling points for the organic bridging ligands. The multidimensional assembly of repeating metal (M) and ligand (L) units, which aggregate through strong metal-ligand coordinate bonds, results in the formation of an organized entity of higher complexity.[24,25] This particular method of self-assembly is often referred to as the directional bonding approach as it uses M-L bonding to direct the structures formed.[8]

The characteristics of the inorganic and organic moieties, such as available coordination sites, coordination geometry preference, ligand flexibility, and potential hydrogen bond interactions, ideally control the extended structure, thereby creating enormous potential for complexity and functionality of these modular materials.[26-33] The metal centres are usually coordinated by capping ligands prior to linking them together in order to exercise a degree of control over the possible structures formed. Thus, with a careful selection of ligand, metal centre(s), and reaction

conditions, control over the architecture of the resultant structural motifs can be achieved (Figure 1.1).[25-32]

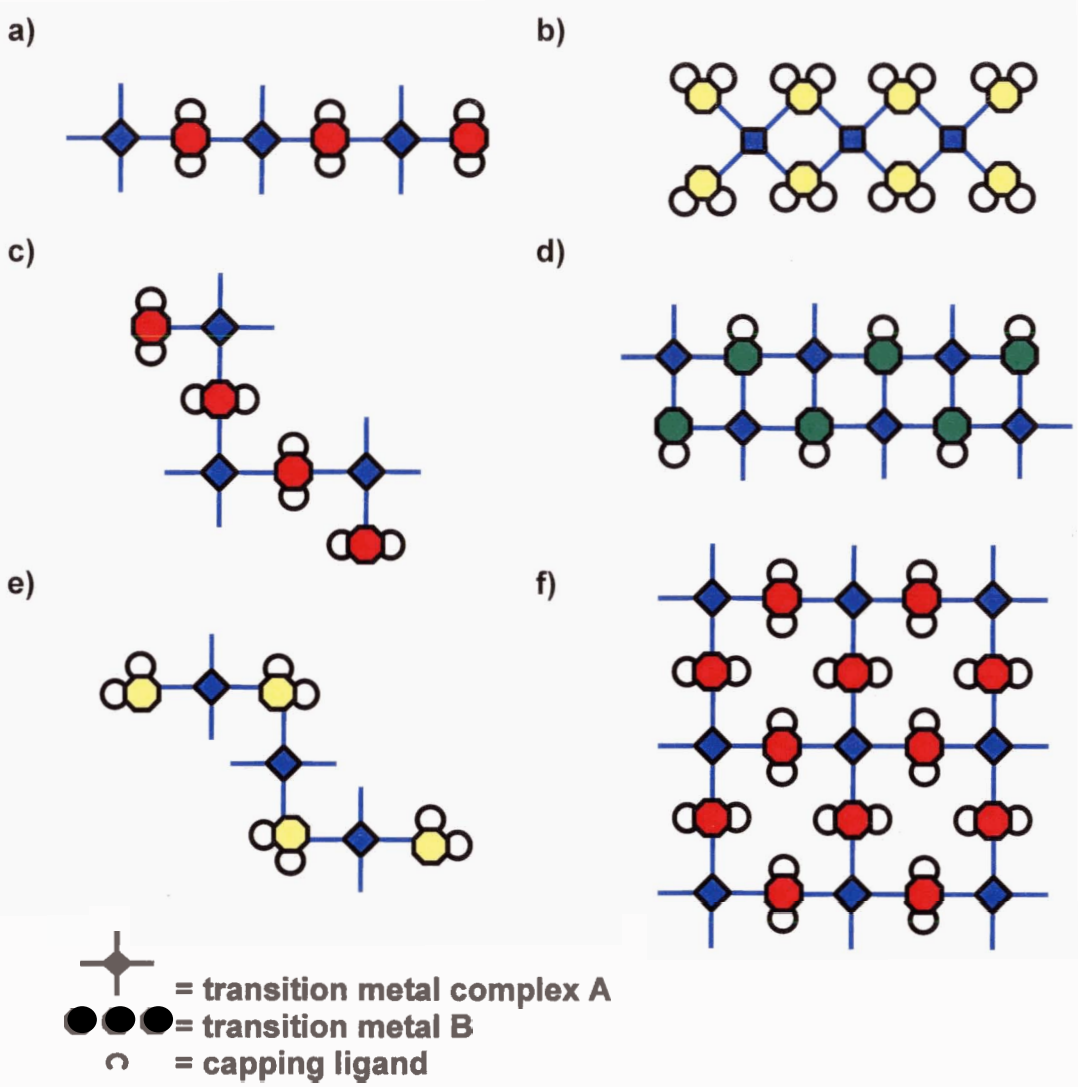

Figure 1.1 Selected supramolecular systems constructed by the directional-bonding approach. a) straight 1-D chain; b) 1-D ribbon; c) extended zig-zag 1-D chain (trans on metal B); d) 1-D ladder; e) extended zig-zag 1-D chain (cis on metal B); f) extended 2-D sheet. Adapted from Iwamoto.[34]

Systems that employ *cyanometallate* building blocks, $[M(CN)_n]^{x-}$, in concert with simple metal ions or their coordinately unsaturated complexes, to create multidimensional networks were among the first prepared coordination polymers to be studied and are of great current interest.[24,34-

[48] Alteration of the metal centre in $[M(CN)_n]^{x-}$ and the consequent adjustment of the geometric, magnetic, and electronic properties, provides the control and flexibility required to assemble solids with tunable properties.[35,37,49] This is illustrated by the Prussian blue analogues such as $\{Cr(II)_3\}$ $[Cr(III)(CN)_6]_2 \cdot 10\ H_2O$,[50] and $\{V(II)_\alpha\}$ $\{V(III)_{(1-\alpha)}\}[Cr(III)(CN)_6]_{0.86} \cdot 2.8\ H_2O$ (α = 0.42),[47,51] two molecule-based magnets that exhibit magnetic ordering at the high temperatures of 240 K and 315 K respectively. Cyanometallates have also been employed extensively to generate inclusion compounds, clathrates, and zeolite-type systems that act as ion exchangers, molecular sieves or materials for storing gases.[34,52-56] Typically, square-planar or tetrahedral cyano-bridging units $[M(CN)_4]^{2-}$ (M = Ni, Pt, Pd, Cd) are used to link various cationic transition metal-ligand complexes to prepare these multidimensional structures.[37,56] Thus, it should be stressed that the generation of high dimensionality systems is one key to accessing materials with potentially useful and interesting material properties.[9-11,22]

Although the tetrahedral $[Hg(CN)_4]^{2-}$ and related $[Cd(CN)_4]^{2-}$ moieties have seen some limited use in the construction of inclusion compounds that are mineralmimetic (resembling SiO_2, clay-layer, and zeolite-cage structures),[34,56-59] the *linear* $Hg(CN)_2$ molecule has not been investigated as a building block to create supramolecular architectures; only a few simple adducts are known.[60,61]

The primary focus of this thesis is to investigate the use of $Hg(CN)_2$ in the formation of supramolecular coordination polymers, there being virtually no known $Hg(CN)_2$ containing coordination polymers in the literature. The goal is to be able to generate a collection of such complexes, including their syntheses, their detailed structural features, and the factors influencing their formation, to be used as a guideline for the predictable formation of new and interesting cyanomercurate polymers with tunable material properties.

1.2 GENERAL ASPECTS OF CYANOMETALLATES

There are several general features of the cyano ligand that make anionic transition metal cyanide (i.e.: cyanometallates) building blocks an attractive choice for the construction of coordination polymers.

Since the cyano group is polar and can participate in hydrogen bonding, cyanometallates are quite soluble in water and other polar media such as methanol and acetonitrile. The cyanometallates are also very stable transition metal complexes with respect to air and water oxidation; few reagents are able to destroy them, with the exception of strong acids.[36,37]

In general, both the carbon and the nitrogen ends of the cyanide ion act as Lewis bases that can coordinate two metal cations acting as the corresponding Lewis acids.[34,36,37] As a result, the cyano group is able to behave as a bridging ligand between two metal centres. Terminal and bridging modes that have been observed for the cyano ligand are depicted in Figure 1.2, the most commonly observed being the carbon-bound terminal mode (a) and the linear bridged mode (b).[37]

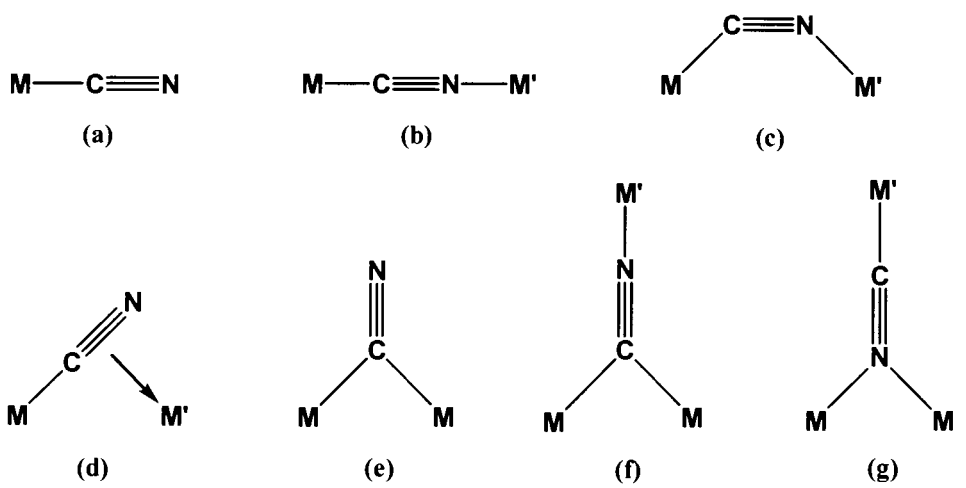

Figure 1.2 Terminal and bridging modes of the cyano group.

All of the coordination polymer cyano groups described in this thesis fall into these two categories. Neutron diffraction and infrared studies have demonstrated that terminal cyanide groups are typically C-bonded structures.[37,62] The cyanide group acts as both a strong σ-donor

and π-acceptor resulting in its ability to stabilize transition metals in both high and low oxidation states.[36,62] As a result, the infrared stretching frequency of the carbon-nitrogen triple bond (ν_{CN}) is very sensitive to its local environment and can be used to characterize cyanometallate complexes, as discussed in section 1.3.2.1.

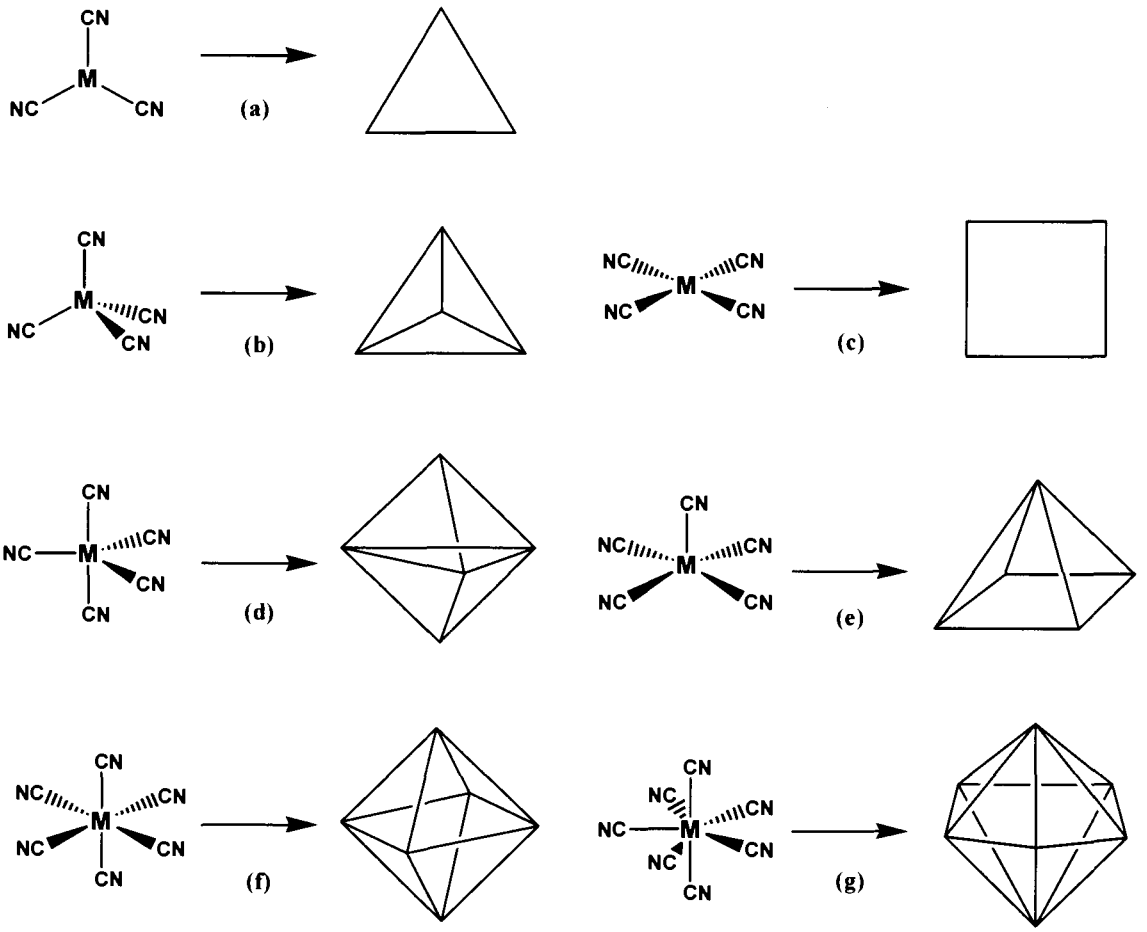

Figure 1.3 Observed geometry for some common cyanometallates.
(a) trigonal $[M(CN)_3]^{n-}$; (b) square planar and (c) tetrahedral $[M(CN)_4]^{n-}$; (d) trigonal bipyramidal and e) square pyramidal $[M(CN)_5]^{n-}$; (f) octahedral $[M(CN)_6]^{n-}$; (g) pentagonal bipyramidal $[M(CN)_7]^{n-}$.

Cyanometallates can assume a number of different geometries depending on the nature of the central metal cation (Figure 1.3).[34,37] They range from two-coordinate linear complexes such as $[Au(CN)_2]^-$ [63] to eight-coordinate complexes such as $[Mo(CN)_8]^{3-}$ [64,65] and provide a large number of different geometric building blocks with which to assemble multidimensional structures,

especially when compared with the three fundamental units of carbon bonding (linear *sp*, trigonal sp^2, tetrahedral sp^3).

By linking a cyanometallate to a second coordination centre, a variety of multidimensional structures such as 1-D chains, ladders, and ribbons, 2-D layers, and 3-D networks can be synthesised, as will be shown. This type of synthetic design is referred to as the 'brick and mortar' method, where the second coordination metal centre is the brick, and the cyanometallate is the mortar.[35,66-68] During the self-assembly process, the central atom of the brick must have vacant coordination sites available to form *N*-cyano linkages with the cyanometallate, permitting polymerization to occur. Typically, the second metal centre is coordinated by a capping ligand(s) in order to exercise a degree of control over the polymeric structure formed, as described in section 1.3.1. The general formula for such a polymer is $[(L_aM')]_b[M(CN)_c]_d$.

Polymers formed from cyanometallates containing paramagnetic metal atoms have been the subject of extensive magnetic studies.[24,35,46,47,69,70] In addition to its structural function (increasing dimensionality), the -M-CN-M'- linkage exhibits an important electronic function: it forms an exchange pathway for the interaction of electron spins between paramagnetic centres of either M' and / or $M(CN)_x$.[47,68]

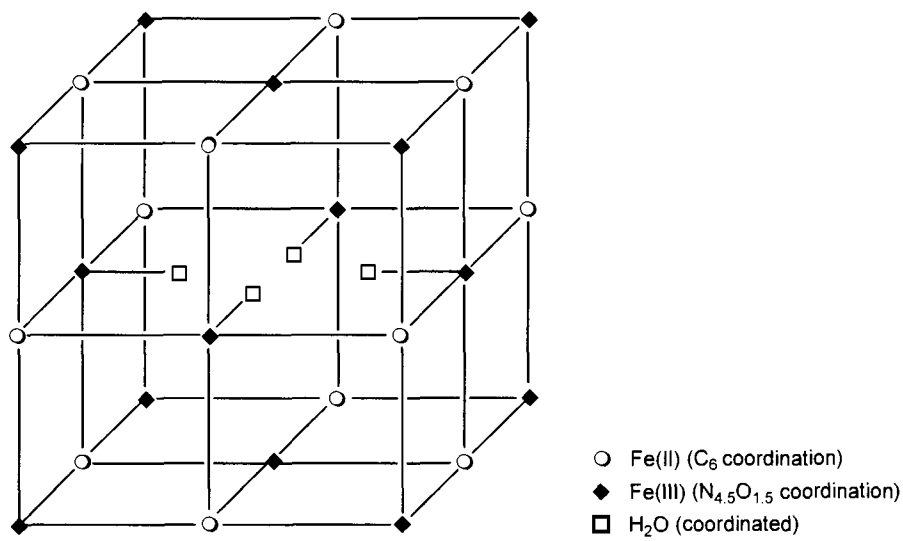

Figure 1.4 Schematic depicting Prussian Blue, $Fe_4[Fe(CN)_6]_3 \cdot 14\ H_2O$.[71]

Octahedral cyanometallates have been extensively employed to form complexes such as the bimetallic Prussian blues (Figure 1.4) which provide significant insights into magnetostructural correlation and design of magnetic materials with high ordering temperatures.[24,37,47,72] The -M-CN-M'- linkage usually ranges in length from 5.0 Å to 6.0 Å.[34,37] Hence, multidimensional structures formed with such linkages contain void spaces that are necessarily filled by either the capping ligand(s) at M', guest molecules, or interpenetration in order to stabilize the adopted crystal structure.[34,37,73,74] Four coordinate tetrahedral and square planar cyanometallates have been extensively used to create numerous structurally diverse materials that behave as inclusion compounds for several molecules of differing size and shape.[34,56,75,76] These compounds are known as Hofmann-type clathrates when the formula is of the type $M'(NH_3)_2M(CN)_4$ and the cyanometallate is square planar (Figure 1.5).[56]

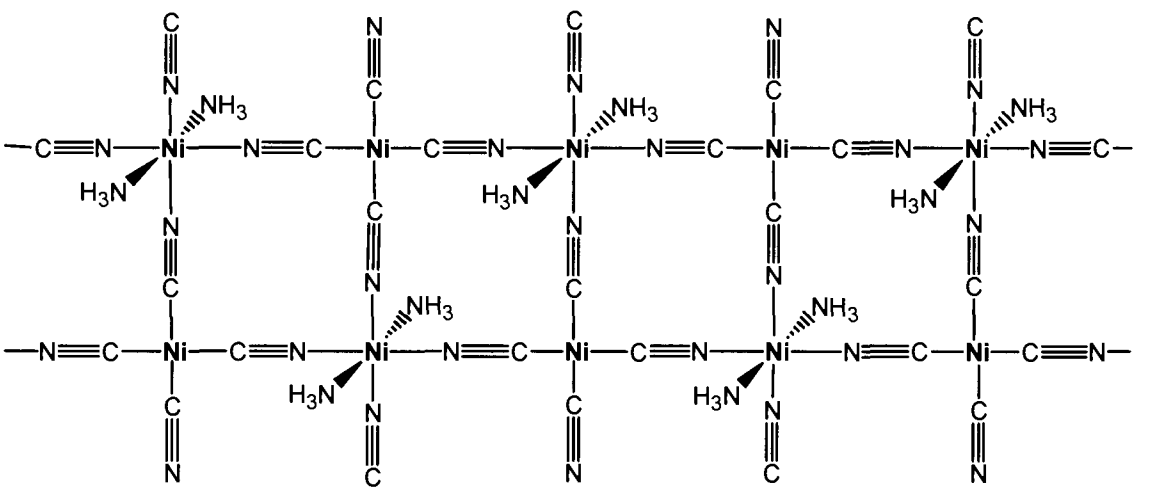

Figure 1.5 $Ni(NH_3)_2Ni(CN)_4 \cdot 2\ C_6H_6$[77,78]-a portion of the 2-D Hoffmann clathrate motif. Benzene guest molecules are not shown.

1.2.1 Linear Cyanometallates

Two-coordinate, linear metal cyanides have not been extensively explored as building blocks in supramolecular inorganic chemistry despite their general utility both as a cyanometallate and a linear-directing building block in the formation of coordination polymers. With this in mind, the Leznoff group has targeted the use of linear anionic $[M(CN)_2]^-$ units (M = Au,[79-81] Ag[82]) as building blocks in coordination polymers. Both the silver and gold cyanometallates were shown

to be capable of forming high dimensionality coordination polymers. Furthermore, they increased structural dimensionality by forming metallophilic (M···M) interactions and although diamagnetic, could propagate significant magnetic interactions.[80,82] These unconventional interactions between the d^{10} metal centres are comparable in strength to the hydrogen bond and are thought to originate from correlation effects.[83] As a comparison, this thesis examines the use of d^{10} *neutral* mercury(II) cyanide, $Hg(CN)_2$, as a potential building block in the formation of coordination polymers. Although mercurophilic interactions cause aggregation of some organomercury(II) compounds such as $Hg(CH_3)_2$[84] and adducts of trimeric perfluoro-ortho-phenylene mercury,[85] more frequently the tendency of neutral Hg(II) salts to form secondary interactions with electronegative atoms, such as Cl, leads to supramolecular self-assembly and increased dimensionality.

1.2.2 Coordination Chemistry of Hg(II): the Universal Glue

Being a soft metal, Hg(II) forms strong complexes with halides, sulphur, phosphorous, selenium, and nitrogen donor ligands;[86-89] many stable compounds with oxygen and carbon donors are also known. Mercuric chloride is an important salt as it is the main reagent in the formation of organomercury compounds.[89] Due to their relative stability in air and water, combined with their thermal and photochemical reactivity, dialkyl- and diarylmercury compounds are useful in preparing other organometallic compounds.[90]

The interference of mercury with biological systems has made it necessary to better understand the ability of mercury to bind donors; many studies have been carried out to understand how proteins interact with Hg(II) in both the solid state and in solution.[86,91-94]

The Hg(II) ion, which has a d^{10} configuration, is larger and softer than most other metal ions. Its complexes frequently have a low coordination number of two as a result of relativistic effects on the 6*s* orbital.[87-89] At the same time, there are fewer steric restrictions to higher coordination numbers, resulting in a wide variety of observed coordination numbers for Hg(II)

compounds.[88,95,96] For atoms to be considered a part of the Hg(II) coordination sphere in the solid state, they must be located at a distance of less than the sum of the van der Waals radii [D(Hg-L) < R(Hg) + R(L)]. According to the convention devised by Grdenić,[88] ligand coordination to mercury is classified into two types. When all x bond lengths are equivalent in a HgL_x system, the mercury atom has a *characteristic coordination* number x.[88] Although characteristic coordination numbers of three and four are not uncommon, coordination numbers of two are especially prevalent (Figure 1.6).

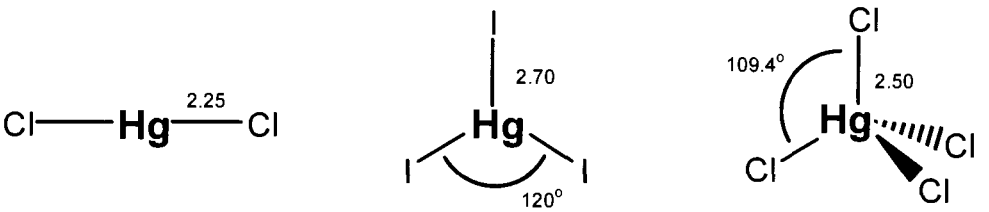

(a) **(b)** **(c)**

Figure 1.6 Examples of characteristic coordination of Hg(II) showing equivalent bond lengths and angles.
a) linear as in mercury chloride;[89] b) trigonal as in $(Me_3S)(HgI_3)$[97] c) tetrahedral as in $[Hg(cyclam)Cl]_2[HgCl_4]$[98] (1,4,8,11-tetraazacyclotetradecane).

The *effective coordination number* is an extension of the characteristic coordination number to include all ligands matching the condition [D(Hg-L) < R(Hg) + R(L)].[88] Only when x = 2, 3 can additional ligands be accommodated. Two or more groups of bond lengths are observed for effective coordination: the shortest ones that represent characteristic coordination, and longer ones due to the close approach of ligands as determined by crystal structures.[88,96] The difference in bond lengths between two or more groups can result in highly distorted geometries, the most common effective coordination being distorted octahedral (Figure 1.7).[88]

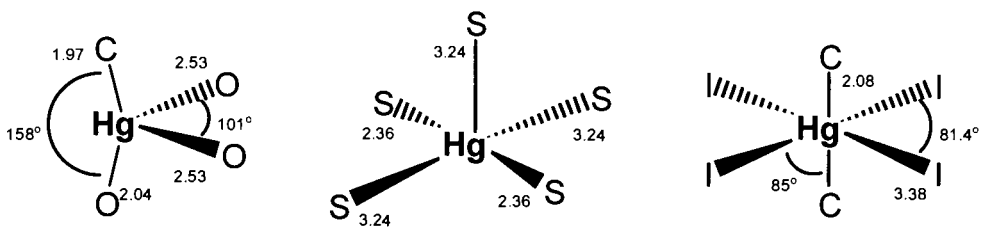

(2+2) (2+3) (2+4)

(a) **(b)** **(c)**

Figure 1.7 Examples of a) seesaw, b) square pyramidal, and c) octahedral effective coordination of Hg(II) based on linear characteristic coordination.
a) mercuric oxycyanide,[99] b) dimethylthio mercury,[100,101] c) $KHg(CN)_2I$.[102]

The fact that mercury can form interactions with a large variety of transition metals and main group elements has made it an attractive candidate as a 'universal glue' in the synthesis of high nuclearity metal clusters.[103] Transition metal-mercury complexes were among the first compounds studied to examine direct metal-metal bonding.[89,103] The recent discovery of redox and photochemical reactivity of some systems has opened up a promising area of mercury cluster research.[103,104]

This concept of using Hg(II) as a 'universal glue' has more recently been employed for the synthesis of extended mixed-metal and organic / inorganic frameworks.[105-112] The pursuit of heterometallic frameworks is motivated by the possibility of enhanced properties that may result from the presence of different metal centres. Novel physical properties are not the sole reason for pursuing the synthesis of bimetallic coordination polymers - the propagation of structural preferences of two different metal centres in bimetallic systems results in a broader spectrum of polymer structural motifs than is achievable in unimetallic systems.[26,28,113,114]

Its transparency in the visible region and its very high polarizability make Hg(II) suitable for the design of new bulk second harmonic generation (SHG) materials used for frequency-doubling of semiconductor lasers by linking together acentric organic building blocks with simple Hg(II) salts.[115] Coordination polymers that show significant third-order non-linear optical properties

have been synthesized.[116] Tunable fluorescent coordination polymers have also been synthesized by the assembly of luminescent organic moieties with HgX_2 (X = Cl, Br).[117]

1.2.3 The Chemistry of Mercury(II) Cyanide

Mercury cyanide is a diamagnetic, white compound that is formed by interaction of most mercury compounds and aqueous cyanide.[36] This linear molecule crystallizes in the $I\bar{4}2d$ tetragonal system, with a = 9.643 Å and c = 8.88 Å.[118] In addition to being bonded to two carbon atoms, the coordinately unsaturated Hg(II) centre is associated with four additional nitrogen atoms (Hg-N = 2.742(3) Å) belonging to four different $Hg(CN)_2$ molecules, resulting in an effective distorted octahedral coordination for the Hg(II) centre (2+4) based on linear characteristic coordination.[87,118]

$Hg(CN)_2$ is readily soluble in polar organic solvents and water. An aqueous solution of $Hg(CN)_2$ is practically a non-electrolyte indicating relatively strong σ-bonding between Hg(II) and the cyano ligands; the rate of cyanide dissociation from $Hg(CN)_2$ is very low.[36] However, in the presence of free cyanide and halides, the low-coordinate unsaturated Hg(II) centre is able to accept these compatible ligands generating higher-coordinate moieties.[119,120] In these reactions the Lewis-acidity of the Hg(II) centre is the key feature controlling the reactivity.[95] Two-coordinate organomercury compounds (HgR_2) show no Lewis acid behaviour, however as the R groups become more electron withdrawing, the Lewis acidity increases, resulting in a higher effective coordination number about the Hg(II) centre.[95] Table 1.1, which contains data for the reaction of several Hg(II) compounds with 4-methylpyridine, shows this gradual change in Lewis acidity.

The $Hg(CN)_2$ unit is also known to react with simple salts such as MX (M = Na, K, Rb, Cs; X = NCO, NCS, N_3, CN, Cl, Br, I; sometimes HgX_2 is also added),[121,122] $(R_4N)CN/M'CN$ (M' = Li, Na, K, Cu)[123] or $M''(NCS)_2$ (M'' = Mg, Ca, Sr, Ba)[124] to yield solid-state 'double salt' arrays of the form $M^{n+}Hg(CN)_2X_n$ (n = 1, 2), $R_4NM'Hg(CN)_4$, or $M''[Hg(CN)_2(SCN)_2]$ respectively. This

provides an interesting design possibility: by accepting additional ligands, higher-coordinate mercury cyanide double salt moieties formed *in situ* could be incorporated during the self-assembly process, possibly increasing the structural and magnetic dimensionality of the coordination polymer as result.[125,126]

Table 1.1 Formation constants of 1:1 adducts of Hg(II) compounds with 4-methylpyridine in benzene solution at 30 °C.[95]

Mercury(II) Compound	*K(L mol^{-1})*
$C_6H_5CH_2HgCl$	1
p-Cl-C_6H_4HgCl	3
$Hg(C_6F_5)_2$	5
$Hg(CN)_2$	11
$Hg(CCl_3)_2$	15
Cl_3CHgCl	22
$C_4H_9HgNO_3$	88
$Hg(SCN)_2$	118
$HgCl_2$	258
HgI_2	266
$HgBr_2$	379

At the same time, the cyano-N atoms of the $Hg(CN)_2$ unit, if not bound to another metal, can participate in hydrogen bonding. There may be either simple or bifurcated hydrogen bonds of the CN···H-X type (where X is an electronegative atom) and these can play an important role in the packing and stabilization of the structures formed.[35,127] Recently, molecular recognition of anionic cyanometallates as hydrogen bond acceptor sites to bis-amidinium dicationic building blocks has been employed in the rational design of 1-D and 2-D hydrogen bonded molecular networks.[128] Cyano-N hydrogen bonding has also been proposed as a possible exchange path for magnetic interactions.[129,130]

The use of $Hg(CN)_2$ as a building block combines the capability of coordinate bonding to a second TM centre via the cyano-nitrogen donors group with the capability of using the

unsaturated Hg(II) centre as a Lewis-acidic glue towards compatible ligands. This method with which to build heterometallic coordination polymers would diverge from that of the metallophilic interactions of $[Au(CN)_2]^-$ and $[Ag(CN)_2]^-$ as observed by the Leznoff group.[79-82]

1.2.4 Previous $Hg(CN)_2$ Results

The linear, but neutral, $Hg(CN)_2$ molecule has not been investigated as a building block to create supramolecular architectures; only a few simple adducts are known. $\{Zn(H_2O)_4[Hg(CN)_2]_2\}(NO_3)_2$ is essentially molecular, consisting of zinc atoms octahedrally coordinated by four water molecules and two *trans*-$Hg(CN)_2$ molecules.[60] Both terminal and bridging cyano groups are present in the IR (ν_{CN} = 2190 cm^{-1} and 2230 cm^{-1} respectively). $Hg(CN)_2$-$Ag(NO_3)$-$2H_2O$ consists of $[Ag(H_2O)_2Hg(CN)_2]_n^{n+}$ one dimensional cation chains (both cyano groups are bridging) that are cross-linked via hydrogen bond interactions and possible argentophilic interactions (Ag···Ag = 3.219 Å).[61] Although $Hg(CN)_2$ is known to form adducts with several chelating amines and $K_4[Fe(CN)_6]$, $K_2[Ni(CN)_4]$, and $K_4[Ru(CN)_6]$, their single X-ray crystal structures are still unknown.[131]

1.3 GENERAL TECHNIQUES

1.3.1 Polymer Preparation

An attractive feature of the cyanometallate self-assembly process is the mild reaction conditions utilized for polymer formation. In general, a solution containing $[TML_y]^{x+}$ is made by dissolving a transition metal (TM) salt in a polar solvent followed by the addition of a stoichiometric amount of capping ligand from a stock solution. An observable colour change typically results upon formation of $[TML_y]^{x+}$. A second solution containing $Hg(CN)_2$ is then added to the $[TML_y]^{x+}$ solution with stirring. Since Hg(II) has a d^{10} configuration and exhibits no paramagnetism, paramagnetic TMs are used as the secondary coordination centre in order to investigate the resultant magnetic properties of any supramolecular system formed. If an immediate precipitate is formed upon mixing of the two solutions, then it is collected via vacuum

filtration, washed and dried. The precipitate is then characterized by a number of methods as described in Section 1.3.2. However, for the majority of reactions described in this thesis, immediate precipitation does not occur. The solutions are left to slowly evaporate until a product is formed, which is then collected, washed, dried, and characterized. Fortunately, many products obtained in this manner are crystalline and can be directly characterized using X-ray crystallography as described in Section 1.3.2.3. Figure 1.8 illustrates the general preparative technique used throughout this thesis.

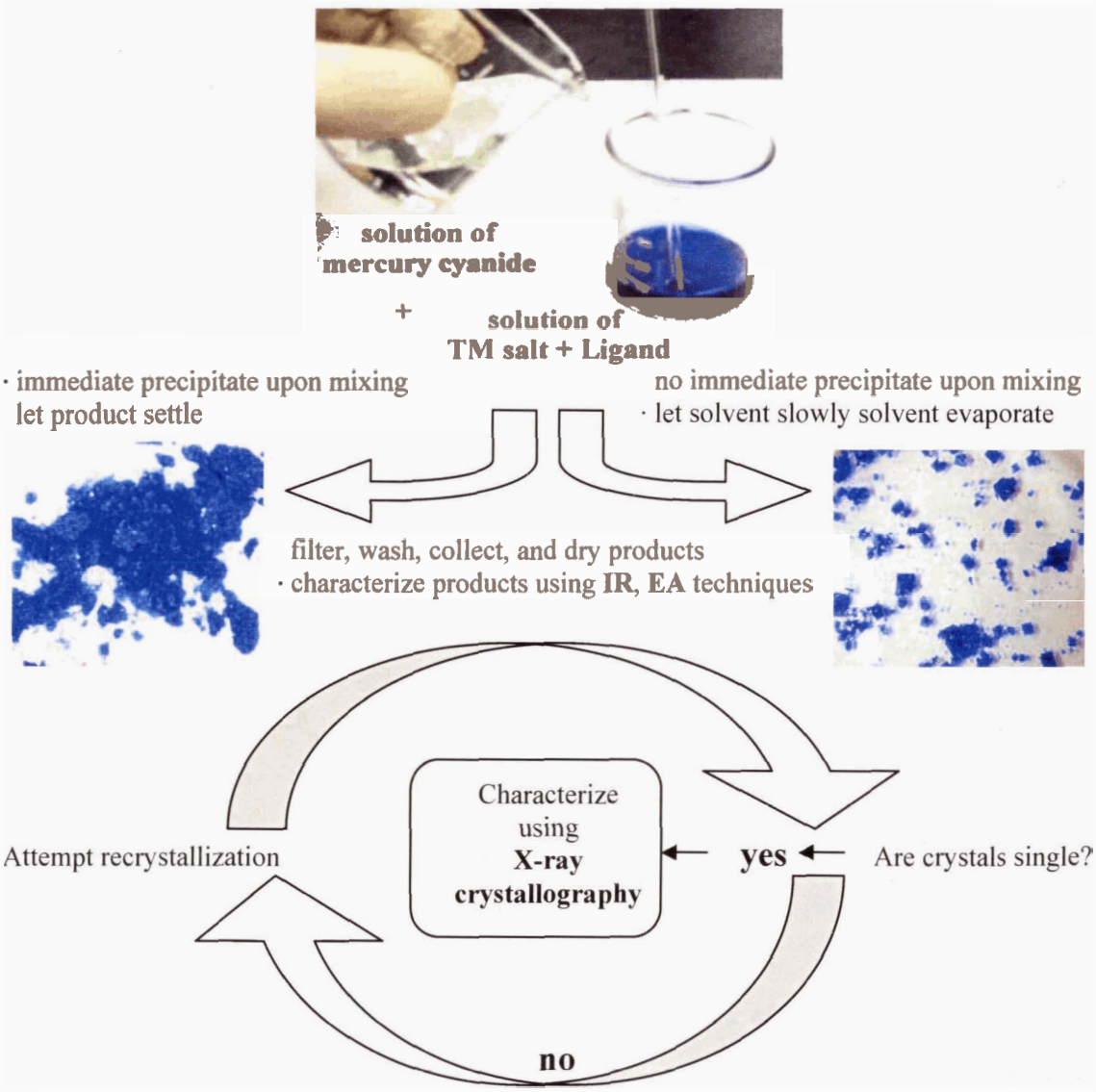

Figure 1.8 General preparative technique for the formation of cyanomercurate-containing coordination polymers.

Chelating amines are employed as capping ligands for the second metal coordination centres for several reasons. Since amine ligands are considered relatively 'hard' ligands, they tend to complex 'hard' metal cations. This gives a degree of control to the experiments; the 'soft' Hg(II) centre will not compete with the transition metal centre for ligands, limiting the possible number of coordination polymers that could form. The number of open coordination sites available on the transition metal is also controlled by the chelating ability of the capping ligand; usually one or two equivalents of ligand are employed. A wide variety of amine ligands with different chelating ability are commercially available, thus providing the means to investigate the effects of ligand shape, basicity, and hydrogen bond donor ability on the resultant polymer formed. The capping ligands used in this thesis are depicted in Figure 1.9.

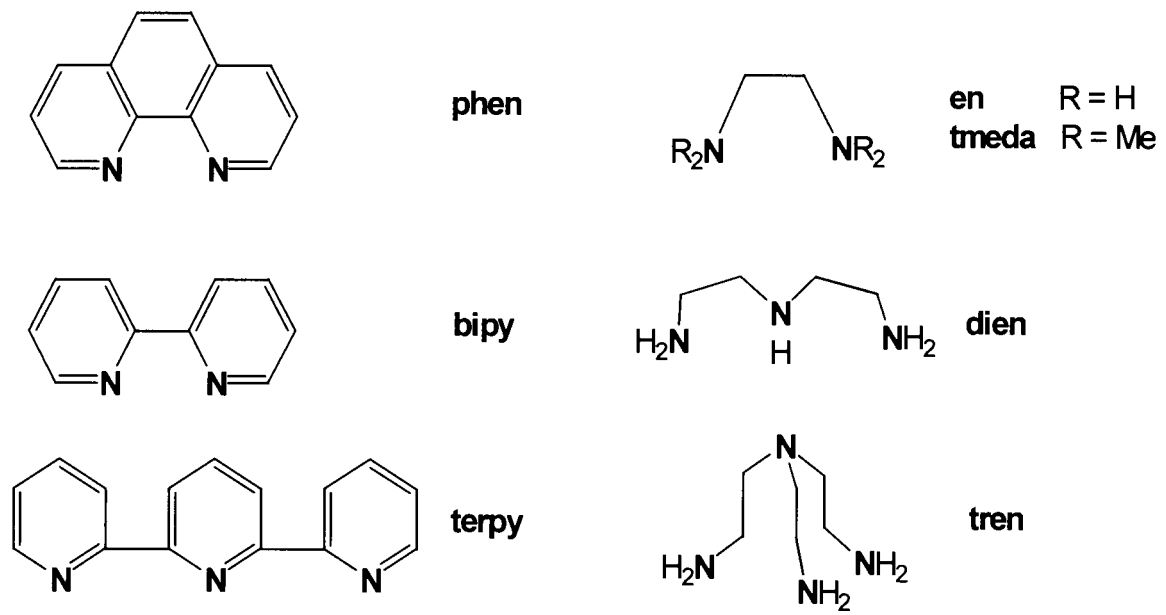

Figure 1.9 Capping ligands for transition metals.

1.3.2 Characterization Methods

1.3.2.1 Infrared Analyses

Infrared spectroscopy (IR) is a valuable tool in determining whether or not cyanometallate moieties have been incorporated into self-assembled coordination polymers. The vibrational spectra of cyano complexes have been extensively studied, the cyano groups being easily

identified by sharp stretching frequencies (ν_{CN}) exhibited between 2250-2000 cm^{-1}.[132] Furthermore, IR can provide a means of distinguishing between bridging and terminal cyanides.[37,132,133] Hence, IR is the first characterization performed on all coordination polymers synthesized in this thesis.

Free cyanide (e.g. aqueous KCN) exhibits a ν_{CN} stretch at 2080 cm^{-1} in aqueous solution,[132] but upon coordination to a metal centre (M-CN) the terminal ν_{CN} stretch usually shifts to higher frequency; the carbon atom is a good σ-donor and electron density is removed from a weakly antibonding orbital relative to the C-N bond.[134,135] On the other hand, electron density from the M *d*-orbitals can be transferred back to the cyano group via good overlap with the cyano antibonding orbital(s) (Figure 1.10); π-back bonding decreases the ν_{CN} stretching frequency for cyano groups.[37]

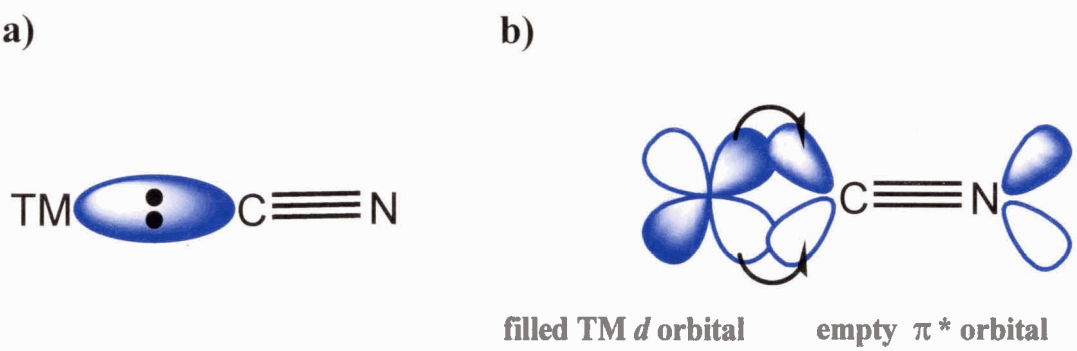

Figure 1.10 Representation of a) cyanometallate σ-bonding and b) cyanometallate π-back bonding.

With this in mind, the ν_{CN} frequencies are affected by the electronegativity, oxidation state, and coordination number of the transition metal.[132] A TM with small electronegativity is not as strong a σ-donor relative to a TM with large electronegativity, thus its ν_{CN} stretching frequency is lower as demonstrated by the order $[Ni(CN)_4]^{2-}$ (2128 cm^{-1}) < $[Pd(CN)_4]^{2-}$ (2143 cm^{-1}) < $[Pt(CN)_4]^{2-}$ (2150 cm^{-1}); there is less electron density available for π-back donation to the cyano groups for TMs of high electronegativity.[37,132] As the oxidation state of a TM increases, the more

electropositive it becomes, decreasing the electron density available for π-back donation in the process. Hence, the ν_{CN} stretching frequency increases with increasing oxidation state as demonstrated by the order $[V(CN)_6]^{5-}$ (1910 cm^{-1}) < $[V(CN)_6]^{4-}$ (2065 cm^{-1}) < $[V(CN)_6]^{3-}$ (2077 cm^{-1}).[37,132] Increasing coordination number results in a decrease in positive charge on the TM which weakens the σ-bonding, thus lowering the ν_{CN} frequency; more electron density is available for π-back donation to the cyano groups. Table 1.2 shows the ν_{CN} stretching frequencies for several cyanomercurate moieties in aqueous solution. Since IR spectroscopy can only detect a change in dipole moment, only the asymmetric ν_{CN} stretching mode is observable for $Hg(CN)_2$.[36,132] Although several more IR-active ν_{CN} modes exist for higher coordinate cyanomercurates, they are degenerate in solution, resulting in a single observable ν_{CN} stretch for each moiety.[119] For the mercury cyanide / chloride double salt units, the ν_{CN} stretch occurs at slightly higher frequencies than the corresponding cyanomercurate analogue.[119] The chloride ligand is able to draw electron density away from the Hg(II) centre making it less available for π-back donation to the cyano groups.

Table 1.2 IR ν_{CN} stretching frequencies of aqueous cyanomercurate moieties.

Cyanomercurate	ν_{CN} *(cm^{-1})*	*Reference*
$Hg(CN)_2$	2194	36
$[Hg(CN)_3]^-$	2161	119
$[Hg(CN)_4]^{2-}$	2143	119
$[Hg(CN)_2Cl]^-$	2187	119
$[Hg(CN)_3Cl]^{2-}$	2157	119

1.3.2.2 Elemental Analysis and Single Crystal X-ray Crystallography

If the IR spectrum suggests the presence of a cyanomercurate, then elemental analysis (EA) is conducted on the coordination polymer formed. From the analysis of the combustion products (carbon dioxide, nitrogen dioxide, and water) combined with the change in weight of the sample, the weight percentage of carbon, nitrogen, and hydrogen of the polymer can be calculated. By

comparing EA results with the expected product percentages, useful information regarding product composition is obtained, such as the presence of a cyanomercurate moiety in a sample. Any polymer sample submitted for EA should appear uniform in composition, containing little or no impurity, the presence of which can roughly be determined by visual inspection through the use of a high powered microscope.

Although EA may successfully predict the number and types of building blocks in a particular coordination polymer, it does not give any information as to how the individual components are assembled together relative to each other. In order to determine this three dimensional arrangement of the individual components in space, X-ray crystallography is employed. This technique is undoubtedly among the most powerful characterization method, providing conclusive evidence of the product's solid state structure. However, for the most part, it is limited to the use of suitable single crystals, which can be difficult to obtain. During the course of my research, approximately sixty crystal structures were successfully solved by myself, of which twenty-five appear in this thesis.

1.3.2.3 Material Properties

A variety of material properties such as the magnetic susceptibility, optical birefringence, and dielectric constant are examined in the latter part of this thesis. Determination of optical and electrical properties usually requires the use of large, single crystals which are difficult to grow. On the other hand, microcrystalline powders are sufficient to collect magnetic data or determine the porosity of a coordination polymer. Typically, the decision to investigate potential material properties of a coordination polymer occurs after the structure has been determined via X-ray crystallography. For instance, if the X-ray crystallographic structure shows promising magnetic pathways, then magnetic susceptibility data is obtained using a SQUID magnetometer. Furthermore, some solid state properties, such as piezoelectricity and non-linear optics require that the compound crystallizes in a non-centrosymmetric space group (i.e.: lack an inversion

centre) while other solid state properties such as pyroelectricity and ferroelectricity require not only a non-centrosymmetric, but also a polar space group. Specific material properties will be described in more detail as required throughout this thesis.

1.4 RESEARCH OBJECTIVES

The general purpose of this thesis is to examine the use of $Hg(CN)_2$ as a potential building block in the preparation of multidimensional coordination polymers. In order to narrow the scope of the research undertaken, the thesis will specifically focus on the development of mercury cyanide / chloride double salt coordination polymers. By doing so the concept of using Hg(II) as a universal glue to generate extended frameworks with increased dimensionality will be assessed. Attention is given to the various factors influencing the formation of such complexes including reactant stoichiometry, ligand basicity, solvent, and hydrogen bonding interactions. This survey should aid in the development of a predictable approach to designing $Hg(CN)_2$ containing coordination polymers with a given dimensionality and their potential material properties. Structural correlations as they relate to measured resultant properties, if any, will be ascertained.

CHAPTER 2
THE BEHAVIOR OF MERCURY CYANIDE / CHLORIDE DOUBLE SALTS: EXTENDED ANIONIC FRAMEWORKS

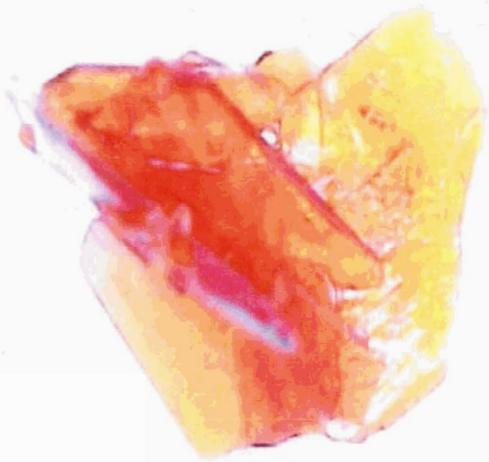

2.1 INTRODUCTION

2.1.1 Related Chloromercurate(II) Frameworks

Some work has been completed that successfully demonstrates that Hg(II) can be used as a 'universal glue' in order to increase dimensionality.[105-110] Two-coordinate, unsaturated, Lewis-acidic Hg(II) centres containing electron withdrawing groups, such as halides, are able to accept compatible ligands (i.e.: Lewis bases) resulting in an increase in effective Hg(II) coordination.[95,136] When the Lewis base is an anion, such as a halide, the formation of structurally diverse complex Hg(II) anions occurs, that can potentially increase dimensionality.[96,122,137] This ability of Hg(II) to accept compatible ligands was first observed in the mid to late 18th century by Daniel Strömholm who reacted $[R_3S]Cl$, $[R_4N]Cl$, or $[PtN_4]Cl_2$ with $HgCl_2$, yielding several different chloromercurate(II) anions with the general formula $Hg_xCl_y^{n-}$.[138] Many of these complex $Hg_xCl_y^{n-}$ anions were rediscovered and structurally characterized by 1968.[139]

$Hg_xCl_y^{n-}$ complex anions are of interest to structural chemists for a number of reasons. Frequently, the configuration of the $Hg_xCl_y^{n-}$ anion does not necessarily follow from the stoichiometry.[87,88,96] For example, $K_2HgCl_4 \cdot H_2O$ does not contain discrete $HgCl_4^{2-}$ anions, but distorted $HgCl_6$ octahedra that share opposite edges, forming anionic 1-D ribbons of $[HgCl_4]_n^{2n-}$ (Figure 2.1).[140] Another observed characteristic of $Hg_xCl_y^{n-}$ anions is the formation of multi-anionic combinations from relatively simple stoichiometries such as reported for the double salt

complex 2 $CaCl_2$-11 $HgCl_2$-16 H_2O which contains both $[Hg_6Cl_{13}]^-$ and $[Hg_5Cl_{13}]^{3-}$ discrete anions.[141]

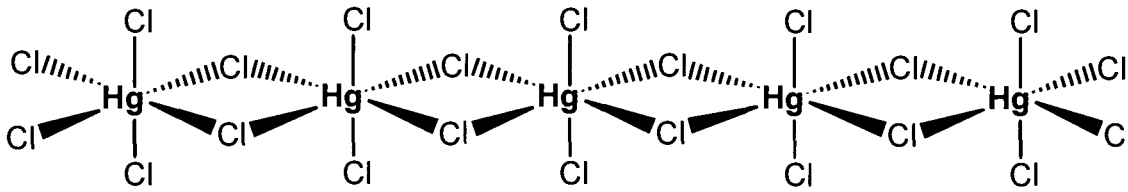

Figure 2.1 Ribbon of $[HgCl_4]_n^{2n-}$ in $K_2HgCl_4 \cdot H_2O$.

This phenomenon is also observed in $Hg_xI_y^{n-}$ systems.[92,142,143] Furthermore, even though a large number of $Hg_xCl_y^{n-}$ anions have been characterized by X-ray crystallography, it is still not possible to predict the particular $Hg_xCl_y^{n-}$ form that will be adopted in the solid state, even for simple stoichiometries such as $[HgCl_3]^-$. However, some generalizations have been made for the most simple chloromercurate anion, $[HgCl_3]^-$. Isolated $[HgCl_3]^-$ anions are quite rare, while $[HgCl_3]_n^{n-}$ chains and $[HgCl_3]_2^{2-}$ bitetrahedra are very common; cations having extended hydrogen bonding networks usually result in more complex structural anionic patterns.[96]

Substitution of $Hg(CN)_2$ for $HgCl_2$ should result in the formation of mercury cyanide / chloride double salt anions which should show similar extended structures to $Hg_xCl_y^{n-}$ anions, however very few have been reported in the literature as described in section 2.1.2. In order to investigate the formation of such extended mercury cyanide / chloride double salt type networks, both organic monocationic chlorides and coordinately saturated transition metal chlorides are utilized in this study, thus eliminating any potential for either chloride or *N*-cyano coordination to the transition metal centre.

2.1.2 Previous Mercury Cyanide / Chloride Double Salt Complexes

As described in Chapter 1, $Hg(CN)_2$ can also accept chloride ligands forming $[Hg(CN)_2Cl]^-$ anions which are referred to as 'double salts'.[86] These anions are known to aggregate to yield multidimensional systems.[102,122] Unlike compounds containing chloromercurate anions, only two

structure types have been reported in the literature. $MHg(CN)_2Cl \cdot x\ H_2O$[122] (M = Na, K, Rb; x = 0, 1) consists of infinite 2-D layers of $[Hg(CN)_2Cl]^-$ separated by M^+ and water molecules (when x = 1). The chlorine atoms form weak equatorial associations with the mercury atoms of the $Hg(CN)_2$ groups increasing the effective Hg(II) coordination from two to six (2+4); the layer then consists of edge sharing $Hg(CN)_2Cl_4$ octahedra. The reaction is summarized in equation 2.1.

$$MCl + Hg(CN)_2 \xrightarrow{H_2O} M[Hg(CN)_2Cl] \cdot x\ H_2O \qquad \text{Equation 2.1}$$

A different 2-D network is observed for $[EtNH_3]_2[Hg(CN)_2Cl_2]$.[144] It belongs to a series of compounds with the general formula $(R_xNH_{4-x})_2MX_4$ with R being an aliphatic or aromatic hydrocarbon, M, a divalent metal, and X, a halogen. Many of these organic-inorganic hybrid perovskites show interesting physical properties such as ferroelectricity or ferroelasticity.[7,144,145] $[EtNH_3]_2[Hg(CN)_2Cl_2]$ consists of 2-D layers of corner-sharing $Hg(CN)_2Cl_4$ octahedra (2+4 Hg(II) effective coordination) that form a chessboard arrangement of half centred chlorine squares. The $[EtNH_3]^+$ cations are located both above and below the non-centred chlorine squares and form hydrogen bonds to neighbouring layers resulting in a 3-D network. The reaction is summarized in equation 2.2.

$$2\ EtNH_3Cl + Hg(CN)_2 \xrightarrow{H_2O} [EtNH_3]_2[Hg(CN)_2Cl_2] \qquad \text{Equation 2.2}$$

2.1.3 Research Objectives

This chapter is focused on the reactions of $Hg(CN)_2$ with organic monocationic chlorides and coordinatively saturated metal-ligand complex chloride salts in order to investigate the possible factors influencing the structure of the double salt anionic motif formed, including cation shape, cation charge, and hydrogen bonding interactions.

2.2 RESULTS AND ANALYSIS

2.2.1 Rational Syntheses of 2.1-2.7

The reaction of an aqueous solution of bis(triphenylphosphoranylidene)ammonium chloride ([PPN]Cl), tetrabutylammonium chloride ([$^{n}Bu_4N$]Cl), or tetraphenylarsonium chloride ([$(C_6H_5)_4As$]Cl) with an aqueous solution containing one equivalent of $Hg(CN)_2$ yielded single crystals of **2.1**, **2.2**, and **2.3** respectively. The reactions can be summarized by general equation 2.3:

$$[Cat]Cl + Hg(CN)_2 \xrightarrow{H_2O} [Cat][Hg(CN)_2Cl] \cdot x\,H_2O \qquad \text{Equation 2.3}$$

where Cat = PPN^+ (x = 1), $^{n}Bu_t^+$ (x = 0.5), and $(C_6H_5)_4As^+$ (x = 0).

Similarly, the reaction of an aqueous solution of $NiCl_2$ with two equivalents of 2,2':6',2"-terpyridine (terpy), or an aqueous solution of $CuCl_2$ with two equivalents of ethylenediamine (en), followed by the addition of two equivalents of $Hg(CN)_2$ yielded single crystals of **2.4** and **2.5** respectively and can be represented by general equation 2.4:

$$1)\ MCl_2 + L_2 \longrightarrow [ML_2]Cl_2$$

$$2)\ [ML_2]Cl_2 + 2\,Hg(CN)_2 \longrightarrow [ML_2][Hg(CN)_2Cl]_2 \qquad \text{Equation 2.4}$$

The reaction of an aqueous solution of $[Co(en)_3]Cl_3$, with 3 equivalents of $Hg(CN)_2$ yielded **2.6** while the reaction of an aqueous solution of $[Co(NH_3)_6]Cl_3$ with 2.5 equivalents of $Hg(CN)_2$ yielded **2.7**. Their resulting double salt formulae were more complex, as described in equations 2.5 and 2.6:

$$[Co(en)_3]Cl_3 + 3\,Hg(CN)_2 \longrightarrow [Co(en)_3][Hg(CN)_2Cl_2]\{[Hg(CN)_2]_2Cl\} \qquad \text{Equation 2.5}$$

$$2\,[Co(NH)_6]Cl_3 + 5\,Hg(CN)_2 \xrightarrow{H_2O} [Co(NH)_6]_2[Hg(CN)_2]_5Cl_6 \cdot 2\,H_2O \qquad \text{Equation 2.6}$$

2.2.2 Structures of $[Cat][Hg(CN)_2Cl]_x \cdot y\ H_2O$ (Cat = PPN^+, x = y = 1 (2.1); $^nBu_4N^+$, x = 1, y = 0.5 (2.2); $Ni(terpy)_2^{2+}$, x = 2, y = 0 (2.4)).

All three structures are molecular and consist of isolated $[Hg(CN)_2Cl]_2^{2-}$ anionic dimers and two $[PPN]^+$ (**2.1**) (Figure 2.2), two $[^nBu_4N]^+$ (**2.2**), and one $[Ni(terpy)_2]^{2+}$ (**2.4**) cations, respectively; the $[(C_6H_5)_4As]^+$ (**2.3**) cation also appears to be balanced by the same $[Hg(CN)_2Cl]_2^{2-}$ unit as shown by a low resolution crystal structure.

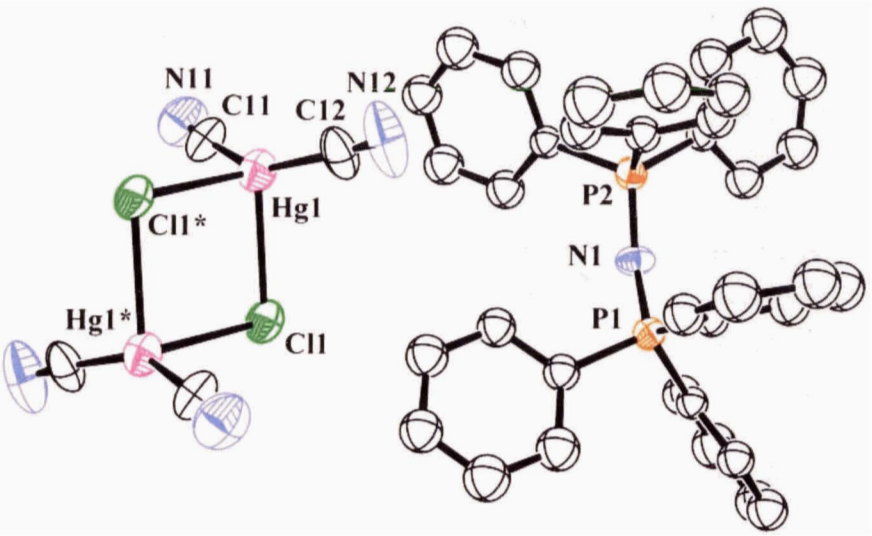

Figure 2.2 Molecular structure of $[PPN][Hg(CN)_2Cl] \cdot H_2O$ (**2.1**).
The second $[PPN]^+$ cation, water molecule and hydrogen atoms have been omitted for clarity (ORTEP 50% ellipsoids).

The bond distances and angles for the $[Hg(CN)_2Cl]_2^{2-}$ anions in **2.1**, **2.2** and **2.4** are gathered in Table 2.1. Each coordinately unsaturated Hg(II) centre accepts a chloride ligand to form a $[Hg(CN)_2Cl]^-$ double salt moiety. These $[Hg(CN)_2Cl]^-$ units self assemble into $[Hg(CN)_2Cl]_2^{2-}$ dimers via two Cl bridges, producing a see-saw geometry around each Hg(II) atom with C-Hg-C angles ranging from 150.5(6)° (**2.4**) to 160.1(6)° (**2.2**), and Cl-Hg-Cl angles ranging from 82.44(10)° (**2.4**) to 93.10(9)° (**2.2**). This effective see-saw coordination of Hg(II) is based on linear Hg(II) characteristic coordination where there are two shorter and two longer Hg(II) bonds ((2+2) according to the convention devised by Grdenić),[88] and is observed in the di-μ-X-

bis[X(bznapH)-Hg(II)] (X = Cl, Br; bznapH = *N*-benzyl-2-oxo-1-napthylideneamine) adducts,[91] and the $HgCl_4^{2-}$ anion of $(ClHgNC_6H_{12}Cl)_2HgCl_4(C_6H_6) \cdot H_2O$.[146]

Table 2.1 Selected Bond Lengths (Å) and Angles (°) for the $[Hg(CN)_2Cl]_2^{2-}$ dimers of **2.1**[a], **2.2**[b], and **2.4**[c].

Compound	**2.1**	**2.2**	**2.4**
Selected Atoms	*Bond Lengths*	*Bond Lengths*	*Bond Lengths*
Hg(1)-Cl(1)	2.713(3)	2.747(3)	2.751(3), 2.711(4)
Hg(1)-Cl(1*)	2.766(3)	2.766(3)	2.799(4), 2.820(3)
Hg(1)-C(11)	2.054(15)	2.056(16)	2.052(15), 2.044(17)
Hg(1)-C(12)	2.054(15)	2.02(2)	2.060(17), 2.060(16)
C(11)-N(11)	1.121(14)	1.107(14)	1.121(16), 1.143(16)
C(12)-N(12)	1.104(15)	1.126(19)	1.114(17), 1.130(16)
Selected Atoms	*Bond Angles*	*Bond Angles*	*Bond Angles*
Cl(1)-Hg(1)-Cl(1*)	85.48(9)	93.10(9)	82.44(10), 87.73(10)
Hg(1)-Cl(1)-Hg(1*)	94.52(9)	86.90(9)	97.56(10), 92.27(10)
C(11)-Hg(1)-C(12)	150.7(5)	160.1(6)	150.5(6), 158.1(6)
Hg(1)-C(11)-N(11)	175.9(13)	177.5(14)	177.4(14), 175.2(17)
Hg(1)-C(11)-N(12)	175.9(14)	175 (2)	177.9(17), 179.8(14)

[a] Symmetry transformations: (*) -x+2, -y+1, -z+2.
[b] Symmetry transformations: (*) -x+1, -y, -z+2.
[c] Symmetry transformations: (*) -x+1, -y+1, -z+1. The second values pertain to the second dimer of compound **2.4**. Symmetry transformations (*) -x, -y+3, -z+2.

The Hg(1)-Cl bond lengths of **2.1**, **2.2**, and **2.4** range from 2.711(4) to 2.820(3) Å, which can be compared with the 2.587(4) and 2.662(5) Å and 2.589(5) and 2.614(5) Å found for the related $[Hg_2Cl_6]^{2-}$ anionic dimers in $[^nBu_4N][HgCl_3]$[147] and $[(C_6H_5)_4As][HgCl_3]$,[148] and the 3.189(2) Å reported for the bridging Hg-Cl distance of $(bznapH)HgCl_2$.[91] No hydrogen bonds are present between the cations and $[Hg(CN)_2Cl]_2^{2-}$ dimers of compounds **2.1-2.4** since $[PPN]^+$, $[^nBu_4N]^+$, $[(C_6H_5)_4As]^+$ and $[Ni(terpy)_2]^{2+}$ lack any significant hydrogen donor sites; no increase in structural dimensionality is observed for compounds **2.1-2.4**. The disordered water molecules in **2.1** and the half equivalent of water in **2.2** do not impact the structure or dimensionality of the $[Hg(CN)_2Cl]_2^2$ anionic dimer as no water is present in **2.3** or **2.4**. No mercurophilic interactions are observed for **2.1-2.4**.

2.2.3 Structure of $[Cu(en)_2][Hg(CN)_2Cl]_2$ (2.5)

The X-ray crystal structure of $[Cu(en)_2][Hg(CN)_2Cl]_2$ (**2.5**) reveals dimeric units of $[Hg(CN)_2Cl]_2^{2-}$ that are linked via weak Hg(1)-Cl(1') interactions to give a $[Hg(CN)_2Cl]_n^{n-}$ one-dimensional anionic ladder motif that runs parallel to the *a*-axis (Figure 2.3). The bond lengths and angles for **2.5** are gathered in Table 2.2.

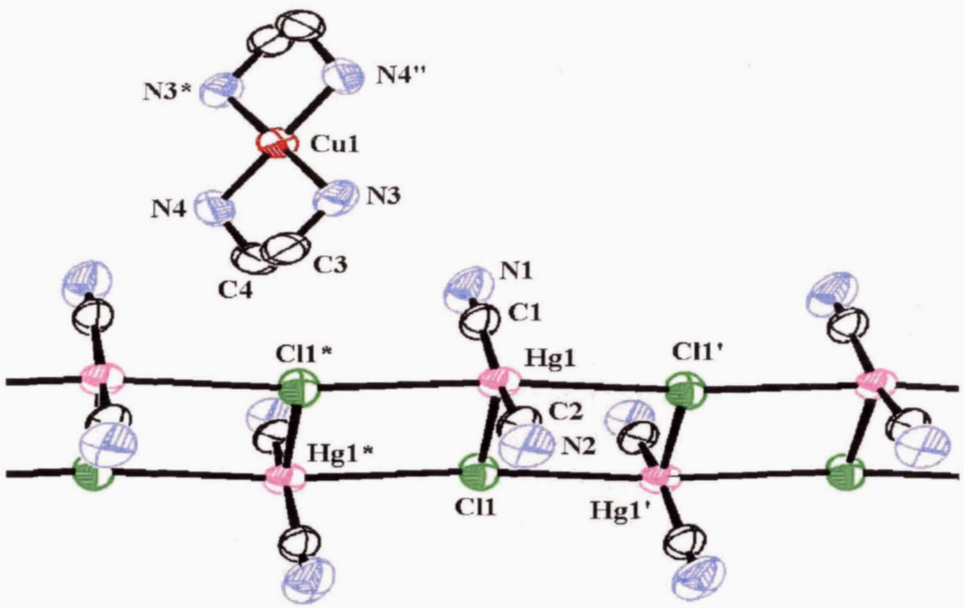

Figure 2.3 Extended 1-D ladder structure of $[Cu(en)_2][Hg(CN)_2Cl]_2$ (**2.5**). Only one $[Cu(en)_2]^{2+}$ cation is shown and hydrogen atoms have been omitted for clarity (ORTEP 50% ellipsoids).

The ladder frame and rungs are made up of three different Hg-Cl bonds (2.7089(17), 3.0978(15), and 3.2186(15) Å) with the cyano ligands lying in the *bc*-plane, perpendicular to the ladder direction. These bond lengths are well within the sum of the Hg/Cl van der Waals radii of 3.30 Å[88,149] and are comparable to the bridging Hg-Cl bond lengths (3.04(1) and 3.21(1) Å) found in the polymeric compound $[(Et_3P)\cdot(HgCl_2)]_n$.[150,151] The effective five-coordinate Hg(II) centres based upon linear characteristic coordination (2+1+1+1) have a distorted square pyramidal geometry (Cl(1*)-Hg(1)-Cl(1') = 173.41(7)°, C(1)-Hg(1)-C(2) = 162.9°(3)) with two chloride

and two cyano ligands occupying the basal plane while the third (but closest) chloride ligand occupies the apical site.

Table 2.2 Selected Bond Lengths (Å) and Angles (°) for $[Cu(en)_2][Hg(CN)_2Cl]_2$ (**2.5**)[a].

Selected Atoms	*Bond Lengths*	*Selected Atoms*	*Bond Lengths*
Hg(1)-C(1)	2.066(8)	N(1)-C(1)	1.103(10)
Hg(1)-C(2)	2.072(7)	N(2)-C(2)	1.064(9)
Hg(1)-Cl(1)	2.709(2)	N(3)-C(3)	1.475(10)
Hg(1)-Cl(1*)	3.0972(15)	N(4)-C(4)	1.476(12)
Hg(1)-Cl(1')	3.2195(16)	Cu(1)-N(3)	1.986(6)
C(3)-C(4)	1.487(13)	Cu(1)-N(4)	2.011(6)
Selected Atoms	*Bond Angles*	*Selected Atoms*	*Bond Angles*
C(1)-Hg(1)-C(2)	162.9(3)	Cl(1)-Hg(1)-Cl(1*)	85.90(6)
Hg(1)-C(1)-N(1)	178.6(8)	Cl(1)-Hg(1)-Cl(1')	88.04(5)
Hg(1)-C(2)-N(2)	176.4(7)	Cl(1*)-Hg(1)-Cl(1')	173.41(7)
Cl(1)-Hg(1)-C(1)	97.1(3)	Hg(1)-Cl(1)-Hg(1*)	94.10(6)
Cl(1)-Hg(1)-C(2)	99.8(2)	Hg(1)-Cl(1)-Hg(1')	91.96(5)
Cl(1*)-Hg(1)-C(1)	92.31(19)	Hg(1*)-Cl(1)-Hg(1')	173.41(7)
Cl(1')-Hg(1)-C(1)	91.10(19)	N(3)-Cu(1)-N(4)	84.8(3)
Cl(1*)-Hg(1)-C(2)	91.51(19)	N(3)-Cu(1)-N(4")	95.2(3)
Cl(1')-Hg(1)-C(2)	86.96(19)		

[a] Symmetry transformations: (*) –x+1, -y, -z-1; (') -x+2, -y, -z-1; (") -x+2, -y+1, -z.

This unusual Hg(II) square pyramidal coordination is also observed in $Hg(SMe_2)_2$ which has two short (2.36 Å) and three long (3.24 Å) Hg-S bonds,[100,101] and in $[ClHgNC_5H_{10}Cl]_2[Hg_2Cl_6]$[146] which also has two short (2.32 Å) and three long (2.80(1), 2.86(1), and 3.39(1) Å) Hg-Cl bonds. In **2.5**, each Cl atom interacts with three different Hg(II) centres and is hence triply bridging, having a slightly distorted T-shaped geometry (Hg(1*)-Cl(1)-Hg(1') = 173.41(7)°). The $[Hg(CN)_2Cl]_n^{n-}$ anionic ladder motif **2.5** is similar to the $[HgBr_3]_n^{n-}$ ribbon motif reported for $[Cu(en)_2][Hg_2Br_6]$,[152] in which the Hg(II) centres have distorted trigonal bipyramidal effective coordination rather than square pyramidal. It also differs from that of the $[Hg_2Cl_6]^{2-}$ anionic dimer found in the chloride analogue $[Cu(en)_2][Hg_2Cl_6]$.[152]

The Cu(II) centre in **2.5** has a distorted square planar geometry comprised of two ethylenediamine ligands; the Cu(1)-N(en) bond lengths are 1.986(6) Å and 2.011(6) Å, respectively. Two cyano ligands can be found in proximity to the open axial sites of each copper centre with a Cu(1)···NC distance of 2.772(7) Å. Although long axial bonds due to bridging cyano groups have been reported in the literature (e.g. 2.731(6) and 2.967(7) Å in the 3-D network $[Cu(en)_2]_3[W(CN)_8]_2 \cdot H_2O$),[127] these contacts should only be considered as weak interactions at best.

Two types of hydrogen bonds are formed between $[Cu(en)_2]^{2+}$ cations and the $[Hg(CN)_2Cl]_n^{n-}$ anionic ladders, consisting of N-H···Cl and N-H···NC donor / acceptor pairs, that result in a three-dimensional, bimetallic network (Figure 2.4). The $[Cu(en)_2]^{2+}$ cations form four weak N-H···NC interactions, each to a different $[Hg(CN)_2Cl]_n^{n-}$ anionic ladder. Two of these interactions are 3.182 Å (N(3)-N(1)) while the other two are 3.389 Å (N(4)-N(2)), and are both comparable to those reported for $[Cu(en)_2]_3[W(CN)_8]_2 \cdot H_2O$ (3.214 Å),[127] $[Cu(en)_2][Ag_2(CN)_4]$ (3.195 Å),[130] and $[NO(CN)_4FeCN\text{-}Cu(en)_2\text{-}NCFe(CN)_4(NO)][Cu(en)_2]$ (several interactions ranging from 3.059 Å - 3.358 Å).[153] Two additional weak N-H···Cl interactions (N(3)-Cl(1) = 3.289 Å) are also present and are comparable to those reported for $[Cu(Hbimam)Cl_3]_2(H_2O)_2$, $[Cu(Hbimam)_2Cl_2]Cl_2(H_2O)_2$ (3.266 Å and 3.277 Å respectively; bimam = bis(imidazol-2-yl)methylaminomethane),[154] *trans*-$[PtCl_2(NH_3)_2]$ (3.41 Å),[155] and 2,6-diphenylpyridinium tetrachloroaurate (3.45 Å, 3.75 Å).[156] The result is a 3-D network of alternating rows of $[Cu(en)_2]^{2+}$ cationic columns and $[Hg(CN)_2Cl]_n^{n-}$ ladders down the *a*-axis, where each cationic column is surrounded by four anionic ladders and *vice versa*. The particular inorganic-organic hybrid framework of **2.5** is very similar to those reported for $[4,4'\text{-}H_2bipy][MCl_4]$ (M = Mn, Pb),[157,158] and $(H_2DAH)BiI_5$ (DAH = 1,6-hexanediamine).[159]

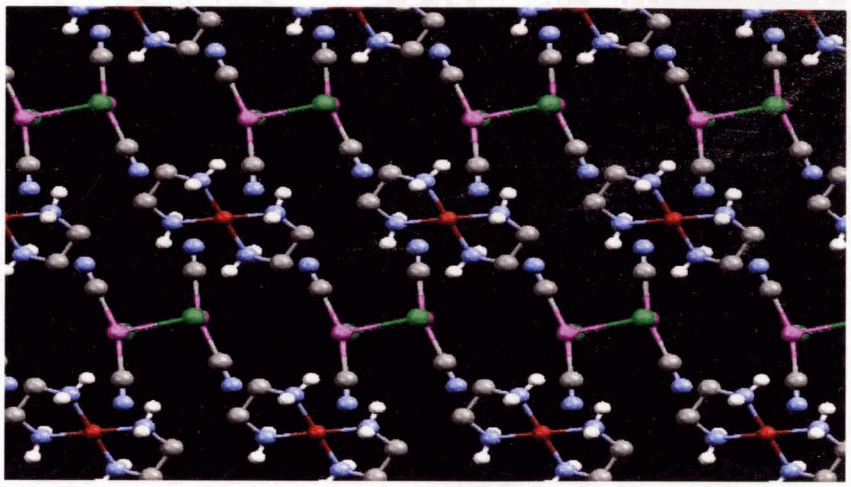

Figure 2.4 The 3-D frameworks of **2.5** showing alternating rows of $[Cu(en)_2]^{2+}$ columns and $[Hg(CN)_2Cl]_n^{n-}$ ladders as viewed down the *a*-axis.
Ethyl hydrogen atoms have been omitted for clarity. Colour scheme: Hg, pink; Cu, red; Cl, green; N, blue; C, grey; H, white.

Although what appear to be small channels that run parallel to the *a*-axis, between each $[Hg(CN)_2Cl]_n^{n-}$ ladder in a row and the $[Cu(en)_2]^{2+}$ columns above and below are observed in **2.5**, a space-filling model (not shown) clearly shows the channels to be filled. No mercurophilic interactions are observed in **2.5**.

2.2.4 Structure of $[Co(en)_3][Hg(CN)_2Cl_2]\{[Hg(CN)_2]_2Cl\}$ (2.6)

This complex has a one-dimensional anionic ribbon motif comprised of $\{[Hg(CN)_2]_2Cl\}^-$ units linked together via bridging Cl(1) atoms (Figure 2.5). The crystallographic inequivalence of the $\{[Hg(CN)_2]_2Cl\}^-$ units result in two sets of similar Hg-Cl bond lengths as presented in Table 2.3. Both Hg(1) and Hg(2) have effective four coordinate (2+1+1) see-saw geometries based upon linear characteristic coordination, while the quadruply bridging Cl(1) atom has a distorted square-planar geometry with two angles less than 90° and two angles greater than 90°. In addition to the $\{[Hg(CN)_2]Cl\}_n^{n-}$ ribbon, an individual $[Hg(CN)_2Cl_2]^{2-}$ anionic unit is present in **2.6**; this Hg(3) centre also shows effective four coordinate (2+1+1) see-saw geometry. The $[Hg(CN)_2Cl_2]^{2-}$ moiety does not show any significant interactions with the $\{[Hg(CN)_2]_2Cl\}_n^{n-}$ ribbon.

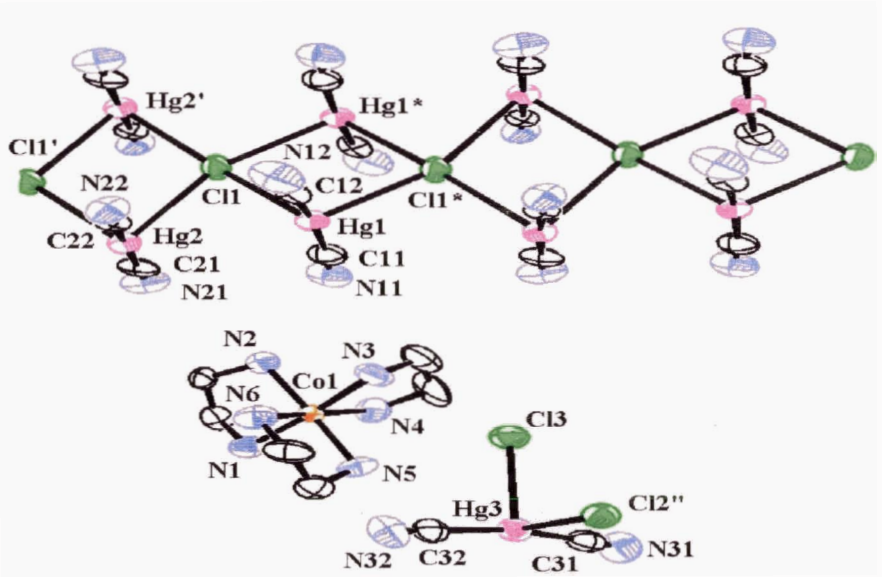

Figure 2.5 Extended 1-D ribbon structure of $[Co(en)_3][Hg(CN)_2Cl_2]\{[Hg(CN)_2]_2Cl\}$ (**2.6**). Only one $[Co(en)_3]^{3+}$ cation and one $[Hg(CN)_2Cl_2]^{2-}$ anion have been shown. Hydrogen atoms have been omitted for clarity (ORTEP 50% ellipsoids).

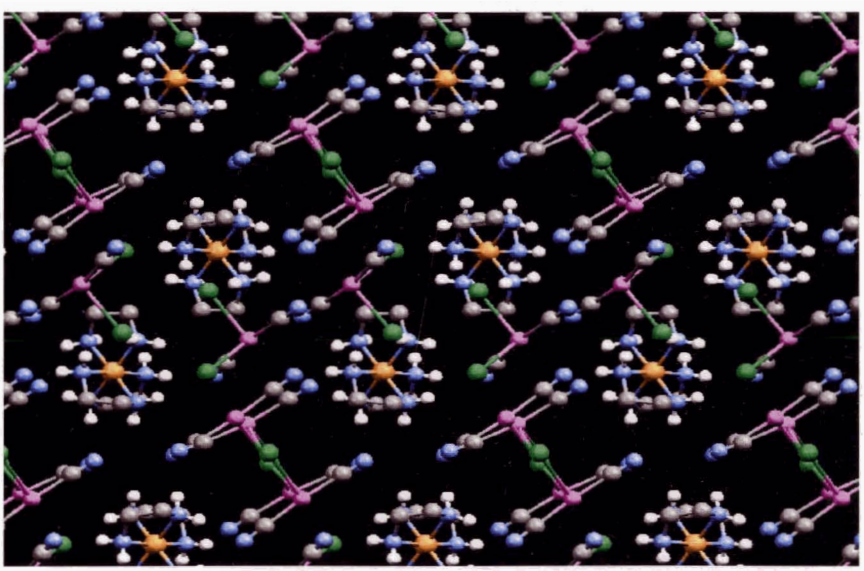

Figure 2.6 The 3-D framework of **2.6** as viewed down the *a*-axis. Ethyl hydrogen atoms have been omitted for clarity. Colour scheme: Hg, pink; Co, orange; Cl, green; N, blue; C, grey; H, white.

Instead, each $[Hg(CN)_2Cl_2]^{2-}$ unit forms a complex network of seven N-H···Cl interactions between three different $[Co(en)_3]^{3+}$ cations (range: N(6)-Cl(2) = 3.297 Å, N(1)-Cl(3) = 3.744 Å) and one N-H···NC interaction (N(5)-N(31) = 3.197 Å) to a fourth $[Co(en)_3]^{3+}$ cation. In turn, each

$[Co(en)_3]^{3+}$ cation forms hydrogen bonds to two different $\{[Hg(CN)_2]_2Cl\}_n^{n-}$ ribbons via seven N-H···NC interactions ranging from 2.954 Å (N(22)-N(1)) to 3.292 Å (N(12)-N(4)), resulting in the complex three-dimensional, bimetallic network shown in Figure 2.6. Rows of the $\{[Hg(CN)_2]_2Cl\}_n^{n-}$ ribbons are separated by columns consisting of the $[Co(en)_3]^{3+}$ and $[Hg(CN)_2Cl_2]^{2-}$ units along the *b*-axis. The resultant alternating anionic-cationic framework in **2.6** is very similar to that found in **2.5** and has a higher dimensionality anionic framework when compared with *trans*-$[Co(en)_2Cl_2][Hg_2Cl_6]$, a molecular complex comprised of discrete $Hg_2Cl_6^{2-}$ bitetrahedral units.[160]

Table 2.3 Selected Bond Lengths (Å) and Angles (°) for $[Co(en)_3]\{[Hg(CN)_2]_2Cl\}[Hg(CN)_2Cl_2]$ (**2.6**)[a].

Selected Atoms	*Bond Lengths*	*Selected Atoms*	*Bond Lengths*
Hg(1)-C(11)	2.045(19)	Hg(2)-C(21)	2.019(15)
Hg(1)-C(12)	2.079(19)	Hg(2)-C(22)	2.053(15)
Hg(1)-Cl(1)	2.915(4)	Hg(3)-Cl(2")	2.939(4)
Hg(1)-Cl(1*)	2.968(4)	Hg(3)-Cl(3)	2.823(4)
Hg(2)-Cl(1')	2.950(4)	Hg(3)-C(31)	2.05(2)
Hg(2)-Cl(1)	3.112(4)	Hg(3)-C(32)	2.09(2)
Co(1)-N(1)	1.952(12)	Co(1)-N(4)	1.984(13)
Co(1)-N(2)	2.000(12)	Co(1)-N(5)	1.983(12)
Co(1)-N(3)	1.957(12)	Co(1)-N(6)	1.981(13)
Selected Atoms	*Bond Angles*	*Selected Atoms*	*Bond Angles*
Cl(1)-Hg(1)-C1(1*)	102.17(10)	Cl(2")-Hg(3)-Cl(3)	93.48(11)
Cl(1)-Hg(1)-C(11)	91.8(5)	Cl(2")-Hg(3)-C(31)	104.9(4)
Cl(1*)-Hg(1)-C(11)	94.5(5)	Cl(3)-Hg(3)-C(31)	92.8(4)
Cl(1)-Hg(1)-C(12)	92.7(5)	Cl(2")-Hg(3)-C(32)	82.5(4)
Cl(1*)-Hg(1)-C(12)	91.3(4)	Cl(3)-Hg(3)-C(32)	97.3(4)
C(11)-Hg(1)-C(12)	171.7(6)	C(31)-Hg(3)-C(32)	167.1(6)
Cl(1')-Hg(2)-C(21)	92.2(5)	Hg(1)-Cl(1)-Hg(1*)	77.83(11)
Cl(1')-Hg(2)-C(22)	93.1(4)	Hg(1)-Cl(1)-Hg(2')	170.6(2)
Cl(1)-Hg(2)-Cl(1')	79.43(12)	Hg(1*)-Cl(1)-Hg(2')	101.00(12)
Cl(1)-Hg(2)-C(21)	91.7(4)	Hg(1)-Cl(1)-Hg(2)	80.49(10)
Cl(1)-Hg(2)-C(22)	91.7(4)	Hg(1*)-Cl(1)-Hg(2)	158.29(15)
C(21)-Hg(2)-C(22)	174.1(5)	Hg(2)-Cl(1)-Hg(2')	100.57(12)

[a] Symmetry transformations: (*) -x, -y-1, -z+1; (') -x+1, -y-1, -z+1; (") -x, -y, -z+2.

2.2.5 Structure of $[Co(NH_3)_6]_2[Hg(CN)_2]_5Cl_6 \cdot 2\ H_2O$ (2.7)

The X-ray single crystal structure of $[Co(NH_3)_6]_2[Hg(CN)_2]_5Cl_6 \cdot 2\ H_2O$ (**2.7**) reveals a two dimensional anionic layer structure (Figure 2.7). This layer is solely comprised of $Hg(CN)_2$ molecules and Cl^- ions that are held together via Hg-Cl bridges that range in length from 3.073(2) Å to 3.118(2) Å.

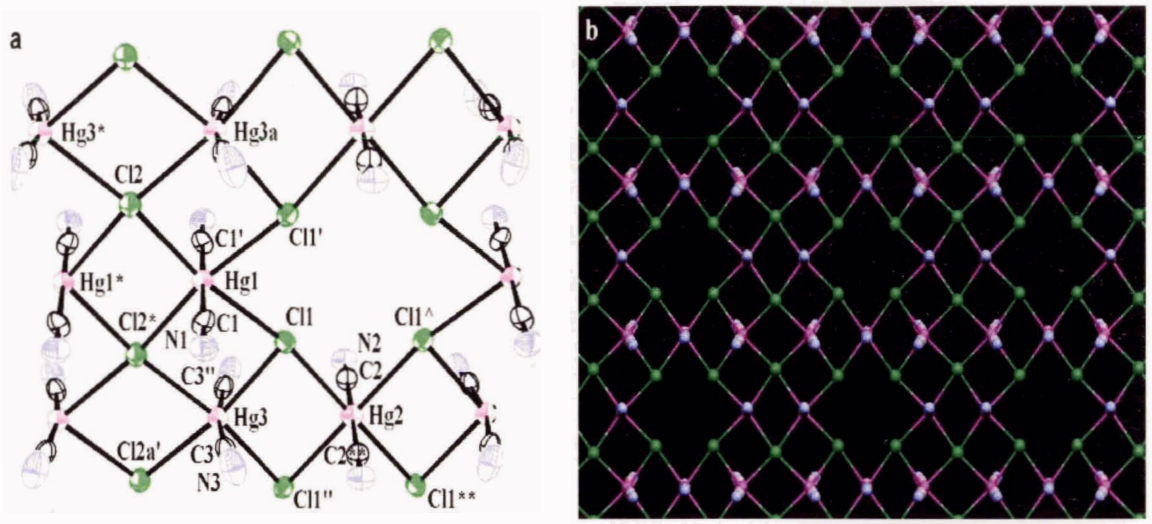

Figure 2.7 Extended 2-D anionic layer structure of $[Co(NH_3)_6]_2[Hg(CN)_2]_5Cl_6 \cdot 2\ H_2O$ (**2.7**). a) (ORTEP 50% ellipsoids); b) Square cavities in 2-D anionic layer as viewed down the *c*-axis. $[Co(NH_3)_6]^{3+}$ cations and H_2O molecules have been omitted for clarity. Colour scheme: Hg, pink; Cl, green; N, blue; C, grey.

Selected bond lengths and angles are shown in Table 2.4. Each Hg(II) centre has distorted octahedral effective geometry based upon linear characteristic coordination (2+4), comprised of four chlorine groups parallel to, and two *trans*-cyano groups perpendicular to the *ab*-plane. This type of Hg(II) coordination is quite common,[88] as observed in $HgBr_2$,[161] both cubic[162,163] and orthorhombic[164,165] amidomercuric bromide, and $KHg(CN)_2I$.[102] Each Cl(2) atom is quadruply bridging to different Hg(II) centres while each Cl(1) atom is only triply bridging to different Hg(II) centres. Along the *b*-axis, double columns consisting of alternating Hg(1) and Hg(3) octahedrons assemble, each sharing three Cl-edges. The Hg(2) centres link these double columns together along the *a*-axis by sharing the fourth Cl-edge of each Hg(3) octahedron.

Table 2.4 Selected Bond Lengths (Å) and Angles (°) for $[Co(NH_3)_6]_2[Hg(CN)_2]_5Cl_6 \cdot 2\ H_2O$ (**2.7**)[a].

Select Atoms	*Bond lengths*	*Select Atoms*	*Bond lengths*
Hg(1)-C(1)	2.025(11)	Hg(2)-Cl(1)	3.087(3)
Hg(2)-C(2)	2.032(12)	Hg(2)-Cl(1^)	3.087(3)
Hg(3)-C(3)	2.040(13)	Hg(1)-Cl(1)	3.119(3)
N(1)-C(1)	1.135(14)	Hg(1)-Cl(2)	3.078(3)
N(2)-C(2)	1.11(2)	Hg(3)-Cl(1)	3.072(2)
N(3)-C(3)	1.124(14)	Hg(3)-Cl(2*)	3.083(2)
Select Atoms	*Bond Angles*	*Select Atoms*	*Bond Angles*
C(1)-Hg(1)-C(1')	180.0(6)	Cl(1)-Hg(2)-Cl(1")	82.72(9)
C(2)-Hg(2)-C(2**)	180	Cl(1^)-Hg(2)-Cl(1")	180
C(3)-Hg(3)-C(3")	168.4(6)	Cl(1)-Hg(3)-Cl(2a')	170.06(7)
Cl(1)-Hg(1)-Cl(1')	78.35(9)	Cl(1)-Hg(3)-Cl(2*)	91.88(7)
Cl(1)-Hg(1)-Cl(2)	169.39(7)	Cl(1')-Hg(3)-Cl(1")	97.90(10)
Cl(1')-Hg(1)-Cl(2)	91.10(6)	Cl(2*)-Hg(3)-Cl(2a')	78.39(11)
Cl(1)-Hg(1)-Cl(2')	91.10(6)	Hg(1)-Cl(1)-Hg(2)	169.86(9)
Cl(1')-Hg(1)-Cl(2')	169.39(7)	Hg(1)-Cl(1)-Hg(3)	88.01(6)
Cl(2)-Hg(1)-Cl(2')	99.46(10)	Hg(2)-Cl(1)-Hg(3)	82.41(6)
Cl(1)-Hg(1)-C(1)	88.8(3)	Hg(1)-Cl(2)-Hg(1*)	80.54(10)
Cl(1')-Hg(1)-C(1)	91.7(3)	Hg(1)-Cl(2)-Hg(3a)	88.544(19)
Cl(2)-Hg(1)-C(1)	89.2(3)	Hg(1)-Cl(2)-Hg(3*)	167.53(13)
Cl(2*)-Hg(1)-C(1)	90.9(3)	Hg(1)-Cl(2)-Hg(3)	167.53(13)
Cl(1)-Hg(2)-Cl(1**)	180	Hg(3*)-Cl(2)-Hg(3a)	101.61(11)
Cl(1)-Hg(2)-Cl(1^)	82.72(9)	Hg(3)-Cl(2)-Hg(3*b)	101.7(1)
Cl(1**)-Hg(2)-Cl(1^)	97.28(9)	Hg(3)-Cl(2)-Hg(3*b)	101.7(1)

[a] Symmetry transformations: (*) –x+2, -y-1, -z; (**) –x+3, -y, -z; (') -x+2, y, -z; (") –x+3, y,-z; (a) x-1, y, z; (a') x+1, y, z; (^) x, -y, z.

Since the fourth Cl-edge of each Hg(1) is left unshared, a series of square cavities arranged in columns along the *b*-axis are formed in the $\{[Hg(CN)_2]_5Cl_6\}_n^{6n-}$ layer as defined by four Hg(1)-Cl(1)-Hg(2) edges (Figure 2.7 b). The $[Co(NH_3)_6]^{3+}$ cations and H_2O molecules are located above and below the cavities as shown in Figure 2.8 Several hydrogen bonds are formed from the NH_3 ligands to the Cl atoms of the neighbouring nets with distances that range from 3.256 Å (N(5)-Cl(1)) to 3.710 Å (N(6)-Cl(1)). Several more hydrogen bonds are formed from the NH_3 ligands to the cyano ligands of the same net (N(1)-N(6) = 3.262 Å; N(2)-N(6) = 3.208 Å) and to

the next net that range from N(3)-N(4) = 3.052 Å to N(1)-N(7) = 3.373 Å. The water molecules also form a series of hydrogen bonds to the $[Co(NH_3)_6]^{3+}$ cations (O(1)-N(7) = 3.085 Å , O(1)-N(5) 3.130 Å), and to the anionic layers (O(1)-N(2) = 3.091 Å, O(1)-N(3) = 3.483 Å). The result is a three dimensional network of $[Co(NH_3)_6]^{3+}$ cations and water molecules sandwiched between two dimensional, $\{[Hg(CN)_2]_5Cl_6\}_n^{6n-}$ anionic layers, held in place by hydrogen bonds. The nets are shifted relative to each other such that the cavities from different nets do not stack into columns forming channels.

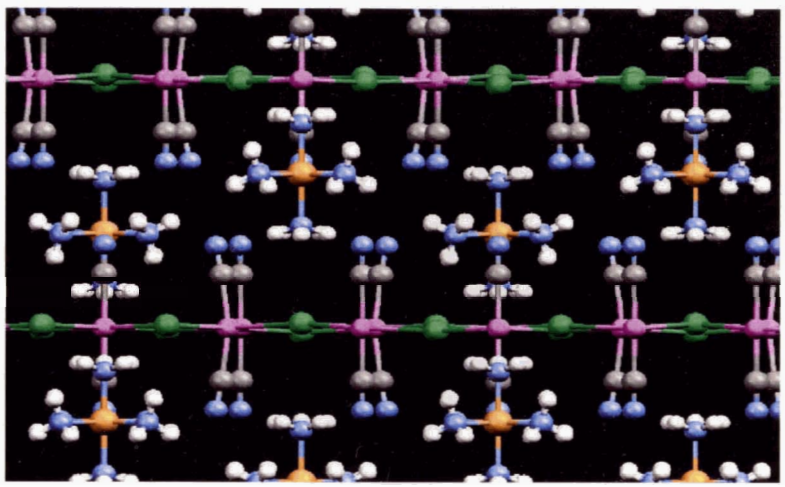

Figure 2.8 A view of the 3-D framework of **2.7** down the *a*-axis. Two $\{[Hg(CN)_2]_5Cl_6\}_n^{6n-}$ anionic nets with $[Co(NH_3)_6]^{3+}$ cations that lie above and below the cavities are shown; H_2O molecules have been omitted for clarity. Colour scheme: Hg, pink; Co, orange; Cl, green; N, blue; C, grey; H, white.

The $\{[Hg(CN)_2]_5Cl_6\}_n^{6n-}$ anionic layer of **2.7** is similar to the corrugated $[Hg(CN)_2I]^-$ anionic layers observed in $KHg(CN)_2I$,[102] and the $[HgCl_3]^-$ anionic layer structure of NH_4HgCl_3.[166] In both cases, the compounds consist of edge-sharing HgX_6 octahedrons along the equatorial plane forming the anionic layers with the cations (K^+ and NH_4^+ respectively) sandwiched in between; however, unlike **2.7**, cavities are not present in these anionic layers. $[NH_3(C_2H_5)]_2[Hg(CN)_2Cl_2]$, a 2-D layer perovskite which contains square cavities arranged in a chess-board manner with the $[NH_3(C_2H_5)]^+$ cations located, both above and below each cavity,[144] also has a similar anionic structure to **2.7**.

When dilute aqueous solutions of $[Co(NH_3)_6]Cl_3$ and $HgCl_2$ are reacted in a 1:3 ratio, $[Co(NH_3)_6][HgCl_3]_3 \cdot H_2O$ is isolated, which consists of $[Hg_3Cl_9]^{3-}$ units that form cross-linked 1-D chains;[160] this coordination polymer is related to, but is structurally different from the 2-D layer of **2.7**. A change in the molar ratio (2:3) results in the formation of a second coordination polymer, $[Co(NH_3)_6]_2[HgCl_4]_3$.[160] A $[Co(NH_3)_6]Cl_3$ / $HgCl_2$ molar ratio of 1:1 results in the formation of the molecular complex $[Co(NH_3)_6][Hg_2Cl_7]$,[160,167] while in the presence of HCl, the molecular complex $[Co(NH_3)_6][HgCl_5]$[160,167,168] has been isolated. Additional mercury-cyanide-chloride double salt structures containing the $[Co(NH_3)_6]^{3+}$ cation could very well be synthesized using different $[Co(NH_3)_6]Cl_3$ / $Hg(CN)_2$ molar ratios and reaction conditions.

2.3 DISCUSSION

In an effort to account for the wide range of structural motifs found for $[Hg(CN)_2Cl]^-$ double salt and related anions, structures **2.1-2.7** can be examined by considering the effects of (a) cation shape, (b) cation charge, and (c) hydrogen bonding interactions from the amine transition metal-bound ligands. All of the transition metal cations utilized in this study were coordinately saturated by the amine ligands, thus eliminating any potential for either chloride or *N*-cyano coordination to the transition metal centre.

2.3.1 Infrared Analysis

The IR spectra of **2.1-2.7** clearly show the presence of the cyano groups and are displayed in Table 2.5. The ν_{CN} stretches range from 2162 cm^{-1} (**2.3**) to 2189 cm^{-1} (**2.5**) and are consistent with terminal cyanide groups on non-linear Hg(II) units with coordination numbers greater than two such as found for $K[Hg(CN)_2Cl] \cdot H_2O$ (ν_{CN} = 2180 cm^{-1}).[122] A representative spectrum is shown for **2.5** in Figure 2.9. Compounds **2.1** shows what appears to be a weak ν_{CN} stretch (2216 cm^{-1}) consistent with bridging cyanomercurate groups, such as found for $\{Zn(H_2O)_4[Hg(CN)_2]_2\}(NO_3)_2$ (ν_{CN} = 2230 cm^{-1}).[60] Strong hydrogen bonding (CN-O = 3.429 Å)

could account for this weak stretch, however no bridging ν_{CN} stretch is observed for **2.2** where the CN-O bond length is even shorter (2.59 Å)

Table 2.5 Comparison of cyanide (ν_{CN}) absorptions (cm^{-1}) for complexes **2.1-2.7** and related systems.

Complex	ν_{CN}	*Reference*
$Hg(CN)_2$	2194 (m)	36
$[PPN][Hg(CN)_2Cl] \cdot H_2O$ (**2.1**)	2216 (w), 2173 (w)	169
$[^nBu_4N][Hg(CN)_2Cl] \cdot 0.5\ H_2O$ (**2.2**)	2175 (w)	169
$[(C_6H_5)_4As][Hg(CN)_2Cl]$ (**2.3**)	2172 (w), 2162 (w)	169
$[Ni(terpy)_2][Hg(CN)_2Cl]_2$ (**2.4**)	2172 (w)	169
$[Cu(en)_2][Hg(CN)_2Cl]_2$ (**2.5**)	2175 (m)	169
$[Co(en)_3][Hg(CN)_2Cl_2]\{[Hg(CN)_2]_2Cl\}$ (**2.6**)	2189 (w), 2185 (w)	169
$[Co(NH_3)_6]_2[Hg(CN)_2]_5Cl_6 \cdot 2\ H_2O$ (**2.7**)	2180 (s)	169
$Na[Hg(CN)_2Cl] \cdot H_2O$	2183 (w)	122
$K[Hg(CN)_2Cl] \cdot H_2O$[122]	2180 (w)	122
$Rb[Hg(CN)_2Cl] \cdot H_2O$[122]	2180 (w)	122
$K[Hg(CN)_2I]$	2181 (w)	102

Values are determined from the maximum of the absorption peak. IR spectrometer resolution = ± 2 cm^{-1}; all spectra were collected as KBr pellets.

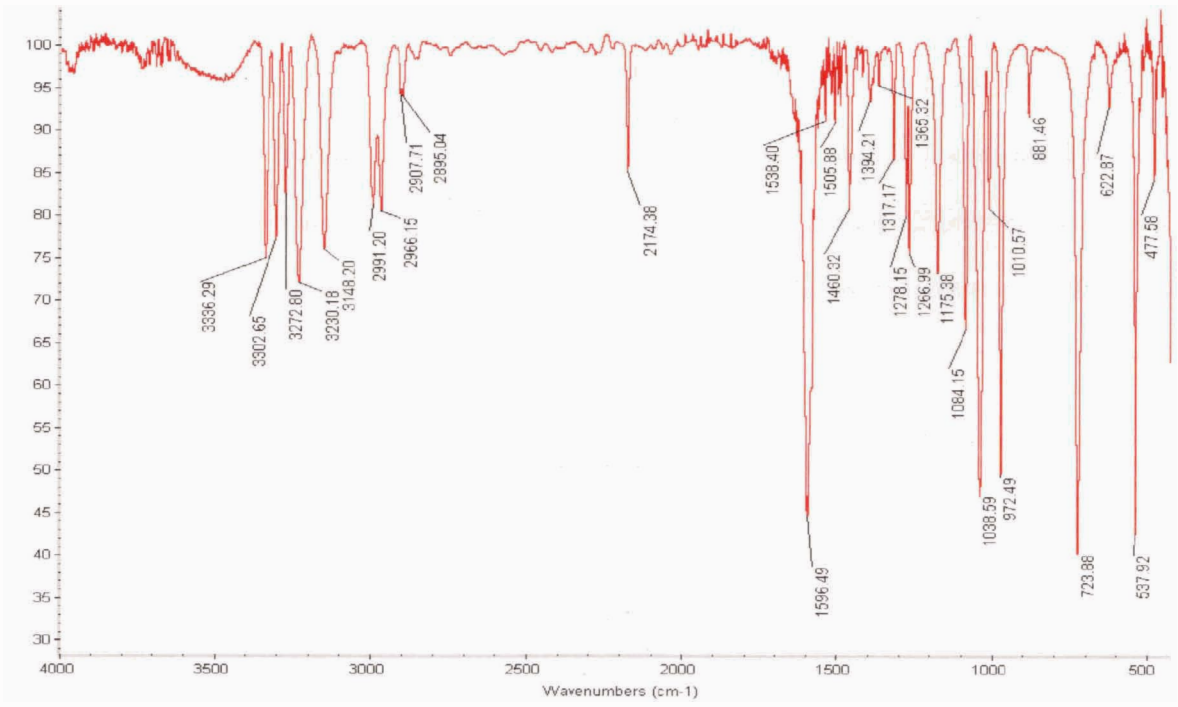

Figure 2.9 IR spectrum of $[Cu(en)_2][Hg(CN)_2Cl]_2$ (**2.5**).

2.3.2 Influence of Cation Shape

By examining structures **2.1-2.3** the effect that cation shape has on the $[Hg(CN)_2Cl]^-$ anionic motif can be determined. All three compounds are salts of 1:1 stoichiometry, with organic monocations and, most importantly, the cations all lack hydrogen bonding donor or acceptor sites. Although interactions between the $[PPN]^+$ phenyl groups, or terpyridine rings, with the anions of the type C-H···X[170], C-H···NC, and Hg···π,[171,172] contribute to the net stabilization of the crystal lattice formed, they are quite weak and do not appear to strongly influence the final anion structure. As described above, all three structures form $[Hg(CN)_2Cl]_2^{2-}$ anionic dimers regardless of whether or not the cation has a dumbbell ($[PPN]^+$, **2.1**), a tetrahedral ($[^nBu_4N]^+$, **2.2**), or a propeller ($[(C_6H_5)_4As]^+$, **2.3**) shape. Thus, (although **2.1-2.3** show different packing) the difference in cation shape has no apparent effect on the adopted anionic motif.

2.3.3 Influence of Cation Charge

In order to investigate the effect of cation charge, structure **2.4** with its $[Ni(terpy)_2]^{2+}$ cation is compared with the +1 cations of structures **2.1-2.3**. The use of two equivalents of terpy constrains the Ni(II) centre to be coordinately saturated while simultaneously eliminating possible strong hydrogen bond donor / acceptor pairs between the cation and anion. Despite the increased cation charge, no structural change is observed for the anionic motif of structure **2.4**; only $[Hg(CN)_2Cl]_2^{2-}$ dimers are formed. The Co(II) analogue is isostructural. Efforts to yield single crystals from the reaction of $[Fe(terpy)_2]Cl_3$ and $Hg(CN)_2$ in order to investigate the effect of a cation with a +3 charge were unsuccessful.

2.3.4 Influence of Hydrogen Bonding Interactions

Comparison of the crystal structures of **2.5-2.7** allows the effects of hydrogen bond interactions of the cations on the $[Hg(CN)_2Cl]_n^{n-}$ double salt structural diversity to be investigated. The presence, number, and profile of hydrogen bond donor sites of the transition metal amine ligands strongly influence the structural motif adopted by the anionic double salt coordination

polymer. When no hydrogen bond donor sites exist, as in **2.1-2.4**, $[Hg(CN)_2Cl]^-$ units form dimers. The four N-H_2 donors of the two en ligands in **2.5** direct the formation of a 1-D ladder motif consisting of $[Hg(CN)_2Cl]_n^{n-}$ units, while the six N-H_2 donors of structure **2.6** direct the formation of a 1-D $\{Hg(CN)_2]_2Cl\}_n^{n-}$ anionic ribbon with additional $[Hg(CN)_2Cl_2]^{2-}$ units also present. It should be noted that the complex cations $[Cu(en)_2]^{2+}$ and $[Co(en)_3]^{3+}$ have different charges; the effect of cation charge does not seem to influence the anion structure, as discussed above. The six N-H_3 donors of the $[Co(NH_3)_6]^{3+}$ cations and the H_2O molecules direct the formation of 2-D anionic layers of $\{[Hg(CN)_2]_5Cl_6\}_n^{6n-}$ in **2.7**. Thus, in general, an increase in the number of hydrogen bonding donor sites on the transition metal complex cation appears to increase the structural dimensionality of the anionic double salt from zero (**2.1-2.4**) to one and two dimensional (**2.5-2.7**). Organic cations with strong hydrogen bonding capability ought to induce similar structural direction of the double salt anions, as was observed with the [4,4'-H_2bipy]$^{2+}$ dications used in the formation of several perhalometallate solid state structures.[157,158] It should be noted that it is not merely the number of hydrogen bond donors that controls polymerization. The flexibility of the d^{10} mercury centre to adopt different effective coordination geometries (see-saw, square pyramidal, octahedral) also plays an important role in the type of anionic motif formed. The concept of directing anionic halometallate networks with organic moieties has recently been employed to fabricate new zeolite-type materials $(HNMe_3)[CuZn_5Cl_{12}]$ and $(H_2NEt_2)[CuZn_5Cl_{12}]$,[173] modular polymeric chlorocadmate(II) compounds[174-176] and other structure types patterned after known chalcogenides.[177]

2.4 CONCLUSIONS

Coordination polymers containing mercury cyanide / chloride double salt building blocks (such as $[Hg(CN)_2Cl]^-$) can aggregate into different structural motifs, including molecular dimers, one-dimensional ladders and ribbons, and two-dimensional layers; the motifs dependent upon the nature of the cation employed. The presence, number, and profile of cation hydrogen bond donor

sites strongly influence the structural motif adopted by the anionic double salt coordination polymer, typically resulting in structures with increased dimensionality. In the absence of cation hydrogen bond donor sites, only in molecular complexes were observed regardless of cation shape and charge.

2.5 EXPERIMENTAL

For these reactions, and all subsequent reactions in proceeding chapters, all manipulations were performed in air using purified solvents. All reagents were obtained from commercial sources and used as received, unless otherwise noted. For all complexes within this thesis, IR spectra were obtained using a Thermo Nicolet 670 FT-IR spectrometer. Microanalyses (C, H, and N) were performed at Simon Fraser University by Mr. Miki Yang.

Unless otherwise indicated, data for all crystal structures described throughout this thesis were collected for each single crystal (mounted on a glass fibre using epoxy adhesive) at room temperature, using the diffractometer control program DIFRAC[178] and an Enraf Nonius CAD4F diffractometer which employed graphite monochromatic Mo Kα radiation. The programs used for all absorption corrections, data reduction, and processing of all structure solutions contained in this thesis were from the *NRCVAX* Crystal Structure System.[179] The structures were refined using *CRYSTALS*.[180] Diagrams were made using ORTEP-3[181] with 50% ellipsoids and MERCURY.[182] Complex scattering factors for neutral atoms[183] were used in the calculation of structure factors. The following example is a typical detailed experimental description for the X-ray crystallographic analysis for compound **2.6**:

2.6 was an orange platelet having dimensions 0.03 x 0.17 x 0.23 mm^3. The following data range was recorded: $4° \leq 2\theta \leq 50°$. The data was corrected for the effects of absorption using a semi-empirical psi-scan method with the following transmission range: 0.0424 - 0.2103. Data reduction for **2.6** included corrections for Lorentz and polarization effects. Final unit-cell dimensions were determined based on the following well-centred reflections: 26 reflections with

range $40° \leq 2\theta \leq 45°$. The coordinates and anisotropic displacement parameters for the non-hydrogen atoms were refined. Hydrogen atoms were placed in calculated positions (d C-H 0.95 Å; d N-H 0.93 Å) and their coordinate shifts were linked with those of the respective carbon or nitrogen atoms during refinement. Isotropic thermal parameters for the hydrogen atoms were initially assigned proportionately to the equivalent isotropic thermal parameters of their respective carbon or nitrogen atoms. Subsequently the isotropic thermal parameters for the C-H hydrogen atoms were constrained to have identical shifts during refinement, as were those of the N-H hydrogen atoms. Extinction parameters[184] were included in the final cycles of full-matrix least-squares refinement.

A summary of crystallographic data and refinement details for all structures in this thesis are collected in Appendix 1. The coordinates are listed in Appendix 2.

2.5.1 Preparation of [PPN][Hg(CN)$_2$Cl] · H$_2$O (2.1)

To a 10 mL methanol / H_2O (50 / 50 % vol.) solution of [PPN]Cl (0.136 g, 0.24 mmol), a 10 mL aqueous solution of $Hg(CN)_2$ (0.059 g, 0.23 mmol) was added and stirred for 2 minutes. The colorless solution was left to slowly evaporate, almost to dryness. Colorless hexagonal crystals of [PPN][$Hg(CN)_2Cl$] · H_2O (**2.1**) were collected via vacuum filtration, washed with two 1 mL portions of cold methanol, and left to air dry. Yield: 0.163 g (84%). Anal. Calcd. for $C_{38}H_{32}N_3ClHgOP_2$: C, 54.03; H, 3.82; N, 4.97. Found: C, 54.01; H, 3.87; N, 4.84. IR (KBr, cm^{-1}): 3056 (m), 3034 (w), 2819 (w), 2694 (w), ν_{CN} **2216 (w)**, **2173 (w)**, 2051 (w), 1918 (w), 1829 (m), 1711 (m), 1588 (m), 1482 (m), 1438 (s), 1363 (w), 1283 (s), 1265 (vs), 1182 (m), 1115 (vs), 1028 (m), 998 (m), 857 (w), 799 (m), 745 (m), 722 (vs), 693 (vs), 550 (vs), 534 (vs), 496 (s).

2.5.2 Preparation of [^{n}Bu$_4$N][Hg(CN)$_2$Cl] · 0.5 H$_2$O (2.2)

To a 10 mL aqueous solution of [^{n}Bu$_4$N]Cl (0.055 g, 0.20 mmol), a 10 mL aqueous solution of $Hg(CN)_2$ (0.050 g, 0.20 mmol) was added and stirred for 2 minutes. The colorless solution was left to slowly evaporate, almost to dryness. Colorless blocks of [^{n}Bu$_4$N][$Hg(CN)_2Cl$] · 0.5

H_2O (**2.2**) were collected via vacuum filtration, washed with two 1 mL portions of cold methanol, and left to air dry. Yield: 0.108 g (59%). Anal. Calcd. for $C_{18}H_{37}N_3ClHgO_{0.5}$: C, 40.07; H, 6.91; N, 7.79. Found: C, 39.85; H, 6.87; N, 7.83. IR (KBr, cm^{-1}): 3599 (s), 3506 (s), 2963 (vs), 2935 (vs), 2876 (vs), 2734 (w), 2408 (w), ν_{CN} **2198 (w), 2175 (w), 2150 (w)**, 1836 (w), 1844 (w), 1829 (w), 1793 (w), 1750 (m), 1711 (s), 1652 (m), 1635 (m), 1484 (s), 1463 (s), 1419 (m), 1383 (s), 1364 (s), 1223 (s), 1178 (w), 1152 (m), 1108 (m), 1091 (w), 1056 (m), 1026 (m), 883 (s), 799 (m), 739 (s), 530 (m), 417 (s), 407 (s).

2.5.3 Preparation of $[(C_6H_5)_4As][Hg(CN)_2Cl]$ (2.3)

To a 10 mL aqueous solution of $[(C_6H_5)_4As]Cl$ (0.083 g, 0.20 mmol), a 10 mL aqueous solution of $Hg(CN)_2$ (0.050 g, 0.20 mmol) was added and stirred for 2 minutes. The colorless solution was left to slowly evaporate, almost to dryness. Colorless blocks of $[(C_6H_5)_4As][Hg(CN)_2Cl]$ (**3**) were collected via vacuum filtration, washed with two 1 mL portions of cold methanol, and left to air dry. Yield: 0.091 g (68%). Anal. Calcd. for $C_{26}H_{20}N_2AsClHg$: C, 46.51; H, 3.00; N, 4.17. Found: C, 46.46; H, 3.03; N, 4.14. IR (KBr, cm^{-1}): 3520 (m), 3452 (m), 3156 (w), 3080 (w), 3058 (m), 3021 (w), 2991 (w), 2657 (w), 2563 (w), ν_{CN} **2172 (w), 2162 (w)**, 1980 (w), 1904 (w), 1826 (w), 1776 (w), 1676 (w), 1632 (w), 1578 (w), 1483 (m), 1439 (s), 1420 (m), 1339 (m), 1308 (m), 1184 (m), 1161 (w), 1081 (s), 1022 (w), 997 (s), 925 (w), 853 (w), 742 (s), 689 (s), 613 (w), 479 (s), 466 (s).

2.5.4 Preparation of $[Ni(terpy)_2][Hg(CN)_2Cl]_2$ (2.4)

To a 5 mL aqueous solution of $NiCl_2 \cdot 6\ H_2O$ (0.015 g, 0.063 mmol), a 5 mL methanolic solution of terpy (0.030 g, 0.128 mmol) was added and stirred for 5 minutes. While stirring, a 5 mL aqueous solution of $Hg(CN)_2$ (0.032 g, 0.127 mmol) was added to this solution. This new dark orange solution was allowed to slowly evaporate. Brown crystal bars of $[Ni(terpy)_2][Hg(CN)_2Cl]_2$ (**2.4**) were collected by vacuum filtration, washed first with two 1 mL portions of cold water followed two 1 mL portions of cold methanol, and were left to air dry.

Yield: 0.050 g (72%). Anal. Calcd. for $C_{34}H_{22}N_{10}Cl_2Hg_2Ni$: C, 37.08; H, 2.01; N, 12.72. Found: C, 37.34; H, 1.97: N, 12.62. IR (KBr, cm^{-1}): 3732 (w), 3108 (m), 3074 (m), 3030 (m), ν_{CN} **2172 (w)**, 2012 (w), 1978 (w), 1879 (w), 1600 (s), 1574 (m), 1563 (m), 1475 (s), 1470 (s), 1450 (s), 1419 (m), 1405 (w), 1321 (m), 1297 (w), 1248 (m), 1184 (m), 1160 (m), 1094 (w), 1052 (w), 1032 (m), 1016 (s), 904 (w), 830 (w), 774 (s), 740 (w), 667 (w), 650 (m), 513 (w), 436 (w), 412 (m).

2.5.5 Preparation of $[Cu(en)_2][Hg(CN)_2Cl]_2$ (2.5)

To a 10 mL aqueous solution of $CuCl_2 \cdot 2\ H_2O$ (0.068 g, 0.40 mmol), an aqueous solution of en (stock solution, 0.80 mmol) was added and stirred for 5 minutes. While stirring, a 10 mL aqueous solution of $Hg(CN)_2$ (0.202 g, 0.80 mmol) was added to this purple solution. This new solution was allowed to slowly evaporate. Purple crystal bars of $[Cu(en)_2][Hg(CN)_2Cl]_2$ (**2.5**) were collected by vacuum filtration, washed first with two 1 mL portions of cold water followed two 1 mL portions of cold methanol, and were left to air dry. Yield: 0.285 g (94%). Anal. Calcd. for $C_8H_{16}N_8Cl_2CuHg_2$: C, 12.64; H, 2.12; N, 14.75. Found: C, 12.52; H, 2.14: N, 14.63. IR (KBr, cm^{-1}): 3338 (s), 3324 (s), 3294 (s), 3276 (s), 3262 (s), 3233 (s), 3143 (m), 2993 (w), 2968 (m), 2955 (m), 2897 (m), ν_{CN} **2175 (m)**, 1709 (m), 1617 (m), 1591 (s), 1458 (m), 1362 (w), 1323 (w), 1274 (m), 1232 (w), 1179 (m), 1095 (m), 1039 (s), 1010 (m), 974 (m), 881 (w), 719 (m), 695 (m), 536 (m), 423 (m), 413 (m).

2.5.6 Preparation of $[Co(en)_3][Hg(CN)_2Cl_2]\{[Hg(CN)_2]_2Cl\}$ (2.6)

To a 10 mL aqueous solution of $[Co(en)_3]Cl_3$ (0.076 g, 0.22 mmol), a 20 mL aqueous solution of $Hg(CN)_2$ (0.151 g, 0.60 mmol) was added and stirred for 5 minutes. This orange solution was allowed to slowly evaporate, almost to dryness. Orange crystal platelets of $[Co(en)_3][Hg(CN)_2Cl_2]\{[Hg(CN)_2]_2Cl\}$ (**2.6**) were collected by vacuum filtration, washed first with two 1 mL portions of cold water followed two 1 mL portions of cold methanol, and were left to air dry. Yield: 0.137 g (62%). Anal. Calcd. for $C_{12}H_{24}N_{12}Cl_3CoHg_3$: C, 13.06; H, 2.19; N,

15.23. Found: C, 12.84; H, 2.10; N, 14.93. IR (KBr, cm^{-1}): 3266 (vs), 3233 (vs), 3162 (vs), 3133 (vs), 2904 (w), 2750 (w), 2612 (w), ν_{CN} **2189 (w), 2185 (w),** 1620 (m), 1583 (m), 1566 (m), 1508 (w), 1462 (m), 1398 (w), 1366 (w), 1320 (m), 1298 (m), 1240 (w), 1149 (m), 1053 (s), 1003 (m), 881 (w), 785 (m), 582 (m), 552 (w), 495 (w), 438 (s).

2.5.7 Preparation of $[Co(NH_3)_6]_2[Hg(CN)_2]_5Cl_6 \cdot 2\ H_2O$ (2.7)

To a 10 mL aqueous solution of $[Co(NH_3)_6]Cl_3$ (0.064 g, 0.24 mmol), a 20 mL aqueous solution of $Hg(CN)_2$ (0.150 g, 0.59 mmol) was added and stirred for 5 minutes. The orange solution was allowed to slowly evaporate. Hexagonal orange crystal platelets of $[Co(NH_3)_6]_2[Hg(CN)_2]_5Cl_6 \cdot 2\ H_2O$ (**2.7**) were collected by vacuum filtration, washed first with two 1 mL portions of cold water followed two 1 mL portions of cold methanol, and were left to air dry. Yield: 0.196 g (92%). Anal. Calcd. for $C_{10}H_{40}N_{22}Cl_6Co_2Hg_5O_2$: C, 6.56; H, 2.20; N, 16.80. Found: C, 6.42; H, 2.20; N, 16.55. IR (KBr, cm^{-1}): 3625 (s), 3448 (m), 3258 (vs), 2771 (m), 2667 (m), 2632 (w), ν_{CN} **2180 (s)**, 1869 (w), 1844 (w), 1771 (m), 1612 (vs), 1412 (m), 1357 (s), 1324 (s), 844 (s), 428 (s).

CHAPTER 3
REACTIONS OF MERCURY CYANIDE WITH COORDINATIVELY UNSATURATED TRANSITION METAL CATION COMPLEXES

3.1 INTRODUCTION

Cyanometallate complexes have been extremely valuable in the study of supramolecular coordination polymers, particularly in molecular magnetism research, as they readily form polymers when reacted with transition metal cations, as well as promoting strong magnetic exchange.[24,37,46,47] Much work has been done in the Leznoff group to successfully demonstrate that two-coordinate linear, anionic $[M(CN)_2]^-$ units (M=Au,[79-81] Ag[82]) are capable of increasing structural dimensionality by forming metallophilic (M···M) interactions and, although diamagnetic, can propagate significant magnetic interactions.[80,82] As detailed in Chapter 2, the use of $Hg(CN)_2$, a linear but *neutral* building block can, by accepting compatible ligands such as chloride ions during polymer formation, form higher coordinate double salt moieties which then aggregate into extended structures having increased structural dimensionality. However, since the transition metal complexes employed were coordinatively saturated, bridging between TM centres could not occur. In order to investigate the ability of cyanomercurate units to propagate magnetic interactions, coordinatively *unsaturated* TM complexes, that is TM complexes with available bridging sites, that are paramagnetic must be used. The formation of double salt mercurate moieties such as $[Hg(CN)_2Cl]^-$ should invoke competition between chloride and *N*-cyano coordination to the coordinatively *unsaturated* TM complexes.

3.1.1 Magnetochemistry

In transition metals, magnetism is due to both the intrinsic spin of unpaired *d*-electrons and the orbital motion of electrons.[185] Specific information concerning the arrangement of unpaired electrons can be obtained from the measurement of *magnetic susceptibility* and its temperature dependence. When a substance is placed in a magnetic field of intensity **H**, the intensity of the field within the substance may either be less than **H**, that is diamagnetic, or greater than **H**, or paramagnetic. Diamagnetism is a property of all matter and originates from electron pairs, while paramagnetism is generally a property of substances possessing unpaired electrons.[185] Magnetic data is obtained from a SQUID (Superconducting Quantum Interference Device) magnetometer which measures the magnetisation (**M**) of a sample. This bulk property is frequently expressed as magnetic molar susceptibility and is given by the formula

$$\chi_M = \mathbf{M} / \mathbf{H} \qquad \text{(Equation 3.1)}$$

Magnetic properties are often expressed in terms of effective magnetic moment (μ_{eff}) which, under certain conditions, relates directly to the number of unpaired electrons. The effective magnetic moment in Bohr magnetons (μ_B) is given by the formula

$$\mu_{eff} = 2.83(\chi'_M T)^{1/2} \qquad \text{(Equation 3.2)}$$

where χ'_M is the susceptibility corrected for diamagnetism of the sample and sample holder. The magnetic moment of atoms or ions containing unpaired electrons can also be calculated using the following formula that considers only the intrinsic spin component:

$$\mu_s = g[S(S+1)]^{1/2} \qquad \text{(Equation 3.3)}$$

where g is approximately equal to 2.0, and S is the sum of the spin quantum numbers of the individual unpaired electrons. For Cu(II), containing one unpaired 3*d* electron, S = ½ and μ_s = 1.73 μ_B The experimental μ_{eff} value and the calculated μ_s value for a sample are often compared

to determine whether or not spin-orbit contributions and / or magnetic interactions between paramagnetic centres are significant.[185]

The temperature dependence of many paramagnetic materials, especially at high temperatures, is governed by the experimentally found Curie law and is given by the formula

$$\chi_M = C / T \qquad \text{(Equation 3.4)}$$

where C is the Curie constant. A Curie response occurs when there is no interaction between the magnetic centres in a complex or in a crystal.[186] Although the unpaired electrons do align in an external field, equation 3.4 shows that this alignment becomes more difficult at higher temperatures resulting in a decrease in χ_M.

When some interactions do occur between adjacent electron spins, equation 3.4 is modified so as to better fit the high temperature data and is called the Curie-Weiss law:

$$\chi_M = C / (T-\theta) \qquad \text{(Equation 3.5)}$$

where θ is the Weiss constant.[186] A plot of χ_M^{-1} *vs.* T for paramagnetic substances showing no interactions will extrapolate to 0 K as shown in Figure 3.1.

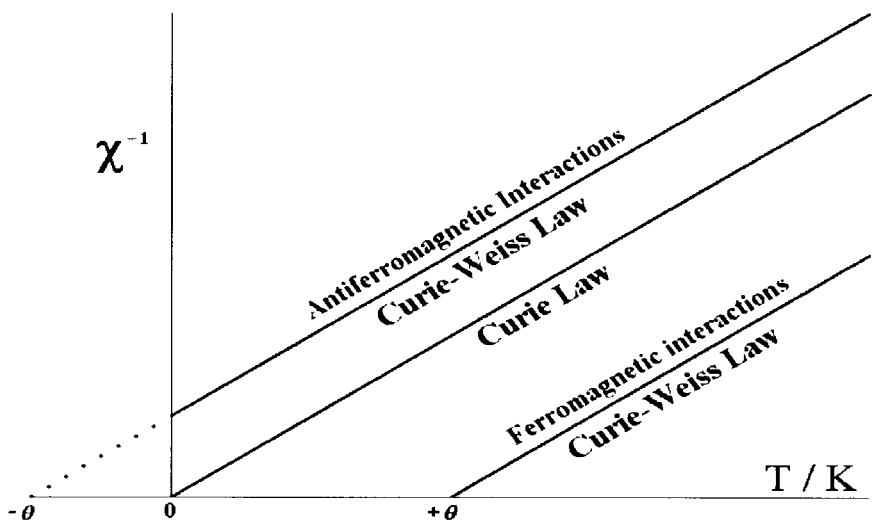

Figure 3.1 Plot of reciprocal magnetic susceptibility *vs.* temperature for paramagnetic substances that may show magnetic interactions at low temperatures.
The slope is equal to C^{-1}.

For a paramagnetic substance that shows some local alignment of spins that is ferromagnetic in nature, χ_M is higher than the simple paramagnetic case and the plot extrapolates to $+\theta$ which is known as the Curie temperature (T_C). Below this temperature the sample is considered have ferromagnetic interactions, where magnetic spins align parallel to each other. When the alignment of some local spins is antiparallel, χ_M is lower than the simple paramagnetic case and the plot extrapolates to $-\theta$. χ_M approaches zero at very low temperatures for samples with antiferromagnetic (AF) behaviour since the magnetic spins are aligning so as to cancel each other out. However, with increasing temperature χ_M increases as thermal disorder disrupts the AF state. χ_M passes through a maximum at the Néel temperature (T_N) and then decreases at higher temperatures following the Curie-Weiss law. On the other hand, for samples with ferromagnetic interactions χ_M is very large at low temperatures, but decreases rapidly with increasing temperature until T_C, above which Curie-Weiss behaviour is generally observed. Figure 3.2 shows generalized plots of both χ_M *vs.* T and μ_{eff} *vs.* T for the spin only (no coupling), ferromagnetic, and antiferromagnetic cases.

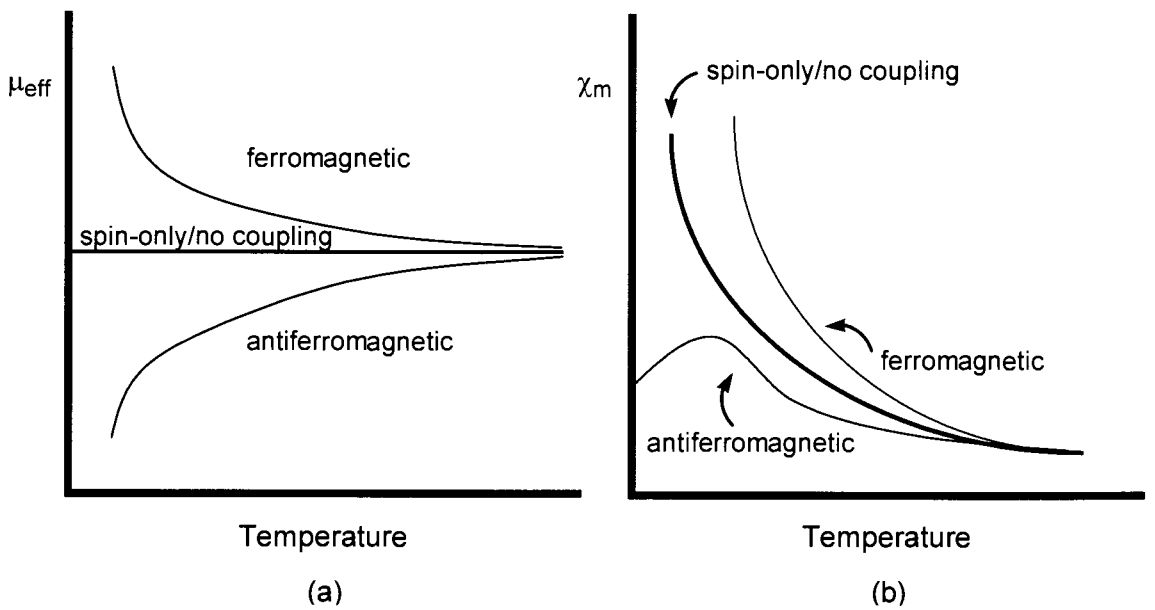

Figure 3.2 Generalized plots of (a) μ_{eff} vs T and (b) χ_M *vs.* T depicting spin-only / no coupling, antiferromagnetic and ferromagnetic behaviour.

The Curie-Weiss law does not account for several factors that affect the observed magnetism such as spin-orbit coupling and crystal field effects. Several mathematical models have been proposed to model the magnetic results of specific systems[68,185] and a few are used in this thesis. Most models are based on a general equation for magnetism, proposed by Van Vleck, which models the magnetic susceptibility under the premise that the distribution of unpaired electrons into quantized energy levels is governed by the Boltzmann distribution.[68,185] Thus, the magnetic susceptibility at any given temperature can be calculated, knowing the appropriate energy level diagram and the magnetic moment for each level. For the simplest case, a system with only one unpaired electron (S = ½), an external magnetic field causes the two degenerate quantum levels (e.g. Kramer's doublet; m_s = +½, -½) to split into two non-degenerate states;[185] this is called Zeeman splitting (Figure 3.3).

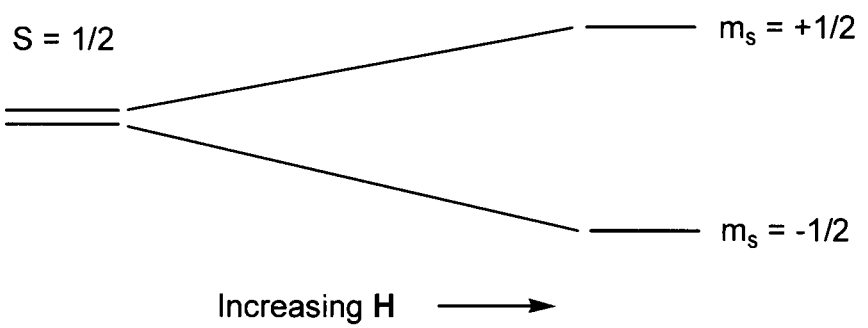

Figure 3.3 Zeeman splitting of a S = ½ doublet.

When two magnetically isolated homometallic magnetic centres of S = ½ interact through a bridge (a Cu(II) dimer for example), the system can be interpreted as being in an antiferromagnetic state (S = 0) or in a ferromagnetic state (S = 1) (Figure 3.4). If orbital contributions, zero-field splitting (see Chapter 4), and intermolecular coupling are ignored, then the following equation is derived from the Van Vleck equation:

$$\chi_M = [(2Ng^2\beta^2) / kT]*[1 / (3 + \exp(-J/kT))] \qquad \text{(Equation 3.6)}$$

where N is Avogadro's number, β is the Bohr magneton, k is the Boltzmann constant, and J is the parameter that represents the coupling of the two spins. Equation 3.6 is known as the Bleaney-Bowers equation.[185,187]

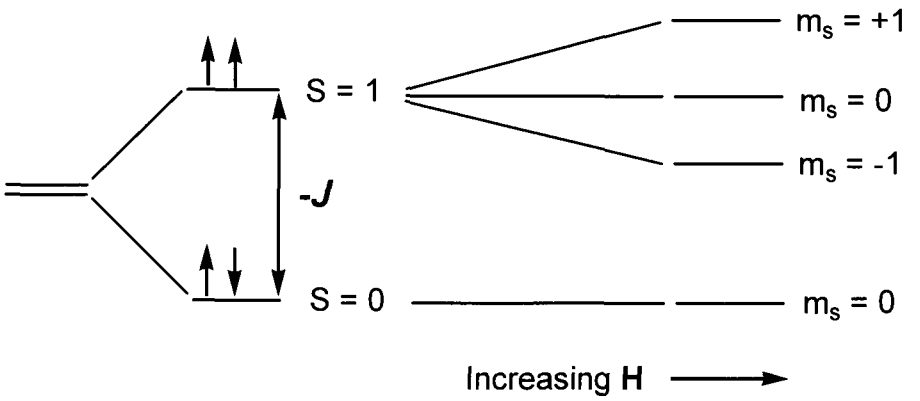

Figure 3.4 Energy level diagram for a homodinuclear complex with two S = ½ centres.

When J is positive, S = 1 is the ground state and the system has ferromagnetic interactions. Conversely, when J is negative, S = 0 is the ground state and the system has antiferromagnetic (AF) interactions. J values below |20| cm^{-1} are weak interactions and typically affect μ_{eff} (or $\chi'_M T$) at temperatures less than 50 K.[68]

For a 1-D uniform chain of S = ½ centres having AF interactions, the Bonner-Fisher model is employed, assuming orbital contributions, zero-field splitting, and interchain coupling are negligible:[188-190]

$$\chi_M = \frac{(Ng^2\beta^2)}{kT} * \frac{(0.25 + 0.074975\,x + 0.075235\,x^2)}{(1.0 + 0.9931\,x + 0.172135\,x^2 + 0.757825\,x^3)} \qquad \text{(Equation 3.7)}$$

where $x = (|J| / kT)$.

The model assumes that the J interaction between adjacent neighbours is the same, while the J interactions between next nearest neighbours is zero. This numerical solution for an infinite chain was determined using a closed ring of S = ½ units of ever increasing size. Additional models are discussed as required throughout the thesis.

3.1.2 Research Objectives

This chapter investigates the synthesis, structural, and magnetic properties of a series of coordinatively *unsaturated* $[L_xTM]Cl_2$ complexes (L = bipy, phen, terpy, en, dien, tren; x = 1 or 2; TM(II) = Mn, Ni, Cu) that have been reacted with coordinately unsaturated $Hg(CN)_2$ to generate transition metal organoamine-double salt cyanomercurates. The available open sites on the TM complex will be limited to two or three. Possible factors influencing $Hg(CN)_2$ nitrile-coordination to transition metal complex cations in the presence of chloride ligands, including transition metal used, the number of open sites available for binding, and ligand basicity are investigated. If X-ray structures show promising magnetic pathways, then magnetic data is obtained in order to examine magnetic exchange through the diamagnetic Hg(II) centre.

3.2 RESULTS AND ANALYSIS*

3.2.1 Rational Syntheses of 3.1-3.10

The reaction of an aqueous / methanolic solution of $[ML_2]Cl_2$ (M = Mn(II), Ni(II); L = 1,10-phenanthroline, 2,2'-bipyridine) with one equivalent of $Hg(CN)_2$ yielded single crystals of **3.1-3.4** as summarized by equation 3.8.

1) $MCl_2 + L_2 \longrightarrow [ML_2]Cl_2$

2) $[ML_2]Cl_2 + Hg(CN)_2 \longrightarrow [ML_2(\mu\text{-}Cl)_2Hg(CN)_2]$ Equation 3.8

The reaction of an aqueous solution of $Cu(terpy)Cl_2$ (terpy = 2,2':6',2"-terpyridine), with an aqueous solution containing one equivalent of $Hg(CN)_2$ yielded single crystals of **3.5**:

1) $CuCl_2 + terpy \longrightarrow [Cu(terpy)]Cl_2$

2) $[Cu(terpy)]Cl_2 + Hg(CN)_2 \longrightarrow [Cu(terpy)Cl_2(\mu\text{-}Hg(CN)_2)]$ Equation 3.9

---

* Draper, N. D.; Batchelor, R. J.; Leznoff, D. B. *Cryst. Growth Des.* **2004**, 4, 621-632. Reproduced in part by permission of the American Chemical Society.

A similar reaction with a methanolic solution of $Cu(dien)Cl_2$ (dien = diethylenetriamine) and a methanolic solution containing one equivalent of $Hg(CN)_2$ yielded single crystals of **3.7**:

1) $CuCl_2 + dien \longrightarrow [Cu(dien)]Cl_2$

2) $[Cu(dien)]Cl_2 + Hg(CN)_2 \longrightarrow [Cu(dien)Cl][Hg(CN)_2Cl]$ Equation 3.10

The reaction of an aqueous solution of two equivalents of $[Cu(phen)_2]Cl_2$ with three equivalents of $Hg(CN)_2$ yielded **3.6,** which has a similar formula to **3.5** and **3.7**.

1) $CuCl_2 + 2phen \longrightarrow [Cu(phen)_2]Cl_2$

2) $2\,[Cu(phen)_2]Cl_2 + 3\,Hg(CN)_2 \longrightarrow \{[Cu(phen)_2Cl]_2Hg(CN)_2[Hg(CN)_2Cl]_2\}$ Equation 3.11

The reaction of an aqueous solution of one equivalent of $CuCl_2$ with one equivalent of tris(2-aminoethyl)amine (tren) and two equivalents of $Hg(CN)_2$ yielded **3.8**:

1) $CuCl_2 + tren \longrightarrow [Cu(tren)]Cl_2$

2) $[Cu(tren)]Cl_2 + 2\,Hg(CN)_2 \longrightarrow [Cu(tren)Hg(CN)_2Cl][HgX_2Cl]$ Equation 3.12

A similar reaction of an aqueous solution of four equivalents of $[Ni(tren)]Cl_2$ with eight equivalents of $Hg(CN)_2$ and one equivalent of $HgCl_2$ yielded single crystals of **3.10**:

1) $NiCl_2 + tren \longrightarrow [Ni(tren)]Cl_2$

2) $4\,[Ni(tren)]Cl_2 + 8\,Hg(CN)_2 + HgCl_2 \longrightarrow \{[Ni(tren)]_4[Hg(CN)_2]_8Cl_6\}HgCl_4$ Equation 3.13

The reaction of an aqueous solution of two equivalent of $NiCl_2$ with four equivalent of ethylenediamine and six equivalents of $Hg(CN)_2$ yielded **3.9:**

1) $NiCl_2 + 2\,en \longrightarrow [Ni(en)_2]Cl_2$

2) $2\,[Ni(en)_2]Cl_2 + 6\,Hg(CN)_2 \longrightarrow \{[Ni(en)_2][Hg(CN)_2]_3Cl_2\}_2$ Equation 3.14

Migration of the labile chloride ligands from the harder Cu(II) and Ni(II) centres to the coordinately unsaturated, softer Hg(II) centres drives the formation of **3.6-3.10**. This halide migration to the Lewis-acidic $Hg(CN)_2$ generates non-linear Hg(II) products with coordination

numbers greater than two, potentially increasing the structural and magnetic dimensionality in the process.

3.2.2 Structures of $[ML_2(\mu\text{-}Cl)_2Hg(CN)_2]$ (M = Mn(II), Ni(II); L = bipy, phen) (3.1-3.4)

The X-ray single crystal structures of $[ML_2(\mu\text{-}Cl)_2Hg(CN)_2]$ (M = Mn(II), Ni(II); L = bipy, phen) reveal simple molecular complexes in which the coordinately unsaturated $Hg(CN)_2$ unit is bound to the chloride ligands, which act as M-Hg bridging groups (Figure 3.5). The Mn(II) and Ni(II) centres in **3.1-3.4** have a distorted, octahedral geometry, with the two amine ligands (bipy or phen) *cis*-oriented and two chloride ligands completing the coordination sphere. These molecular complexes are analogous to the nickel organoamine-halocadmates $[Ni(phen)_2Cl_2CdI_2]$, $[Ni(phen)_2X_2CdX_2]$ (X = site of mixed Br, Cl occupancy) and $[Ni(bipy)_2Cl_2CdCl_2]_2$.[174] The bond distances and angles for **3.1-3.4** are gathered in Table 3.1. The M-N bond lengths range from 2.057(9) Å (**3.3**) to 2.295(11) Å (**3.2**) while the M-Cl bond lengths range from 2.4473(18) Å (**3.4**) to 2.505(4) Å (**3.2**).

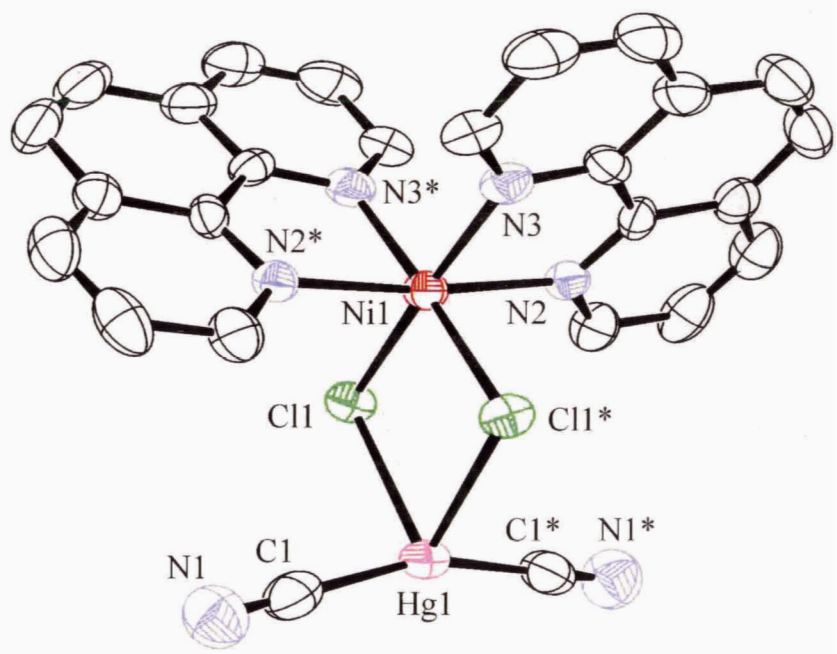

Figure 3.5 Molecular structure of $[Ni(phen)_2(\mu\text{-}Cl)_2Hg(CN)_2]$ (**3.4**).
The hydrogen atoms have been omitted for clarity (ORTEP 50% ellipsoids).

These values are comparable to those reported for $Ni(bipy)_2Cl_2 \cdot CH_3OH$ (Ni-N = 2.073(3), 2.077(3), 2.084(3), 2.100(4) Å; Ni-Cl = 2.3940(13), 2.4213(13) Å),[191] $Mn(phen)_2Cl_2$ (Mn-N = 2.073(3), 2.077(3), 2.084(3), 2.100(4) Å; Mn-Cl = 2.3940(13), 2.4213(13) Å),[192] and $Mn(bipy)_2Cl_2$ (Mn-N = 2.281(4), 2.299(4), 2.341(4), 2.371(4) Å; Mn-Cl = 2.4396(14), 2.4544(13) Å).[193]

Table 3.1 Selected Bond Lengths (Å) and Angles (°) for the $[M(L)_2][(\mu\text{-}Cl)_2Hg(CN)_2]$ complexes **3.1-3.4**.

Compound	**3.1**[a]	**3.2**	**3.3**[b]	**3.4**[c]
M, L	Mn, bipy	Mn, phen	Ni, bipy	Ni, phen
Selected Atoms	*Bond Lengths*			
M(1)-N(2)	2.280(3)	2.272(12), 2.250(11)	2.056(9)	2.109(6)
M(1)-N(3)	2.238(3)	2.240(11), 2.295(11)	2.066(8)	2.078(5)
M(1)-Cl(1)	2.4951(9)	2.481(4), 2.505(4)	2.451(3)	2.4473(18)
Hg(1)-Cl(1)	2.8199(9)	2.813(4), 2.829(4)	2.771(3)	2.7744(17)
Hg(1)-C(1)	2.036(4)	2.061(19), 2.070(19)	2.045(14)	2.034(9)
Selected Atoms	*Bond Angles*			
Cl(1)-Hg(1)-Cl(1*)	80.70(3)	81.50(11)	78.76(11)	79.90(7)
Cl(1)-Hg(1)-C(1)	92.01(12)	92.1(5), 90.9(5)	94.5(4)	94.2(2)
Cl(1*)-Hg(1)-C(1)	99.81(13)	102.0(5), 99.5(5)	99.2(4)	100.9(2)
C(1)-Hg(1)-C(1*)	164.5(2)	163.8(6)	162.2(7)	160.6(3)
Cl(1)-M(1)-Cl(1*)	94.06(4)	95.22(13)	91.66(15)	93.44(7)
Cl(1)-M(1)-N(2)	169.48(7)	170.3(3), 168.4(3)	174.3(3)	174.37(15)
Cl(1*)-M(1)-N(2)	89.79(3)	89.9(2), 90.0(3)	88.7(3)	88.29(16)
N(2)-M(1)-N(2*)	88.14(6)	86.5(4)	91.5(5)	90.5(3)
Cl(1)-M(1)-N(3)	97.50(8)	97.6(3), 95.9(3)	95.4(3)	94.97(16)
Cl(1*)-M(1)-N(3)	95.12(8)	91.5(5), 97.2(3)	89.9(3)	90.11(16)
N(3)-M(1)-N(3*)	161.44(15)	162.7(4)	172.4(5)	172.6(3)
N(2)-M(1)-N(3)	72.4(1)	73.9(4), 73.1(4)	78.9(4)	79.7(2)
N(2)-M(1)-N(3*)	94.1(1)	90.4(4), 98.1(4)	95.7(4)	95.1(2)
Hg(1)-Cl(1)-M(1)	92.62(3)	91.91(13), 91.04(13)	94.79(9)	93.33(6)

[a] Symmetry transformations: (*) -x+1, y, -z+1/2.
[b] Symmetry transformations: (*) -x+1, y, -z+3/2.
[c] Symmetry transformations: (*) -x+1/2, y, -z+3/2.

The chloride ligands bridge to the $Hg(CN)_2$ metal centres via Hg-Cl bonds that range in length from 2.771(3) Å (**3.3**) to 2.829(4) Å (**3.2**) and can be compared to the Hg-Cl bonds lengths

of 2.670(3) Å, found in the molecular $[Cu(bipy)_2(\mu\text{-}Cl)_2HgBr_2]$[194] and the 2.710(1) and 2.820(1) Å found in the molecular $[Cu(bipy)_2(\mu\text{-}Cl)_2Hg(CN)_2]$, a Cu(II) isostructural analogue to **3.1** and **3.3** which is presented in Chapter 5.[195] This results in an effective see-saw coordination sphere, based on linear Hg(II) characteristic coordination (2+2), for the Hg(II) centre with C-Hg-C angles ranging from 160.6(3)° (**3.4**) to 164.8(1)° (**3.1**) and Cl-Hg-Cl angles ranging from 78.76(11)° (**3.3**) to 81.50(11)° (**3.2**) which can be compared to the C-Hg-C and Cl-Hg-Cl angles of **2.1-2.4** as discussed in Chapter 2. The M-Hg distances range from 3.805 Å (**3.4**) to 3.850 Å (**3.3**) indicating that there are no significant intermolecular interactions between the two metal centres.

In all four cases, there is extended $\pi\cdots\pi$ stacking of neighbouring conjugated ring systems characterized by interplanar distances of 3.4-3.6 Å that are slightly larger than the 3.3-3.5 Å range found for $Mn(phen)_2Cl_2$,[192,196,197] but are smaller than the 3.949 Å distance observed in $[Cu(bipy)_2(\mu\text{-}Cl)_2HgBr_2]$.[194] One-D chains are thus formed from the molecular units of **3.1-3.4**. More importantly, the addition of $Hg(CN)_2$ to ML_2Cl_2 (M = Mn, Ni; L = bipy, phen) does not induce chloride migration and no increase in structural dimensionality is observed as a result of Hg-Cl interactions. The rational synthesis of $[Cu(phen)_2(\mu\text{-}Cl)_2Hg(CN)_2]$ was attempted but only complex **3.6** could be isolated.

3.2.3 Structure of $[Cu(terpy)Cl_2(\mu\text{-}Hg(CN)_2)]$ (3.5)

The X-ray single crystal structure of $[Cu(terpy)Cl_2(\mu\text{-}Hg(CN)_2)]$ (**3.5**) reveals a one-dimensional chain motif of $[Cu(terpy)Cl_2(\mu\text{-}Hg(CN)_2)]_n$ that runs parallel to the *a*-axis (Figure 3.6). Rather than forming two chloride bridges to a single Hg(II) centre, the $Cu(terpy)Cl_2$ unit forms two chloride bridges to different Hg(II) centres. This bonding arrangement is similar to that observed for *cis*-$[Rh(en)_2Cl_2][HgCl_3]$.[198] The bond distances and angles for **3.5** are gathered in Table 3.2. The Hg-Cl bond lengths of 2.8080(9) and 2.9121(9) Å are well within the sum of the Hg/Cl van der Waals radii of 3.30 Å[88,149] and are shorter than most bridging Hg-Cl bond

lengths, such as those found in $[Cu(en)_2][Hg(CN)_2Cl]_2$ (**2.5**) (2.7089(17) to 3.2186(15) Å), and $[Co(NH_3)_6]_2[Hg(CN)_2]_5Cl_6 \cdot 2\ H_2O$ (**2.7**) (3.072(2) Å to 3.119(3)Å).

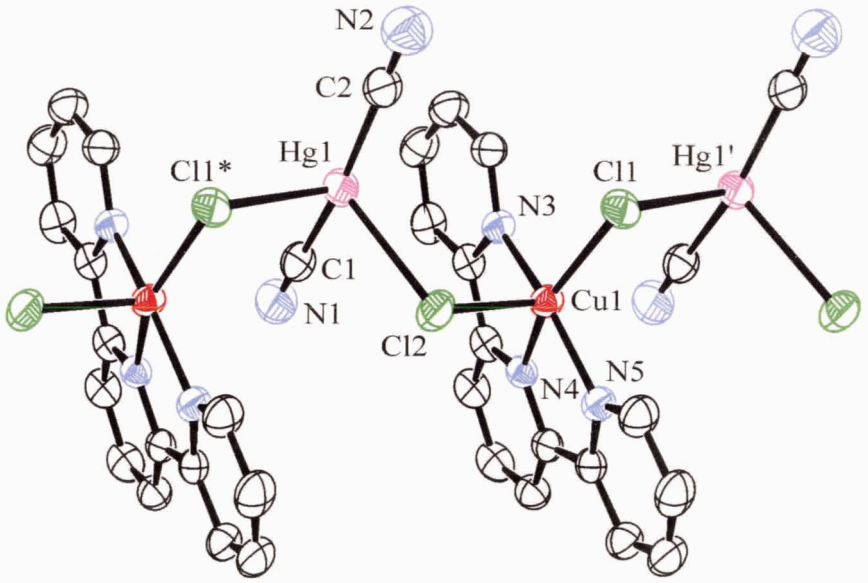

Figure 3.6 1-D chain segment of $[Cu(terpy)Cl_2(\mu\text{-}Hg(CN)_2)]_n$ (**3.5**) as viewed along the *a*-axis. The hydrogen atoms have been omitted for clarity (ORTEP 50% ellipsoids).

Table 3.2 Selected Bond Lengths (Å) and Angles (°) for $[Cu(terpy)Cl_2(\mu\text{-}Hg(CN)_2)]$ (**3.5**)[a].

Selected Atoms	*Bond Lengths*	*Selected Atoms*	*Bond Lengths*
Hg(1)-C(1)	2.046(4)	Hg(1)-C(2)	2.043(4)
Hg(1)-Cl(1*)	2.9121(9)	Hg(1)-Cl(2)	2.8080(9)
Cu(1)-Cl(1)	2.2673(9)	Cu(1)-Cl(2)	2.516(1)
Cu(1)-N(3)	2.029(3)	Cu(1)-N(4)	1.943(3)
Selected Atoms	*Bond Angles*	*Selected Atoms*	*Bond Angles*
C(1)-Hg(1)-C(2)	165.16(15)	Cl(1)-Cu(1)-Cl(2)	100.55(4)
Cl(1*)-Hg(1)-Cl(2)	100.25(3)	Cl(1)-Cu(1)-N(3)	98.28(8)
Cl(1*)-Hg(1)-C(1)	92.68(11)	Cl(2)-Cu(1)-C(3)	95.18(8)
Cl(2)-Hg(1)-C(1)	92.18(11)	Cl(1)-Cu(1)-N(4)	155.30(9)
Cl(1*)-Hg(1)-C(2)	94.20(12)	Cl(2)-Cu(1)-N(4)	104.15(9)
Cl(2)-Hg(1)-C(2)	155.30(9)	N(3)-Cu(1)-N(4)	79.45(11)
Hg(1)-C(1)-N(1)	178.7(4)	Cl(1)-Cu(1)-N(5)	97.79(9)
Hg(1)-C(2)-N(2)	178.7(4)	Cl(2)-Cu(1)-N(5)	96.44(9)
N(3)-Cu(1)-N(5)	158.07(11)	N(4)-Cu(1)-N(5)	79.70(11)
Hg(1')-Cl(1)-Cu(1)	100.58(3)	Hg(1)-Cl(2)-Cu(1)	105.78(3)

[a] Symmetry transformations: (*) -x-1, -y, -z; (') -x+2, -y, -z.

The Cu(II) centre in **3.5** has square pyramidal geometry comprised of three nitrogen donors from the terpy ligand and one chloride ligand (Cu(1)-Cl(1) = 2.2673(9) Å) forming the base, while the second chloride ligand resides in the apical position (Cu(1)-Cl(2) = 2.516(1) Å). This square pyramidal Cu(II) coordination sphere is also found for $Cu(terpy)Cl_2 \cdot H_2O$ ($Cu\text{-}Cl_{eq}$ = 2.231(2) Å, $Cu\text{-}Cl_{ax}$ = 2.565(2) Å)[199] and is similar to that found for $\{[Cu(bipy)Hg(CN)_2Cl_2]_2Hg(CN)_2\}$ ($Cu\text{-}Cl_{eq}$ = 2.3090(16) Å, $Cu\text{-}Cl_{ax}$ = 2. 5560(17),[195] a 1-D Cu_2Hg_2 rectangular cluster discussed in Chapter 5, and $[Cu(terpy)CN]NO_3 \cdot H_2O$ ($Cu\text{-}C_{eq}$ = 1.92(2) Å, $Cu\text{-}NC_{ax}$ = 2.21(1) Å), a 1-D $[Cu(terpy)CN]^+$ chain.[200] The Hg(II) centre has an effective see-saw geometry based on linear characteristic coordination (2+2) with C(1)-Hg(1)-C(2) = 165.16(15)°, and Cl(1*)-Hg(1)-Cl(2) = 100.25(3)°, similar to the Hg(II) centres in **3.1-3.4**. The Cu(1)-Hg(1) and Cu(1)-Hg(1') distances are 4.006 Å and 4.250 Å respectively. Although the addition of $Hg(CN)_2$ to $Cu(terpy)Cl_2$ does not induce chloride migration from the hard Cu(II) centre to the softer Hg(II) centre, the structural dimensionality has increased in the process due to the Hg-Cl interactions.

3.2.4 Structure of $\{[Cu(phen)_2Cl]_2Hg(CN)_2[Hg(CN)_2Cl]_2\}$ (3.6)

Unlike the molecular complexes **3.2** and **3.4,** reaction of an aqueous solution containing one equivalent of $[Cu(phen)_2]Cl_2$ with one equivalent of $Hg(CN)_2$ results in the formation of single crystals of $\{[Cu(phen)_2Cl]_2Hg(CN)_2[Hg(CN)_2Cl]_2\}$ (**3.6**) (Figure 3.7). The copper(II) centre of the $[Cu(phen)_2Cl]^+$ cation is five coordinate with a distorted geometry as exemplified by its tau parameter of $\tau = 0.72$ (where the τ range from 0 to 1 represents the geometric distortions from a perfect square pyramid to a trigonal bipyramid, respectively).[201] The bond distances and angles for **3.6** are gathered in Table 3.3. This copper(II) coordination sphere and the Cu(1)-Cl(2) bond length of 2.3340(17) Å is very similar to that found in the molecular complex $[Cu(bipy)_2Hg_2Cl_6]_2$ ($\tau = 0.47$, Cu-Cl = 2.320(7) Å),[195] as will be discussed in Chapter 5.

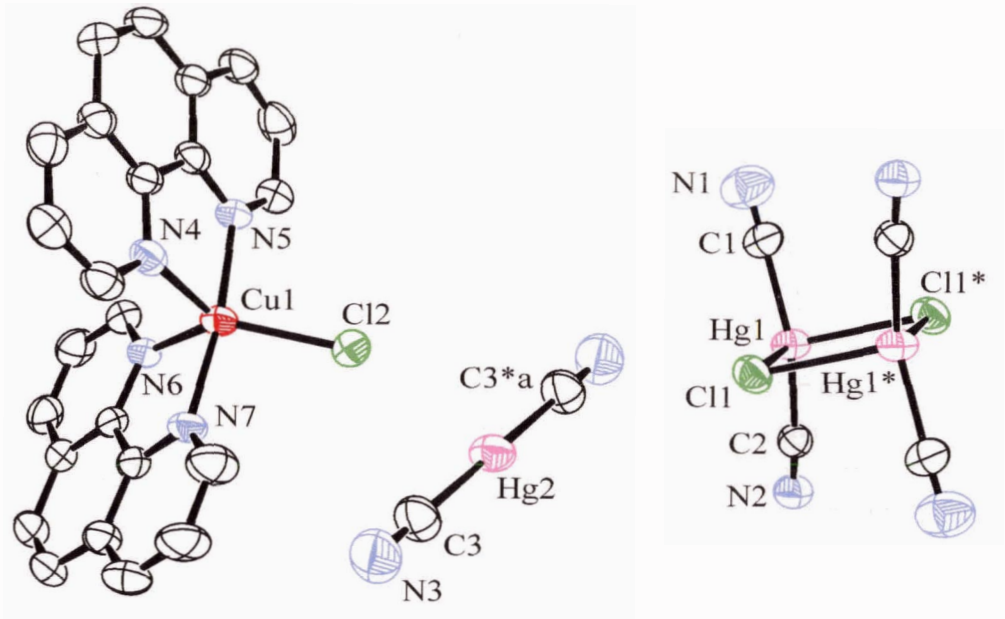

Figure 3.7 Three moieties that constitute $\{[Cu(phen)_2Cl]_2Hg(CN)_2[Hg(CN)_2Cl]_2\}$ (**3.6**). One $[Cu(phen)_2Cl]^+$ cation and the hydrogen atoms have been omitted for clarity (ORTEP 50% ellipsoids).

One chloride ligand has migrated to generate an $[Hg(CN)_2Cl]^-$ anion which in turn dimerizes via Hg-Cl bridges to form a $[Hg(CN)_2Cl]_2^{2-}$ double salt moiety with distorted see-saw effective coordination (2+2) as observed in the molecular dimers $[PPN][Hg(CN)_2Cl] \cdot H_2O$ (**2.1**), $[^nBu_t][Hg(CN)_2Cl] \cdot 0.5\ H_2O$ (**2.2**), and $[Ni(terpy)_2][Hg(CN)_2Cl]_2$ (**2.4**).[169] The additional, neutral $Hg(CN)_2$ unit serves two functions: 1) to act as bridging units between the $[Hg(CN)_2Cl]_2^{2-}$ anions via *N*-cyano interactions from the anion to the neutral $Hg(CN)_2$ metal centre (N(2)-Hg(2) = 3.010(5) Å), and 2) to act as bridging units for the $[Cu(phen)_2Cl]^+$ cations via chloride bridges (Cl(2)-Hg(2) = 3.2800(16) Å). The net result is the formation of a 1-D anionic chain of $\{[Hg(CN)_2Cl]_2Hg(CN)_2\}_n^{2n-}$ with associated $[Cu(phen)_2Cl]^+$ units that dangle along its length (Figure 3.8). This $Hg(CN)_2$ bridging mode is related to those reported for the 1-D complexes $[Cu(bipy)Hg(CN)_2Cl_2]_2Hg(CN)_2$[195] and $\{[Cu(bipy)(OH)(Cl)]_2[Hg(CN)_2\} \cdot 2\ H_2O$[195] (see Chapter 5). It is also similar to an example where $HgCl_2$ bridges Cu_4 clusters,[125] and where $HgCl_2$ bridges $[Co(NH_3)_5Cl]^{2+}$ cations.[96]

Table 3.3 Selected Bond Lengths (Å) and Angles (°) for $\{[Cu(phen)_2Cl]_2[Hg(CN)_2Hg(CN)_2Cl]_2\}$ (**3.6**)[a].

Selected Atoms	*Bond Lengths*	*Selected Atoms*	*Bond Lengths*
Hg(1)-Cl(1)	2.7217(15)	Hg(1)-Cl(1*)	2.7831(17)
Hg(1)-C(1)	2.077(7)	Hg(1)-C(2)	2.061(7)
Hg(2)-Cl(2)	3.2800(16)	Hg(2)-Cl(2*a)	3.2800(16)
Hg(2)-N(2')	3.010(5)	Hg(2)-N(2*b)	3.010(5)
Hg(2)-C(3)	2.034(7)	Cu(1)-Cl(2)	2.3340(17)
Cu(1)-N(4)	2.105(5)	Cu(1)-N(5)	1.998(4)
Cu(1)-N(6)	2.100(5)	Cu(1)-N(7)	1.994(4)
Selected Atoms	*Bond Angles*	*Selected Atoms*	*Bond Angles*
Cl(1)-Hg(1)-Cl(1*)	91.98(4)	Cl(1)-Hg(1)-C(1)	97.74(18)
Cl(1*)-Hg(1)-C(1)	93.7(2)	Cl(1)-Hg(1)-C(2)	101.74(17)
Cl(1*)-Hg(1)-C(2)	104.16(18)	C(1)-Hg(1)-C(2)	152.9(3)
Cl(2)-Hg(2)-Cl(2*a)	180	Cl(2)-Hg(2)-N(2')	94.51(12)
Cl(2*a)-Hg(2)-N(2')	85.49(12)	Cl(2)-Hg(2)-N(2*b)	85.49(12)
Cl(2*a)-Hg(2)-N(2*b)	94.51(12)	N(2')-Hg(2)-N(2*b)	180
Cl(2)-Hg(2)-C(3)	94.2(2)	Cl(2*a)-Hg(2)-C(3)	85.8(2)
N(2')-Hg(2)-C(3)	91.0(2)	N(2*b)-Hg(2)-C(3)	89.0(2)
C(3)-Hg(1)-C(3*a)	180	Cl(2)-Cu(1)-N(4)	128.75(14)
N(4)-Cu(1)-N(5)	80.92(19)	N(4)-Cu(1)-N(6)	105.00(18)
N(5)-Cu(1)-N(6)	94.17(19)	Cl(2)-Cu(1)-N(7)	93.98(15)
N(4)-Cu(1)-N(7)	93.74(19)	N(5)-Cu(1)-N(7)	171.8(2)
N(6)-Cu(1)-N(7)	81.14(19)	Hg(1)-Cl(1)-Hg(1*)	88.02(4)
Hg(2)-Cl(2)-Cu(1)	143.87(7)		

[a] Symmetry transformations: (*) -x, -y+1, -z+1; (*a) -x+1, -y+1, -z+2; (*b) -x+1, -y+1, -z+1; (') x, y, z+1.

The Hg(2) centre is rendered pseudo-octahedral based upon linear characteristic coordination (2+4) as a result (N(2')-Hg(2)-N(2*b) = Cl(2)-Hg(2)-Cl(2*a) = C(3)-Hg(2)-N(3*a) = 180°). The Hg···NC bond is longer than the Hg···NC interaction of 2.742(3) Å responsible for the solid-state aggregation of $Hg(CN)_2$[118] and can be compared with the related $[Cu(dien)][Au(CN)_4]_2$ and $[Cu(dmeda)_2Au(CN)_4][Au(CN)_4]$ (-AuCN-Au = 3.002(14) Å and 2.963(13) Å, respectively) gold(III) complexes[202] and $[Cu(en)_2][Ag_2(CN)_3][Ag(CN)_2]$ (-AgCN-Ag = 2.572(3) Å) silver(I) complex.[82] Thus, the addition of $Hg(CN)_2$ to $Cu(phen)_2Cl_2$ induces the migration of one chloride ligand from the harder Cu(II) to the softer Hg(II) centre, increasing the structural dimensionality

from 0 to 1 in complex **3.6**. Extended $\pi\cdots\pi$ stacking of the conjugated ring systems characterized by interplanar distances of 3.7-4.4 Å further increases the dimensionality from 1 to 2. Similar $\pi\cdots\pi$ interactions between pyridine rings have been reported for many phen-containing Cu(II) complexes.

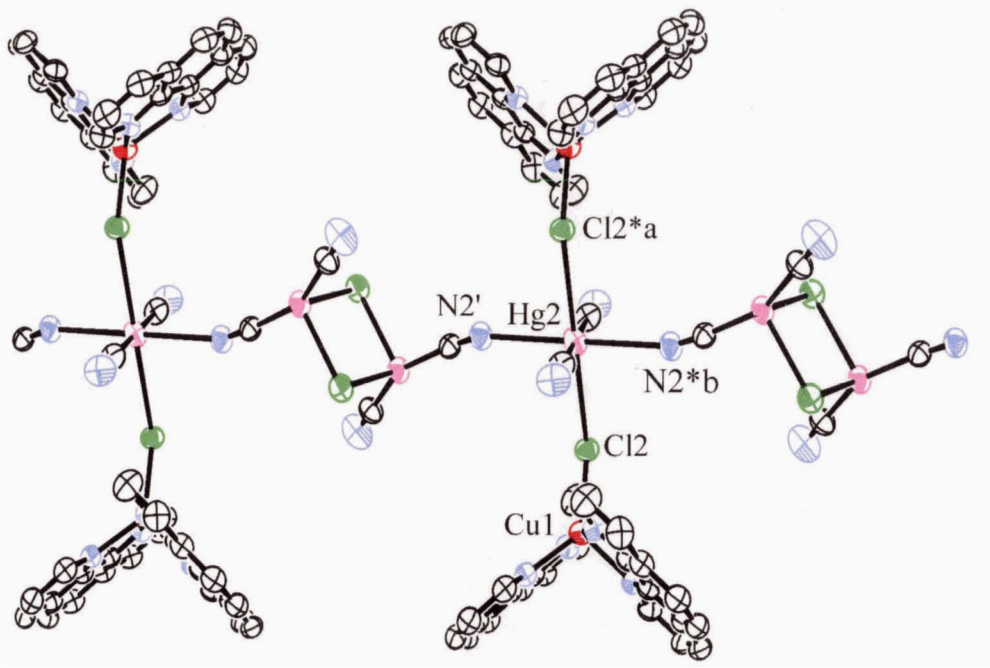

Figure 3.8 1-D chain segment of **3.6** as viewed along the *c*-axis.
The hydrogen atoms have been omitted for clarity (ORTEP 50% ellipsoids).

3.2.5 Structure of [Cu(dien)Cl][Hg(CN)$_2$Cl] (3.7)

The slow evaporation of a solution containing $Hg(CN)_2$ and one equivalent of $Cu(dien)Cl_2$ yielded single crystals of [Cu(dien)Cl][$Hg(CN)_2Cl$] (**3.7**). Migration of one chloride ligand occurs from the copper(II) centre to a $Hg(CN)_2$ unit to form a $[Hg(CN)_2Cl]^-$ double salt moiety. In contrast to the self-assembled $[Hg(CN)_2Cl_2]^{2-}$ dimers observed in **3.6**, a 1-D chain of $[Hg(CN)_2Cl]_n^{n-}$ is formed with Hg(1)-Cl(2) bond lengths of 2.9219(16) and 2.9345(16) Å (Figure 3.9 a). The bond distances and angles for **3.7** are gathered in Table 3.4.

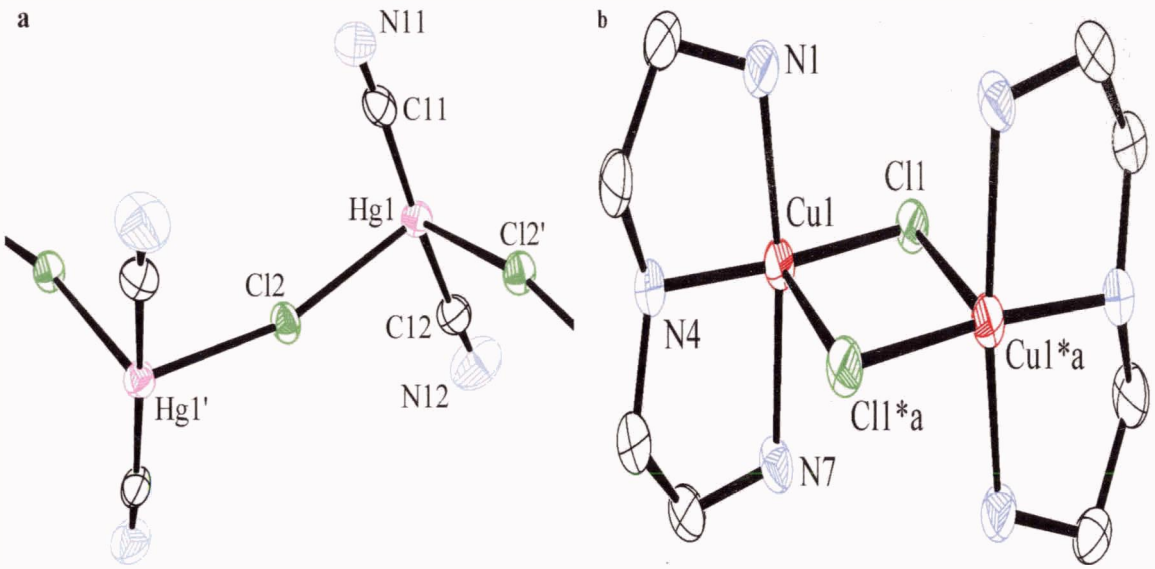

Figure 3.9 a) A segment of the $[Hg(CN)_2Cl]_n^{n-}$ 1-D chain and b) a dimeric $[Cu_2(dien)_2(\mu\text{-}Cl)_2]^{2+}$ cation of [Cu(dien)Cl][$Hg(CN)_2Cl$] (**3.7**).
Hydrogen atoms have been removed for clarity (ORTEP 50% ellipsoids).

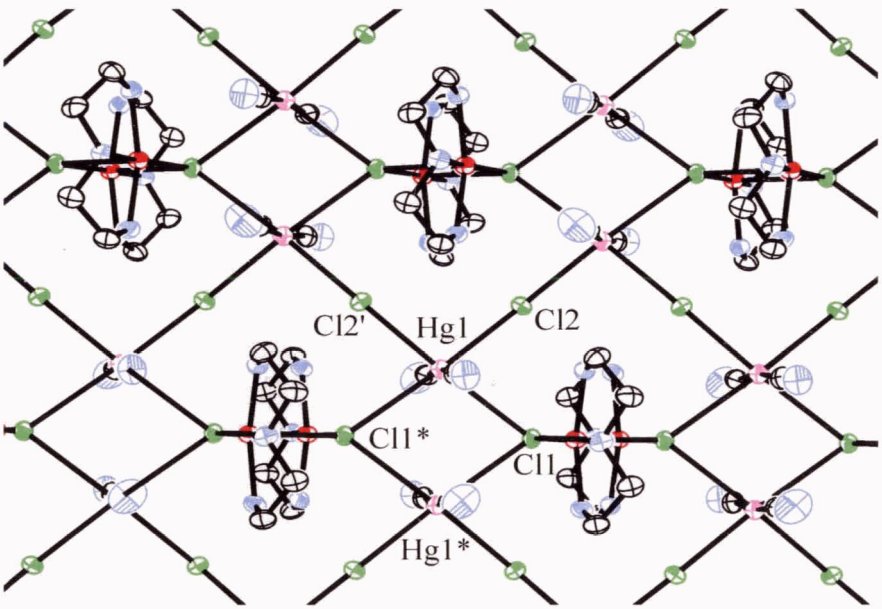

Figure 3.10 2-D layer structure of [Cu(dien)Cl][$Hg(CN)_2Cl$] (**3.7**).
Hydrogen atoms have been omitted for clarity (ORTEP 50% ellipsoids).

This 1-D anionic chain motif is similar to the $[Hg_3Cl_9]_n^{3n-}$ chains reported for $[Co(NH_3)_6][Hg_3Cl_9] \cdot H_2O$.[160] As in **3.5** and **3.6**, the second chloride ligand remains bound to the copper(II) centre but in **3.7** the cations dimerize via two chloride bridges to form $[Cu_2(dien)_2(\mu\text{-}$

$Cl)_2]^{2+}$ (Figure 3.9 b). Each Cu(II) centre has a distorted square pyramidal geometry where the three N atoms of the dien ligand and one chloride ligand (Cl1) form the basal plane while the second chloride (Cl1*) occupies the apical position. The three Cu-N distances are very similar (2.014(5), 2.015(5), 2.001(5) Å) while the Cu-Cl apical bond is much longer than the basal one (2.7608(17) *versus* 2.2875(17) Å). The Cu(II) centres in the dimer are separated from each other by 3.528 Å and the Cu-Cl-Cu and Cl-Cu-Cl angles are 88.13(6)° and 91.87(6)° respectively. This can be compared with the Cu-Cl-Cu bond angle of $[Cu_2(dien)_2Cl_2][NO_3]_2$ (90.62(1)°),[203] and the related $[(terpy)CuCl]_2[PF_6]_2$ (89.9(1)°).[204]

Table 3.4 Selected Bond Lengths (Å) and Angles (°) for [Cu(dien)Cl][Hg(CN)$_2$Cl] (**3.7**)[a].

Selected Atoms	*Bond Lengths*	*Selected Atoms*	*Bond Lengths*
Hg(1)-Cl(1)	3.2143(15)	Hg(1)-Cl(1*)	3.2483(16)
Hg(1)-Cl(2)	2.9219(16)	Hg(1)-Cl(2')	2.9345(16)
Hg(1)-C(11)	2.066(8)	Hg(1)-C(12)	2.055(7)
Cu(1)-Cl(1)	2.2875(16)	Cu(1)-Cl(1*a)	2.7608(17)
Cu(1)-N(1)	2.014(5)	Cu(1)-N(4)	2.001(5)
Cu(1)-N(7)	2.017(5)		
Selected Atoms	*Bond Angles*	*Selected Atoms*	*Bond Angles*
Cl(1)-Hg(1)-Cl(1*)	103.17(4)	Cl(1)-Hg(1)-Cl(2)	79.94(4)
Cl(1*)-Hg(1)-Cl(2)	175.19(4)	Cl(1)-Hg(1)-Cl(2')	174.68(4)
Cl(1*)-Hg(1)-Cl(2')	79.37(4)	Cl(2)-Hg(1)-Cl(2')	97.835(12)
Cl(1)-Hg(1)-C(11)	83.0(2)	Cl(1*)-Hg(1)-C(11)	91.4(2)
Cl(2)-Hg(1)-C(11)	92.6(2)	Cl(2')-Hg(1)-C(11)	92.3(2)
Cl(1)-Hg(1)-C(12)	91.9(2)	Cl(1*)-Hg(1)-C(12)	83.5(2)
Cl(2)-Hg(1)-C(12)	92.8(2)	Cl(2')-Hg(1)-C(12)	93.0(2)
C(11)-Hg(1)-C(12)	171.9(3)	Cl(1)-Cu(1)-Cl(1*a)	91.87(6)
Cl(1)-Cu(1)-N(1)	96.82(16)	Cl(1*a)-Cu(1)-N(1)	87.08(16)
Cl(1)-Cu(1)-N(4)	167.45(17)	Cl(1*a)-Cu(1)-N(4)	100.65(16)
Cl(1)-Cu(1)-N(7)	95.53(15)	Cl(1*a)-Cu(1)-N(7)	86.62(17)
N(1)-Cu(1)-N(4)	84.9(2)	N(1)-Cu(1)-N(7)	166.3(2)
N(4)-Cu(1)-N(7)	84.4(2)	Hg(1)-Cl(1)-Hg(1*)	76.83(4)
Hg(1)-Cl(1)-Cu(1)	108.04(6)	Hg(1*)-Cl(1)-Cu(1)	108.04(6)
Hg(1)-Cl(1)-Cu(1*a)	136.39(6)	Hg(1*)-Cl(1)-Cu(1*a)	137.11(5)
Cu(1)-Cl(1)-Cu(1*a)	88.13(6)	Hg(1)-Cl(2)-Hg(1')	160.82(7)

[a] Symmetry transformations: (*) -x, -y-1/2, -z+1/2; (*a) -x, -y+1/2, -z+1/2; (') -x-1/2, y-1/2, -z+1/2

The chlorine atoms of the $[Cu_2(dien)_2(\mu\text{-}Cl)_2]^{2+}$ cations form two additional bridges to the open coordination site on the Hg(II) centres (Cl(1)-Hg(1) = 3.2143(15) Å, Cl(1*)-Hg(1) = 3.2483(16) Å) of the anionic 1-D $[Hg(CN)_2Cl]_n^{n-}$ chains resulting in a 2-D brick-wall layer motif (Figure 3.10). Each Hg(II) centre has octahedral effective coordination based upon linear characteristic coordination (2+4) with bridging chlorine atoms all in the equatorial plane and the cyano ligands perpendicular to the layer. The layer is related to $[NH_3(C_2H_5)]_2[Hg(CN)_2Cl_2]$[144], a 2-D chess-board layer perovskite-like structure with Hg-Cl bond lengths of 2.901(2) and 3.432(2) Å. Weak N-H···NC interactions (N(11)···N(4) = 3.057 Å) between the cyano groups of one 2-D layer and the amine protons from the layer above and below increase the structural dimensionality of **3.7** from 2 to 3, and are shorter than those reported for $[Cu(en)_2]_3[W(CN)_8]_2 \cdot H_2O$ (3.214 Å),[127] and $[Cu(en)_2][Ag_2(CN)_4]$ (3.195 Å).[130]

3.2.6 Structure of [Cu(tren)Hg(CN)$_2$Cl][HgX$_2$Cl] (3.8)

The reaction of $Cu(tren)Cl_2$ with two equivalents of $Hg(CN)_2$ not only induces complete migration of the chloride ligands from the Cu(II) centre to the coordinately unsaturated Hg(II) centres, but in the process opens a site for *N*-cyano binding between the $[Hg(CN)_2Cl]^-$ double salt unit formed and the $[Cu(tren)]^{2+}$ cation. These units then assemble into a 1-D cationic chain with the formula $[Cu(tren)Hg(CN)_2Cl]_n^{n+}$ via Hg-Cl bridges (Hg(1)-Cl(1) = 2.795(4) Å, Hg(1)-Cl(1*) = 2.772(3) Å (Figure 3.11 a). The bond distances and angles for **3.8** are gathered in Table 3.5.

The cationic Cu(II) centre in **3.8** has a distorted five-coordinate geometry (τ = 0.65), with one tren and one strongly *N*-bound $Hg(CN)_2$ completing the coordination sphere (Cu-NC = 1.966(11) Å). This coordination sphere is very similar to the five-coordinate Cu(II) centre reported for the molecular complex $[Cu(tren)Au(CN)_2][Au(CN)_2]$ (τ = 0.74; Cu-NC = 1.950(9) Å).[79] Simultaneous chloride migration from harder Cu(II) to softer Hg(II) and cyano bridging from $Hg(CN)_2$ units to an octahedral Cu(II) centre has been observed in $\{Cu(tmeda)[Hg(CN)_2]_2\}HgCl_4$ ($Cu\text{-}NC_{eq}$ = 1.975(11) Å, $Cu\text{-}NC_{ax}$ = 2.583(13) Å),[205] as described in Chapter 4.

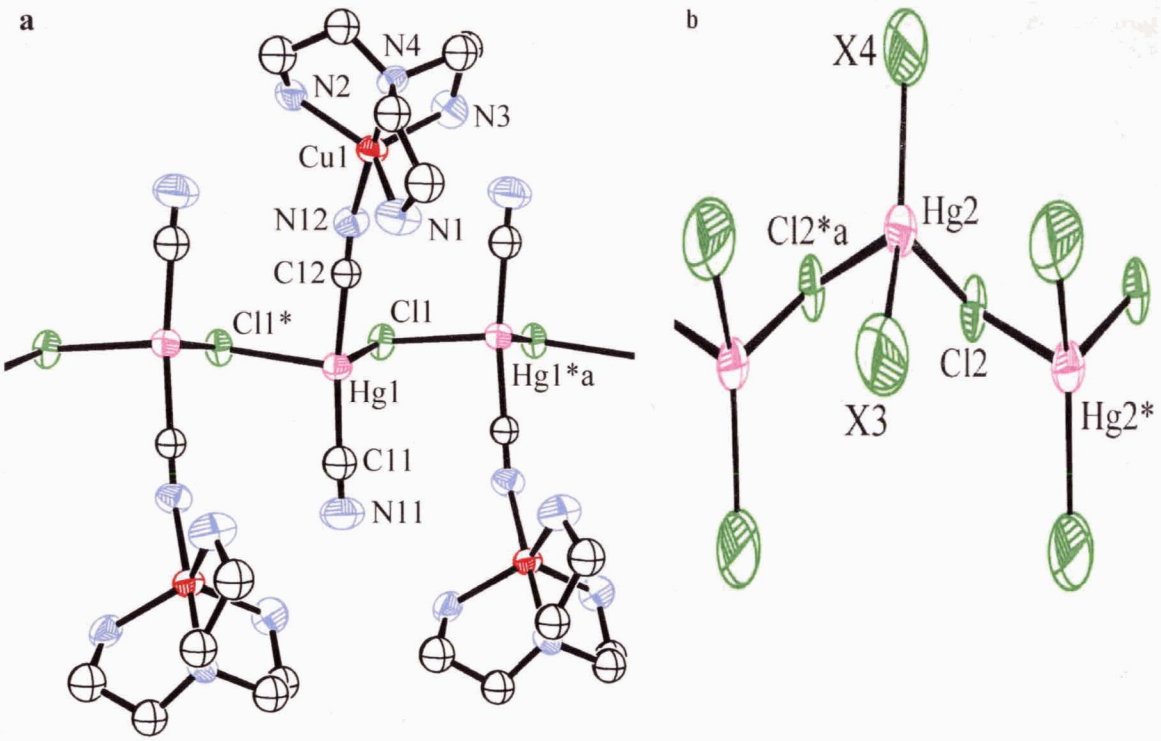

Figure 3.11 a) 1-D cationic chain of $[Cu(tren)Hg(CN)_2Cl]_n^{n+}$ and b) 1-D anionic chain of $[HgX_2Cl]_n^{n-}$ observed in $[Cu(tren)Hg(CN)_2Cl][HgX_2Cl]$ (**3.8**).
X sites are of 1:1 mixed Cl / CN occupancy; hydrogen atoms have been omitted for clarity (ORTEP 50% ellipsoids).

The Hg(1) centres have an effective see-saw geometry (2+2) (C-Hg-C = 164.2(6)°, Cl-Hg-Cl = 90.1(1)°) as found for structures **3.1-3.5**. A second 1-D chain is also formed but it is anionic, comprised of $[HgX_2Cl]^-$ units; where X represents sites of 1:1 mixed Cl / CN occupancy (Hg(2)-Cl(2) = 2.632(4) Å, Hg(2*)-Cl(2) = 2.754(4) Å) (Figure 3.11 b). The Hg(2) centre shows a distorted effective tetrahedral geometry (2+2) (Cl(2*a)-Hg(2)-Cl(2) = 83.0(2)°, X(3)-Hg(2)-X(4) ≅ 142.4°). Unlike structures **3.6** and **3.7**, no additional Hg-Cl or Hg-NC bridging takes place to connect the cationic and anionic components of **3.8**. Rather, weak N-H···NC (N(4)-N(11) = 3.106 Å, N(3)-N(11) = 3.274 Å) and N-H···Cl (N(1)-Cl(2) = 3.521 Å, N(3)-X(4) ≅ 3.695 Å) interactions bind the $[HgX_2Cl]_n^{n-}$ chain between the crescent-shaped cleft formed by the $[Cu(tren)Hg(CN)_2Cl]_n^{n+}$ chain to generate a neutral $[Cu(tren)Hg(CN)_2Cl][HgX_2Cl]$ (**3.8**) column.

Additional N-H···Cl interactions (N(4)-Cl(1) = 3.437 Å) bind different columns together, forming the 2-D layer motif shown in Figure 3.12.

Table 3.5 Selected Bond Lengths (Å) and Angles (°) for $[Cu(tren)Hg(CN)_2Cl][HgX_2Cl]$ (**3.8**)[a].

Selected Atoms	*Bond Lengths*	*Selected Atoms*	*Bond Lengths*
Hg(1)-Cl(1)	2.757(3)	Hg(1)-Cl(1*)	2.776(2)
Hg(1)-C(11)	2.028(12)	Hg(1)-C(12)	2.054(11)
Hg(2)-Cl(2)	2.658(3)	Hg(2)-Cl(2*a)	2.761(3)
Hg(2)-C[b](10)	2.050(5)	Hg(2)-C[c](20)	2.054(5)
Hg(2)-Cl[b](3)	2.364(7)	Hg(2)-Cl[c](4)	2.306(6)
Cu(1)-N(1)	2.051(13)	Cu(1)-N(2)	2.018(11)
Cu(1)-N(3)	2.135(12)	Cu(1)-N(4)	2.053(12)
Selected Atoms	*Bond Angles*	*Selected Atoms*	*Bond Angles*
Cl(1)-Hg(1)-Cl(1*)	90.19(7)	Cl(1)-Hg(1)-C(11)	97.6(3)
Cl(1*)-Hg(1)-C(11)	98.2(3)	Cl(1)-Hg(1)-C(12)	92.9(3)
Cl(1*)-Hg(1)-C(12)	93.1(3)	C(11)-Hg(1)-C(12)	164.4(4)
Cl(2)-Hg(2)-Cl(2*a)	92.85(7)	Cl(2)-Hg(2)-Cl[b](3)	101.7(2)
Cl(2*a)-Hg(2)-Cl[b](3)	100.2(3)	Cl(2)-Hg(2)-Cl[c](4)	108.1(3)
Cl(2*a)-Hg(2)-Cl[c](4)	96.4(11)	Cl[b](3)-Hg(2)-Cl[c](4)	145.0(4)
N(1)-Cu(1)-N(2)	84.1(5)	N(1)-Cu(1)-N(3)	114.6(6)
N(2)-Cu(1)-N(3)	85.3(4)	N(1)-Cu(1)-N(4)	133.6(6)
N(2)-Cu(1)-N(4)	84.9(5)	N(3)-Cu(1)-N(4)	109.2(5)
N(1)-Cu(1)-N(12)	89.0(5)	N(2)-Cu(1)-N(12)	172.5(5)
N(3)-Cu(1)-N(12)	100.2(5)	N(4)-Cu(1)-N(12)	98.0(5)
Hg(1)-Cl(1)-Hg(1*a)	91.3(1)	Hg(2)-Cl(2)-Hg(2*)	104.72(13)
C[b](10)-Hg(2)-C[c](20)	151.1(17)		

[a] Symmetry transformations: (*) x-1/2, -y+1/2, z; (*a) x+1/2, -y+1/2, z.
[b] X3 = 1:1 mixed Cl(3) / C(10)occupancy.
[c] X4 = 1:1 mixed Cl(4) / C(20)occupancy.

These weak N-H···Cl interactions are comparable to those N-Cl distances reported for $[Cu(Hbimam)Cl_3]_2(H_2O)_2$, $[Cu(Hbimam)_2Cl_2]Cl_2(H_2O)_2$ (3.266 Å and 3.277 Å respectively; bimam = bis(imidazol-2-yl)methylaminomethane),[154] *trans*-$[PtCl_2(NH_3)_2]$ (3.41 Å),[155] and 2,6-diphenylpyridinium tetrachloroaurate (3.45 Å, 3.75 Å).[156]

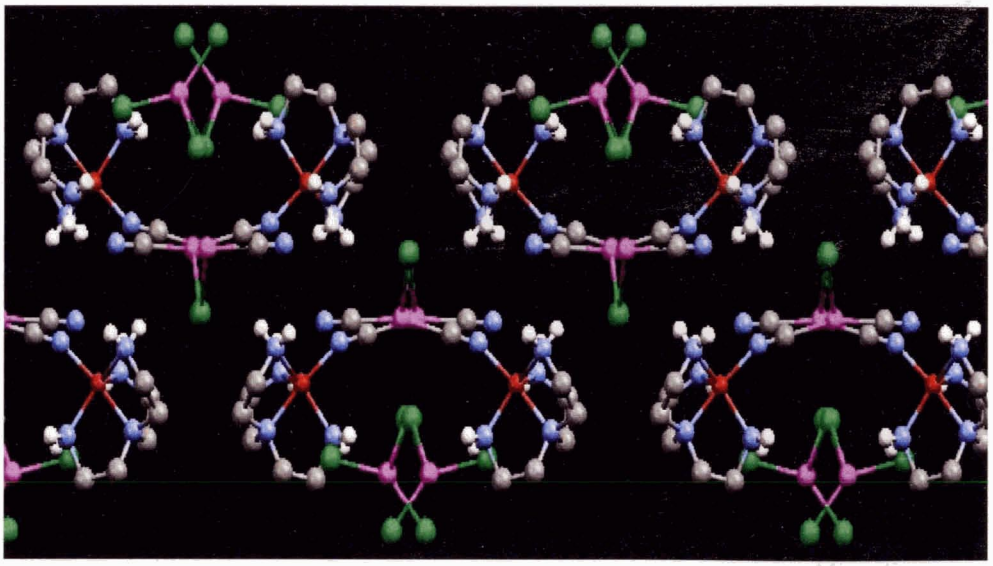

Figure 3.12 Extended 2-D motif of $[Cu(tren)Hg(CN)_2Cl][HgX_2Cl]$ (**3.8**). Methylene hydrogen atoms have been omitted for clarity. Colour scheme: Hg, pink; Cu, red; Cl, green; N, blue; C, grey; H, white.

3.2.7 Structure of $\{[Ni(en)_2][Hg(CN)_2]_3Cl_2\}_2$ (3.9)

Reaction of an aqueous solution containing one equivalent of $Ni(en)_2Cl_2$ with three equivalents of $Hg(CN)_2$ results in the formation of single crystals of $\{[Ni(en)_2][Hg(CN)_2]_3Cl_2\}_2$ (**3.9**). Complete migration of both chloride ligands from Ni(II) to Hg(II) drives the formation of the product. The IR spectrum clearly shows two blue-shifted ν_{CN} (2217 cm^{-1}, 2207 cm^{-1}) bands relative to free $Hg(CN)_2$, consistent with the formation of bridging cyanide ligands. The crystal structure consists of a 1-D battlement arrangement of anionic $\{[Hg(CN)_2]_3Cl_2\}_{2n}^{4n-}$ units held together via several Hg-Cl bridges ranging from 2.696(7) Å (Hg(1)-Cl(1)) to 3.239(9) Å (Hg(6)-Cl(3)) (Figure 3.13). The bond distances and angles for **3.9** are gathered in Table 3.6. This unusual 1-D anionic motif is similar to the battlement-like 1-D coordination polymer $[Cd(tren)][Pd(CN)_4]$ which is formed by the alternating *cis*-arrangement of $[Cd(tren)]^{2+}$ and $[Pd(CN)_4]^{2-}$ ions.[206] For **3.9**, the battlement consists of a repeating -Hg(1)-Cl(1)-Hg(2)-Cl(2)-Hg(4)-Cl(3)-Hg(5)-Cl(4)- 'square wave' chain.

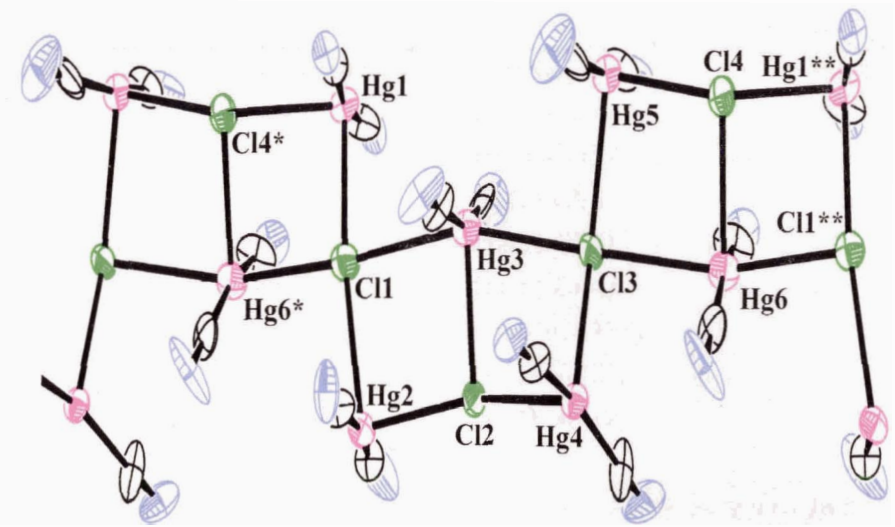

Figure 3.13 1-D anionic battlement arrangement observed in $\{[Ni(en)_2][Hg(CN)_2]_3Cl_2\}_2$ (**3.9**). (ORTEP 50% ellipsoids).

These four Hg(II) centres have effective see-saw geometry based on linear characteristic coordination (2+2) with C-Hg-C angles that range from 160.4(14)° to 168.9(13)° and Cl-Hg-Cl angles that range from 78.4(2)° to 90.6(2)°. Each square wave is roughly centred by additional $Hg(CN)_2$ moieties via three Hg-Cl interactions. These effective five-coordinate Hg(3) and Hg(6) centres (2+3) have a distorted square pyramidal geometry with two chloride and two cyano ligands occupying the basal plane and the third chloride ligand occupying the apical site, similar to the Hg(II) centres observed in **2.5**. The resultant $\{[Hg(CN)_2]_3Cl_2\}_{2n}^{4n-}$ battlement motif has structural characteristics of an amalgamated 1-D anionic ladder (**2.5**) and ribbon (**2.6**). $[Ni(en)_2]^{2+}$ cations bridge the 1-D anionic chains together to form an alternating corrugated 2-D layer structure (Figure 3.14). Both Ni(II) centres in **3.9** have octahedral geometries comprised of two equatorial en ligands and two axial *N*-cyano bridging groups. Ni-N(en) bond lengths range from 2.04(2) Å to 2.11(2) Å and are in the expected range for Ni-N(amine) bonds. Ni-N(cyano) bond lengths range from 2.11(2) Å to 2.13(2) Å and is comparable to those reported for the molecular complex $[Ni(en)_2][Au(CN)_4]_2 \cdot H_2O$ (2.129(5) Å),[202] the 2-D $[Ni(en)_2Ag_2(CN)_3][Ag(CN)_2]$ (2.0832(18) Å),[82] and the 3-D $[Ni(en)_2]_3[Fe(CN)_6](PF_6)_2$ (2.104(3) Å).[207]

Table 3.6 Selected Bond Lengths (Å) and Angles (°) for $\{[Ni(en)_2][Hg(CN)_2]_3Cl_2\}_2$ (**3.9**)[a].

Selected Atoms	*Bond Lengths*	*Selected Atoms*	*Bond Lengths*
Hg(1)-Cl(1)	2.696(7)	Hg(2)-Cl(2)	2.820(8)
Hg(3)-Cl(2)	2.813(7)	Hg(4)-Cl(3)	2.767(7)
Hg(3)-Cl(1)	3.216(9)	Hg(3)-Cl(3)	3.079(9)
Hg(4)-Cl(2)	2.901(8)	Hg(5)-Cl(4)	2.837(9)
Hg(5)-Cl(3)	2.889(7)	Hg(6)-Cl(4)	2.916(7)
Hg(1)-Cl(4*)	3.012(9)	Hg(6)-Cl(1**)	3.070(9)
Hg(6)-Cl(3)	3.239(9)	Ni(1)-N(12')	2.08(2)
Ni(1)-N(52)	2.12(2)	Ni(2)-N(11a)	2.11(2)
Ni(2)-N(41)	2.13(2)		
Selected Atoms	*Bond Angles*	*Selected Atoms*	*Bond Angles*
C(11)-Hg(1)-C(12)	168.3(12)	C(11)-Hg(1)-Cl(1)	94.9(9)
C(22)-Hg(2)-C(21)	168.9(13)	C(21)-Hg(2)-Cl(2)	96.9(10)
Cl(2)-Hg(2)-Cl(1)	90.6(2)	C(32)-Hg(3)-C(31)	157.7(11)
C(32)-Hg(3)-Cl(2)	105.2(8)	C(42)-Hg(4)-C(41)	160.4(14)
C(42)-Hg(4)-Cl(3)	95.6(12)	Cl(3)-Hg(4)-Cl(2)	82.3(2)
C(52)-Hg(5)-C(51)	163.1(16)	C(52)-Hg(5)-Cl(4)	90.2(11)
Cl(4)-Hg(5)-Cl(3)	90.4(2)	C(62)-Hg(6)-C(61)	165.9(13)
Cl(4*)-Hg(1)-Cl(1)	86.6(2)	Cl(2)-Hg(3)-Cl(1)	84.6(2)
Cl(3)-Hg(3)-Cl(1)	160.9(2)	Cl(3)-Hg(3)-Cl(2)	78.4(2)
Cl(3)-Hg(6)-Cl(1**)	160.0(2)	Cl(4)-Hg(6)-Cl(1**)	81.8(2)
N(52)-Ni(1)-N(12')	177.3(10)	Cl(4)-Hg(6)-Cl(3)	82.4(2)
N(1)-Ni(1)-N(4)	173.6(14)	N(41)-Ni(2)-N(11a)	173.9(10)
N(52)-Ni(1)-N(1)	92.4(12)	N(2)-Ni(1)-N(3)	175.8(13)
N(4)-Ni(1)-N(3)	80.3(15)	N(52)-Ni(1)-N(4)	89.7(11)
N(8)-Ni(2)-N(11a)	92.5(9)	N(4)-Ni(1)-N(2)	103.3(16)
N(41)-Ni(2)-N(8)	91.8(9)	N(6)-Ni(2)-N(11a)	87.4(9)
N(41)-Ni(2)-N(6)	96.6(10)	N(41)-Ni(2)-N(7)	89.7(10)
N(8)-Ni(2)-N(5)	175.7(10)	N(7)-Ni(2)-N(6)	172.8(8)
N(8)-Ni(2)-N(7)	82.5(9)	N(7)-Ni(2)-N(5)	101.7(10)
N(7)-Ni(2)-N(11a)	86.5(9)	N(5)-Ni(2)-N(11a)	87.5(9)
Hg(1)-Cl(1)-Hg(2)	170.5(4)	Hg(3)-Cl(2)-Hg(2)	96.4(2)
Hg(3)-Cl(2)-Hg(4)	94.7(2)	Hg(2)-Cl(2)-Hg(4)	151.0(3)
Hg(4)-Cl(3)-Hg(5)	146.1(3)	Hg(1**)-Cl(4)-Hg(6)	88.3(2)
Hg(1**)-Cl(4)-Hg(5)	155.4(3)	Hg(6)-Cl(4)-Hg(5)	96.0(2)

[a] Symmetry transformations as *x, y, z*: (*) x, y-1, z; (**) x, y+1, z; (') –x+5/2, y+1/2, -z+2; (a) –x+2, -y, -z+1.

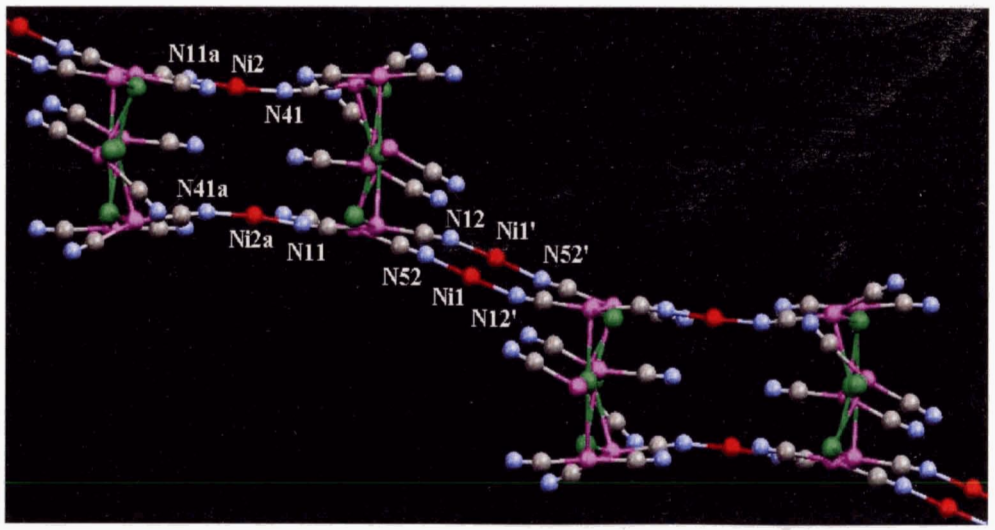

Figure 3.14 2-D layer structure of $\{[Ni(en)_2][Hg(CN)_2]_3Cl_2\}_2$ (**3.9**). Alternating cations and 1-D anionic $\{[Hg(CN)_2]_3Cl_2\}_{2n}^{4n-}$ chains are shown; en ligands have been omitted for clarity. Colour scheme: Hg, pink; Ni, red; Cl, green; N, blue; C, grey.

3.2.8 Structure of $\{[Ni(tren)]_4[Hg(CN)_2]_8Cl_6\}HgCl_4$ (3.10)

Reaction of an aqueous solution containing four equivalents of $Ni(tren)Cl_2$ with eight equivalents of $Hg(CN)_2$ and one equivalent of $HgCl_2$ results in the formation of single crystals of $\{[Ni(tren)]_4[Hg(CN)_2]_8Cl_6\}HgCl_4$ (**3.10**). Complete migration of both chloride ligands from Ni(II) to Hg(II) drives the formation of the product, similar to that found with complexes **3.8** and **3.9**. The IR spectrum clearly shows a blue-shifted ν_{CN} (2215 cm^{-1}) band relative to free $Hg(CN)_2$, consistent with the formation of a bridging cyanide ligand. The crystal structure has an asymmetric unit consisting of a six-coordinate Ni(II) centre with distorted octahedral geometry (one tren ligand, one bridging $Hg(CN)_2$, and one bridging $[Hg(CN)_2Cl]^-$ unit), an additional Cl atom and a $[HgCl_4]^{2-}$ moiety (Ni-N(1)cyano = 2.13(3) Å, Ni-N(3)cyano = 2.06(3) Å) (Figure 3.15). The bond distances and angles for **3.10** are gathered in Table 3.7. Similar cyano-bridging to Ni(II) centres is reported for $[Ni(tren)Au(CN)_2][Au(CN)_2]$ (Ni-NC = 2.12(1) Å, 2.05(2) Å),[208] $[Ni(tren)Ag(CN)_2][Au(CN)_2]$ (Ni-NC = 2.098(3) Å, 2.039(3) Å),[82] and $[Ni(tren)][N(CN)_2]_2$ (Ni-NC = 2.108(3) Å, 2.064(3) Å).[209] The Ni-N distances range from 2.03(3) Å to 2.11(3) Å for the Ni-N(tren) which are in the expected range for Ni-N(amine) bonds. The Ni(II)-bound

$[Hg(CN)_2Cl]^-$ moiety (Hg(2)-Cl(2) = 2.754(9) Å) forms a second chloride bridge to a different Ni(II)-bound $[Hg(CN)_2Cl]^-$ unit (Hg(2)-Cl(2*) =2.768(9) Å) that is inverted with respect to its Ni(II) centre, resulting in an alternating chain of effective four coordinate (2+2) see-saw Hg(2) centres.

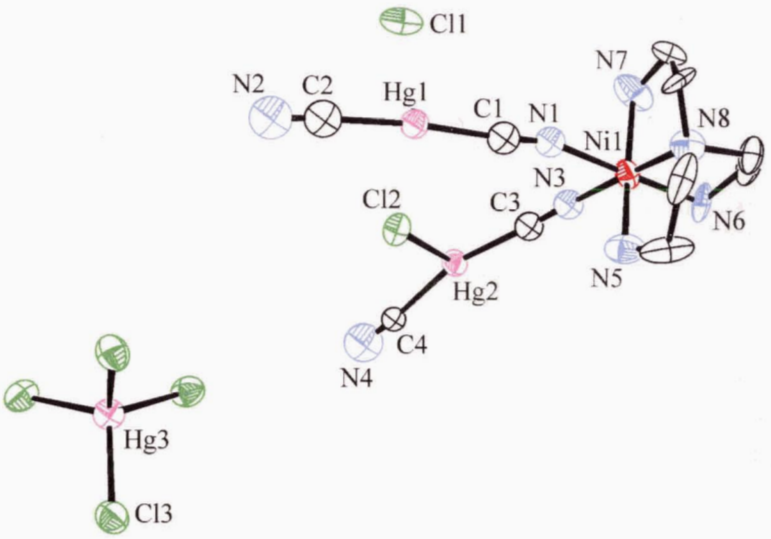

Figure 3.15 Contents of the asymmetric unit cell for $\{[Ni(tren)]_4[Hg(CN)_2]_8Cl_6\}HgCl_4$ (**3.10**). (ORTEP 50% ellipsoids).

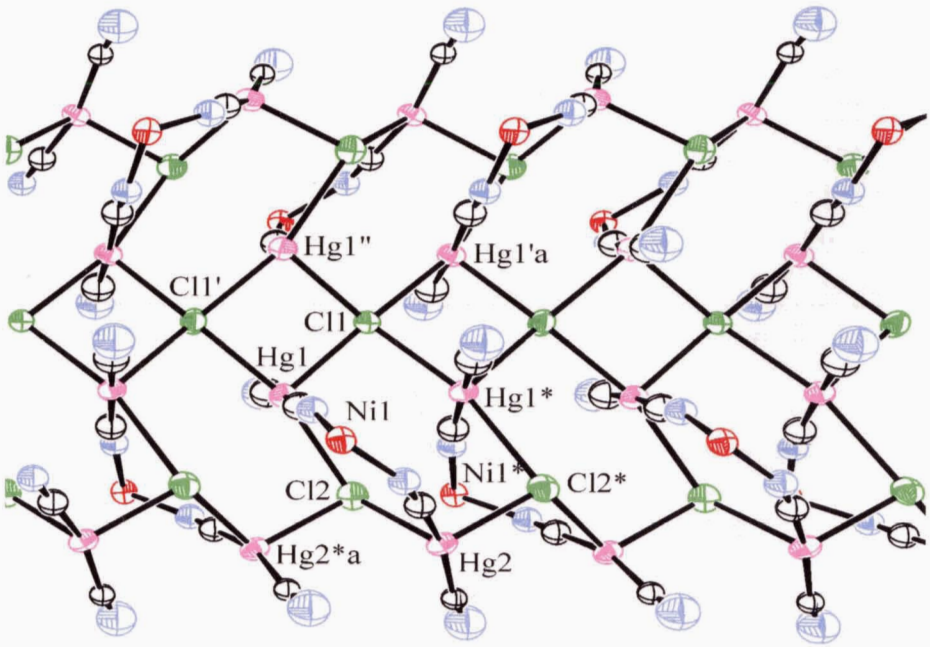

Figure 3.16 1-D cationic $\{[Ni(tren)]_4[Hg(CN)_2]_8Cl_6\}^{2+}$ ribbon segment of **3.10**. Tren ligands have been omitted for clarity (ORTEP 50% ellipsoids).

Table 3.7 Selected Bond Lengths (Å) and Angles (°) for $\{[Ni(tren)]_4[Hg(CN)_2]_8Cl_6\}HgCl_4$ (**3.10**)[a].

Selected Atoms	*Bond Lengths*	*Selected Atoms*	*Bond Lengths*
Hg(1)-C(1)	2.06(3)	Hg(1)-C(2)	2.04(4)
Hg(1)-Cl(1')	2.92(1)	Hg(2)-C(3)	2.06(3)
Hg(1)-Cl(1)	2.825(9)	Hg(1)-Cl(2)	3.187(9)
Hg(2)-Cl(2)	2.754(9)	Hg(2)-Cl(2*)	2.768(9)
Hg(2)-C(4)	2.09(3)	Hg(3)-Cl(3)	2.48(1)
Ni(1)-N(5)	2.10(3)	Ni(1)-N(6)	2.11(3)
Ni(1)-N(7)	2.03(3)	Ni(1)-N(8)	2.01(3)
Ni(1)-N(1)	2.13(3)	Ni(1)-N(3)	2.06(3)
Selected Atoms	*Bond Angles*	*Selected Atoms*	*Bond Angles*
C(1)-Hg(1)-C(2)	174.0(15)	Cl(1)-Hg(1)-C(1)	95.0(11)
Cl(1)-Hg(1)-Cl(2)	106.0(3)	Cl(1')-Hg(1)-Cl(2)	164.2(3)
Cl(1)-Hg(1)-Cl(1')	89.72(4)	Cl(1')-Hg(1)-C(1)	98.5(11)
Cl(1)-Hg(1)-C(2)	90.1(12)	Cl(1')-Hg(1)-C(2)	84.8(12)
Cl(2)-Hg(2)-C(3)	91.5(10)	Cl(2*)-Hg(2)-C(3)	94.1(10)
Cl(2)-Hg(2)-C(4)	94.6(8)	Cl(2*)-Hg(2)-C(4)	99.2(8)
C(3)-Hg(2)-C(4)	163.5(12)	Cl(2)-Hg(2)-Cl(2*)	104.6(3)
N(5)-Ni(1)-N(6)	93.7(11)	N(5)-Ni(1)-N(7)	163.0(13)
N(6)-Ni(1)-N(7)	94.4(13)	N(5)-Ni(1)-N(8)	82.0(12)
N(6)-Ni(1)-N(8)	84.2(11)	N(7)-Ni(1)-N(8)	83.9(13)
N(5)-Ni(1)-N(1)	87.4(11)	N(6)-Ni(1)-N(1)	178.8(11)
N(7)-Ni(1)-N(1)	84.5(13)	N(8)-Ni(1)-N(1)	95.8(11)
N(5)-Ni(1)-N(3)	95.0(12)	N(6)-Ni(1)-N(3)	96.4(11)
N(7)-Ni(1)-N(3)	99.0(12)	N(8)-Ni(1)-N(3)	177.0(13)
N(1)-Ni(1)-N(3)	83.7(11)	Hg(2)-Cl(2)-Hg(2*a)	101.9(3)
Hg(1)-Cl(1)-Hg(1")	92.9(4)	Hg(1)-Cl(1)-Hg(1'a)	166.25(7)
Hg(1")-Cl(1)-Hg(1'a)	91.33(4)	Hg(1)-Cl(1)-Hg(1*)	91.33(4)
Hg(1")-Cl(1)-Hg(1*)	166.25(4)	Hg(1'a)-Cl(1)-Hg(1*)	88.3(4)

[a] Symmetry transformations as *x, y, z*: (*) y+1/2, x-1/2, z+1/2; (*a) y+1/2, x-1/2, z-1/2, (') -y+3/2, -x+3/2, z-1/2; ('a) -y+3/2, -x+3/2, z+1/2; (") -x+2, -y+1, z.

A third chloride bridge to the $Hg(CN)_2$ unit, N-bound to the same Ni(II) centre (Hg(1)-Cl(2) = 3.187(9) Å) is also formed. The Cl(1) atoms forms two chloride bridges between two different Hg(1) centres (Cl(1)-Hg(1) = 2.825(9) Å, Cl(1)-Hg(1'a) = 2.92(1) Å) of the same Hg(2) containing chain and another two chloride bridges between two different Hg(1) centres of a second Hg(2) containing chain resulting in a complex 1-D $\{[Ni(tren)]_4[Hg(CN)_2]_8Cl_6\}^{2+}$ ribbon

(Figure 3.16). The Hg(1) centres have an effective distorted square pyramidal geometry (2+3) with two chloride and two cyano ligands in *trans* positions making up the basal plane; a third Cl ligand is found in the apical position, as observed for the 1-D $[Hg(CN)_2Cl]_n^{n-}$ ladders of $[Cu(en)_2][Hg(CN)_2Cl]_2$ (**2.5**).[169]

The double salt complex **3.10** crystallizes in the non-centrosymmetric, tetragonal space group $P\bar{4}2_1c$, suggesting that interesting optical properties such as second harmonic generation (SHG) may be accessed.[205] The tetrahedral $[HgCl_4]^{2-}$ moieties, which charge-balance the cationic ribbons, template the 3-D packing of the $\{[Ni(tren)]_4[Hg(CN)_2]_8Cl_6\}^{2+}$ ribbons via the formation of weak N-H···Cl interactions (Cl(3)-Namine = 3.500 Å, 3.569 Å, 3.590 Å) into a 3-D superstructure (Figure 3.17).

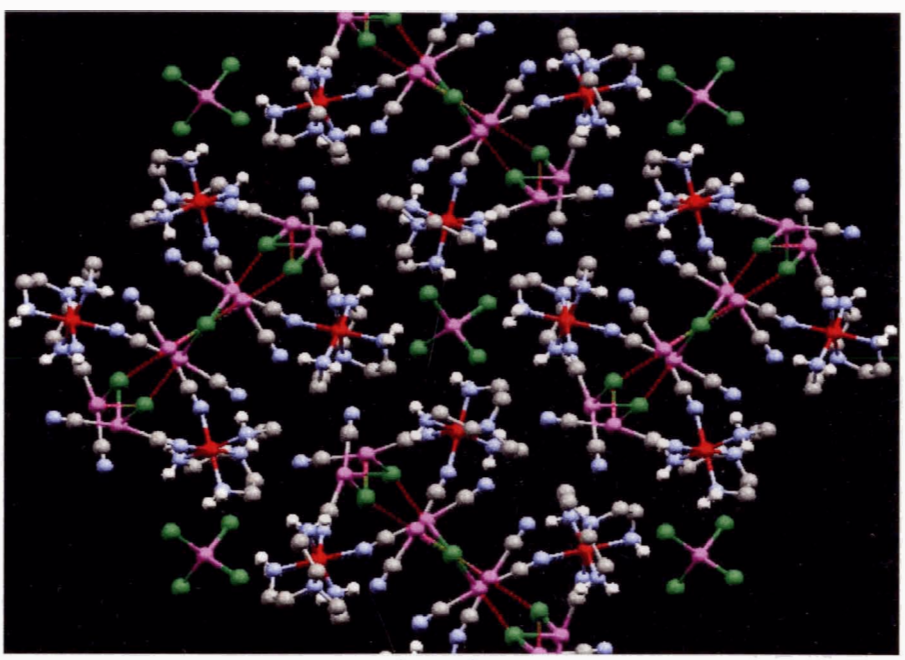

Figure 3.17 3-D extended structure of $\{[Ni(tren)]_4[Hg(CN)_2]_8Cl_6\}HgCl_4$ (**3.10**) as viewed down the *c*-axis.
Methylene hydrogen atoms have been omitted for clarity. Colour scheme: Hg, pink; Ni, red; Cl, green; N, blue; C, grey; H, white.

3.2.9 Magnetic Properties

For most of the reported complexes, the paramagnetic transition metal centres are well separated in space with no viable magnetic coupling pathway. However **3.5**, **3.6**, and **3.7** all have

structural features that might mediate magnetic interactions. Accordingly, the temperature (T) dependence of the molar magnetic susceptibility (χ_M) of polycrystalline samples of these three compounds were measured from 1.8-300 K.

For **3.6**, μ_{eff} = 2.65 μ_B (per Cu(II)-pair) at 300 K, and remains constant until 30 K, at which point it decreases, reaching 2.18 μ_B at 1.8 K. No maximum in χ_M *vs.* T is observed. This behaviour is consistent with weak antiferromagnetic (AF) exchange between S = ½ Cu(II) centres. The data can be fit to the Curie-Weiss Law, with C = 0.892(1) and θ = -0.868(9) K, consistent with weak antiferromagnetic coupling between the Cu(II) centres. From the X-ray structure, the two Cu(II) centres are connected via a nearly linear Cl-Hg-Cl chain (Figure 3.8); each pair of such Cu(II) centres is magnetically (but not structurally) isolated from the next. Thus, **3.6** can be treated as a simple bimetallic Cu(II) species and accordingly, the magnetic data was fitted with the Bleaney-Bowers dimer model (using $\hat{H} = -2JS_1S_2$)[187] to yield J = -0.70(1) cm^{-1} and g = 2.16(1). This interaction is quite weak on account of the long Hg-Cl bonds (3.2800(16) Å) that disrupt the exchange pathway.

The magnetic behaviour of **3.5** is very similar to **3.6**. The μ_{eff} = 1.92 μ_B at 300 K and is temperature-independent until 30 K, upon which it drops to 1.58 μ_B at 2 K. The data can be fit to the Curie-Weiss Law, with C = 0.4642(9) and θ = -0.87(2) K, consistent with weak antiferromagnetic coupling between the Cu(II) centres. The pathway for the AF interactions in **3.5** is also a Cl-Hg-Cl bridge but in this case the Cu(II) centres form a 1-D chain (Figure 3.6), hence the magnetic data was fitted using the theoretical expression for a 1-D AF chain of S = ½ centers[190] to give best-fit values of J = -0.45(1) cm^{-1} and g = 2.22(1). Unlike **3.6**, the Cl-Hg-Cl bridge in **3.5** is not linear but kinked, and the Cu(II) centres are connected in an equatorial / axial fashion. Despite this difference, the magnitude of the coupling interaction is similar and weak, but stronger than that found in {[Cu(bipy)Hg(CN)$_2$Cl$_2$]$_2$Hg(CN)$_2$} which has a linear, axial / axial Cl-Hg-Cl bridge mediating Cu(II) magnetic exchange.[195]

As would be expected, **3.7**, which contains a chloro-bridged Cu(dien) dimer cation, shows the strongest magnetic interaction. At 300 K, $\mu_{eff} = 2.57\ \mu_B$ (per dimer) and this remains unchanged until 4 K, at which point it drops reaching 1.58 μ_B at 1.8 K. Importantly, there is a maximum in χ_M at 3.5 K (Figure 3.14), indicative of significant AF interactions.[68] The data can be fit to the Curie-Weiss Law, with C = 0.884(17) and θ = -1.75(19) K, consistent with antiferromagnetic coupling between the Cu(II) centres. An examination of the structure (Figure 3.10) shows that the $[Cu(dien)(\mu\text{-}Cl)]_2^{2+}$ dimers are connected in a 2-D array via Cl-Hg-Cl bridges similar to **3.5**. Thus the magnetic data was fitted using the Bleaney-Bowers equation with an additional magnetic field parameter (zJ') to account for the weaker interdimer interactions and a paramagnetic impurity factor (P).[68] This gave best fit values of J = -1.16(11) cm^{-1}, g = 2.08(5), P = 0.003, and zJ' = -0.14(1) cm^{-1}; the fit is shown as a solid line in Figure 3.18. The edge-sharing apical / basal coordination geometry of **3.7** is less common than edge-shared basal / basal systems.[210] Other examples similar to **3.7** include $[Cu(dien)(\mu\text{-}Cl)]_2(ClO_4)_2$[211] and $[Cu(terpy)(\mu\text{-}Cl)]_2(PF_6)_2$,[204] which show magnetic exchange interactions of J = -5.9 and +0.4 cm^{-1} respectively. A magnetostructural correlation[210] based on the Cu-Cl-Cu angle has been proposed and it predicts an antiferromagnetic interaction of -11.5 cm^{-1}, however only three compounds were used to define the correlation. The J-value in **3.7** is found to be significantly smaller than the Cu-Cl-Cu angle-based prediction due to the extreme asymmetry of the Cu-Cl bond lengths in **3.7** (2.7608(17) and 2.2875(17) Å); the related complexes used for the magnetostructural correlation have more symmetric copper-chloride cores than that found in **3.7**. That said, theoretical calculations[212] suggest that the coupling in these apical / basal systems should generally be weak and this is certainly reflected in the magnetic data for **3.7**. Also, the weak interdimer interaction (zJ') in **3.7** is consistent with the fact that it is mediated by long (> 3.2 Å) Hg-Cl bonds, as is the case for the weak coupling in **3.6**.

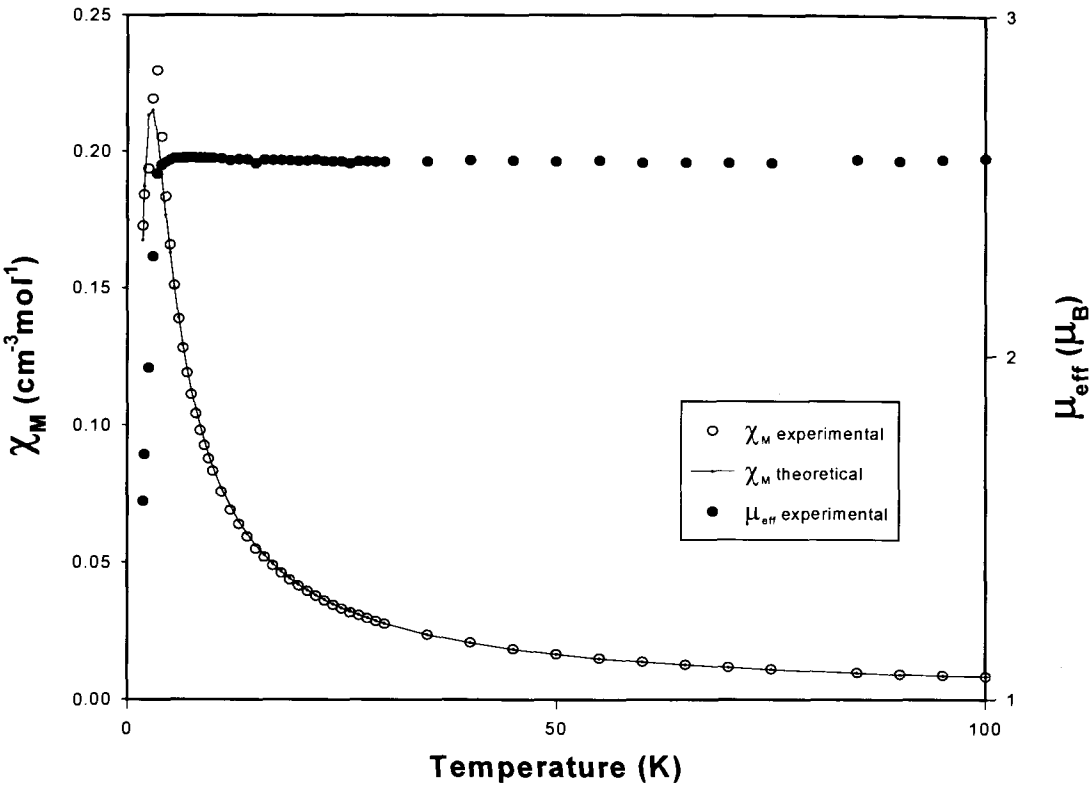

Figure 3.18 Temperature dependence of χ_M and μ_{eff} for **3.7**; a maximum at 4 K is observable. The solid line is theory (see text).

3.3 DISCUSSION

In an effort to comprehend the type of bridging mode (chloride *versus* *N*-cyano) favoured in the transition metal organoamine double salt mercurates, structures **3.1-3.10** can be examined by considering the effects of (a) the transition metal used, (b) the effective coordination sphere of the transition metal (i.e.: capping ligand employed), and (c) the capping ligand basicity. None of the transition metal cations utilized here in this study are coordinately saturated, thus ensuring either chloride or *N*-cyano coordination to the transition metal centre.

3.3.1 Infrared Analysis

The IR spectra for **3.1-3.6** (Table 3.8) which contain aromatic-amine capping ligands, are unusual in that there is a lack of consistency between the expected structure as predicted by the cyanide stretches, and the observed structure as shown by X-ray crystallography. The observed ν_{CN} stretches for **3.1-3.5** have such weak intensities (with the exception of **3.3**) that it is difficult

to assess whether or not $Hg(CN)_2$ had been incorporated in the compound formed; X-ray crystallography and elemental analysis confirmed the presence of $Hg(CN)_2$ moieties.

Table 3.8 Comparison of cyanide (ν_{CN}) absorptions (cm^{-1}) for complexes **3.1-3.10**.

Complex	*Bridging* ν_{CN}	*Terminal* ν_{CN}
$[Mn(bipy)_2(\mu\text{-}Cl)_2Hg(CN)_2]$ (**3.1**)[213]		2180 (vw), 2147 (vw)
$[Mn(phen)_2(\mu\text{-}Cl)_2Hg(CN)_2]$ (**3.2**)[213]		2180 (vw)
$[Ni(bipy)_2(\mu\text{-}Cl)_2Hg(CN)_2]$ (**3.3**)[213]		2172 (m), 2150 (vw)
$[Ni(phen)_2(\mu\text{-}Cl)_2Hg(CN)_2]$ (**3.4**)[213]		2173 (vw)
$[Cu(terpy)Cl_2(\mu\text{-}Hg(CN)_2)]$ (**3.5**)[213]		2177 (vw)
$\{[Cu(phen)_2Cl]_2Hg(CN)_2[Hg(CN)_2Cl]_2\}$(**3.6**)[213]		2166 (m)
$[Cu(dien)Cl][Hg(CN)_2Cl]$ (**3.7**)[213]		2178 (w)
$[Cu(tren)Hg(CN)_2Cl][HgX_2Cl]$ (**3.8**)[213]	2214 (m)	2178 (w)
$\{[Ni(en)_2][Hg(CN)_2]_3Cl_2\}_2$ (**3.9**)	2217 (w), 2207 (w)	2186 (w)
$\{[Ni(tren)]_4[Hg(CN)_2]_8Cl_6\}HgCl_4$ (**3.10**)[213]	2215 (m)	2184 (w)
$[Cu(en)_2][Hg(CN)_2Cl]_2$ (**2.5**)[169]		2175 (w)

Values are determined from the maximum of the absorption peak. IR spectrometer resolution = ± 2 cm^{-1}; all spectra were collected as KBr pellets.

The ν_{CN} stretches range from 2147 cm^{-1} (**3.1**) to 2180 cm^{-1} (**3.1** and **3.2**) and are consistent with terminal cyanide groups on non-linear Hg(II) units with coordination numbers greater than two. No reasonable explanation can be given as to why the two molecular complexes containing bipy (**3.1** and **3.3**) show two ν_{CN} stretches while those containing phen (**3.2** and **3.4**) show only one ν_{CN} stretch, even though the Hg(II) effective coordination and C-N bond lengths of **3.1-3.4** are nearly identical (see Table 3.1).

The minimal effect of Hg-NC interactions on the cyanide stretching frequency is apparent from the IR spectrum of **3.6** which shows no shifted bands despite the presence of such interactions (Figure 3.7). There is a general consistency between the expected structure as predicted by the cyanide stretches and the observed structure from X-ray analysis for compounds **3.7-3.10** which contain alkylamine ligands. The IR spectra of **3.7-3.10** clearly show the presence of the cyano groups and are displayed in Table 3.8. All four compounds show ν_{CN} stretches

consistent with that of terminal cyanide groups on non-linear Hg(II) units with coordination numbers greater than two (2178 cm^{-1} to 2186 cm^{-1}), comparable with those reported in Table 2.8. Compounds **3.8-3.10** show additional ν_{CN} stretches consistent with bridging cyanomercurate groups (2207 cm^{-1} to 2217 cm^{-1}) such as those found for $\{Zn(H_2O)_4[Hg(CN)_2]_2\}(NO_3)_2$ (ν_{CN} = 2230 cm^{-1}).[60] Compound **3.8** shows a single terminal ν_{CN} stretch and a single bridging ν_{CN} stretch consistent with the two cyano groups shown in Figure 3.7 a. Compound **3.9** shows a single terminal ν_{CN} stretch and two bridging ν_{CN} stretches, although there are eight different terminal and four different bridging cyano groups. Compound **3.10** shows a single terminal ν_{CN} stretch and a single bridging ν_{CN} stretch, although there are two different terminal and two different bridging cyano groups.

3.3.2 Influence of Transition Metal and Its Coordination Sphere

When two equivalents of bipy and phen are employed with Mn(II) or Ni(II) centres, blocking four of six possible coordination sites, only molecular complexes incorporating $Hg(CN)_2$ units are obtained (**3.1-3.4**) after the addition of $Hg(CN)_2$; migration of the chloride ligands does not occur and there is no increase in structural dimensionality. However, changing the transition metal to Cu(II) causes partial migration of the chloride ligands (from Cu(II) to Hg(II)) to occur, resulting in the formation of new moieties (e.g. $[Hg(CN)_2Cl]_2^{2-}$) and an increase in structural dimensionality to a 1-D chain in the case of **3.6**. The increased lability of Cu(II) *vs.* the more inert Mn(II) or Ni(II) centres may enable this facile chloride migration to occur. Although chloride migration from Cu(II) does not occur upon substitution of bipy or phen for one equivalent of terpy, an increase of dimensionality also occurs (complex **3.5**). In this case, the plasticity of the Cu(II) centre enables a facile change in coordination sphere of the Cu(II) from octahedral to distorted trigonal bipyramidal geometry also resulting in the formation of a 1-D chain. Typically, an increase in the number of available coordination sites at the transition metal site by changing the amine ligand should result in an increase in structural dimensionality. In this

case, with the use of neutral $Hg(CN)_2$, it is difficult to ascertain the impact of different denticity amines due to the fact that the chloride atoms can act as ligands themselves - there is not a clear correlation of capping amine denticity and structural dimensionality.

3.3.3 Influence of Ligand Basicity

On the other hand, the basicity of the amine capping ligand appears to be a very important factor influencing the type of structure that is observed. Thus, systems containing the basic trialkylamine ligand tren have $Hg(CN)_2$ units N-bound to the transition metal; this generally results in an increase in structural dimensionality and particularly complicated, interesting structures that may have useful materials properties (e.g. **3.10**). In the highly birefringent 2-D layer structure $\{Cu(tmeda)[Hg(CN)_2]_2\}HgCl_4$, which has four N-bound cyano units per copper(II), the capping ligand is also a trialkylamine (tmeda),[205] as described in Chapter 4. Compounds containing the much less basic heterocyclic amine ligands bipy, phen and terpy as capping ligands do not, for the most part, have N-bound $Hg(CN)_2$ units and generally have a lower overall dimensionality as compared with the tren-containing structures. The dien capping group has an intermediate basicity and thus **3.7** shows elements of systems containing both types of ligand.

The impact of ligand basicity can be rationalized in terms of its influence on the transition-metal electron density. In these syntheses, both chloro- and *N*-cyano ligands are present and either (or both) can bind to the transition-metal (which also has a particular lability, as described above). A more electron-deficient transition-metal cation would likely opt to ligate the Cl^- units, which are good π-donors, rather than the π-accepting nitrile moieties of $Hg(CN)_2$, resulting in the chloride-bound structures observed in **3.1**-**3.7**. Upon use of a basic capping ligand such as tren, however, the resulting electron-rich transition-metal cation more appropriately interacts with the π-accepting nitrile donors, yielding the *N*-cyano bridged structures **3.8** and **3.10**. It was observed that ligand basicity was not observed to have a significant impact in a related study of amine-

capped transition metal cations with $[M(CN)_2]^-$ (M=Au, Ag)[79,82] as, in these cases, the nitrile donors are significantly more basic in their own right.

The use of two equivalents of ethylenediamine with Ni(II) results in *N*-cyano coordination of $Hg(CN)_2$ to the Ni(II) centre and an increase in structural dimensionality, as observed for the 2-D layer structure of **3.9**. Although the en ligand is a monoalkylamine and less basic than tren, two en equivalents donate sufficient electron density to the Ni(II) centre so that the neutral $Hg(CN)_2$ moieties are ligated rather than the Cl^- anions. This enables the Cl^- anions to fully migrate from Ni(II) to the more Lewis-acidic Hg(II) centres forming 1-D mercury cyanide / chloride anionic chains. The two en ligands used in **2.5** also results in full migration of the Cl^- anions from the Cu(II) centre to the unsaturated Hg(II) centres, but *N*-cyano coordination of $Hg(CN)_2$ does not occur as indicated by the lack of bridging ν_{CN} stretches in the IR (Table 3.8). In this case, the plasticity of the Cu(II) centre enables a facile change in coordination sphere of the Cu(II) from Jahn-Teller distorted octahedral to square planar geometry, effectively eliminating the requirement of *N*-cyano coordination to the Cu(II) centres.

3.4 CONCLUSIONS

The bimetallic coordination polymers formed by the addition of $Hg(CN)_2$ to $[TML_x]Cl_2$ show several structural motifs including molecular dimers, one-dimensional chains and ribbons, two-dimensional layers, and three dimensional extended structures. The d^{10} Hg(II) centres do not form metallophilic bonds like their gold and silver counterparts, but increase dimensionality by acting as low-coordinate Lewis acids, accepting chloride ligands from transition metal complexes in both bridging and non-bridging fashions. It has been illustrated that the formation of higher coordinate mercury cyanide / chloride double salt moieties invokes competition between halide and *N*-cyano coordination to unsaturated transition metal complexes. Although there is no correlation of capping amine ligand denticity and structural dimensionality, the amine's basicity significantly influences the structure type. Basic alkylamines promote *N*-cyano binding of

$Hg(CN)_2$ to the transition metal cations, yielding complex, high-dimensionality structures. By expanding the range of capping ligand basicities, further control and an increase in structural dimensionality in $Hg(CN)_2$-based coordination polymers should be attainable, thereby potentially enhancing their useful bulk materials properties. It was also shown that the $Hg(CN)_2$ units can mediate magnetic exchange through the diamagnetic Hg(II) centre, thereby increasing the magnetic dimensionality of the coordination polymers.

3.5 EXPERIMENTAL

General experimental details were as indicated in Chapter 2, with the following exceptions:

3.5.1 X-ray Crystallography

Dr. R. Batchelor collected the data and solved the X-ray structure for complex **3.7**. The diffraction data for **3.1**, **3.5-3.8**, and **3.10** were acquired on an Enraf Nonius CAD4F diffractometer as described in Chapter 2. However, the diffraction data for **3.2-3.4** and **3.9** were acquired on a Rigaku RAXIS-Rapid curved image plate area detector with graphite monochromatic Cu Kα radiation. Indexing was performed from three, 5° oscillations that were exposed for 90 seconds. The data were collected at a temperature of 293 K. The following data ranges were recorded: **3.2** = $6.9° \leq 2\theta \leq 136.5°$; **3.3** = $11.0° \leq 2\theta \leq 136.5°$; **3.4** = $10.0° \leq 2\theta \leq 136.5°$; **3.9** = $8° \leq 2\theta \leq 137°$; A total of 18 images each were collected for **3.2** and 27 images for **3.3**, **3.4**, and **3.9**. A sweep of data for **3.2** was done using ω scans from 50.0° to 230.0° in 30° steps, at $\chi = 50.0°$ and $\phi = 0.0°$. A second sweep was performed done using ω scans from 50.0° to 230.0° in 30° steps, at $\chi = 50.0°$ and $\phi = 90.0°$. A final sweep was performed done using ω scans from 50.0° to 230.0° in 30° steps, at $\chi = 50.0°$ and $\phi = 180.0°$. The exposure rate for **3.2-3.4**, and **3.9** was 90 sec/°. A sweep of data for **3.3, 3.4**, and **3.9** was done using ω scans from 50.0° to 230.0° in 20° steps, at $\chi = 50.0°$ and $\phi = 0.0°$. A second sweep was performed done using ω scans from 50.0° to 230.0° in 20° steps, at $\chi = 50.0°$ and $\phi = 90.0°$. A final sweep was

performed done using ω scans from 50.0° to 230.0° in 20° steps, at χ = 50.0° and ϕ = 180.0°. In each case, the crystal-to-detector distance was 127.40 mm. An empirical absorption correction[214] was applied which resulted in the following transmission ranges: **3.2** = 0.3388 – 1; **3.3** = 0.2363 – 1; **3.4** = 0.2718 – 1; **3.9** = 0.1794 – 1.[214] The data were worked up using RAPID-AUTO[215] and the resultant '*h k l*' files were inputted into *CRYSTALS*[180] where the structures were solved and refined.

3.5.2 Magnetic Susceptibility

For complexes **3.5-3.7**, variable temperature magnetic susceptibility data were collected using a Quantum Design SQUID MPMS-5S (**3.5**) or an Evercool XL-7 magnetometer (**3.6**, **3.7**) working down to 2 K or 1.8 K at a field strength of 1 T. Sample **3.5** was measured in a cylindrical, airtight sample holder constructed from PVC[216] while **3.6** and **3.7** were measured in low background gel caps and straws. The data were corrected for TIP, the diamagnetism of the sample holder and the constituent atoms (by use of Pascal constants).[68]

3.5.3 Preparation of $[Mn(bipy)_2(\mu\text{-}Cl)_2Hg(CN)_2]$ (3.1)

To a 5 mL methanolic solution of $MnCl_2 \cdot 4\ H_2O$ (0.078 g, 0.39 mmol), a 10 mL methanolic solution of bipy (0.124 g, 0.79 mmol) was added, while stirring. A 5 mL methanolic solution of $Hg(CN)_2$ (0.100 g, 0.40 mmol) was added to this pale yellow solution and was stirred for 2 minutes. After leaving the mixture covered for one day, small yellow crystal bars of $[Mn(bipy)_2(\mu\text{-}Cl)_2Hg(CN)_2]$ (**3.1**) were collected by vacuum filtration, washed with two 1 mL portions of cold methanol, and were left to air dry. Yield: 0.186 g (68%). Anal. Calcd. for $C_{22}H_{16}N_6Cl_2HgMn$: C, 38.25; H, 2.33; N, 12.16. Found: C, 38.09; H, 2.25: N, 11.82. IR (KBr, cm^{-1}): 3190 (w), 3106 (m), 3073 (m), 3060 (m), 3031 (w), 2983 (w), 2950 (w), ν_{CN} **2180** (**vw**), **2147** (**vw**), 2040 (w), 1996 (w), 1960 (m), 1923 (w), 1887 (w), 1853 (w), 1617 (m), 1602(s), 1596 (s), 1574 (m), 1563 (m), 1539 (w), 1507 (m), 1492 (s), 1477 (s), 1443 (s), 1399 (m), 1363 (w), 1340 (w), 1317 (m), 1283 (w), 1249 (m), 1218 (w), 1184 (m), 1160 (s), 1120 (w), 1102 (m), 1074

(m), 1062 (s), 1041 (w), 1015 (s), 962 (w), 910 (w), 892 (m), 816 (m), 773 (s), 766 (s), 738 (s), 649 (s), 627 (m), 412 (s).

3.5.4 Preparation of $[Mn(phen)_2(\mu\text{-}Cl)_2Hg(CN)_2]$ (3.2)

To a 5 mL methanolic solution of $MnCl_2 \cdot 4\ H_2O$ (0.078 g, 0.39 mmol), a 10 mL methanolic solution of phen (0.157 g, 0.79 mmol) was added, while stirring. A 5 mL aqueous solution of $Hg(CN)_2$ (0.100 g, 0.40 mmol) was added to this pale yellow solution and was stirred for 2 minutes. After leaving the mixture covered for one day, small yellow crystal bars of $[Mn(phen)_2(\mu\text{-}Cl)_2Hg(CN)_2]$ (**3.2**) were collected by vacuum filtration, washed with two 1 mL portions of cold methanol, and were left to air dry. Yield: 0.232 g (80%). Anal. Calcd. for $C_{26}H_{16}N_6Cl_2HgMn$: C, 42.26; H, 2.18; N, 11.37. Found: C, 42.43; H, 2.25: N, 11.11. IR (KBr, cm^{-1}): 3734 (w), 3093 (w), 3051 (m), 3018 (w), 2994 (w), 2940 (w), 2915 (w), 2877 (w), 2830 (w), 2650 (w), 2620 (w), 2600 (w), ν_{CN} **2180 (vw)**, 1983 (m), 1837 (w), 1803 (w), 1777 (w), 1625 (s), 1589 (s), 1576 (m), 1540 (m), 1514 (s), 1499 (m), 1456 (m), 1425 (vs), 1363 (w), 1341 (m), 1302 (w), 1260 (w), 1228 (w), 1149 (m), 1104 (s), 1088 (w), 1031 (w), 985 (w), 940 (w), 898 (w), 864 (vs), 857 (vs), 785 (m), 730 (vs), 723 (vs), 639 (m), 555 (w), 510 (w), 474 (w), 421 (s).

3.5.5 Preparation of $[Ni(bipy)_2(\mu\text{-}Cl)_2Hg(CN)_2]$ (3.3)

To a 5 mL aqueous solution of $NiCl_2 \cdot 6\ H_2O$ (0.094 g, 0.40 mmol), a 10 mL methanolic solution of bipy (0.124 g, 0.79 mmol) was added, while stirring. After reducing the total volume to 5 mL, a 5 mL aqueous solution of $Hg(CN)_2$ (0.100 g, 0.40 mmol) was added to this pale purple solution and was stirred for 2 minutes. The solution was allowed to slowly evaporate. Small pale green crystal blocks of $[Ni(bipy)_2(\mu\text{-}Cl)_2Hg(CN)_2]$ (**3.3**) were collected by vacuum filtration, washed with two 1 mL portions of cold water followed by two 1 mL portions of cold methanol, and were left to air dry. Yield: 0.154 g (56%). Anal. Calcd. for $C_{22}H_{16}N_6Cl_2HgNi$: C, 38.04; H, 2.32; N, 12.01. Found: C, 37.87; H, 2.32: N, 11.88. IR (KBr, cm^{-1}): 3199 (w), 3108 (m), 3078 (m), 3057 (m), 3035 (m), 2986 (w), 2963 (w), 2913 (w), 2882 (w), 2777 (w), 2677 (w), 2627 (w),

ν_{CN} **2172 (m), 2150 (vw)**, 2040 (w), 1994 (w), 1963 (w), 1917 (w), 1887 (w), 1850 (w), 1783 (w), 1678 (w), 1617 (m), 1600 (s), 1566 (m), 1537 (m), 1507 (m), 1494 (s), 1475 (s), 1449 (s), 1417 (m), 1403 (w), 1360 (w), 1316 (s), 1283 (m), 1251 (m), 1223 (w), 1181 (m), 1162 (s), 1125 (w), 1107 (m), 1060 (m), 1043 (m), 1023 (s), 999 (m), 960 (m), 905 (m), 892 (m), 815 (s), 768 (s), 736 (s), 654 (s), 664 (m), 462 (w), 449 (m), 441 (m), 418 (s), 414 (s).

3.5.6 Preparation of $[Ni(phen)_2(\mu\text{-}Cl)_2Hg(CN)_2]$ (3.4)

To a 5 mL aqueous solution of $NiCl_2 \cdot 6\ H_2O$ (0.094 g, 0.40 mmol), a 10 mL methanolic solution of phen (0.157 g, 0.79 mmol) was added with stirring. After reducing the total volume to 5 mL, a 5 mL aqueous solution of $Hg(CN)_2$ (0.100 g, 0.40 mmol) was added to this pink solution and was stirred for 2 minutes. The solution was allowed to slowly evaporate. Small pale blue crystal platelets of $[Ni(phen)_2(\mu\text{-}Cl)_2Hg(CN)_2]$ (**3.4**) were collected by vacuum filtration, washed with two 1 mL portions of cold water followed by two 1 mL portions of cold methanol, and were left to air dry. Yield: 0.182 g (62%). Anal. Calcd. for $C_{22}H_{16}N_6Cl_2HgNi$: C, 42.05; H, 2.17; N, 11.32. Found: C, 41.79; H, 2.21: N, 11.21. IR (KBr, cm^{-1}): 3090 (w), 3053 (m), 3019 (w), 2990 (w), 2923 (w), 2881 (w), ν_{CN} **2173 (vw)**, 1994 (m), 1886 (w), 1842 (w), 1803 (w), 1777 (w), 1716 (w), 1626 (m), 1600 (m), 1580 (m), 1539 (m), 1514 (s), 1500 (m), 1456 (m), 1426 (s), 1342 (m), 1307 (m), 1256 (w), 1230 (m), 1201 (w), 1150 (s), 1107 (m), 1050 (m), 986 (m), 945 (w), 905 (w), 869 (s), 857 (vs), 812 (w), 786 (s), 728 (vs), 643 (m), 509 (w), 484 (w), 425 (s), 414 (m), 404 (m).

3.5.7 Preparation of $[Cu(terpy)Cl_2(\mu\text{-}Hg(CN)_2)]$ (3.5)

To a 10 mL aqueous solution of $CuCl_2 \cdot 2\ H_2O$ (0.075 g, 0.44 mmol), a 5 mL methanolic solution of terpy (0.103 g, 0.44 mmol) was added, while stirring. A 5 mL aqueous solution of $Hg(CN)_2$ (0.112 g, 0.44 mmol) was added to the green solution and was stirred for 2 minutes. The solution was allowed to slowly evaporate. Large dark green crystal bars of $[Cu(terpy)Cl_2(\mu\text{-}Hg(CN)_2)]$ (**3.5**) were collected by vacuum filtration, washed with two 1 mL portions of cold

water followed by two 1 mL portions of cold methanol, and were left to air dry. Yield: 0.252 g (91%). Anal. Calcd. for $C_{17}H_{15}N_5Cl_2CuHg$: C, 32.92; H, 1.72; N, 11.29. Found: C, 33.20; H, 1.79; N, 11.14. IR (KBr, cm^{-1}): 3195 (w), 3137 (w), 3074 (m), 3035 (w), 2997 (w), 2927 (w), 2860 (w), 2770 (w), ν_{CN} **2177 (vw)**, 2037 (w), 1936 (w), 1893 (w), 1860 (w), 1807 (w), 1764 (w), 1599 (s), 1574 (m), 1566 (m), 1539 (w), 1500 (m), 1475 (s), 1450 (s), 1419 (m), 1410 (m), 1387 (m), 1363 (w), 1328 (s), 1302 (s), 1289 (m), 1255 (s), 1244 (m), 1187 (m), 1176 (m), 1141 (w), 1118 (w), 1098 (m), 1070 (m), 1038 (m), 1021 (s), 1009 (m), 978 (w), 902 (w), 834 (m), 784 (vs), 734 (s), 726 (m), 671 (m), 651 (s), 539 (w), 515 (m), 438 (m), 423 (m), 411 (m).

3.5.8 Preparation of $\{[Cu(phen)_2Cl]_2Hg(CN)_2[Hg(CN)_2Cl]_2\}$ (3.6)

To a 10 mL aqueous solution of $CuCl_2 \cdot 2\ H_2O$ (0.135 g, 0.79 mmol), a 20 mL methanolic solution of phen (0.314 g, 1.58 mmol) was added, while stirring. A 15 mL aqueous solution of $Hg(CN)_2$ (0.300 g, 1.19 mmol) was added to this green solution and was stirred for 2 minutes. After leaving the mixture covered for one day, small green crystal platelets of $\{[Cu(phen)_2Cl]_2Hg(CN)_2[Hg(CN)_2Cl]_2\}$ (**3.6**) were collected by vacuum filtration, washed with two 2 mL portions of cold water followed by two 2 mL portions of cold methanol, and were left to air dry. Crystals suitable for X-ray crystallographic studies were obtained upon slow evaporation of the solution mixture. These larger crystals has identical IR spectra and elemental analysis with the smaller crystals originally collected. Yield: 0.594 g (86%). Anal. Calcd. for $C_{54}H_{32}N_{14}Cl_4Cu_2Hg_3$: C, 37.11; H, 1.85; N, 11.22. Found: C, 37.09; H, 1.94; N, 11.05. IR (KBr, cm^{-1}): 3092 (m), 3070 (m), 3059 (m), 3013 (m), 2621 (w), 2513 (w), 2293 (w), ν_{CN} **2166 (m)**, 2000 (w), 1975 (w), 1955 (w), 1936 (w), 1899 (w), 1833 (w), 1809 (w), 1783 (w), 1760 (w), 1627 (m), 1608 (m), 1582 (s), 1519 (s), 1495 (s), 1456 (m), 1427 (vs), 1341 (m), 1322 (m), 1312 (m), 1255 (w), 1224 (s), 1208 (m), 1145 (s), 1106 (s), 1037 (w), 1004 (w), 987 (m), 952 (m), 911 (w), 870 (s), 854 (vs), 846 (vs), 787 (m), 774 (m), 724 (vs), 649 (s), 557 (w), 508 (w), 430 (s), 417 (m).

3.5.9 Preparation of [Cu(dien)Cl][Hg(CN)$_2$Cl] (3.7)

To a 5 mL methanolic solution of $CuCl_2 \cdot 2\ H_2O$ (0.067 g, 0.39 mmol), a 10 mL methanolic solution of dien (0.041 g, 0.39 mmol) was added, while stirring. A 5 mL methanolic solution of $Hg(CN)_2$ (0.100 g, 0.40 mmol) was added to this dark blue solution and was stirred for 2 minutes. The solution was allowed to slowly evaporate. Dark blue crystal bars of [Cu(dien)Cl][Hg(CN)$_2$Cl] (**3.7**) were collected by vacuum filtration, washed with two 1 mL portions of cold methanol, and were left to air dry. Yield: 0.133 g (69%). Anal. Calcd. for $C_6H_{13}N_5Cl_2CuHg$: C, 14.70; H, 2.67; N, 14.29. Found: C, 14.80; H, 2.79; N, 14.05. IR (KBr, cm^{-1}): 3286 (vs), 3244 (vs), 3234 (vs), 3136 (m), 2971 (m), 2959 (m), 2918 (w), 2884 (m), ν_{CN} **2178 (w)**, 1844 (w), 1830 (w), 1712 (s), 1636 (w), 1594 (m), 1580 (m), 1460 (m), 1436 (m), 1362 (m), 1318 (w), 1301 (w), 1223 (m), 1136 (m), 1124 (m), 1092 (s), 1024 (s), 1000 (m), 954 (s), 922 (w), 882 (w), 833 (w), 659 (m), 637 (w), 529 (m), 460 (w).

3.5.10 Preparation of [Cu(tren)Hg(CN)$_2$Cl][HgX$_2$Cl] (3.8)

To a 5 mL aqueous solution of $CuCl_2 \cdot 2\ H_2O$ (0.067 g, 0.39 mmol), a 20 mL aqueous solution of tren (0.058 g, 0.39 mmol) was added, while stirring. A 5 mL aqueous solution of $Hg(CN)_2$ (0.200 g, 0.80 mmol) was added to this blue solution and was stirred for 2 minutes. The solution was allowed to slowly evaporate. Blue crystal bars of [Cu(tren)Hg(CN)$_2$Cl][HgX$_2$Cl] (**3.8**) were collected by vacuum filtration, washed with two 1 mL portions of cold water followed by two 1 mL portions of cold methanol, and were left to air dry. Yield: 0.115 g (56%). Anal. Calcd. for $C_9H_{18}N_7Cl_3CuHg_2$: C, 13.59; H, 2.28 N, 12.33. Found: C, 13.94; H, 2.26; N, 12.48. IR (KBr, cm^{-1}): 3351 (vs), 3293 (s), 3293 (vs), ν_{CN} **2214 (m)**, **2178 (w)**, 1631 (m), 1587 (s), 1480 (m), 1450 (m), 1389 (w), 1311 (m), 1271 (w), 1226 (w), 1117 (m), 1059 (s), 1038 (m), 1013 (m), 992 (s), 902 (m), 867 (m), 748 (w), 665 (w), 616 (w), 545 (m), 476 (m), 419 (vs).

3.5.11 Preparation of $\{[Ni(en)_2][Hg(CN)_2]_3Cl_2\}_2$ (3.9)

To a 5 mL aqueous solution of $NiCl_2 \cdot 6\ H_2O$ (0.047 g, 0.20 mmol), a 5 mL methanolic solution of en (0.058 g, 0.40 mmol) was added, while stirring. A 10 mL aqueous solution of $Hg(CN)_2$ (0.150 g, 0.59 mmol) was added to this purple solution and was stirred for 2 minutes. The solution was allowed to slowly evaporate. Pink crystal platelets of $\{[Ni(en)_2][Hg(CN)_2]_3Cl_2\}_2$ (**3.9**) were collected by vacuum filtration, washed with two 1 mL portions of cold water followed by two 1 mL portions of cold methanol, and were left to air dry. Yield: 0.124 g (63%). Anal. Calcd. for $C_{10}H_{16}N_{10}Cl_2Hg_3Ni$: C, 11.92; H, 1.60 N, 13.90. Found: C, 11.70; H, 1.62; N, 13.81. IR (KBr, cm^{-1}): 3386 (m), 3353 (s), 3343 (s), 3287 (s), 3185 (m), 2974 (s), 2950 (s), 2888 (s), 2743 (w), 2724 (w), ν_{CN} **2217 (w), 2207 (w), 2186 (w)**, 1585 (s), 1539 (w), 1503 (m), 1463 (m), 1454 (m), 1437 (w), 1419 (w), 1395 (w), 1331 (m), 1279 (m), 1149 (m), 1102 (m), 1017 (vs), 972 (m), 880 (w), 871 (w), 855 (w), 693 (s), 627 (w), 614 (w), 580 (w), 526 (s), 481 (w), 462 (m), 425 (m).

3.5.12 Preparation of $\{[Ni(tren)]_4[Hg(CN)_2]_8Cl_6\}HgCl_4$ (3.10)

To a 5 mL aqueous solution of $NiCl_2 \cdot 6\ H_2O$ (0.094 g, 0.40 mmol), a 20 mL aqueous solution of tren (0.058 g, 0.39 mmol) was added, while stirring. A 5 mL aqueous solution of $Hg(CN)_2$ (0.200 g, 0.79 mmol) was added to this purple solution, followed by a dropwise addition of a 5 mL aqueous solution of $HgCl_2$ (0.027 g, 0.01 mmol), and was stirred for 2 minutes. The solution was allowed to slowly evaporate. Purple crystal bars of $\{[Ni(tren)]_4[Hg(CN)_2]_8Cl_6\}HgCl_4$ (**3.10**) were collected by vacuum filtration, washed with two 1 mL portions of cold water followed by two 1 mL portions of cold methanol, and were left to air dry. Yield: 0.228 g (68%). Anal. Calcd. for $C_{40}H_{72}N_{32}Cl_{10}Hg_9Ni_4$: C, 14.15; H, 2.14; N, 13.20. Found: C, 14.01; H, 2.23; N, 13.09. IR (KBr, cm^{-1}): 3338 (s), 3309 (m), 3277 (m), 3259 (m), 3176 (m), 2990 (m), 2943 (w), 2930 (w), 2905 (m), 2865 (s), ν_{CN} **2215 (m), 2184 (vw)**, 1987 (w), 1880 (w), 1598 (vs), 1581 (vs), 1539 (m), 1479 (s), 1470 (s), 1397 (w), 1373 (w), 1347 (m), 1329 (m), 1318 (m), 1254 (m), 1236 (m),

1167 (m), 1140 (m), 1107 (m), 1081 (s), 1053 (s), 1036 (m), 1026 (s), 996 (s), 980 (vs), 896 (m), 880 (s), 852 (m), 748 (m), 650 (m), 615 (s), 583 (w), 560 (w), 538 (s), 516 (w), 460 (s).

CHAPTER 4
SELF-ASSEMBLY OF A NON-CENTROSYMMETRIC 2-D LAYER SYSTEM AND ITS MATERIAL PROPERTIES

4.1 INTRODUCTION

4.1.1 Material Properties of Crystals

As described in Chapter 3, basic alkylamines promote *N*-cyano binding of $Hg(CN)_2$ to transition metal cations, yielding high-dimensional structures that may have useful materials properties. Of particular interest are the properties related to non-centrosymmetric arrangements of molecules in the structure. Crystals with this feature may exhibit pyroelectric effects, piezoelectric effects, and significant optical non-linearity. Upon heating or cooling a pyroelectric crystal, opposite charges migrate to the two ends of the polar axis and can be detected on a macroscopic level.[217] Hence, pyroelectric crystals are typically used as thermal detectors. Piezoelectric crystals polarize upon the application of mechanical stress, developing electrical charges on opposite crystal faces.[217,218] They are commonly used in devices that transform mechanical energy into electrical energy and *vice versa* such as microphone pick-ups, sonar generators, and solenoid ignition systems.[218] Optical non-linearity is potentially useful for frequency doubling into short wavelengths via so-called second harmonic generation (SHG); this is desirable for high-density information storage and telecommunication applications such as tunable laser light.[25]

The introduction of Hg(II) in the form of a tetrahedral moiety could increase the probability of a non-centrosymmetric product, as observed for $\{[Ni(tren)]_4[Hg(CN)_2]_8Cl_6\}HgCl_4$ **(3.10)** (space group = $P\bar{4}2_1c$) which contains a $[HgCl_4]^{2-}$ building block. As demonstrated in Chapter 3,

the addition of $HgCl_2$ could be used as a means of generating the desired tetrahedral $[HgCl_4]^{2-}$ moieties *in situ*. Since $HgCl_2$ is more Lewis-acidic than $Hg(CN)_2$ [95] (Table 1.1), it would be the principal acceptor for labile chloride ligands from the transition metal chloride salts.

Another important property of crystals is birefringence, especially the principal birefringence (Δn), which is defined as the difference in the refractive indices of two waves vibrating in the same plane along two different crystallographic axes:

$$\Delta n = n_a - n_b \qquad \text{(Equation 4.1)}$$

where n_a and n_b correspond to the indices of refraction along the *a*- and *b*-axis respectively for a light beam that has entered a crystal collinear to the *c*-axis.

Birefringence can be useful in SHG materials. Greatly amplified harmonics are possible if the velocities of the fundamental and harmonic waves are made equal. This kind of phase matching is possible if the difference in refractive indices due to dispersion can be matched by birefringence.[219] Birefringence is related to the structural anisotropy of the crystals. For instance, low dimensional polymers have been shown to exhibit high birefringence because of high structural anisotropy.[220,221] The use of *linear* mercury cyanide is particularly appealing with respect to generating high anisotropy and thereby strong birefringence.

4.1.2 Magnetochemistry: Zero-Field Splitting

When a compound has a total spin quantum number (S) greater than ½, the effect of the crystal field about the paramagnetic metal centre can result in a splitting of energy levels in the absence of a magnetic field.[185] This zero-field splitting results in anisotropic behaviour for the magnetic susceptibility (χ_M); χ_M has both a parallel and perpendicular component relative to the applied magnetic field. Figure 4.1 depicts the zero-field spitting for a Ni(II) centre, where S = 1. Application of the Van Vleck formula in the case of zero-field splitting for an S = 1 centre results in two equations for χ_M:

$$\chi_{parallel} = [(2Ng_z^2\beta^2) / kT]*[\exp(-D/kT) / (1 + 2 \exp(-D/kT))] \quad \text{(Equation 4.2)}$$

$$\chi_{perp} = [(2Ng_x^2\beta^2) / D]*[(1- \exp(-D/kT)) / (1 + 2 \exp(-D/kT))] \quad \text{(Equation 4.3)}$$

where $\chi_{parallel}$ and χ_{perp} are the parallel and perpendicular components of the susceptibility. The experimental χ_M of powdered samples is the weighted average of equations 4.1 and 4.2:[185]:

$$\chi_{Avg} = (\chi_{parallel} + 2\ \chi_{perp}) / 3 \quad \text{(Equation 4.4)}$$

Zero-field splitting is prominent at lower temperatures; as the temperature decreases, so does μ_{eff}. Differentiation between weak antiferromagnetic interactions and zero-field splitting is difficult because both effects occur simultaneously. For Ni(II), D typically ranges from between 0.1 -6.0 cm^{-1}.[185]

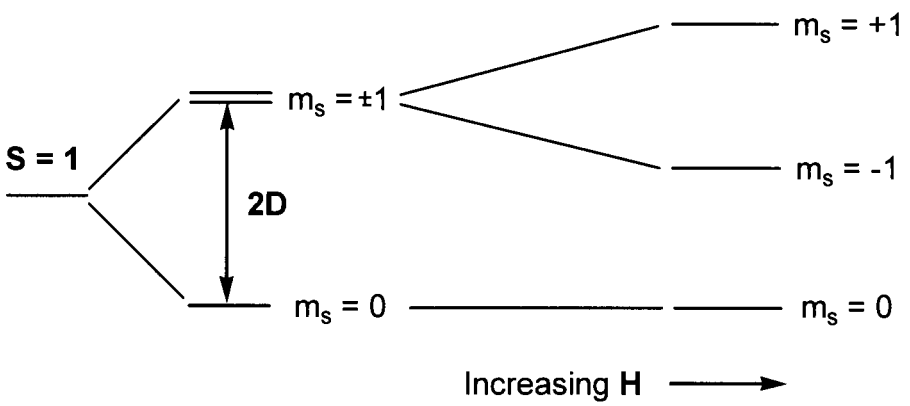

Figure 4.1 Zero-field splitting energy diagram of a S = 1 metal centre.

4.1.3 Dielectric Materials

Many materials such as glass, plastics, and wood do not conduct electricity very easily; these insulating materials are known as dielectrics. In the mid-1800s, Michael Faraday performed experiments which demonstrated that the presence of a dielectric between the two conductors of a capacitor increases the capacitance.[222] The dielectric constant, ε', of a material is defined by the following equation:

$$\varepsilon' = C_d / C_o \quad \text{(Equation 4.5)}$$

where C_o is the capacitance of a capacitor in a vacuum and C_d is the capacitance measured with a dielectric placed between the conductors.[222] The dielectric constant is larger than 1 for all materials and depends on not only the material, but on external conditions such as temperature and the frequency of oscillating fields.[218] When a dielectric material is placed in a charged capacitor, the permanent or induced electric dipoles of the dielectric become aligned with the electric field; that is the dielectric is polarized. When the field is removed, the polarization disappears. If a residual polarization remains on the dielectric after the electric field has been removed, then the material is termed ferroelectric.[218,222]

The magnitude of ε' depends upon the degree of polarization that can occur in the material. For most ionic solids, ε' = 5-10 (Table 4.1), while ε' = 10^3-10^4 for ferroelectric materials.[218]

Table 4.1 Dielectric properties of selected materials at room temperature.

Material	*Dielectric Constant, ε'*	*Frequency (Hz)*	*Reference*
Vacuum	1.0	not applicable	222
Asphalt	2.68	$< 3 \times 10^6$	223
$HgCl_2$	3.2	1×10^6	223
SiO_2	4.34, 4.27	3×10^7, 3×10^7	223
$CuSO_4 \cdot 5\ H_2O$	10.3	6×10^7	223
$PbSO_4$	14.3	1×10^6	223
$Ag_2(C_3H_3N_3O_3)$	22000	not reported	224

The dielectric constant of a material can be related to its index of refraction (n) by the following equation:

$$\varepsilon' = n^2 \qquad \text{(Equation 4.6)}$$

It should be noted that the dielectric constant and the index of refraction is dependent on the frequency of the electromagnetic wave.[222]

Dielectric materials are used as capacitors, substrates, and electrical insulators in a variety of applications. They should be able to withstand high voltages and alternating electric fields

without degradation, that is, the loss of electrical energy in the form of heat, in order to have practical applications.[218]

4.1.4 Research Objectives

This chapter investigates the use of HgX_2 and $Hg(CN)_2$ moieties in conjunction with $[(tmeda)M]X_2$ complexes (M = Cu(II), Ni(II); X = Cl, Br, I). The use of the bidentate basic trialkylamine ligand *tmeda* serves two main functions: 1) to induce *N*-cyano coordination of the neutral $Hg(CN)_2$ moieties; and 2) to increase the number of open sites at the transition metal complex available for *N*-cyano bridging to take place. Both functions should aid to increase the structural dimensionality in $Hg(CN)_2$-based coordination polymers. By simultaneously using the more Lewis-acidic HgX_2 units to accept the labile halide ligands, tetrahedral $[HgX_4]^{2-}$ moieties should be generated, thereby potentially enhancing the chance of forming non-centrosymmetric coordination polymers with useful bulk materials properties. Material properties such as the magnetic susceptibility, birefringence, and dielectric constant are investigated.

4.2 RESULTS, ANALYSIS AND DISCUSSION*

4.2.1 Synthesis of $\{(tmeda)M[Hg(CN)_2]_2\}HgX_4$ (M = Cu(II), Ni(II); X = Cl, Br, I) (4.1-4.6)

The chloride complex $\{(tmeda)Cu[Hg(CN)_2]_2\}HgCl_4$ (**4.1**) spontaneously self-assembles in good yields (49-91%) from several different starting points (Figure 4.2), indicating that it is the most thermodynamically stable product. In reactions 1 and 3, the migration of two labile chloride ligands from Cu(II) to Hg(II) drives the formation of the product;[126,152] in reaction 2, additional chloride is added. This halide migration from the harder Cu(II) to the softer Hg(II) effectively opens two additional coordination sites on the Cu(II) for *N*-cyano binding. Interestingly, the crystal morphology of **4.1** ranges from block-like (reactions 1, 3) to plate-shaped (reaction 2) and

---

* Draper, N. D.; Batchelor, R. J.; Sih, B. C.; Ye, Z. G.; Leznoff, D. B. *Chem. Mater.* **2003**, *15*, 1612-1616. Reproduced in part by permission of the American Chemical Society.

is highly influenced by the solvent employed. When water is used as the solvent for reaction 3, platelets of **4.1** crystallize in lieu of the blocks obtained when methanol is the solvent.

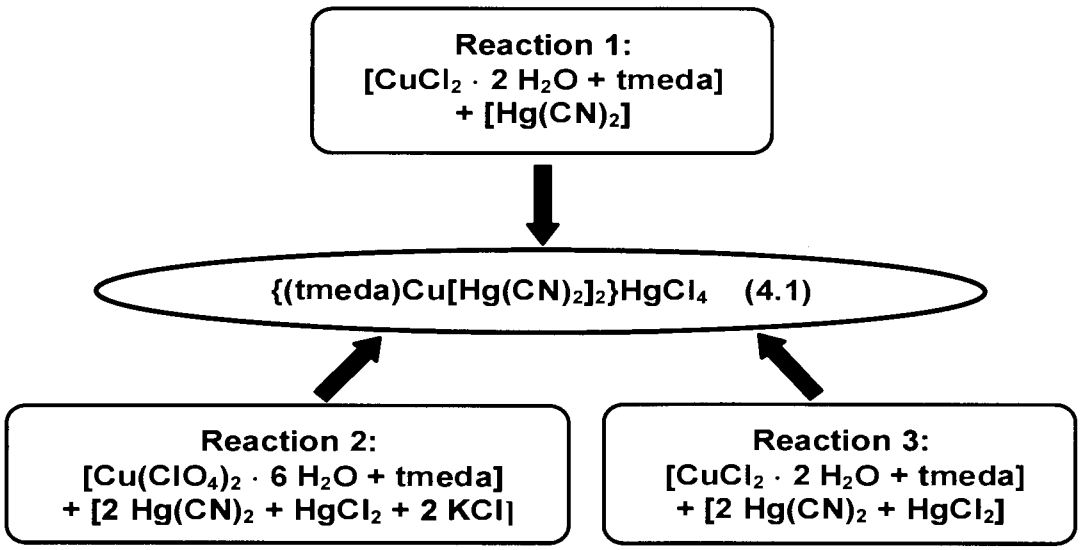

Figure 4.2 Scheme of the three reaction pathways for the synthesis of $\{(tmeda)Cu[Hg(CN)_2]_2\}HgCl_4$ (**4.1**).

It should be noted that an additional undesirable green side product is obtained in reaction 1 that is not formed in reactions 2 and 3. Complexes **4.2-4.6** also spontaneously self-assemble from similar reactions as those in Figure 4.2 upon substitution with the analogous starting materials. For example, crystals of the bromide complex $\{(tmeda)Cu[Hg(CN)_2]_2\}HgBr_4$ (**4.2**) are obtained in high yields via reaction 3 when $CuBr_2$ and $HgBr_2$ are substituted for $CuCl_2$ and $HgCl_2$ using water, rather than methanol, as the solvent.

However, the differences in starting material solubilities and the reduction in lability of the TM centre upon replacement of Cu(II) with Ni(II) alter the precise experimental preparation for each complex, as described in experimental section 4.5. For example, both iodide complexes are difficult to prepare due to interference from the following equilibrium reaction:[225]

$$HgI_2 + Hg(CN)_2 \rightleftharpoons 2\,Hg(CN)I \qquad K_{eq} = 0.14$$

4.2.2 Structures of $\{(tmeda)M[Hg(CN)_2]_2\}HgX_4$ (M = Cu(II), Ni(II); X = Cl, Br, I) (4.1-4.6)

The X-ray diffraction studies performed on **4.1-4.6** all reveal a 2-D cationic $\{(tmeda)M[Hg(CN)_2]_2\}^{2+}$ network consisting of six-coordinate M centres (M = Cu(II), Ni(II)) and bridging $Hg(CN)_2$ groups, impregnated with a layer of $[HgX_4]^{2-}$ anions.

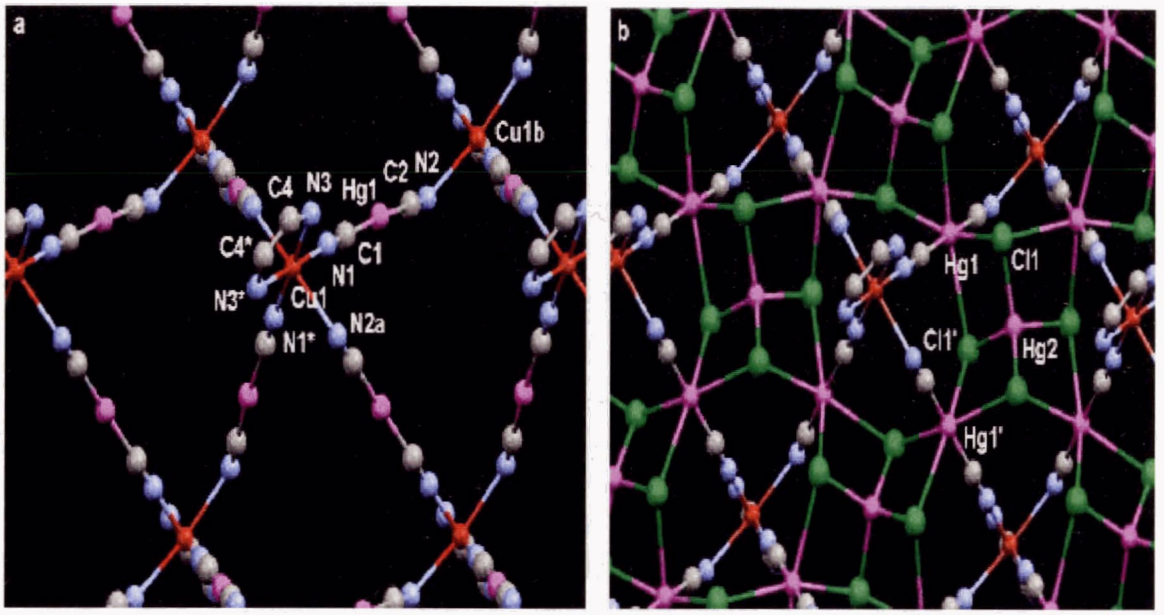

Figure 4.3 (a) A view of the cationic 2-D framework of $\{(tmeda)Cu[Hg(CN)_2]_2\}HgCl_4$ (**4.1**), showing corrugated cavities and (b) the cavities filled with $[HgCl_4]^{2-}$ anions as viewed down the *c*-axis.
Tmeda methyl groups and methylene hydrogen atoms have been omitted for clarity.
Colour scheme: Hg, pink; Cu, red; Cl, green; N, blue, C, grey.

The six complexes, which are isostructural and isomorphous, crystallize in the non-centrosymmetric, tetragonal space group $P\bar{4}2_1m$. For compounds **4.1-4.3**, the Cu(II) centre adopts a Jahn-Teller distorted octahedral geometry by coordinating to one tmeda molecule and four cyanide bridged $Hg(CN)_2$ moieties as shown for **4.1** in Figure 4.3. Each $Hg(CN)_2$ unit bridges in an axial / equatorial fashion to a different $[(tmeda)Cu]^{2+}$ centre, thus propagating the corrugated 2-D array that lies in the *ab*-plane (for **4.1**: Cu-N(1, eq-CN) = 1.975(11) Å; Cu-N(2a, ax-CN) = 2.583(13) Å; Cu-N(3, tmeda) = 2.050(7) Å) (Table 4.1). Analogous structures (**4.4-4.6**) are obtained upon the replacement of Cu(II) for Ni(II), which show no axial Jahn-Teller distortion

(for **4.4**: Ni-N(1)cyano = 2.052(15) Å; Ni-N(2a)cyano = 2.159(14) Å) (Table 4.1). The approximately 11 Å diameter cavities delineated by four M(II) centres (Figure 4.3 a) are filled by tetrahedral $[HgX_4]^{2-}$ anions, thus stabilizing the cationic 2-D array (Figure 4.3 b).

Table 4.2 Selected Bond Lengths (Å) and Angles (°) for $\{(tmeda)M[Hg(CN)_2]_2\}HgX_4$ (**4.1-4.6**)[a].

Compound	**4.1**[a]	**4.2**	**4.3**	**4.4**	**4.5**	**4.6**
M(II), X	Cu, Cl	Cu, Br	Cu, I	Ni, Cl	Ni, Br	Ni, I
Selected Atoms	*Bond Lengths*	*Bond Lengths*	*Bond Lengths*	*Bond Lengths*	*Bond Lengths*	*Bond Lengths*
Hg(1)-X(1)	3.0514(2)	3.182(6)	3.351(2)	3.136(4)	3.268(3)	3.465(5)
Hg(1)-X(1')	3.217(2)	3.315(5)	3.488(2)	3.180(4)	3.282(3)	3.465(5)
Hg(2)-X(1)	2.4807(2)	2.619(5)	2.783(1)	2.479(3)	2.605(3)	2.797(4)
Hg(1)-C(1)	2.049(13)	2.07(6)	2.03(4)	2.044(16)	2.01(3)	2.14(10)
Hg(1)-C(2)	2.014(12)	2.12(6)	2.09(3)	2.02(2)	2.03(5)	1.86(8)
M(1)-N(1)	1.975(11)	2.03(5)	1.96(2)	2.052(15)	2.03(3)	1.87(8)
M(1)-N(2a)	2.583(13)	2.54(6)	2.62(3)	2.159(14)	2.15(3)	2.13(7)
C(2)-N(2)	1.116(17)	1.06(6)	1.05(4)	1.12(2)	1.15(5)	1.40(10)
C(1)-N(1)	1.120(17)	1.05(6)	1.15(4)	1.11(2)	1.15(4)	1.21(11)
M(1)-N(3)	2.050(7)	2.05(6)	2.06(2)	2.116(15)	2.15(3)	2.16(8)
Selected Atoms	*Bond Angles*	*Bond Angles*	*Bond Angles*	*Bond Angles*	*Bond Angles*	*Bond Angles*
N(3)-M(1)-N(1)	90.3(4)	90(2)	90.7(1)	90.7(6)	91.1(11)	88(3)
N(3)-M(1)-N(1*)	178.3(4)	180(2)	180.0(11)	177.0(7)	175.6(13)	174(3)
N(3)-M(1)-N(3*)	88.0(5)	90(3)	89.3(15)	86.2(11)	84.6(15)	86(5)
N(3)-M(1)-N(2a)	97.75(17)	96.7(8)	95.5(5)	96.4(3)	95.6(5)	93.8(14)
N(1)-M(1)-N(1*)	91.3(3)	89(2)	89.4(14)	92.3(9)	93.3(19)	98(4)
N(1)-M(1)-N(2a)	82.48(16)	83.2(8)	84.5(5)	84.0(3)	84.8(4)	86.6(13)
C(1)-Hg(1)-C(2)	172.4(4)	173(2)	173.5(12)	176.3(8)	175.5(14)	178(4)
Hg(1)-X(1)-Hg(2)	89.31(6)	86.50(13)	84.34(4)	87.88(10)	85.10(8)	82.11(11)
X(1)-Hg(1)-C(1)	85.9(2)	84.2(12)	85.3(7)	83.9(5)	82.6(6)	81(2)
X(1)-Hg(1)-X(1')	85.91(7)	80.87(19)	78.77(5)	84.65(13)	80.67(10)	77.64(16)
X(1)-Hg(1)-C(2)	99.6(2)	100.9(11)	99.7(5)	98.9(3)	100.8(9)	100.9(18)
X(1)-Hg(2)-X(1')	105.52(5)	107.14(9)	109.01(3)	105.61(9)	107.72(9)	108.73(16)

[a] Symmetry transformations: (*) -x, -y-1, z; (') -y,x,-z-1; (a).y, -x,-1, -z-1; (b) y, -x, -z,-1.

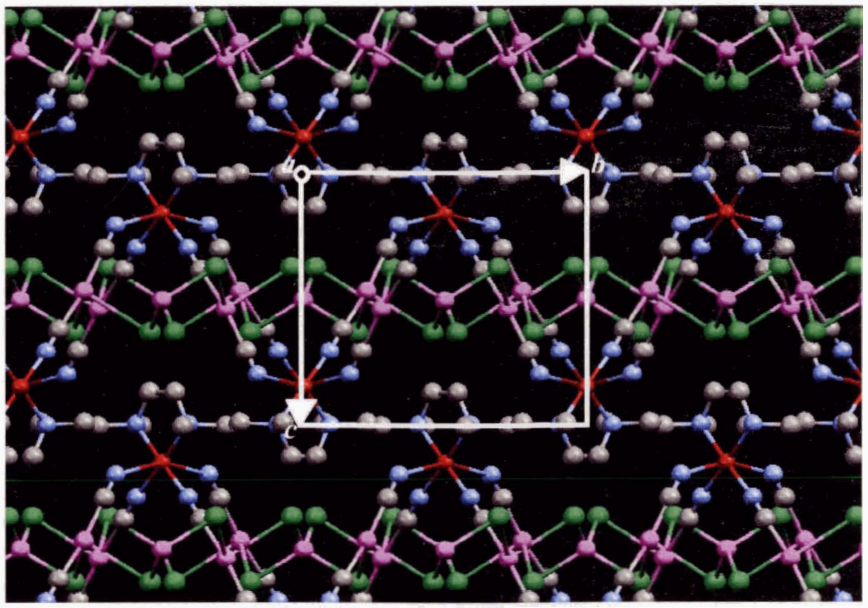

Figure 4.4 Packing diagram of **4.1** viewed down the *a*-axis, showing the unit cell. Colour scheme: Hg, pink; Cu, red; Cl, green; N, blue, C, grey.

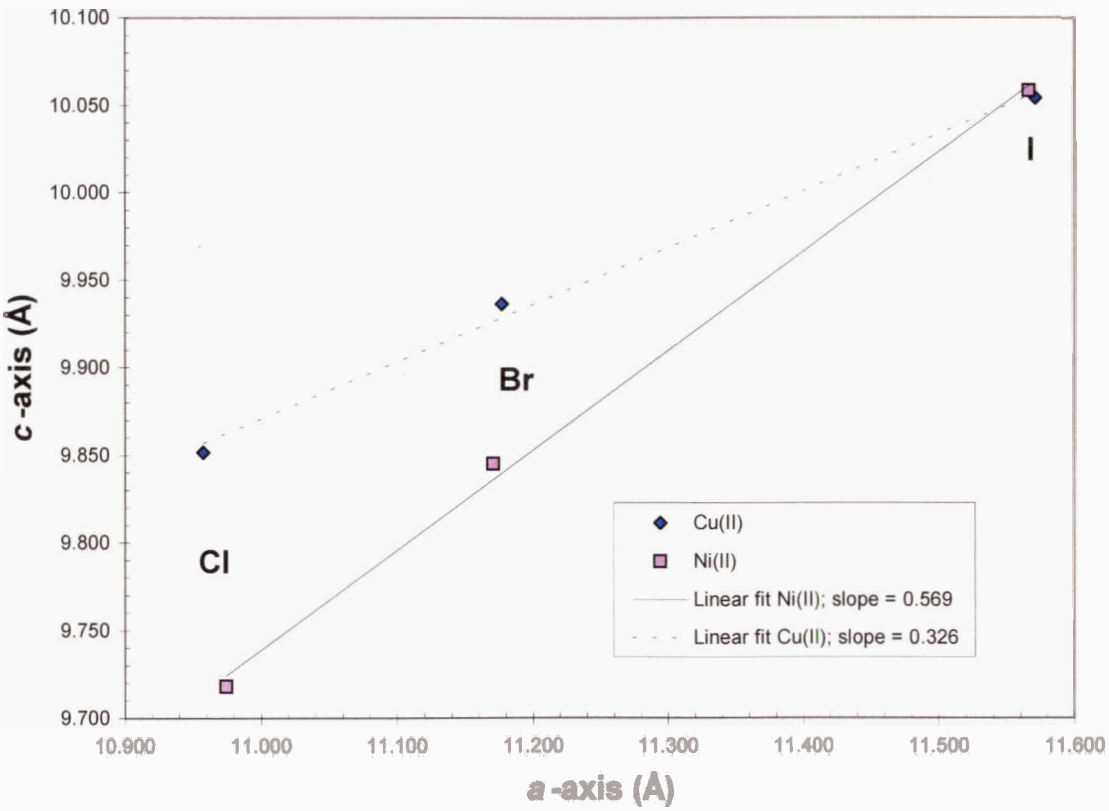

Figure 4.5 Unit cell comparisons for complexes **4.1-4.6.**

Each halide atom further interacts with its two closest bridging mercury atoms resulting in an effective distorted octahedral geometry, based on linear characteristic coordination (2+4), about each mercury cyanide's metal centre. The Hg-Cl bond interactions in **4.1** (3.051(2) and 3.217(2) Å), can be compared with the pseudo-octahedral chain structure of $K_2HgCl_4 \cdot H_2O$, which has two short Hg-Cl distances of 2.383(1) Å and two longer pairs at 2.897(1) and 3.251(1) Å.[140,226]

The 2-D sheets in **4.1-4.6** are stacked together in a corrugated fashion, held together only by weak hydrophobic interactions between tmeda ligands, forming zig-zag channels (~ 4 Å) between each sheet, as shown in Figure 4.4. This unusual structure, containing two different 2-D layers embedded in each other, is perhaps more closely related to some organic / inorganic hybrid materials[227] than to interpenetrated coordination polymers, which normally involve interpenetration of one network with itself.[74]

An examination of the unit cells for compounds **4.1-4.6** show the following two trends as depicted in Figure 4.5. First of all, the Cu(II) chloride and bromide complexes are more corrugated (i.e.: they have significantly longer *c*-axes but similar *a*-axes length) than their Ni(II) analogues, probably as a result of Jahn-Teller distortion. Coincidentally, both iodide complexes have very similar unit cell dimensions. Secondly, the unit cell expands in a linear fashion as the halide increases in size for both the Cu(II) and Ni(II) complexes. In both cases, expansion occurs not only between the 2-D layers, but predominately within the layers (the *ab*-plane) as shown by the fractional values obtained for the slope (Cu(II) 0.362; Ni(II) 0.569).

4.2.3 Infrared Analysis

The IR spectra of **4.1-4.6** clearly show the presence of bridging cyano groups and are displayed in Table 4.3. The ν_{CN} stretches range from 2248 cm^{-1} (**4.1**) to 2189 cm^{-1} (**4.3**) and are comparable with those found for $[Cu(tren)Hg(CN)_2Cl][HgX_2Cl]$ (**3.8**) (ν_{CN} = 2214 cm^{-1}) and $\{[Ni(en)_2][Hg(CN)_2]_3Cl_2\}_2$ (**3.9**) (ν_{CN} = 2217 cm^{-1}, 2207 cm^{-1}). Compounds **4.1-4.6** each show two bridging ν_{CN} stretches that are consistent with the two cyano groups found in the asymmetric

unit cell. There are two notable trends present in Table 4.3: 1) as the halide increases in size, both ν_{CN} stretches become less strongly shifted relative to free $Hg(CN)_2$; and 2) the second ν_{CN} stretch is more strongly shifted and has greater intensity, upon changing the transition metal from Cu(II) to Ni(II) while keeping the halides the same. The first trend is likely a result of an increase in electron donation from the halides to the Hg(1) centres in going from Cl to I (i.e.: how strong the secondary interactions are relative to linear characteristic coordination of the $Hg(CN)_2$ units). The lack of Jahn-Teller distortion in compounds **4.4-4.6** results in more tightly bridged cyano groups, accounting for the second observed trend.

Table 4.3 Comparison of cyanide (ν_{CN}) absorptions (cm^{-1}) for complexes **4.1-4.6**.

Complex	*Bridging ν_{CN}*
$\{(tmeda)Cu[Hg(CN)_2]_2\}HgCl_4$ (**4.1**)[205]	2248 (s), 2197 (w)
$\{(tmeda)Cu[Hg(CN)_2]_2\}HgBr_4$ (**4.2**)	2245 (s), 2196 (w)
$\{(tmeda)Cu[Hg(CN)_2]_2\}HgI_4$ (**4.3**)	2236 (s), 2189 (w)
$\{(tmeda)Ni[Hg(CN)_2]_2\}HgCl_4$ (**4.4**)	2247 (m), 2210 (m)
$\{(tmeda)Ni[Hg(CN)_2]_2\}HgBr_4$ (**4.5**)	2244 (m), 2209 (m)
$\{(tmeda)Ni[Hg(CN)_2]_2\}HgI_4$ (**4.6**)	2235 (m), 2206 (m)

Values are determined from the maximum of the absorption peak. IR spectrometer resolution = ± 2 cm^{-1}; all spectra were collected as KBr pellets.

4.2.4 Magnetic Properties

The magnetic susceptibility of **4.1** (Cu / Cl) was measured as a function of temperature. However, despite the 2-D structural nature, **4.1** shows very little magnetic interaction between the Cu(II) centres; μ_{eff} = 1.87 μ_B at 300 K and is temperature independent until 5 K. Very weak antiferromagnetic coupling is observed between the Cu(II) centres below 5 K, upon which μ_{eff} drops to 1.80 μ_B at 1.8 K. The data can be fit to the Curie-Weiss Law, with C = 0.4289(2) and θ = -0.105(4) K, consistent with weak antiferromagnetic coupling between the Cu(II) centres even though the Cu(II) centres are connected in an axial / equatorial fashion, typical of systems showing ferromagnetic interactions.[228] The antiferromagnetic interaction can be attributed to the N(1)-Cu(1)-N(2a) bond angle of 82.48(16)° *vs.* the 90° angle required for strict orthogonality,

which generates ferromagnetic coupling.[68] A significant ferromagnetic interaction is observed in [Cu(tmeda)][$Au(CN)_2]_2$,[80] a related axial / equatorial 1-D chain that is mediated by d^{10} Au(I) centres, having an N-Cu-N angle of 89.3(4)°.

The Jahn-Teller distorted weak axial bonding of the cyanides ($Cu(1)\text{-}N(2a)_{ax}$ = 2.583(13) Å *vs.* $Cu(1)\text{-}N(1)_{eq}$ = 1.975(11) Å) effectively disrupts coupling interactions between Cu(II) centres,[81] as a result of poor orbital overlap. For this reason, the susceptibility of the bromide (**4.2**) and iodide (**4.3**) Cu(II) complexes were not measured.

On the other hand, there is no Jahn-Teller distortion to disrupt coupling between the M(II) centres of the nickel isostructural analogues, hence the magnetic susceptibility of **4.5** (Ni / Br) as a function of temperature was measured. However, the magnetic behaviour of **4.5** also showed very little magnetic interactions between the Ni(II) centres.

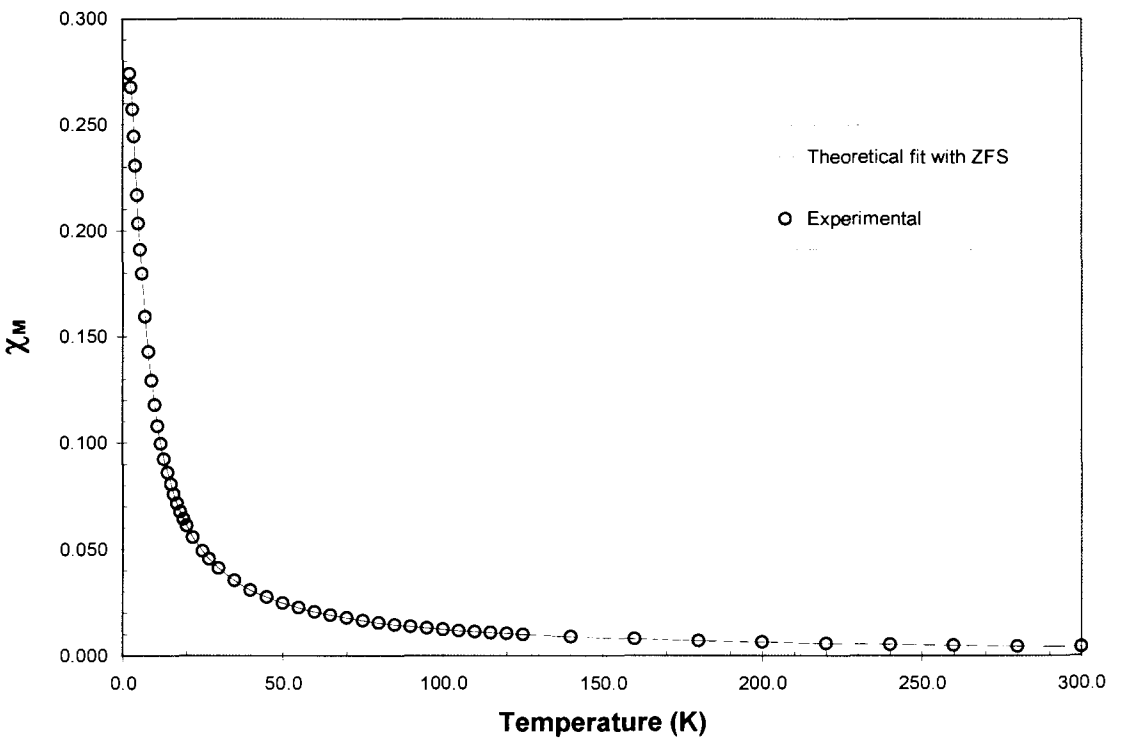

Figure 4.6 χ_M *vs.* T plot for **4.5** with data fitted using a zero-field splitting parameter.

The $\mu_{eff} = 3.16\ \mu_B$ at 300 K and is temperature-independent until 25 K, upon which it drops to 2.11 μ_B. at 2 K. No maximum in χ_M *vs.* T is observed, indicative of weak antiferromagnetic interactions. The antiferromagnetic behaviour is consistent with a N(1)-Ni(1)-N(2a) bond angle of 84.8(4)°, which is significantly shifted from the 90° required for ferromagnetic coupling in an axial / equatorial complex.

The investigation of weak antiferromagnetic interactions is complicated by the zero-field splitting of isolated S = 1 octahedral Ni(II) centres. The data can be modelled using a zero-field splitting parameter of D = +6.21(3) cm^{-1} and g = 2.223(1) (Figure 4.6); these are reasonable values for magnetically dilute Ni(II) centres,[185] but there may be some weak AF interactions present.

The magnetic susceptibility of the chloride (**4.4**) and iodide (**4.6**) Ni(II) complexes were not measured.

4.2.5 Thermogravimetric Analysis

From thermogravimetric analysis, **4.1** begins to decompose at 138 °C with eventual loss of all material except $CuCl_2$ (86.91 % calculated weight loss, 86.07 % observed) (Figure 4.7). A single crystal of **4.1** decomposed in air between 133-138 °C, as observed in a melting point apparatus.

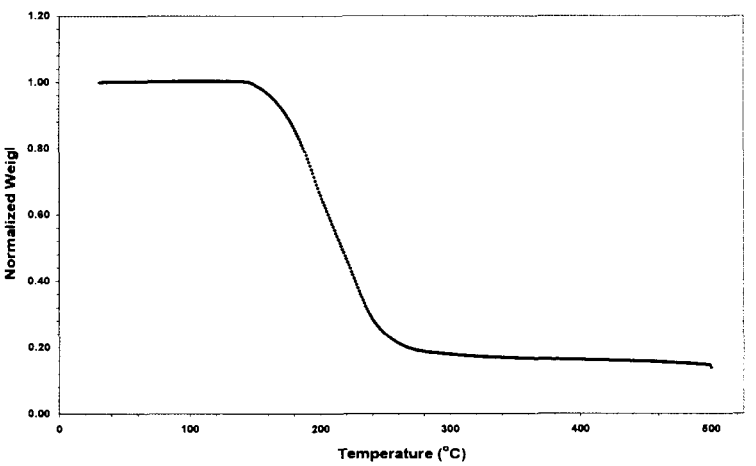

Figure 4.7 Thermogravimetric analysis of **4.1**.

4.2.6 Birefringence Properties

The birefringence of a crystal is an important characteristic of the material. The unusual structural features of the $\{(tmeda)M[Hg(CN)_2]_2\}HgX_4$ crystals, as described above, provide an ideal case to study the optical properties related to the structural anisotropy due to the stacking of 2-D sheets. To investigate such a structure-property relationship, the optical birefringence of **4.1** (M = Cu(II); X = Cl) was measured along different crystallographic directions by means of polarized light microscopy. The *c*-oriented crystal plates are optically isotropic when observed along the [001] direction, with extinction at any positions between the crossed polarizers, consistent with the tetragonal point group.[220] The *a*- or *b*-oriented crystal plates (with the *c*-axis lying in the plane of the platelets) are strongly birefringent with a birefringence value of Δn = 6.38 x 10^{-2} at room temperature, as measured at λ = 546.1 nm (Figure 4.8).

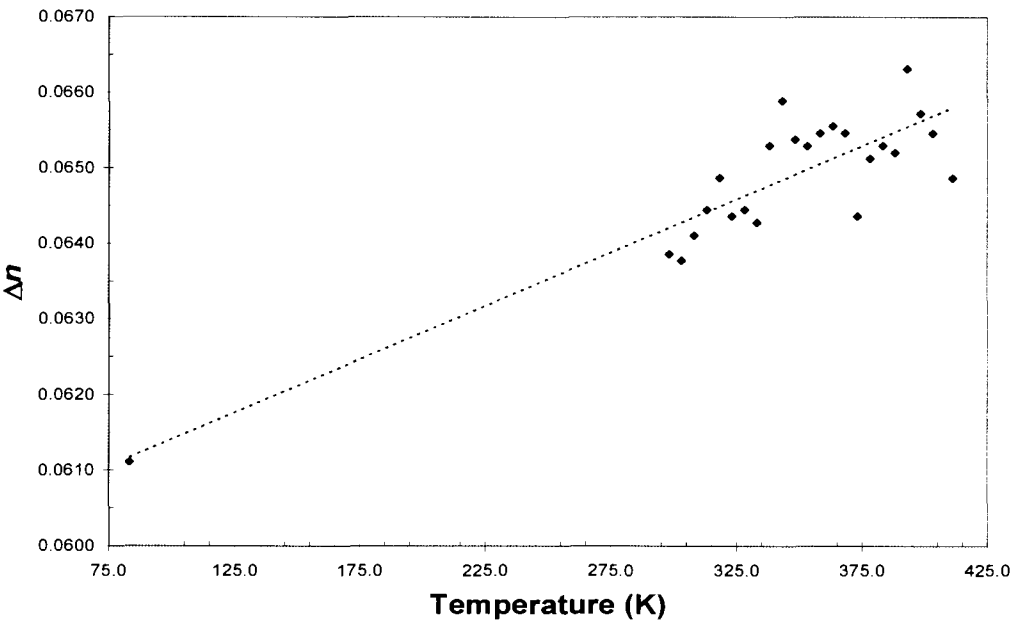

Figure 4.8 Birefringence of **4.1** as a function of temperature.

The blue crystals of **4.1** do not absorb light at 546.1 nm, hence the birefringence measurement is unimpeded by the optical absorption profile. This value of birefringence can be compared with 0.105 for the coordination polymer [hydrotris(1,2,4-triazolyl)borato]silver(I)[229]

and 0.0155 for [Na⊂(dibenzo-24-crown-8)(I(1,3-dioxolane)][221] or even with the value of very strongly birefringent inorganic crystals, e.g. $KNbO_3$ ($\Delta n = n_b - n_a = 0.171$).[230] Upon cooling, the birefringence of **4.1** decreases slightly to reach a value of $\Delta n = 6.12 \times 10^{-2}$ at 90 K, while upon warming, the birefringence increases slightly to a value of $\Delta n = 6.55 \times 10^{-2}$ at 400 K. As the temperature increases, the structural anisotropy increases slightly, probably due to the thermal expansion of the polymer interlayers.

The correlation between the optical indicatrix and the crystallographic axes shows that the refractive index along the *a*- or *b*-axis (n_o, for the ordinary beam component) is larger than that along the *c*-axis, which is also the optical axis (n_e, for the extraordinary beam component), as indicated in Figure 4.9. Therefore, the birefringence corresponds to $\Delta n = n_o - n_e$, the principal birefringence of the tetragonal crystal. Since $n_e < n_o$, **4.1** exhibits an optically negative indicatrix.[231] The optical character of the {(tmeda)Cu[$Hg(CN)_2$]$_2$}$HgCl_4$ crystals can be understood with respect to the crystal structure and chemical bonding. It is known that the refractive index *n* of a crystal depends on its packing density and atomic or ionic polarizability, with a large *n* arising from a dense packing of highly polarizable atoms or ionic groups.[219]

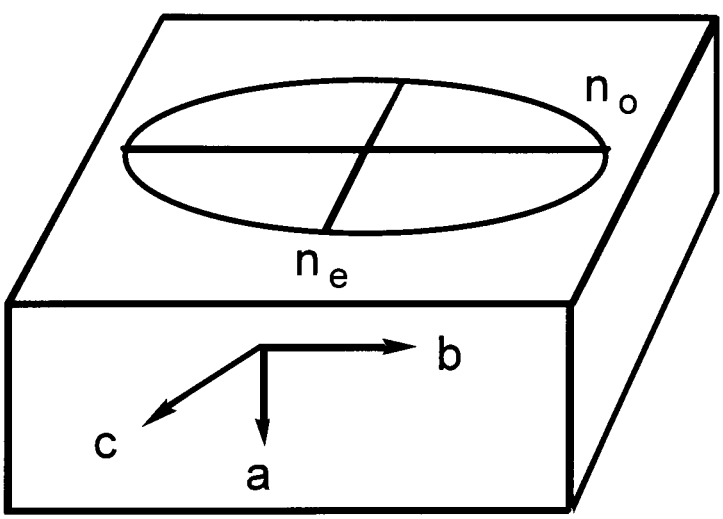

Figure 4.9 Orientation of the *b*-*c* section of the optical indicatrix with respect to the crystallographic axes, illustrating the optical anisotropy along the *a*-axis and the optically negative character of the {(tmeda)M[$Hg(CN)_2$]$_2$}HgX_4 crystals.

Figure 4.4 clearly shows that the *ab*-plane contains densely packed layers of $[HgCl_4]^{2-}$ anions and the $\{(tmeda)Cu[Hg(CN)_2]_2\}^{2+}$ moieties; the 2-D sheets are only weakly packed along the *c*-axis. The electric vector of light propagating along the *a*- or *b*-axis encounters stronger interactions through the dense layers of highly polarizable Hg(II) groups, giving rise to a substantially larger value of the refractive index n_o (along the *a*- or *b*-axis) than n_e (along the *c*-axis) resulting in the high birefringence and the optically negative character.

The principal reason for synthesizing the bromide (**4.2**, **4.5**) and iodide (**4.3**, **4.6**) analogues was to make the $[HgX_4]^{2-}$ anions in the *ab*-plane more polarizable and hence increase the birefringence. However, birefringence measurements were not performed on **4.2-4.6** because suitable single crystals of the proper orientation (*a*- or *b*-oriented) and size could not be grown, despite numerous efforts.

4.2.7 Dielectric Constant

The dielectric constant of **4.1** was measured as a function of temperature using a polished *c*-axis oriented single crystal. The dielectric constant showed no temperature dependence between 30 °C and 115 °C, having an average value of ε' = 37.1 measured at an oscillating frequency of 10 kHz (Figure 4.10).

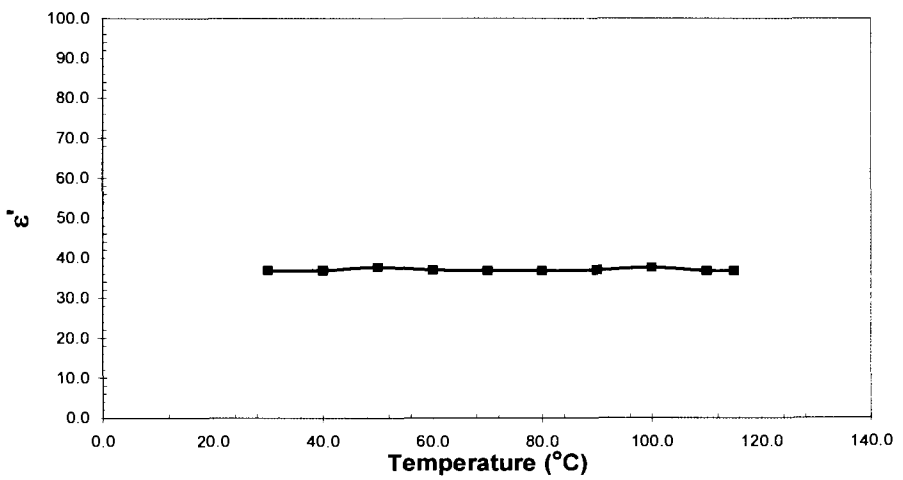

Figure 4.10 Temperature dependence of the dielectric constant (ε') for complex **4.1**.at 10 kHz. The crystal was oriented along the *c*-axis.

The dielectric constant was also measured as a function of frequency at 30 °C and showed only a slight change between 1 kHz (ε' = 35.4) and 100 kHz (ε' = 36.4) (Figure 4.11). Dielectric constants of ε' < 10 are common for most dielectrics that are non-ferroelectric materials.[218] Even $HgCl_2$, which contains polarizable mercury atoms, has a low dielectric constant (Table 4.1).

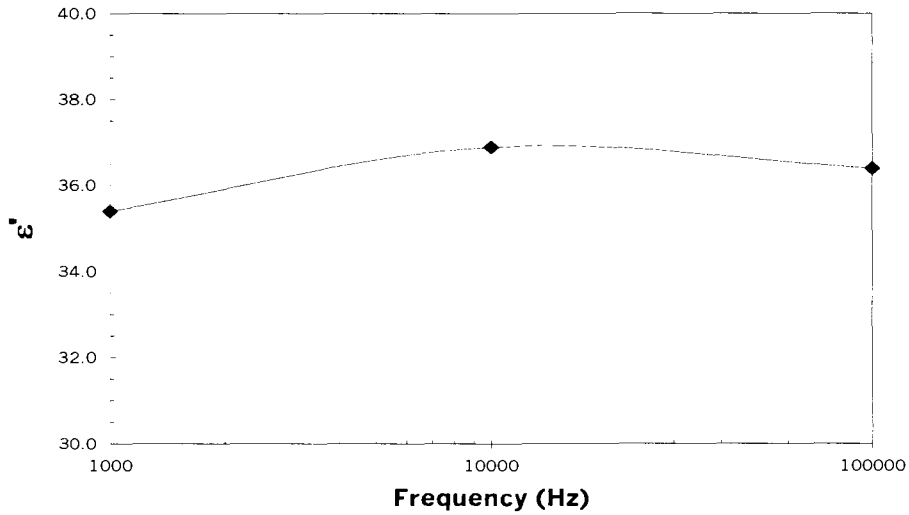

Figure 4.11 Frequency dependence of the dielectric constant (ε') for complex **4.1** at 30 °C.

The dielectric constant of **4.1** was not measured for an *a*- or *b*-axis oriented crystal because the crystals grown were too small. Since the 2-D layers consist of densely packed $[HgCl_4]^{2-}$ anions and $\{(tmeda)Cu[Hg(CN)_2]_2\}^{2+}$ moieties containing polarizable Hg(II) atoms along the *ab*-plane (Figure 4.3), it is expected that the measured dielectric constant would be greater along the *a*- or *b*-axis than along the *c*-axis where the 2-D sheets are only weakly packed.

Dielectric constant measurements were not performed on complexes **4.2-4.6** since the crystals grown were too small.

4.3 CONCLUSIONS

A series of self-assembled isostructural M(II) / Hg(II) coordination polymers with the general formula $\{(tmeda)M[Hg(CN)_2]_2\}HgX_4$ (M = Cu(II), Ni(II); X = Cl, Br, I) have been prepared. As expected, halide migration occurs from the harder M(II) centres, not to the $Hg(CN)_2$ units, but to

the more Lewis-acidic HgX_2 units forming tetrahedral $[HgX_4]^{2-}$ anions. Complexes **4.1-4.6** crystallize in the tetragonal, non-centric $P\bar{4}2_1m$ space group The structure adopted is composed of a 2-D cationic layer of $[(tmeda)M[Hg(CN)_2]_2]^{2+}$ units (M = Cu(II), Ni(II)) in which the six-coordinate M(II) centres are capped by the basic trialkylamine tmeda which induces *N*-cyano bridging of four separate $Hg(CN)_2$ groups. This robust array is interspersed with a layer of $[HgX_4]^{2-}$ anions (X = Cl, Br, I), which form additional bridging Hg-X bonds with the $Hg(CN)_2$ units. The strongly anisotropic 2-D layer crystal structure, including the highly polarizable Hg(II) ions, is responsible for a significant optical birefringence and dielectric constant as measured for complex **4.1**. It is expected that the bromide and iodide analogues would be even more strongly birefringent and have higher dielectric constants than that of the chloride analogues since they contain more polarizable atoms. However, despite numerous efforts, large single crystals of these complexes with the proper orientation could not be grown for birefringence and electronic measurements.

Although viable magnetic pathways are present between the paramagnetic M(II) centres, magnetic susceptibility measurements showed no significant interactions between the M(II) centres.

Efforts to grow large single crystals in both orientations are ongoing in order to expand the investigation of material properties for this interesting 2-D layer system. For instance, since many non-centric crystals that contain tetrahedral groups can have their tetrahedra distorted by the application of mechanical stress, **4.1-4.6** may also be piezoelectric.[218]

Although compounds **4.1-4.6** crystallize in the polar, non-centric $P\bar{4}2_1m$ space group, their SHG optical properties were not investigated because they absorb in the visible spectrum. SHG materials should be colourless so that the laser light employed is not absorbed causing overheating and subsequent melting of the crystal.[25] If crystals of Zn(II) structural analogues could be synthesized, then second-order non-linear optical properties could be investigated.

4.4 EXPERIMENTAL

CAUTION: Although we have experienced no difficulties, perchlorate salts are potentially explosive and should only be used in small quantities and handled with care. General experimental details were as indicated in Chapter 2, with the following exceptions:

4.4.1 X-ray Crystallography

Dr. R. Batchelor collected the data and solved the X-ray structure for complex **4.1**. The diffraction data for **4.1**, **4.3**, and **4.4** were acquired on an Enraf Nonius CAD4F diffractometer, as described in Chapter 2. However, the diffraction data for **4.2**, **4.5** and **4.6** were acquired on a Rigaku RAXIS-Rapid curved image plate area detector, as described in Chapter 3. An empirical absorption correction was applied to **4.1**, and **4.3-4.6**, while a numerical absorption correction was applied to **4.2**. The data for **4.2** was worked up using CRYSTALCLEAR[232] control program and the resultant '*h k l*' files were inputted into *CRYSTALS*[180] where the structure was solved and refined.

4.4.2 Magnetic Susceptibility and Thermogravimetric Analysis

For complexes **4.1** and **4.5**, variable temperature magnetic susceptibility data were collected using an Evercool XL-7 magnetometer (**4.1**) or a Quantum Design SQUID MPMS-5S (**4.5**) working down to 1.8 K or 2 K at a field strength of 1 T. Sample **4.1** was measured in a low background gel cap and straw while **4.5** was measured in a cylindrical, airtight sample holder constructed from PVC.[216] The data were corrected for TIP, the diamagnetism of the sample holder and the constituent atoms (by use of Pascal constants).[68] Thermogravimetric analysis data were collected using a Shimadzu TGA-50 instrument. Solid-state visible spectra were obtained using a diode-array HP 8453 spectrometer and a suspension of sample in a customized cell.

4.4.3 Birefringence

The optical birefringence was measured, with assistance from B.C. Sih of Prof. Z.-G. Ye's group and Prof. Z.-G. Ye along different crystallographic directions by means of polarized light microscopy (Olympus BX60) on polished platelets of different orientations.

After determining the anisotropic orientation through the use of crossed polars on the microscope (i.e.: the crystal lightens and darkens upon rotating the crystal on the microscope stage), crystals with an *a*-(or *b*-) axis orientation were mounted on a cylindrical brass die with a low melting-point wax. Care was taken to ensure the brass die was not heated above 100 °C so that decomposition of the crystal did not occur. While the die returned to room temperature, a thin coating of fine alumina powder (< 10 μm) was spread over a piece of Kodac photographic paper upon which a couple of drops of silicon oil were added. The crystal was then gently polished by moving the die (crystal side down) in a 'figure eight' motion on the photographic paper. During polishing, the thickness of the crystal (d) was carefully monitored using a Mitutoyo ID-C112E digital micrometer; polishing ceased once $d \cong 50$ μm. It should be noted that it is necessary to polish both sides of the crystal. The polished crystal was then placed in diethyether for an hour in order to remove any residual residue from the polishing process.

Using a 4-1 Berek tilting compensator (U-CBE, 3λ) at the wavelength of $\lambda = 546.1$ nm (e-line, $\omega = 1.37859$, $\xi = 1.39043$), the optical retardation (Γ) was calculated using the following equation:

$$\Gamma = \mathbf{C} * 2[(1-\sin^2\theta/\omega^2)^{1/2} - (1-\sin^2\theta/\xi^2)^{1/2}] / (1/\xi^2 - 1/\omega^2) \qquad \text{(Equation 4.7)}$$

where **C** is the compensator constant and θ is mean value of the compensator angle measurements. The birefringence was then calculated by dividing the measured retardation by the crystal thickness:

$$\Delta n = \Gamma / d \qquad \text{(Equation 4.8)}$$

A heating / cooling stage (Linkam HTMS600) mounted on the microscope was used for studying the temperature dependence of the birefringence.

4.4.4 Dielectric Constant

The dielectric constant was measured, by Wenzhi Chen of Prof. Z.-G. Ye's group, along a *c*-oriented (1.0 x 1.0 x 0.25) mm^3 platelet polished to a crystal thickness of d = 250 μm using the same method as described above. The dielectric constant and tan (δ) *vs.* temperature using frequency as parameters for the crystal was measured by using a Solotran 1290 impedance analyzer in conjunction with a 1296 dielectric interface. The applied peak voltage was 0.5 V.

4.4.5 Preparation of {(tmeda)Cu[Hg(CN)$_2$]$_2$}HgCl$_4$ (4.1)

Reaction 1: a 10 mL methanolic solution of $Hg(CN)_2$ (0.100 g, 0.40 mmol) was added to a blue methanolic solution of comprised of $CuCl_2 \cdot 2\ H_2O$ (0.067 g, 0.40 mmol) and tmeda (0.046 g, 0.40 mmol) at room temperature. The solution was decanted after the precipitation of a green side-product. The solution was allowed to slowly evaporate. Dark blue block-like crystals of {(tmeda)Cu[$Hg(CN)_2$]$_2$}$HgCl_4$ (**4.1**) were collected by vacuum filtration, washed with two 1 mL portions of cold methanol, and were left to air dry. Yield: 0.198 g (49%). Reaction 2: a 10 mL aqueous solution of $Hg(CN)_2$ (0.200 g, 0.791 mmol), $HgCl_2$ (0.107 g, 0.40 mmol), and KCl (0.059 g, 0.79 mmol) was added, with stirring, to a 10 mL blue aqueous solution comprised of $Cu(ClO_4)_2 \cdot 6\ H_2O$ (0.147 g, 0.40 mmol) and tmeda (0.046 g, 0.40 mmol) at room temperature. The solution was allowed to slowly evaporate. Dark blue plate-like crystals of **4.1** were collected by vacuum filtration, washed with two 1 mL portions of cold methanol, and were left to air dry. Yield: 0.321 g (79%). Reaction 3: a 10 mL methanolic solution of $Hg(CN)_2$ (0.200 g, 0.79 mmol) and $HgCl_2$ (0.107 g, 0.40 mmol) was added, with stirring, to a blue methanolic solution comprised of $CuCl_2 \cdot 2\ H_2O$ (0.067 g, 0.40 mmol) and tmeda (0.046 g, 0.40 mmol) at room temperature. The solution was allowed to slowly evaporate. Dark blue block-like crystals of **4.1** were collected by vacuum filtration, washed with two 1 mL portions of cold methanol, and were left to air dry. Yield: 0.370

g (91%). Anal. Calcd. for $C_{10}H_{16}N_6Cl_4CuHg_3$: C, 11.69; H, 1.57; N, 8.18. Found: C, 11.72; H, 1.57; N, 8.01. IR (KBr, cm^{-1}): 3018 (s), 2992 (m), 2976 (m), 2938 (m), 2856 (w), 2817 (w), ν_{CN} **2248 (s)**, **2197 (w)**, 1632 (m), 1463 (vs), 1437 (m), 1428 (m), 1419 (w), 1388 (w), 1280 (s), 1241 (m), 1205 (w), 1120 (m), 1103 (w), 1059 (m), 1043 (m), 1008 (s), 994 (m), 946 (s), 806 (s), 760 (m), 592 (m), 499 (s), 468 (w), 426 (m).

4.4.6 Preparation of {(tmeda)Cu[Hg(CN)$_2$]$_2$}HgBr$_4$ (4.2)

To a 5 mL aqueous solution of $CuBr_2$ (0.090 g, 0.40 mmol), a 5 mL aqueous solution of tmeda (0.046 g, 0.40 mmol) was added, with stirring. Meanwhile, a second aqueous solution consisting of $HgBr_2$ (0.142 g, 0.39 mmol), $Hg(CN)_2$ (0.200 g, 0.79 mmol), and 2 mL of methanol was prepared. The Hg(II) solution was slowly added with stirring to the blue Cu(tmeda)Br_2 solution, was covered and left to stand over night. Dark blue platelets of {(tmeda)Cu[Hg(CN)$_2$]$_2$}HgBr$_4$ (**4.2**) were collected by vacuum filtration, washed with two 1 mL portions of cold water followed by two 1 mL portions of cold methanol, and were left to air dry. Additional crystals of **4.2** were obtained by slowly evaporating the remaining filtrate. Yield: 0.346 g (73%). Anal. Calcd. for $C_{10}H_{16}N_6Br_4CuHg_3$: C, 9.97; H, 1.34; N, 6.97. Found: C, 9.91; H, 1.33; N, 6.82. IR (KBr, cm^{-1}): 3736 (vw), 3019 (s), 2989 (m), 2973 (m), 2934 (m), 2854 (w), 2815 (w), ν_{CN} **2244 (s)**, **2195 (vw)**, 1614 (m), 1462 (vs), 1437 (m), 1419 (m), 1387 (w), 1370 (vw), 1340 (vw), 1280 (m), 1240 (m), 1197 (w), 1171 (vw), 1119 (m), 1103 (w), 1058 (w), 1043 (m), 1007 (s), 995 (m), 947 (s), 807 (s), 761 (m), 592 (m), 508 (s), 498 (s), 466 (w), 423 (m).

4.4.7 Preparation of {(tmeda)Cu[Hg(CN)$_2$]$_2$}HgI$_4$ (4.3)

A 30 mL aqueous solution comprised of HgI_2 (0.180 g, 0.40 mmol), KI (0.131 g, 0.79 mmol), 5 mL of ethanol, and 10 mL of methanol was prepared with stirring. Meanwhile, a methanolic solution of $Hg(CN)_2$ (0.200 g, 0.79 mmol) was added to a blue aqueous solution of comprised of $Cu(ClO_4)_2 \cdot 6\ H_2O$ (0.147 g, 0.40 mmol) and tmeda (0.046 g, 0.40 mmol) at room temperature. The pale yellow solution containing $HgI_4^{2-}{}_{(aq)}$ was added with stirring to the Cu(II) solution

resulting in the immediate formation of a green / grey precipitate. The mixture was covered and allowed to stand for 2.5 hours. The precipitate was filtered, washed with three 2 mL portions of ethanol followed by three 2 mL portions of methanol, and was discarded. The pale blue filtrate was allowed to slowly evaporate. Blue platelets of $\{(tmeda)Cu[Hg(CN)_2]_2\}HgI_4$ (**4.3**) were collected by vacuum filtration, washed with two 1 mL portions of cold water followed by two 1 mL portions of cold ethanol, and were left to air dry. Yield: 0.122 g (22%). Anal. Calcd. for $C_{10}H_{16}N_6CuHg_3I_4$: C, 8.62; H, 1.16; N, 6.03. Found: C, 8.84; H, 1.17; N, 6.14. IR (KBr, cm^{-1}): 3741 (vw), 3018 (m), 2987 (m), 2969 (m), 2920 (m), 2850 (w), 2811 (w), ν_{CN} **2236 (s), 2189 (vw)**, 2129 (m), 1918 (vw), 1869 (w), 1844 (w), 1830 (w), 1793 (w), 1712 (vs), 1653 (m), 1635 (m), 1472 (s), 1463 (s), 149 (m), 1365 (s), 1279 (m), 1228 (s), 1170 (vw), 1118 (w), 1091 (w), 1059 (w), 1043 (m), 1007 (s), 996 (m), 948 (s), 807 (s), 763 (m), 593 (m), 532 (m), 494 (s), 463 (w), 420 (m).

4.4.8 Preparation of $\{(tmeda)Ni[Hg(CN)_2]_2\}HgCl_4$ (4.4)

To a 15 mL ethanolic solution of $NiCl_2 \cdot 6\ H_2O$ (0.094 g, 0.40 mmol), a 2 mL ethanolic solution of tmeda (0.046 g, 0.40 mmol) was refluxed with stirring for 1 hour. Meanwhile, a 25 mL ethanolic solution containing $Hg(CN)_2$ (0.200 g, 0.79 mmol) and $HgCl_2$ (0.108 g, 0.40 mmol) was prepared. The Hg(II) solution was slowly added to the pale $Ni(tmeda)Cl_2$ solution and was refluxed for 1 hour. While still warm, the mixture was filtered to remove a small amount of insoluble material. The filtrate was covered and left over night. Purple crystal platelets and a blue polycrystalline material were collected by vacuum filtration, washed with two 1 mL portions of cold water, and were left to air dry. The purple crystals of $\{(tmeda)Ni[Hg(CN)_2]_2\}HgCl_4$ (**4.4**) were separated by hand. Yield: 0.098 g (24%). Anal. Calcd. for $C_{10}H_{16}N_6Cl_4Hg_3Ni$: C, 11.75; H, 1.58; N, 8.22. Found: C, 12.02; H, 1.63; N, 8.33. IR (KBr, cm^{-1}): 3013 (s), 2982 (m), 2970 (m), 2941 (m), 2918 (w), 2892 (w), 2851 (w), 2811 (w), ν_{CN} **2247 (m), 2210 (m)**, 1633 (m), 1470 (vs), 1436 (m), 1419 (m), 1387 (m), 1352 (m), 1283 (s), 1241 (m), 1195 (w), 1169 (w), 1120 (m), 1101

(w), 1059 (m), 1041 (m), 1014 (s), 1001 (m), 949 (s), 880 (vw), 804 (s), 763 (m), 589 (m), 492 (s), 440 (m), 424 (m).

4.4.9 Preparation of {(tmeda)Ni[Hg(CN)$_2$]$_2$}HgBr$_4$ (4.5)

To a 5 mL aqueous solution of $NiBr_2$ (0.088 g, 0.40 mmol), a 5 mL aqueous solution of tmeda (0.046 g, 0.40 mmol) was added with stirring for 30 minutes. A 10 mL aqueous solution $Hg(CN)_2$ (0.200 g, 0.79 mmol) was added to the pale blue Ni(tmeda)Br_2 solution with stirring. Immediate precipitation occurred following the subsequent addition of a 2 mL methanolic solution of $HgBr_2$ (0.142 g, 0.39 mmol). The mixture was covered and left to settle over night. Pink microcrystalline {(tmeda)Ni[Hg(CN)$_2$]$_2$}HgBr$_4$ (**4.5**) was collected by vacuum filtration, washed with three 2 mL portions of cold water, followed by three 5 mL portions of methanol, and was left to air dry. Yield: 0.204 g (43%). Anal. Calcd. for $C_{10}H_{16}N_6Br_4Hg_3Ni$: C, 10.01; H, 1.34; N, 7.00. Found: C, 10.30; H, 1.47; N, 7.12. IR (KBr, cm^{-1}): 3735 (vw), 3012 (s), 2978 (m), 2967 (m), 2932 (m), 2916 (m), 2899 (m), 2849 (m), 2809 (m), ν_{CN} **2244 (m)**, **2209 (m)**, 1621 (m), 1470 (vs), 1441 (m), 1419 (m), 1385 (m), 1351 (m), 1283 (s), 1240 (m), 1194 (w), 1169 (m), 1119 (m), 1101 (m), 1059 (m), 1041 (m), 1014 (s), 1002 (m), 949 (s), 804 (s), 763 (m), 590 (m), 490 (s), 441 (m), 415 (vw). Small single crystals of **4.5** were obtained upon slow evaporation of the filtrate. The crystals and microcrystalline powder had comparable IR spectra.

4.4.10 Preparation of {(tmeda)Ni[Hg(CN)$_2$]$_2$}HgI$_4$ (4.6)

To a 25 mL ethanolic solution of NiI_2 (0.137 g, 0.40 mmol), a 2 mL ethanolic solution of tmeda (0.046 g, 0.40 mmol) was refluxed with stirring for 1 hour. Meanwhile, a 25 mL ethanolic solution of $Hg(CN)_2$ (0.200 g, 0.79 mmol) and HgI_2 (0.108 g, 0.40 mmol) was prepared. The Hg(II) solution was slowly added to the dark orange Ni(tmeda)I_2 solution and was refluxed for 1 hour. The solution was covered and left to stand for 45 days. Small pink platelets of {(tmeda)Ni[Hg(CN)$_2$]$_2$}HgI$_4$ (**4.6**) were collected by vacuum filtration, washed with several 5 mL portions of ethanol to remove some impurities, and were left to air dry. Yield: 0.153 g (28%).

Anal. Calcd. for $C_{10}H_{16}N_6Hg_3I_4Ni$: C, 8.65; H, 1.16; N, 6.05. Found: C, 8.75; H, 1.25; N, 5.85. IR (KBr, cm^{-1}): 3734 (vw), 3010 (s), 2979 (m), 2963 (m), 2929 (w), 2914 (m), 2889 (m), 2847 (m), 2805 (m), ν_{CN} **2235 (m)**, **2206 (m)**, 2171 (vw), 1631 (m), 1469 (vs), 1455 (m), 1427 (m), 1394 (w), 1354 (w), 1283 (m), 1268 (w), 1240 (m), 1193 (vw), 1168 (m), 1118 (m), 1100 (w), 1059 (w), 1042 (w), 1014 (s), 1003 (m), 950 (s), 931 (vw), 850 (vw), 805 (s), 766 (m), 591 (w), 482 (s), 442 (m).

CHAPTER 5
REACTION OF MERCURY CYANIDE WITH UNSATURATED COPPER(II) BIPYRIDINE COMPLEX CATIONS

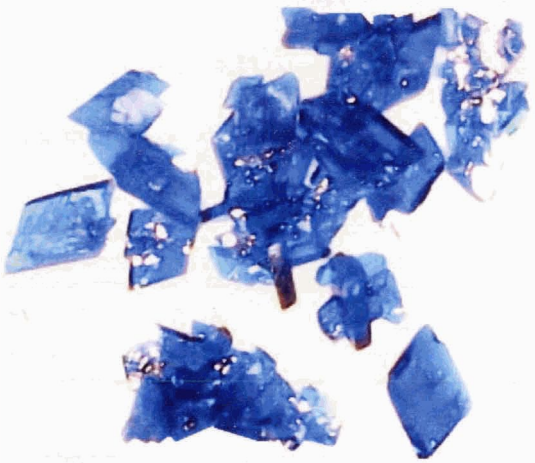

5.1 INTRODUCTION

5.1.1 Research Objectives

As detailed in Chapter 4, a series of self-assembled isostructural coordination polymers with the general formula $\{(tmeda)M[Hg(CN)_2]_2\}HgX_4$ (M = Cu(II), Ni(II); X = Cl, Br, I) were prepared. The use of Lewis acidic HgX_2 units induced halide migration from the harder M(II) centres to the softer, unsaturated, more Lewis-acidic $HgCl_2$ centres, forming tetrahedral $[HgX_4]^{2-}$ in the process. These anionic building blocks induce the formation of the non-centrosymmetric 2-D layer adopted by complexes **4.1**-**4.6**.

In an effort to test the robustness of this 2-D layered system, this chapter investigates the replacement of the bidentate *tmeda* capping ligand with bidentate *2,2'-bipyridine* (bipy) using a similar reaction scheme as developed for the $\{(tmeda)Cu[Hg(CN)_2]_2\}HgCl_4$ complex (**4.1**).

5.2 RESULTS, ANALYSIS AND DISCUSSION*

The reaction of an aqueous solution of $CuCl_2$ containing one equivalent of bipy with an aqueous solution containing two equivalents of $Hg(CN)_2$ and one equivalent of $HgCl_2$ yielded three minor crystalline products after partial evaporation of the resulting solution. Blue-green platelets of $[Cu(bipy)_2(\mu\text{-}Cl)_2Hg(CN)_2]$ (**5.1**), dark blue platelets of $[Cu(bipy)_2Hg_2Cl_6]_2$ (**5.2**), and dark blue blocks of $\{[Cu(bipy)Hg(CN)_2Cl_2]_2Hg(CN)_2\}$ (**5.3**) were isolated and characterised.

* Leznoff, D. B.; Draper, N. D.; Batchelor, R. J. *Polyhedron* **2003**, *22*, 1735-1743. Reproduced by permission of Elsevier B.V.

Upon further evaporation of the remaining solution, the majority product, a blue polycrystalline compound, was obtained. An IR spectra of this compound showed two ν_{CN} stretches (2225 cm^{-1}, 2185 cm^{-1}) similar to those found for $\{(tmeda)Cu[Hg(CN)_2]_2\}HgCl_4$ (**4.1**) (ν_{CN} = 2248 cm^{-1}, 2197 cm^{-1}). Table 5.1 shows the elemental analysis results for the polycrystalline compound.

Table 5.1 Elemental analysis for blue polycrystalline majority product.

Compound		*% C*	*% H*	*% N*
$\{(bipy)Cu[Hg(CN)_2]_2\}HgCl_4$	Calculated	15.75	0.76	7.87
Blue polycrystalline product	Experimental	17.21	0.98	7.21

Although there is a significant difference between the calculated and experimental %C, this could be attributed to a possible impurity in the polycrystalline sample. In an attempt at recrystallization, the compound was then dissolved in concentrated NH_4OH and allowed to slowly evaporate. Dark blue platelets of $\{[Cu(bipy)(OH)(Cl)]_2Hg(CN)_2\} \cdot 2\ H_2O$ (**5.4**) were the only crystals isolated and characterized using this recrystallization technique.[35,233,234] Although the IR spectra and EA analysis both support the possible formation of $\{(bipy)Cu[Hg(CN)_2]_2\}HgCl_4$, this evidence remains inconclusive.

The reaction of an aqueous solution of $Cu(ClO_4)_2$ containing one equivalent of bipy with an aqueous solution containing two equivalents of $Hg(CN)_2$, one equivalent of $HgCl_2$, and two equivalents of KCl only yielded crystals of $Cu(bipy)_2(ClO_4)_2$ as confirmed by IR and EA analyses.

The structural and magnetic properties of **5.1-5.4** are investigated below.

5.2.1 Rational Synthesis of Complexes 5.1-5.4

Complexes **5.1-5.4** could also be synthesized by different means with higher yields (see section 5.4). Single crystals of **5.1** and **5.2** were obtained by slow evaporation of solutions containing $Cu(bipy)_2Cl_2$ and one equivalent of $Hg(CN)_2$ or two equivalents of $HgCl_2$ respectively, as summarized by equations 5.1 and 5.2.

1) $CuCl_2 + 2\ bipy \longrightarrow [Cu(bipy)_2]Cl_2$

2) $[Cu(bipy)_2]Cl_2 + Hg(CN)_2 \longrightarrow [Cu(bipy)_2(\mu\text{-}Cl)_2Hg(CN)_2]$ Equation 5.1

1) $CuCl_2 + 2\ bipy \longrightarrow [Cu(bipy)_2]Cl_2$

2) $[Cu(bipy)_2]Cl_2 + 2\ HgCl_2 \longrightarrow [Cu(bipy)_2Hg_2Cl_6]_2$ Equation 5.2

The slow evaporation of a solution containing a 10% excess of $Hg(CN)_2$ and only one equivalent of bipy per $CuCl_2$ moiety yielded single crystals of **5.3**.

1) $CuCl_2 + bipy \longrightarrow [Cu(bipy)]Cl_2$

2) $2\ [Cu(bipy)]Cl_2 + 3\ Hg(CN)_2 \longrightarrow \{[Cu(bipy)Hg(CN)_2Cl_2]_2Hg(CN)_2\}$ Equation 5.3

If solutions containing one equivalent of $Cu(bipy)Cl_2$ and two equivalents of $Hg(CN)_2$ are made basic via addition of NH_4OH prior to solvent evaporation,[234] then single crystals of **5.4** are obtained:

1) $CuCl_2 + bipy \longrightarrow [Cu(bipy)]Cl_2$

2) $2\ [Cu(bipy)]Cl_2 + Hg(CN)_2 \xrightarrow{OH^-/H_2O} \{[Cu(bipy)OHCl]_2Hg(CN)_2\} \cdot 2\ H_2O$ Equation 5.4

5.2.2 Structure of $[Cu(bipy)_2(\mu\text{-}Cl)_2Hg(CN)_2]$ (5.1)

The X-ray crystal structure of $[Cu(bipy)_2(\mu\text{-}Cl)_2Hg(CN)_2]$ (**5.1**) reveals a simple molecular complex, in which the coordinately unsaturated $Hg(CN)_2$ unit is bound to the chloride ligands, which act as Cu-Hg bridging groups, isostructural to the Mn(II) (**3.1**) and the Ni(II) (**3.3**) complexes (see Figure 3.4). The Cu(II) centre in **5.1** has an axially-distorted, octahedral geometry, with two 2,2'-bipyridine ligands *cis*-oriented and two chloride atoms completing the coordination sphere. The Cu(1)-N bond lengths range from 1.996(3) and 2.087(4) Å in the equatorial plane to 2.189(4) Å in the Jahn-Teller distorted axial site (Table 5.2). The equatorial and axial Cu(1)-Cl bond lengths are 2.443(1) and 2.786(1) Å respectively, which can be compared with the 2.218(19) and 2.723(3) Å found in the equatorial / axial Cu-Cl bonds[204] in the

chloride-bridged $[(terpy)CuCl]_2[PF_6]_2$ or the 2.481(1) and 2.545(2) Å found in the distorted, chloride-bridged $[(dpt)CuCl]_2(Cl)_2$ (dpt = dipropylenetriamine).[210] The addition of $Hg(CN)_2$ to coordinatively saturated $Cu(bipy)_2Cl_2$ does not induce halide migration and no coordination sites are opened on the Cu(II) centre; extended $\pi\cdots\pi$ stacking of neighbouring conjugated ring systems characterized by interplanar distances of 3.4-3.6 Å form 1-D chains from the molecular units of **5.1**. These results are analogous to those described in Chapter 3 for complexes **3.1-3.4**.

Table 5.2 Selected Bond Lengths (Å) and Angles (°) for $[Cu(bipy)_2(\mu\text{-}Cl)_2Hg(CN)_2]$ (**5.1**).

Selected Atoms	*Bond Lengths*	*Selected Atoms*	*Bond Lengths*
Cu(1)-N(1)	1.999(3)	Cu(1)-N(2)	2.189(4)
Cu(1)-N(3)	1.996(3)	Cu(1)-N(4)	2.087(4)
Cu(1)-Cl(1)	2.443(1)	Cu(1)-Cl(2)	2.786(1)
Hg(1)-C1(1)	2.820(1)	Hg(1)-Cl(2)	2.710(1)
Hg(1)-C(12)	2.059(5)	Hg(1)-C(12)	2.051(5)
Selected Atoms	*Bond Angles*	*Selected Atoms*	*Bond Angles*
N(1)-Cu(1)-N(2)	78.64(14)	N(1)-Cu(1)-N(3)	173.28(17)
N(1)-Cu(1)-N(4)	95.05(14)	N(2)-Cu(1)-N(3)	96.79(14)
N(2)-Cu(1)-N(4)	93.77(14)	N(3)-Cu(1)-N(4)	80.24(14)
N(1)-Cu(1)-Cl(1)	89.03(11)	N(1)-Cu(1)-Cl(2)	96.23(11)
N(2)-Cu(1)-Cl(1)	92.10(10)	N(2)-Cu(1)-Cl(2)	174.60(10)
N(3)-Cu(1)-Cl(1)	96.11(12)	N(3)-Cu(1)-Cl(2)	88.20(10)
N(4)-Cu(1)-Cl(1)	173.40(10)	N(4)-Cu(1)-Cl(2)	84.90(10)
Cu(1)-Cl(1)-Hg(1)	95.86(4)	Cu(1)-Cl(2)-Hg(1)	90.86(4)
Cl(1)-Hg(1)-C(11)	93.94(16)	Cl(1)-Hg(1)-C(12)	98.30(16)
Cl(2)-Hg(1)-C(11)	100.39(17)	Cl(2)-Hg(1)-C(12)	95.82(16)
Cl(1)-Cu(1)-Cl(2)	89.54(4)	Cl(1)-Hg(1)-Cl(2)	83.71(4)
C(11)-Hg(1)-C(12)	160.6(2)		

5.2.3 Structure of $[Cu(bipy)_2Hg_2Cl_6]_2$ (5.2)

The structure of $[Cu(bipy)_2Hg_2Cl_6]_2$ (**5.2**) is essentially molecular (Figure 5.1). However, the Cu(II) centre in **5.2** is only five-coordinate, with a distorted geometry as exemplified by its tau parameter of $\tau = 0.47$. The $[Cu(bipy)_2Cl]^+$ unit resembles the dangling $[Cu(phen)_2Cl]^+$ cations of complex **3.6** ($\tau = 0.72$). The Cu(1)-Cl(4) distance of 3.856 Å (Table 5.3) indicates that this chloride does not bind to the open Cu(II) coordination site. One chloride ligand has migrated to

generate an $[HgCl_3]^-$ anion, while the remaining chloride ligand (Cu(1)-Cl(3) = 2.320(7) Å) bridges to another Hg(II) centre, resulting in the formation of a $[Hg_2Cl_6]^{2-}$ unit.

Table 5.3 Selected Bond Lengths (Å) and Angles (°) for $[Cu(bipy)_2Hg_2Cl_6]_2$ (**5.2**)[a].

Selected Atoms	*Bond Lengths*	*Selected Atoms*	*Bond Lengths*
Cu(1)-N(1)	1.978(17)	Cu(1)-N(2)	2.125(17)
Cu(1)-N(3)	1.973(16)	Cu(1)-N(4)	2.042(16)
Cu(1)-Cl(3)	2.320(7)	Hg(2)-Cl(3)	2.728(6)
Hg(2)-C1(4)	2.338(8)	Hg(2)-Cl(1)	2.337(7)
Hg(2)-Cl(2)	2.884(6)	Hg(1)-Cl(1)	3.112(7)
Hg(1)-Cl(2)	2.541(6)	Hg(1)-Cl(5)	2.359(6)
Hg(1)-Cl(6)	2.361(6)	Hg(1)-Cl(5*)	3.029(7)
Selected Atoms	*Bond Angles*	*Selected Atoms*	*Bond Angles*
N(1)-Cu(1)-N(2)	77.8(7)	N(1)-Cu(1)-N(3)	172.0(8)
N(1)-Cu(1)-N(4)	92.3(7)	N(2)-Cu(1)-N(3)	100.9(7)
N(2)-Cu(1)-N(4)	109.0(7)	N(3)-Cu(1)-N(4)	80.6(7)
N(1)-Cu(1)-Cl(3)	93.7(6)	N(2)-Cu(1)-Cl(3)	107.0(5)
N(3)-Cu(1)-Cl(3)	94.2(5)	N(4)-Cu(1)-Cl(3)	144.0(5)
Cu(1)-Cl(3)-Hg(2)	107.3 (2)	Cl(3)-Hg(2)-Cl(1)	93.2(2)
Cl(3)-Hg(2)-Cl(2)	97.39(19)	Cl(3)-Hg(2)-Cl(4)	100.5(3)
Cl(1)-Hg(2)-Cl(2)	87.78(19)	Cl(1)-Hg(2)-Cl(4)	162.6(3)
Cl(4)-Hg(2)-Cl(2)	100.9(2)	Cl(1)-Hg(1)-Cl(2)	79.49(18)
Cl(1)-Hg(1)-Cl(5)	92.6(2)	Cl(1)-Hg(1)-Cl(6)	89.5(2)
Cl(1)-Hg(1)-Cl(5*)	170.24(19)	Cl(2)-Hg(1)-Cl(5)	110.5(2)
Cl(2)-Hg(1)-Cl(5*)	93.8(2)	Cl(2)-Hg(1)-Cl(6)	107.8(2)
Cl(5)-Hg(1)-Cl(5*)	83.1(2)	Cl(5)-Hg(1)-Cl(6)	141.4(3)
Hg(1)-Cl(5)-Hg(1*)	96.9(2)	Cl(5*)-Hg(1)-Cl(6)	99.4(2)
Hg(1)-Cl(2)-Hg(2)	96.72(19)		

[a] Symmetry transformation: (*) $-x+1, -y+1, -z+1$.

The molecule dimerizes via Hg-Cl bridges to yield the final structure: a dinuclear Cu(II) complex with an impressive $[Hg_4Cl_{12}]^{4-}$ ribbon-like bridge. The Hg-Cl bond lengths in the bridge range from 2.337(7) to 3.112(7) Å and can be compared with the Hg-Cl bond lengths of 2.35 Å, 2.40 Å , 2.81 Å, and 3.27 Å in $NaHgCl_3$, which is composed of twofold polymeric ribbons of $[Hg_2Cl_6]^{2-}$ units in the solid state structure.[235] The substantially higher Lewis acidity of $HgCl_2$ as compared with $Hg(CN)_2$,[95] may also account for the increased halide migration in **5.2** *vs.* the

cyanide-containing **5.1**. The Cu(1)-Hg(2) and Hg(1)-Hg(2) distances are 4.073 Å and 4.059 Å respectively. There are no significant intermolecular interactions between neighbouring $[Cu(bipy)_2Hg_2Cl_6]_2$ molecules.

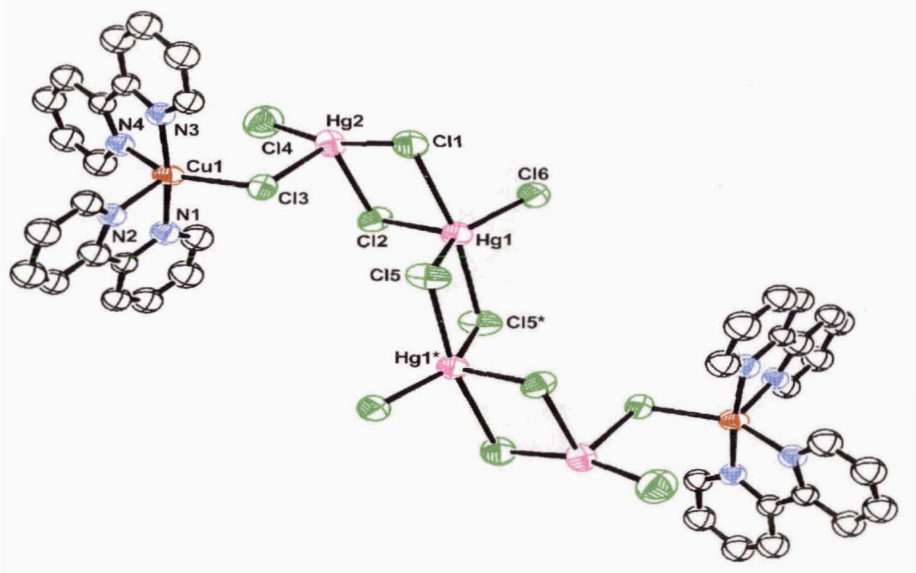

Figure 5.1 Molecular structure of $[Cu(bipy)_2Hg_2Cl_6]_2$ (**5.2**).
Hydrogen atoms have been removed for clarity (ORTEP 50% ellipsoids).

5.2.4 Structure of $\{[Cu(bipy)Hg(CN)_2Cl_2]_2Hg(CN)_2\}$ (5.3)

The X-ray crystal structure of $\{[Cu(bipy)Hg(CN)_2Cl_2]_2Hg(CN)_2\}$ (**5.3**), as depicted in Figure 5.2, reveals that some general structural features of **5.1** are present in **5.3** as well: the chloride ligands have not migrated from the Cu(II) centre, but bridge to a $Hg(CN)_2$ unit via Hg(1)-Cl bonds of 2.7867(16) and 2.923(16) Å to yield a $[(bipy)Cu(\mu\text{-}Cl)(Cl)Hg(CN)_2]$ moiety. The Cu(II) centre has a five-coordinate, square-pyramidal geometry, with one bipy, one chloride (Cu(1)-Cl(2) = 2.3090(16) Å) and one cyano-nitrogen from the adjacent $[(bipy)Cu(\mu\text{-}Cl)_2Hg(CN)_2]$ group in the basal plane and the other chloride (Cu(1)-Cl(2) = 2.5560(17) Å) in the apical position completing the coordination sphere (Table 5.4). The Cu(1)-*N*-cyano bond length of 1.967(5) Å is typical of an equatorially bound N-cyanide to Cu(II) ; this interaction is clearly visible as a bridging stretch in the IR spectrum of **5.3** (ν_{CN} = 2242 cm^{-1}).

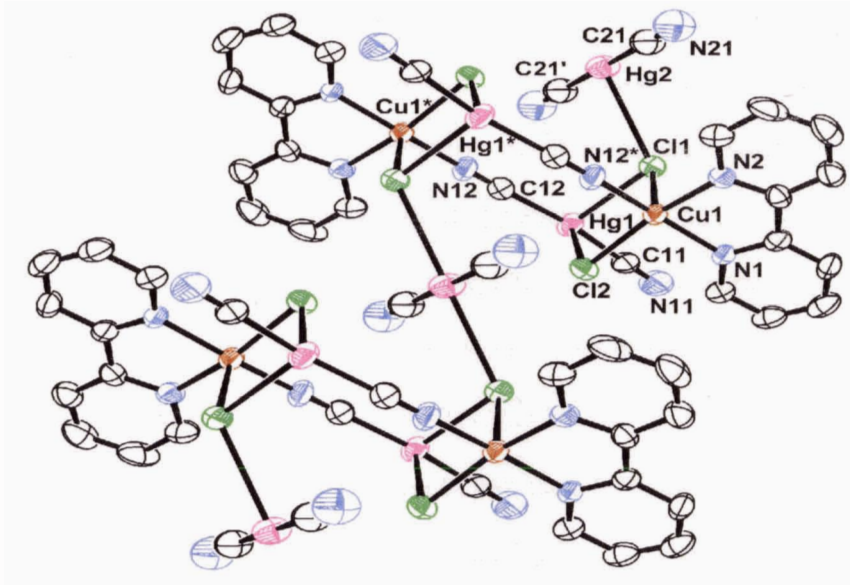

Figure 5.2 Extended 1-D chain structure of $\{[Cu(bipy)Hg(CN)_2Cl_2]_2Hg(CN)_2\}$ (5.3). Hydrogen atoms have been removed for clarity (ORTEP 50% ellipsoids).

Table 5.4 Selected Bond Lengths (Å) and Angles (°) for $\{[Cu(bipy)Hg(CN)_2Cl_2]_2Hg(CN)_2\}$ (5.3)[a].

Selected Atoms	*Bond Lengths*	*Selected Atoms*	*Bond Lengths*
Cu(1)-N(1)	1.994(5)	Cu(1)-N(2)	1.998(5)
Cu(1)-Cl(1)	2.5560(17)	Cu(1)-Cl(2)	2.3090(16)
Cu(1)-N(12*)	1.967(5)	Hg(2)-Cl(1)	3.1450(16)
Hg(1)-C1(1)	2.7867(16)	Hg(1)-Cl(2)	2.9523(16)
Hg(1)-C(11)	2.043(6)	Hg(1)-C(12)	2.042(7)
C(11)-N(11)	1.100(8)	C(12)-N(12)	1.122(8)
Hg(2)-C(21)	2.005(7)	C(21)-N(21)	1.140(9)
Selected Atoms	*Bond Angles*	*Selected Atoms*	*Bond Angles*
N(1)-Cu(1)-N(2)	80.6(2)	N(1)-Cu(1)-N(12*)	165.2(2)
N(1)-Cu(1)-Cl(1)	96.95(13)	N(1)-Cu(1)-Cl(2)	94.73(14)
N(2)-Cu(1)-Cl(1)	96.27(14)	N(2)-Cu(1)-Cl(2)	164.61(15)
N(2)-Cu(1)-N(12*)	92.1(2)	Cl(1)-Cu(1)-Cl(2)	98.87(6)
Cl(1)-Cu(1)-N(12*)	96.80(18)	Cl(1)-Hg(1)-Cl(2)	80.21(4)
Cl(2)-Cu(1)-N(12*)	88.94(16)	Cl(1)-Hg(1)-C(11)	96.93(19)
Cl(1)-Hg(1)-C(12)	93.68(18)	Cl(2)-Hg(1)-C(11)	98.79(19)
Cl(2)-Hg(1)-C(12)	89.5(2)	C(11)-Hg(1)-C(12)	167.5(3)
C(12)-N(12)-Cu(1*)	177.3(6)	C(21)-Hg(2)-C(21')	180
Cl(1)-Hg(2)-C(21)	94.6(2)	Cl(1)-Hg(2)-C(21')	85.4(2)
Hg(1)-Cl(1)-Cu(1)	89.93(5)	Hg(1)-Cl(2)-Cu(1)	90.98(5)

[a] Symmetry transformations: (*) $-x, -y+1, -z+2$; (') $-x+1, -y+1, -z+2$.

The $Hg(CN)_2$ units thus act as bridging ligands via the Hg(II) centre to one copper, and via one cyano group to another copper. This unusual binding motif generates a "Chinese kite"-shaped Cu_2Hg_2 unit (Figure 5.2) with C_i symmetry. Each tetranuclear cluster is bridged to the next one via two copper-bound chloride ligands at opposite ends of the cluster, which donate not only to Hg(1) but also to another equivalent of $Hg(CN)_2$ situated between the clusters; each of these Hg(2) centres has an effective square-planar coordination (2+2) based on linear characteristic coordination as a result. This Hg(2)-Cl(1) interaction of 3.1450(16) Å generates a 1-D chain of Cu_2Hg_2 clusters; a similar example has been reported where $HgCl_2$ bridges Cu_4 clusters.[125] Thus the use of coordinately unsaturated $Hg(CN)_2$, which accepts chloride ligands, increases the structural dimensionality from zero to one in complex **5.3** and is also instrumental in constructing the clusters described. Extended $\pi\cdots\pi$ stacking of neighbouring conjugated ring systems characterized by interplanar distances of 3.3-3.7 Å form 2-D sheets along the *ac*-plane.

5.2.5 Structure of $\{[Cu(bipy)(OH)(Cl)]_2Hg(CN)_2\} \cdot 2\ H_2O$ (5.4)

The X-ray structure, shown in Figure 5.3, indicates that dinuclear $[(bipy)Cu(\mu\text{-}OH)]_2$ units are produced in which each Cu(II) centre is square-pyramidal, with a chloride ligand in the apical position (Cu(1)-Cl(2) = 2.6709(11) Å). Within the dimer, the Cu-N, Cu-O and Cu-Cu' distances are all comparable with those found in other $[(bipy)Cu(\mu\text{-}OH)]$ systems.[236] Each dinuclear unit in **5.4** is connected to the next via the apical chloride ligands, which bridge to an $Hg(CN)_2$ molecule; each Hg(1) thus becomes effectively square-planar (2+2 based on linear characteristic coordination), with Hg(1)-Cl(2) bonds of 2.980(1) Å (Table 5.5). This motif is similar to that of $\{[Cu(phen)_2Cl]_2Hg(CN)_2[Hg(CN)_2Cl]_2\}$ (**3.7**) and $\{[Cu(bipy)Hg(CN)_2Cl_2]_2Hg(CN)_2\}$ (**5.3**); the chloride ligands bridge via the coordinatively unsaturated $Hg(CN)_2$ acceptors to yield a 1-D chain of alternating $[(bipy)Cu(\mu\text{-}OH)(Cl)]_2$ and $Hg(CN)_2$ units (Figure 5.3). Thus, the $Hg(CN)_2$ units have effectively increased the structural dimensionality from zero to one.

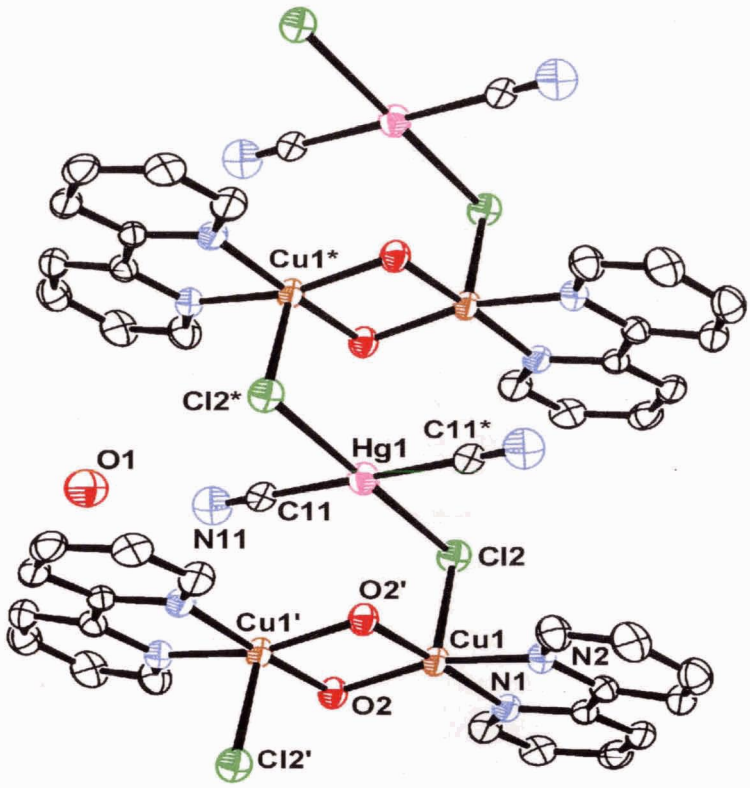

Figure 5.3 Extended 1-D chain structure of $\{[Cu(bipy)(OH)(Cl)]_2Hg(CN)_2\} \cdot 2\ H_2O$ (**5.4**). Hydrogen atoms have been removed for clarity (ORTEP 50% ellipsoids).

Table 5.5 Selected Bond Lengths (Å) and Angles (°) for $\{[Cu(bipy)(OH)(Cl)]_2Hg(CN)_2\} \cdot 2\ H_2O$ (**5.4**)[a].

Selected Atoms	*Bond Lengths*	*Selected Atoms*	*Bond Lengths*
Cu(1)-N(1)	2.008(3)	Cu(1)-N(2)	2.008(3)
Cu(1)-O(2)	1.943(3)	Cu(1)-O(2')	1.952(3)
Cu(1)-Cl(2)	2.6709(11)	Hg(1)-C(11)	2.081(4)
C(11)-N(11)	1.077(5)	Hg(1)-Cl(2*)	2.980(1)
Selected Atoms	*Bond Angles*	*Selected Atoms*	*Bond Angles*
N(1)-Cu(1)-N(2)	80.82(13)	N(1)-Cu(1)-O(2)	97.08(12)
N(1)-Cu(1)-O(2')	175.36(13)	N(2)-Cu(1)-O(2)	159.51(14)
N(2)-Cu(1)-O(2')	97.94(13)	N(1)-Cu(1)-Cl(2*)	87.6(1)
N(2)-Cu(1)-Cl(2*)	100.1(1)	Cl(2)-Cu(1)-O(2)	97.03(9)
Cl(2)-Cu(1)-O(2')	100.19(9)	C(11)-Hg(1)-C(11*)	180
O(2)-Cu(1)-O(2')	82.51(12)	Cu(1)-Cl(2)-Hg(1)	86.46(3)
N(11)-C(11)-Hg(1)	176.9(4)	Cl(2)-Hg(1)-C(11)	86.93(11)
Cl(2)-Hg(1)-C(11*)	93.07(11)	Cu(1)-O(2)-Cu(1')	97.49(12)

[a] Symmetry transformation: (*) $-x, -y, -z+2$; (') $-x+1, -y, -z+2$.

These chains are connected by H_2O molecules which form hydrogen bonds with the chlorides of one chain and *N*-cyano atom on the other (not shown) but this interaction is not magnetically significant as the distance between Cu(II) centres is > 10 Å. Other coordination polymers that utilize Cu(II) dimers as "complex ligands" have been reported.[237,238]

5.2.6 Infrared Analysis

Unlike the IR spectra for **3.1-3.6** which contain aromatic-amine capping ligands, the ν_{CN} stretches for **5.1**, **5.3**, and **5.4** can easily be identified. The ν_{CN} stretches range from 2146 cm^{-1} (**5.1**) to 2242 cm^{-1} (**5.3**) and are consistent with either terminal cyanide groups on non-linear Hg(II) units or bridging cyanide groups (Table 5.6).

Table 5.6 Comparison of cyanide (ν_{CN}) absorptions (cm^{-1}) for complexes **5.1-5.4**.

Complex	*Bridging* ν_{CN}	*Terminal* ν_{CN}
$[Cu(bipy)_2(\mu\text{-}Cl)_2Hg(CN)_2]$ (**5.1**)[195]		2172 (w), 2146 (vw)
$[Cu(bipy)_2Hg_2Cl_6]_2$ (**5.2**)[195]	not applicable	not applicable
$\{[Cu(bipy)Hg(CN)_2Cl_2]_2Hg(CN)_2\}$ (**5.3**)[195]	2242 (m)	2182 (w)
$\{[Cu(bipy)(OH)(Cl)]_2Hg(CN)_2\} \cdot 2\ H_2O$ (**5.4**)[195]		2182 (w)

Values are determined from the maximum of the absorption peak. IR spectrometer resolution = ± 2 cm^{-1}; all spectra were collected as KBr pellets.

Complex **5.1** shows two ν_{CN} stretches (2146 cm^{-1}, 2172 cm^{-1}) consistent with terminal cyanide groups on non-linear Hg(II) units with coordination numbers greater than two. These results are also consistent with the ν_{CN} stretches observed for the isomorphous complexes Mn(II) (**3.1**) and Ni(II) (**3.3**).

There is a general consistency between the expected structure as predicted by the cyanide stretches and the observed structure from X-ray analysis for compounds **5.3** and **5.4**. Compound **5.3** shows a single bridging ν_{CN} stretch and a single terminal ν_{CN} stretch, although there are two different terminal cyano groups as shown in Figure 5.2. Compound **5.4** shows a single terminal ν_{CN} stretch consistent with the two equivalent cyano groups shown in Figure 5.3.

5.2.7 Magnetic Properties

For **5.1**, the paramagnetic transition metal centres are well separated in space with no viable magnetic coupling pathway. However complexes **5.2-5.4** have structural features that might mediate magnetic interactions. Accordingly, the temperature (T) dependence of the molar magnetic susceptibility (χ_M) of polycrystalline samples of these three compounds were measured from 2-300 K.

In $[Cu(bipy)_2Hg_2Cl_6]_2$ (**5.2**), the Cu(1)-Cu(1*) distance of 15.4 Å precludes any significant magnetic interactions between the two d^9 centres. However, the magnetic susceptibility as a function of temperature was measured from 2-300 K and although Curie Law behaviour was observed as the temperature was lowered from 300 to 15 K (μ_{eff} = 1.87 μ_B), a small but discernable drop in magnetic moment to μ_{eff} = 1.81 μ_B at 2 K was also noted. The data can be fit to the Curie-Weiss Law, with C = 0.4371(2) and θ = -0.132(4) K, consistent with weak antiferromagnetic coupling between the Cu(II) centres. This apparent weak antiferromagnetic (AF) interaction may be mediated by the highly polarizable and covalent $[Hg_4Cl_{12}]^{4-}$ bridge, but the possibility that a small structural change at low temperature could activate a shorter pathway (e.g. an Hg-Cl bridge between molecular units) cannot be excluded. In any event, the magnitude of this coupling is very small and hence was not analyzed further.

The temperature (T) dependence of the molar magnetic susceptibility (χ_M) of a polycrystalline sample of **5.3** was measured in the temperature range 2-300 K. The plot of μ_{eff} *vs.* T is shown in Figure 5.4. At 300 K, μ_{eff} = 1.95 μ_B, consistent with isolated S = ½ Cu(II) centres. The μ_{eff} value remains constant until 25 K, at which point it begins to decrease, reaching a value of μ_{eff} = 1.49 μ_B at 2 K. The data can be fit to the Curie-Weiss Law, with C = 0.4853(9) and θ = -1.33(2) K, that is consistent with the presence of weak AF interactions. Examining the X-ray structure from the point of view of magnetic exchange, the Cu(1)-Cu(1*) distance within one cluster is 6.282 Å. The two through-bond magnetic pathways delineated by Cu-Cl-Hg-CN-Cu, in

which the copper centres are connected in an equatorial / equatorial fashion, can mediate significant magnetic interactions.[239] In addition, copper centres on adjacent clusters are connected by axial Cl-Hg-Cl linkages, with a Cu(1)-Cu(1*) distance of 10 Å. This intercluster pathway is expected to yield weaker exchange interactions due to the longer Cu-Cu distance and axial / axial linkage. With this structural analysis in mind, the magnetic data were fitted with two different models. Firstly, using the simple Bleaney-Bowers dimer model, with $\hat{H} = -2JS_1S_2$ (assuming no intercluster interactions),[68,187] the best-fit values of J = -0.99(2) cm^{-1} and g = 2.260(3) are obtained. If the second pathway is included, then the system can in principle be treated as a 1-D chain of Cu(II) dimers. Thus, using the theoretical expression for an alternating 1-D chain of AF coupled S = ½ Cu(II) centres, which uses an additional molecular field parameter to account for the interdimer interactions,[240] the best-fit values of J_1 = -0.92(1) cm^{-1}, α = 0.17(1) (i.e., the second coupling constant is αJ_1, or -0.16 cm^{-1}) and g = 2.260(2) are obtained; this fit is indicated as a solid line in Figure 5.4.

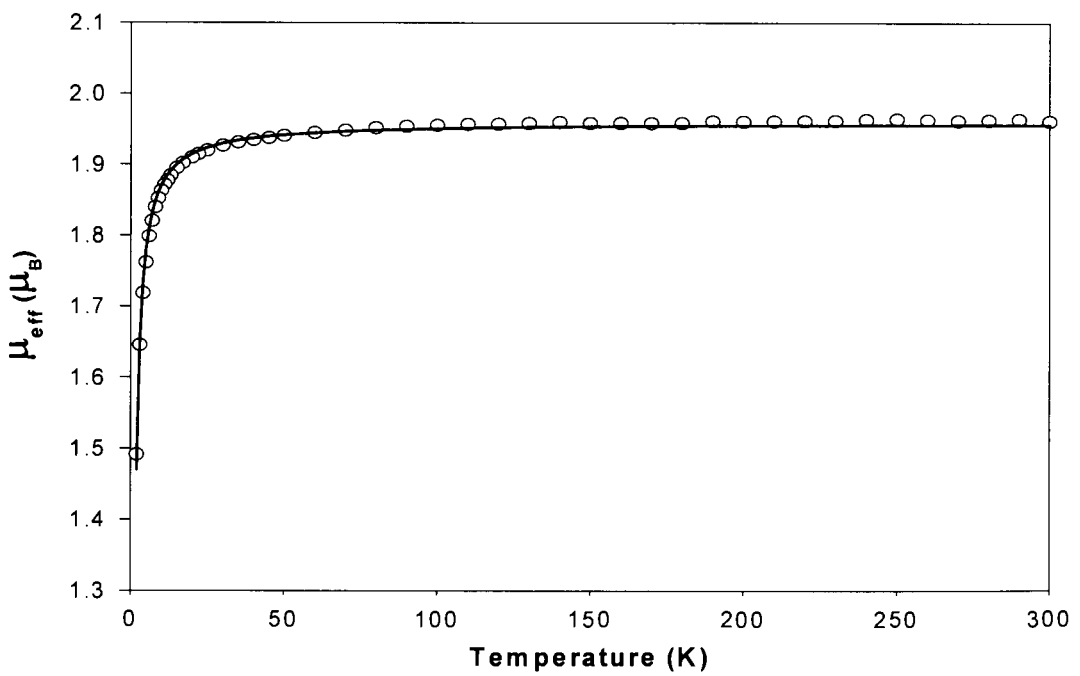

Figure 5.4 Temperature dependence of μ_{eff} for **5.3** treated as an alternating 1-D chain of AF coupled Cu(II) centres; the solid line is theory (see text).

Even though they are weak, both pathways represent unusual examples of Hg(II) (a diamagnetic d^{10} metal centre) mediating a magnetic interaction. As previously mentioned, other d^{10} metal centres, including copper(I), gold(I), silver(I), and zinc(II) have been shown by the Leznoff group and others to be capable of mediating magnetic exchange.[80,82,241,242]

Copper(II) hydroxo-bridged dimers have been extensively studied both experimentally and theoretically; the Cu-O-Cu angle and the out-of-plane O-H/R angle are known to be key geometric features that control the sign and magnitude of the coupling between S = ½ Cu(II) centres.[243-245] Specifically, Cu-O-Cu angles > 97.5° generally yield AF coupling, while angles < 97.5° generate ferromagnetic (F) interactions.[246] The [(bipy)Cu(μ-OH)]-containing structures that have been previously reported all exhibit strongly ferromagnetic intradimer interactions, in keeping with their Cu-O-Cu angles, which range from 94.5° to 97.3°;[247] this angle is anion-dependent.[236] The critical Cu-O-Cu angle in **5.4** is 97.5°, which is larger than that found in other [(bipy)Cu(μ-OH)] systems; on this basis alone, a small *J*-coupling should be observed. However, the angle of the O-H group (O-H hydrogen atoms were located and refined in **5.4**) relative to the Cu_2O_2 plane is 56°, which is predicted to lead to significant ferromagnetic interactions.[243,244] To explore this point, the temperature (T) dependence of the molar magnetic susceptibility (χ_M) of a polycrystalline sample of **5.4** was measured and the results are depicted as a μ_{eff} *vs.* T plot in Figure 5.5. As the temperature is lowered, μ_{eff} increases slowly from 2.04 μ_B at 300 K to 2.22 μ_B at 25 K, consistent with the presence of ferromagnetic interactions. Below 25 K, μ_{eff} decreases to a value of 2.08 μ_B at 2 K. The data were fitted assuming an intradimer ferromagnetic interaction and a much weaker interdimer AF interaction mediated through the Cl-Hg-Cl bonds; a similar intercluster pathway was identified in **5.3**. The data could be successfully fitted using the Bleaney-Bowers equation and an additional molecular field parameter (zJ')[68] used under the assumption that zJ' is a much smaller value as compared to *J*.

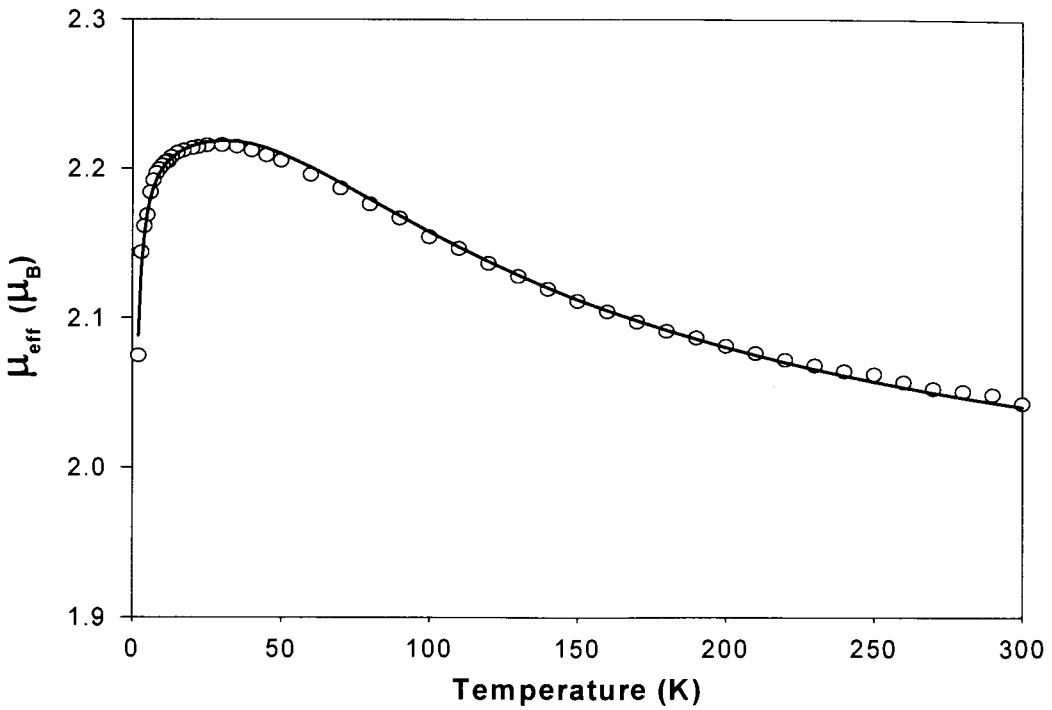

Figure 5.5 Temperature dependence of μ_{eff} for **5.4** fitted using the Bleaney-Bower's equation with an intradimer F interaction and a much weaker interdimer AF interaction. The solid line is theory (see text).

This results in the best-fit values of J = 56.3(8) cm^{-1}, g = 2.23(2) and zJ' = -0.060(4) cm^{-1}. The result illustrates the importance of the O-H/R angle relative to the Cu_2O_2 plane in determining the sign and magnitude of the Cu-Cu coupling, as has been stressed recently.[243,244] It is predicted that if the hydrogen atom remains in the Cu_2O_2 plane, then the magnetism for most hydroxo-bridged Cu(II) dimers will be antiferromagnetic. Conversely, a large out of plane angle results in ferromagnetic Cu(II) dimer interactions,[243,244] as observed for **5.4**. The data could not be fitted with the 1-D chain model for alternating F / AF coupled S = ½ centres[237,248] due to the relative weakness of J_{AF} *vs.* J_F. The slightly larger interdimer coupling constant in **5.3** compared to **5.4** can be attributed both to the shorter Cu-Cl distances (2.5560(17) *vs.* 2.6709(11) Å) and larger Cu-Cl-Hg angle (122.05(3)° *vs.* 86.46(3)°) in **5.3** *vs.* **5.4**, both of which enhance the orbital overlap necessary for magnetic exchange.

5.3 CONCLUSIONS

While attempting to synthesize single crystals of $\{(bipy)Cu[Hg(CN)_2]_2\}HgCl_4$, three different coordination polymers that incorporate linear, neutral $Hg(CN)_2$ units as ligands have been isolated, as well as a related complex using $HgCl_2$. As previously demonstrated, these d^{10} centres can increase structural dimensionality by acting as low-coordinate Lewis acids, accepting, chloride ligands from complex cations in a bridging fashion and the $Hg(CN)_2$ units can mediate magnetic exchange through the diamagnetic Hg(II) centre, thereby increasing the magnetic dimensionality of the coordination polymers as demonstrated by complexes **5.3** and **5.4**.

Unexpectedly, the use of the more Lewis-acidic $HgCl_2$ unit did not induce the formation of tetrahedral $[HgCl_4]^{2-}$ units in any of the single crystal products formed as was observed for complexes **3.10**, **4.1**, and **4.4**. Even though IR and EA analysis of one product indicated possible $\{(bipy)Cu[Hg(CN)_2]_2\}HgCl_4$ formation, no X-ray crystallographic data could be obtained to support this result. However, it remains possible that the use of other recrystallization techniques, such as the use of different solvents or hydrothermal reaction conditions, may result in the formation of $\{(bipy)Cu[Hg(CN)_2]_2\}HgCl_4$ as single crystals.

Although the bipy ligand was shown to induce *N*-cyano coordination of the $Hg(CN)_2$ units (complex **5.3**), the use of different bidentate ligands should be investigated to form $\{(L)Cu[Hg(CN)_2]_2\}HgCl_4$ 2-D layer structural analogues. Investigation into the formation of structural analogues having different tetrahedral units, such as $[MoO_4]^{2-}$ for example, should also be examined.

5.4 EXPERIMENTAL

5.4.1 Preparation of $[Cu(bipy)_2(\mu\text{-}Cl)_2Hg(CN)_2]$ (5.1)

To a 15 mL aqueous solution of $CuCl_2 \cdot 2\ H_2O$ (0.067 g, 0.39 mmol), a methanolic solution of bipy (stock solution, 0.79 mmol) was added dropwise with stirring. A 10 mL aqueous solution of $Hg(CN)_2$ (0.100 g, 0.40 mmol) was added to this blue solution and was stirred for 5 minutes.

The solution was allowed to slowly evaporate. Blue-green crystal blocks of $[Cu(bipy)_2(\mu\text{-}Cl)_2Hg(CN)_2]$ (**5.1**) were collected by vacuum filtration, washed with two 1 mL portions of cold water followed by two 1 mL portions of cold methanol, and were left to air dry. Yield: 0.207 g (75%). Anal. Calcd. for $C_{22}H_{16}N_6Cl_2CuHg$: C, 37.78; H, 2.31; N, 12.02. Found: C, 38.05; H, 2.27; N, 12.05. IR (KBr, cm^{-1}): 3735 (vw), 3202 (w), 3109 (m), 3073 (m), 3056 (m), 3033 (m), 2987 (w), 2918 (vw), 2883 (vw), 2776 (vw), ν_{CN} **2172 (w), 2146 (vw)**, 2046 (w), 1961 (w), 1913 (w), 1892 (w), 1849 (w), 1715 (vw), 1676 (vw), 1605 (s), 1566 (m), 1538 (m), 1494 (s), 1477 (s), 1443 (s), 1419 (m), 1396 (m), 1361 (m), 1319 (s), 1282 (w), 1252 (m), 1221 (w), 1186 (m), 1163 (s), 1105 (w), 1063 (m), 1027 (s), 1013 (s), 958 (w), 906 (w), 891 (w), 814 (m), 775 (vs), 733 (s), 658 (s), 631 (m), 439 (vw), 409 (s).

5.4.2 Preparation of $[Cu(bipy)_2Hg_2Cl_6]_2$ (5.2)

To a 10 mL aqueous solution of $CuCl_2 \cdot 2\ H_2O$ (0.067 g, 0.39 mmol), a methanolic solution of bipy (stock solution, 0.79 mmol) was added dropwise with stirring. A 10 mL aqueous solution of $HgCl_2$ (0.213 g, 0.78 mmol) was added, with stirring, to this blue solution resulting in an immediate white precipitate that was left to settle. The mixture was then decanted, and the pale blue solution was allowed to slowly evaporate. Small blue crystal platelets of $[Cu(bipy)_2Hg_2Cl_6]_2$ (**5.2**) were collected by vacuum filtration, washed with two 1 mL portions of cold water followed by two 1 mL portions of cold methanol, and were left to air dry. Yield: 0.103 g (26%). Anal. Calcd. for $C_{20}H_{16}N_4Cl_6CuHg_2$: C, 24.27; H, 1.63; N, 5.66. Found: C, 24.01; H, 1.60: N, 5.50. IR (KBr, cm^{-1}): 3733 (vw), 3108 (vw), 3084 (w), 3060 (w), 3052 (w), 3034 (vw), 2017 (vw), 1974 (vw), 1935 (vw), 1862 (w), 1602 (m), 1567 (m), 1493 (m), 1474 (m), 1443 (s), 1419 (m), 1392 (w), 1340 (w), 1316 (m), 1251 (m), 1215 (w), 1172 (m), 1157 (m), 1105 (m), 1066 (w), 1044 (w), 1028 (m), 1014 (m), 973 (vw), 901 (w), 810 (w), 769 (vs), 729 (m), 660 (m), 634 (w), 496 (vw), 439 (vw), 419 (m).

5.4.3 Preparation of {[Cu(bipy)Hg(CN)$_2$Cl$_2$]$_2$Hg(CN)$_2$} (5.3)

To a 15 mL aqueous solution of $CuCl_2 \cdot 2\ H_2O$ (0.067 g, 0.39 mmol), a methanolic solution of bipy (stock solution, 0.39 mmol) was added dropwise with stirring. A 10 mL aqueous solution of $Hg(CN)_2$ (0.150 g, 0.59 mmol) was added to this blue solution and was stirred for 10 minutes. The solution was allowed to slowly evaporate. Dark blue crystal blocks of {[Cu(bipy)Hg(CN)$_2$Cl$_2$]$_2$Hg(CN)$_2$} (**5.3**) were collected by vacuum filtration, washed with two 1 mL portions of cold water followed by two 1 mL portions of cold methanol, and were left to air dry. Yield: 0.171 g (65%). Anal. Calcd. for $C_{16}H_8N_8Cl_2CuHg_3$: C, 23.32; H, 1.20; N, 10.46. Found: C, 23.12; H, 1.21; N, 10.43. IR (KBr, cm^{-1}): 3737 (vw), 3207 (vw), 3113 (w), 3095 (w), 3084 (w), 3063 (w), 3034 (vw), 2983 (vw), ν_{CN} **2242 (m)**, **2182 (w)**, 2034 (w), 1952 (w), 1874 (w), 1612 (m), 1602 (s), 1567 (m), 1539 (w), 1498 (m), 1474 (m), 1445 (s), 1399 (w), 1339 (w), 1312 (s), 1280 (vw), 1251 (m), 1224 (w), 1173 (m), 1154 (m), 1110 (m), 1061 (m), 1033 (m), 1020 (m), 977 (m), 905 (m), 808 (m), 778 (vs), 748 (m), 730 (s), 662 (m), 650 (m), 640 (m), 502 (m), 434 (m), 421 (m).

5.4.4 Preparation of {[Cu(bipy)(OH)(Cl)]$_2$Hg(CN)$_2$} · 2 H$_2$O (5.4)

To a 15 mL aqueous solution of $CuCl_2 \cdot 2\ H_2O$ (0.067 g, 0.39 mmol), a methanolic solution of bipy (stock solution, 0.39 mmol) was added dropwise with stirring. A 10 mL aqueous solution of $Hg(CN)_2$ (0.050 g, 0.20 mmol) was added to this blue solution with stirring. The solution was made basic by the addition of 10 mL NH_4OH (conc.) and allowed to slowly evaporate. Dark blue plate-shaped crystals of {[Cu(bipy)(OH)(Cl)]$_2$Hg(CN)$_2$} · 2 H$_2$O (**5.4**) were collected by vacuum filtration, washed with two 1 mL portions of cold water followed by two 1 mL portions of cold methanol, and were left to air dry. Yield: 0.080 g (49%). Anal. Calcd. for $C_{22}H_{22}N_6O_4Cl_2Cu_2Hg$: C, 31.72; H, 2.66; N, 10.09. Found: C, 31.61; H, 2.60; N, 9.89. IR (KBr, cm^{-1}): 3735 (w), 3493 (vs), 3436 (vs), 3114 (w), 3082 (m), 3057 (m), 3036 (m), 2987 (vw), 2948 (vw), 2922 (vw), 2892 (vw), 2784 (vw), ν_{CN} **2182 (w)**, 2035 (vw), 1931 (vw), 1879 (vw), 1605 (s), 1578 (m), 1568 (w),

1538 (w), 1500 (m), 1479 (m), 1446 (s), 1392 (w), 1361 (w), 1321 (s), 1255 (m), 1215 (vw), 1178 (w), 1162 (m), 1108 (m), 1079 (vw), 1032 (m), 1018 (m), 979 (m), 949 (m), 913 (w), 808 (vw), 770 (s), 747 (m), 732 (s), 661 (m), 638 (m), 535 (w), 483 (m), 429 (m), 411 (s).

APPENDIX 1

SUMMARY OF CRYSTALLOGRAPHIC DATA

The following pages contain summary tables of the crystallographic data and refinement details for all reported structures contained in this thesis. The complete list of fractional atomic coordinates and equivalent isotropic thermal parameters (U(iso) in $Å^2$) are collected in Appendix 2. Details regarding the collection data methods can be found in the experimental sections of Chapters 2, 3, 4, and 5.

Table A1.1 Summary of Crystallographic Data for Chapter 2.

	2.1	**2.2**	**2.4**	**2.5**	**2.6**	**2.7**
Empirical Formula	$C_{38}H_{32}N_3ClHgOP_2$	$C_{18}H_{37}N_3ClHgO_{0.5}$	$C_{34}H_{22}N_{10}Cl_2Hg_2Ni$	$C_8H_{16}N_8Cl_2CuHg_2$	$C_{12}H_{24}N_{12}Cl_3CoHg_3$	$C_{10}H_{40}N_{22}Cl_6Co_2Hg_5O_2$
FW(g mol^{-1})	844.67	539.55	1101.39	759.90	1103.46	1834.10
Crystal habit	colorless block	colorless block	brown bar	purple bar	orange platelet	orange platelet
Crystal dimensions (mm^3)	0.11 x 0.14 x 0.20	0.12 x 0.18 x 0.23	0.03 x 0.11 x 0.34	0.05 x 0.15 x 0.34	0.03 x 0.17 x 0.23	0.05 x 0.23 x 0.31
Space Group	$P2_1/n$	$P2_1/n$	$P\bar{1}$	$P\bar{1}$	$P\bar{1}$	$I2/m$
a(Å)	10.949(2)	12.580(2)	8.840(2)	6.3063(13)	8.393(1)	8.5648(9)
b(Å)	12.761(3)	14.710(4)	12.509(3)	8.132(3)	11.853(3)	12.8938(9)
c(Å)	25.921(6)	13.075(2)	17.779(4)	9.9615(15)	13.838(3)	19.0120(15)
α(°)	90	90	92.488(19)	70.43(2)	100.12(2)	90
β(°)	90.414(17)	94.189(14)	91.35(2)	85.675(18)	91.51(2)	97.088(6)
γ(°)	90	90	110.442(19)	72.63(2)	105.94(2)	90
Z	4	4	2	1	2	2
U(Å)	3621.6	2413.1	1838.9	459.2	1299.1	2083.5
Final unit cell reflections; 2θ limits(°)	26; 29-30	28; 30-32	24; 30-34	19; 40-49	26; 40-45	40; 34-35
D_{calc}(g cm^{-3})	1.549	1.485	1.989	2.748	2.821	2.924
Data collection 2θ limits(°)	4-45	4-45	4-45	4-54	4-50	4-51
Absorption correction transmission range	0.4566-0.5756	0.2694-0.3599	0.2093-0.4446	0.0482-0.2188	0.0424-0.2103	0.0106-0.0460
Parameters / Observed data	235 / 2513	134 / 1476	293 / 2725	99 / 1692	282 / 3089	126 / 1348
R_1, R_w [I=2.5σ(I)]	0.038, 0.043	0.034, 0.036	0.034, 0.035	0.027, 0.030	0.042, 0.046	0.032, 0.043

Table A1.2 Summary of Crystallographic Data for Chapter 3: Complexes **3.1-3.4**.

	3.1	**3.2**	**3.3**	**3.4**
Empirical Formula	$C_{22}H_{16}N_6Cl_2HgMn$	$C_{24}H_{16}N_6Cl_2HgMn$	$C_{22}H_{16}N_6Cl_2HgNi$	$C_{24}H_{16}N_6Cl_2HgNi$
FW(g mol^{-1})	690.84	738.88	694.59	742.63
Crystal habit	yellow platelet	yellow block	pale green block	pale blue platelet
Crystal dimensions (mm^3)	0.06 x 0.17 x 0.23	0.10 x 0.17 x 0.20	0.06 x 0.09 x 0.20	0.06 x 0.17 x 0.20
Space Group	*I*2/*c*	*P*2/*n*	*C*2/*c*	*P*2/*n*
a(Å)	16.071(2)	15.998(5)	22.521(15)	8.088(2)
b(Å)	9.015(1)	8.853(3)	8.887(7)	8.742(2)
c(Å)	16.252(2)	18.797(8)	16.147(12)	17.763(6)
α(°)	90	90	90	90
β(°)	90.127(8)	107.42(3)	135.47(4)	97.08(2)
γ(°)	90	90	90	90
Z	4	4	4	2
U(Å)	2354.6	2540.1	2266.1	1246.3
Final unit cell reflections; 2θ limits(°)	76; 40-54	not applicable	not applicable	not applicable
D_{calc}(g cm^{-3})	1.949	1.932	2.036	1.979
Data collection 2θ limits(°)	4-54	6-137	11-137	10-137
Absorption correction transmission range	0.3235 – 0.5188	0.3388 – 1	0.2363 – 1	0.2718 – 1
Parameters / Observed data	148 / 2169	326 / 2713	148 / 1489	166 / 1795
R_1, R_w [$I=2.5\sigma(I)$]	0.020, 0.025	0.064, 0.064	0.047, 0.060	0.037, 0.045

Table A1.3 Summary of Crystallographic Data for Chapter 3: Complexes **3.5-3.10**.

	3.5	**3.6**	**3.7**	**3.8**	**3.9**	**3.10**
Empirical Formula	$C_{17}H_{15}N_5Cl_2CuHg$	$C_{54}H_{32}N_{14}Cl_4Cu_2Hg_3$	$C_6H_{13}N_5Cl_2CuHg$	$C_9H_{18}N_7Cl_3CuHg_2$	$C_{20}H_{32}N_{20}Cl_4Hg_6Ni_2$	$C_{40}H_{72}N_{32}Cl_{10}Hg_9Ni_4$
FW(g mol^{-1})	624.38	1747.6	490.24	795.37	2015.35	3395.83
Crystal habit	dark green block	green platelet	dark blue platelet	blue platelet	pink platelet	purple block
Crystal dimensions (mm^3)	0.17 x 0.29 x 0.57	0.07 x 0.29 x 0.43	0.07 x 0.17 x 0.40	0.06 x 0.09 x 0.51	0.03 x 0.10 x 0.10	0.11 x 0.14 x 0.43
Space Group	$P\bar{1}$	$P\bar{1}$	$A2/a$	$P2_1/a$	$P2_1/a$	$P\bar{4}2_1c$
a(Å)	7.3434(9)	10.339(2)	15.7274(18)	7.837(2)	17.205(7)	22.358(3)
b(Å)	9.510(1)	10.911(2)	8.6102(8)	17.148(2)	12.412(6)	22.358(3)
c(Å)	13.3533(17)	12.723(3)	19.2642(17)	14.423(2)	21.488(9)	8.1101(13)
α(°)	85.57(1)	69.811(17)	90	90	90	90
β(°)	82.47(1)	77.55(2)	97.735(8)	95.67(2)	98.87(4)	90
γ(°)	87.594(8)	82.228(18)	90	90	90	90
Z	2	1	8	4	4	2
U(Å)	921.2	1312.5	2484.9	1928.8	4534.0	4054.1
Final unit cell reflections; 2θ limits(°)	20; 33-35	16; 30-35	36; 48-52	38; 38-44	not applicable	40; 33-34
D_{calc}(g cm^{-3})	2.236	2.211	2.519	2.739	2.952	2.821
Data collection 2θ limits(°)	4-51	4-56	4-52	4-55	8-137	4-50
Absorption correction transmission range	0.1237 – 0.2273	0.0773 – 0.2979	0.0883 – 0.1857	0.1406 – 0.2328	0.1794-1	0.0858 – 0.1489
Flack Parameter						0.01(2)
Parameters / Observed data	237 / 3054	350 / 4065	138 / 1705	201 / 2205	457 / 3753	178 / 1454
R_1, R_w [I=2.5σ(I)]	0.017, 0.022	0.031, 0.034	0.022, 0.027	0.035, 0.033	0.051, 0.059	0.031, 0.030

Table A1.4 Summary of Crystallographic Data for Chapter 4.

	4.1	**4.2**	**4.3**	**4.4**	**4.5**	**4.6**
Empirical Formula	$C_{10}H_{16}N_6Cl_4CuHg_3$	$C_{10}H_{16}N_6Br_4CuHg_3$	$C_{10}H_{16}N_6CuHg_3I_4$	$C_{10}H_{16}N_6Cl_4Hg_3Ni$	$C_{10}H_{16}N_6Br_4Hg_3Ni$	$C_{10}H_{16}N_6Hg_3I_4Ni$
FW(g mol^{-1})	1027.40	1205.21	1393.21	1022.55	1200.35	1388.36
Crystal habit	blue block	blue platelet	blue platelet	pink block	pink platelet	pink platelet
Crystal dimensions (mm^3)	0.11 x 0.21 x 0.23	0.03 x 0.09 x 0.29	0.04 x 0.23 x 0.23	0.09 x 0.23 x 0.40	0.03 x 0.11 x 0.11	0.06 x 0.14 x 0.14
Space Group	$P\bar{4}2_1m$	$P\bar{4}2_1m$	$P\bar{4}2_1m$	$P\bar{4}2_1m$	$P\bar{4}2_1m$	$P\bar{4}2_1m$
a(Å)	10.9576(12)	11.1771(8)	11.5716(12)	10.9744(10)	11.171(2)	11.567(5)
b(Å)	10.9576(12)	11.1771(8)	11.5716(12)	10.9744(10)	11.171(2)	11.567(5)
c(Å)	9.8516(13)	9.9361(9)	10.0540(13)	9.7180(9)	9.845(3)	10.058(7)
α(°)	90	90	90	90	90	90
β(°)	90	90	90	90	90	90
γ(°)	90	90	90	90	90	90
Z	2	2	2	2	2	2
U(Å)	1182.87(20)	1249(17)	1346.2(2)	1170.41(15)	1228.4(5)	1345.7(12)
Final unit cell reflections; 2θ limits (°)	48; 40-49	not applicable	48; 36-42	62; 43-48	not applicable	not applicable
D_{calc} (g cm^{-3})	2.885	3.235	3.437	2.902	3.234	3.386
Data collection 2θ limits (°)	4-52	8-145	4-58	4-60	8-137	8-137
Absorption correction transmission range	0.0399 – 0.1430	0.020-0.290	0.0211-0.1638	0.0331-0.1602	0.1459-1	0.1188-1
Flack Parameter	-0.01(3)	-0.01(6)	-0.04(2)	0.03(3)	0.05(5)	0.04(2)
Parameters / Observed data	48 / 1081	51 / 354	56 / 777	57 / 846	58 / 448	44 / 371
R_1, R_w [I=2.5σ (I)]	0.024, 0.028	0.033[a], 0.042[a]	0.044, 0.055	0.035, 0.044	0.038, 0.041	0.068, 0.083

[a] R_1, R_w [I=1.8σ (I)]

Table A1.5 Summary of Crystallographic Data for Chapter 5.

	5.1	**5.2**	**5.3**	**5.4**
Empirical Formula	$C_{22}H_{16}N_6Cl_2CuHg$	$C_{20}H_{16}N_4Cl_6CuHg_2$	$C_{13}H_8N_5Cl_2Cu_1Hg_{1.5}$	$C_{11}H_{11}N_3O_2ClCuHg_{0.5}$
FW(g mol^{-1})	699.45	989.82	669.58	416.52
Crystal habit	blue/green block	blue needle	dark blue block	blue platelet
Crystal dimensions (mm^3)	0.23 x 0.31 x 0.43	0.03 x 0.06 x 0.34	0.23 x 0.25 x 0.42	0.06 x 0.11 x 0.31
Space Group	$P\bar{1}$	$P\bar{1}$	$P\bar{1}$	$P\bar{1}$
a(Å)	8.963 (4)	9.754 (2)	7.913 (3)	7.185 (2)
b(Å)	12.107 (4)	11.557 (2)	8.384 (1)	9.460 (2)
c(Å)	12.141 (7)	12.504 (3)	13.584 (3)	10.627 (2)
α(°)	83.30 (5)	82.02 (2)	81.35 (2)	106.35 (2)
β(°)	69.60 (4)	70.91 (2)	73.33 (3)	96.51 (2)
γ(°)	68.19 (3)	85.56 (2)	75.60 (2)	109.28 (2)
Z	2	2	2	2
U(Å)	1146.34	1318.35	833.16	637.04
Final unit cell reflections; 2θ limits (°)	16; 43-45	22; 24-26	20; 40-50	32; 40-44
D_{calc} (g cm^{-3})	2.026	2.494	2.669	2.171
Data collection 2θ limits (°)	4-50	4-45	4-58	4-52
Absorption correction transmission range	0.1289-0.2068	0.0571-0.3370	0.0693-0.2473	0.2050-0.3095
Parameters / Observed data	290 / 3204	199 / 1691	207 / 3164	180 / 2044
R_1, R_w [$I=2.5\sigma(I)$]	0.029, 0.028	0.042, 0.045	0.029, 0.035	0.021, 0.022

APPENDIX 2

FRACTIONAL ATOMIC COORDINATES

Note: Unless otherwise stated, the occupancies for all the atoms in the tables contained in this appendix are 1.0.

A2.1 Fractional Atomic Coordinates and Equivalent Isotropic Thermal Parameters (U(iso) in $Å^2$) for $[PPN][Hg(CN)_2Cl] \cdot H_2O$ (**2.1**).

Atom	x	y	z	U(iso)($Å^2$)	Occ
Hg1	1.17139(5)	0.44579(4)	0.99151(2)	0.0570	1.0000
Cl1	0.9876(3)	0.5125(2)	0.9286(1)	0.0580	1.0000
P1	1.2478(2)	0.0422(2)	0.8273(1)	0.0356	1.0000
P2	1.0001(2)	0.0513(2)	0.7820(1)	0.0355	1.0000
N1	1.1397(7)	0.0782(6)	0.7912(3)	0.0395	1.0000
N11	1.3544(11)	0.6390(11)	0.9948(5)	0.0849	1.0000
N12	1.1354(13)	0.2006(11)	0.9868(6)	0.1127	1.0000
C11	1.2867(13)	0.5730(11)	0.9946(5)	0.0643	1.0000
C12	1.1434(11)	0.2868(12)	0.9880(6)	0.0666	1.0000
C1	1.2100(9)	-0.0550(9)	0.8741(4)	0.041(3)	1.0000
C2	1.2168(10)	-0.1598(8)	0.8616(4)	0.047(3)	1.0000
C3	1.1735(10)	-0.2351(9)	0.8951(4)	0.054(3)	1.0000
C4	1.1239(12)	-0.2066(10)	0.9413(5)	0.067(4)	1.0000
C5	1.1197(12)	-0.1019(11)	0.9554(5)	0.075(4)	1.0000
C6	1.1597(10)	-0.0256(9)	0.9205(4)	0.053(3)	1.0000
C7	1.3669(9)	-0.0124(8)	0.7882(4)	0.036(3)	1.0000
C8	1.3552(10)	-0.0144(8)	0.7358(4)	0.049(3)	1.0000
C9	1.4486(11)	-0.0570(10)	0.7054(5)	0.061(3)	1.0000
C10	1.5483(12)	-0.0950(9)	0.7285(5)	0.066(4)	1.0000

C13	1.5641(13)	-0.0959(10)	0.7809(5)	0.072(4)	1.0000
C14	1.4705(10)	-0.0528(9)	0.8112(4)	0.058(3)	1.0000
C15	1.3104(9)	0.1545(8)	0.8598(4)	0.034(3)	1.0000
C16	1.3873(10)	0.1421(9)	0.9018(4)	0.052(3)	1.0000
C17	1.4402(11)	0.2302(9)	0.9247(5)	0.059(3)	1.0000
C18	1.4130(11)	0.3272(10)	0.9071(4)	0.056(3)	1.0000
C19	1.3350(10)	0.3417(9)	0.8665(4)	0.057(3)	1.0000
C20	1.2816(10)	0.2532(8)	0.8422(4)	0.050(3)	1.0000
C21	0.9584(9)	-0.0830(7)	0.7966(4)	0.037(3)	1.0000
C22	0.8956(10)	-0.1078(9)	0.8402(4)	0.050(3)	1.0000
C23	0.8730(12)	-0.2134(10)	0.8519(5)	0.067(4)	1.0000
C24	0.9134(12)	-0.2893(10)	0.8192(5)	0.067(4)	1.0000
C25	0.9760(12)	-0.2651(10)	0.7773(5)	0.066(4)	1.0000
C26	1.0010(10)	-0.1614(9)	0.7642(4)	0.052(3)	1.0000
C27	0.9029(10)	0.1340(8)	0.8198(4)	0.041(3)	1.0000
C28	0.9483(10)	0.1847(8)	0.8627(4)	0.047(3)	1.0000
C29	0.8721(11)	0.2433(9)	0.8937(4)	0.055(3)	1.0000
C30	0.7516(11)	0.2524(9)	0.8822(5)	0.058(3)	1.0000
C31	0.7037(12)	0.2025(9)	0.8397(5)	0.065(4)	1.0000
C32	0.7797(11)	0.1433(9)	0.8076(5)	0.059(3)	1.0000
C33	0.9648(9)	0.0720(8)	0.7148(4)	0.037(3)	1.0000
C34	0.8690(10)	0.0223(8)	0.6908(4)	0.047(3)	1.0000
C35	0.8441(11)	0.0390(9)	0.6391(4)	0.056(3)	1.0000
C36	0.9141(11)	0.1041(10)	0.6115(5)	0.062(4)	1.0000
C37	1.0116(13)	0.1551(11)	0.6346(5)	0.076(4)	1.0000
C38	1.0368(11)	0.1390(9)	0.6872(4)	0.056(3)	1.0000
H2	1.2506(10)	-0.1799(8)	0.8294(4)	0.086(8)	1.0000
H3	1.1808(10)	-0.3073(9)	0.8867(4)	0.097(8)	1.0000
H4	1.0922(12)	-0.2594(10)	0.9633(5)	0.107(8)	1.0000
H5	1.0868(12)	-0.0831(11)	0.9879(5)	0.114(8)	1.0000
H6	1.1553(10)	0.0465(9)	0.9294(4)	0.096(8)	1.0000
H8	1.2835(10)	0.0132(8)	0.7200(4)	0.091(8)	1.0000
H9	1.4417(11)	-0.0588(10)	0.6688(5)	0.107(8)	1.0000
H10	1.6114(12)	-0.1233(9)	0.7077(5)	0.108(8)	1.0000
H13	1.6365(13)	-0.1229(10)	0.7963(5)	0.120(8)	1.0000
H14	1.4782(10)	-0.0532(9)	0.8477(4)	0.101(8)	1.0000
H16	1.4070(10)	0.0739(9)	0.9139(4)	0.095(8)	1.0000

H17	1.4927(11)	0.2226(9)	0.9538(5)	0.110(8)	1.0000
H18	1.4499(11)	0.3867(10)	0.9228(4)	0.097(8)	1.0000
H19	1.3176(10)	0.4104(9)	0.8543(4)	0.105(8)	1.0000
H20	1.2262(10)	0.2620(8)	0.8142(4)	0.094(8)	1.0000
H22	0.8661(10)	-0.0531(9)	0.8617(4)	0.089(8)	1.0000
H23	0.8328(12)	-0.2314(10)	0.8830(5)	0.112(8)	1.0000
H24	0.8943(12)	-0.3606(10)	0.8259(5)	0.110(8)	1.0000
H25	1.0066(12)	-0.3198(10)	0.7562(5)	0.115(8)	1.0000
H26	1.0454(10)	-0.1444(9)	0.7339(4)	0.092(8)	1.0000
H28	1.0324(10)	0.1776(8)	0.8712(4)	0.085(8)	1.0000
H29	0.9048(11)	0.2781(9)	0.9231(4)	0.095(8)	1.0000
H30	0.7003(11)	0.2934(9)	0.9037(5)	0.100(8)	1.0000
H31	0.6190(12)	0.2087(9)	0.8322(5)	0.112(8)	1.0000
H32	0.7477(11)	0.1088(9)	0.7780(5)	0.104(8)	1.0000
H34	0.8206(10)	-0.0255(8)	0.7099(4)	0.088(8)	1.0000
H35	0.7748(11)	0.0065(9)	0.6238(4)	0.098(8)	1.0000
H36	0.8972(11)	0.1147(10)	0.5759(5)	0.104(8)	1.0000
H37	1.0630(13)	0.1994(11)	0.6148(5)	0.114(8)	1.0000
H38	1.1027(11)	0.1742(9)	0.7037(4)	0.102(8)	1.0000
O1	1.3411(16)	0.0457(14)	1.0509(8)	0.164(7)	0.626(14)
O2	1.4516(13)	0.881(3)	0.9577(14)	0.164(7)	0.374(14)
H40	1.2888(16)	0.0829(14)	1.0348(8)	0.197(7)	0.626(14)
H41	1.4275(13)	0.821(3)	0.9670(14)	0.197(7)	0.374(14)
H1	1.4281	0.1213	1.0563	0.197(7)	1.0000

A2. 2 Fractional Atomic Coordinates and Equivalent Isotropic Thermal Parameters (U(iso) in $Å^2$) for $[^nBu_4N][Hg(CN)_2Cl] \cdot 0.5\ H_2O$ (**2.2**).

Atom	x	y	z	U(iso)($Å^2$)	Occ
Hg1	0.39658(4)	0.46277(4)	1.08980(4)	0.1034	1.0000
Cl1	0.5462(3)	0.3706(2)	0.9873(3)	0.1105	1.0000
N1	0.3550(6)	0.2120(6)	0.7094(6)	0.0769	1.0000
N12	0.5254(15)	0.4889(16)	1.3032(12)	0.2313	1.0000
N11	0.1992(11)	0.4279(9)	0.9308(12)	0.1635	1.0000
C12	0.4828(14)	0.4771(15)	1.2256(14)	0.1654	1.0000

C11	0.2692(12)	0.4382(9)	0.9859(12)	0.1194	1.0000
C1	0.2980(8)	0.1561(7)	0.7857(7)	0.083(3)	1.0000
C2	0.2918(9)	0.1976(8)	0.8895(8)	0.100(4)	1.0000
C3	0.2385(10)	0.1365(10)	0.9583(9)	0.131(5)	1.0000
C4	0.2222(11)	0.1791(10)	1.0633(10)	0.155(6)	1.0000
C5	0.4715(8)	0.2282(8)	0.7475(9)	0.092(3)	1.0000
C6	0.5383(9)	0.1443(8)	0.7633(9)	0.112(4)	1.0000
C7	0.6507(10)	0.1676(9)	0.8037(10)	0.132(5)	1.0000
C8	0.7137(11)	0.0845(10)	0.8286(11)	0.148(5)	1.0000
C9	0.3500(8)	0.1587(8)	0.6094(8)	0.091(3)	1.0000
C10	0.4022(10)	0.2014(9)	0.5221(9)	0.123(4)	1.0000
C13	0.3833(11)	0.1442(11)	0.4266(11)	0.156(6)	1.0000
C14	0.4335(15)	0.1839(14)	0.3470(15)	0.252(10)	1.0000
C15	0.3057(8)	0.3045(8)	0.6953(8)	0.095(4)	1.0000
C16	0.1915(9)	0.3036(9)	0.6578(9)	0.116(4)	1.0000
C17	0.1460(11)	0.3998(10)	0.6394(11)	0.138(5)	1.0000
C18	0.0370(11)	0.3985(11)	0.5938(11)	0.167(6)	1.0000
H11	0.3331(8)	0.0991(7)	0.7939(7)	0.073(6)	1.0000
H12	0.2271(8)	0.1469(7)	0.7576(7)	0.073(6)	1.0000
H21	0.3620(9)	0.2084(8)	0.9187(8)	0.088(6)	1.0000
H22	0.2540(9)	0.2534(8)	0.8835(8)	0.088(6)	1.0000
H31	0.2796(10)	0.0826(10)	0.9681(9)	0.121(6)	1.0000
H32	0.1707(10)	0.1219(10)	0.9258(9)	0.121(6)	1.0000
H41	0.1864(11)	0.1366(10)	1.1034(10)	0.151(6)	1.0000
H42	0.2895(11)	0.1935(10)	1.0970(10)	0.151(6)	1.0000
H43	0.1806(11)	0.2328(10)	1.0547(10)	0.151(6)	1.0000
H51	0.4722(8)	0.2605(8)	0.8105(9)	0.081(6)	1.0000
H52	0.5038(8)	0.2643(8)	0.6981(9)	0.081(6)	1.0000
H61	0.5063(9)	0.1069(8)	0.8116(9)	0.103(6)	1.0000
H62	0.5409(9)	0.1125(8)	0.7003(9)	0.103(6)	1.0000
H71	0.6473(10)	0.2029(9)	0.8642(10)	0.129(6)	1.0000

H72	0.6837(10)	0.2021(9)	0.7534(10)	0.129(6)	1.0000
H81	0.7835(11)	0.1018(10)	0.8539(11)	0.147(6)	1.0000
H82	0.6813(11)	0.0498(10)	0.8791(11)	0.147(6)	1.0000
H83	0.7177(11)	0.0490(10)	0.7683(11)	0.147(6)	1.0000
H91	0.3830(8)	0.1015(8)	0.6230(8)	0.078(6)	1.0000
H92	0.2771(8)	0.1497(8)	0.5875(8)	0.078(6)	1.0000
H101	0.4769(10)	0.2045(9)	0.5388(9)	0.115(6)	1.0000
H102	0.3748(10)	0.2609(9)	0.5106(9)	0.115(6)	1.0000
H131	0.4058(11)	0.0835(11)	0.4402(11)	0.157(6)	1.0000
H132	0.3090(11)	0.1449(11)	0.4074(11)	0.157(6)	1.0000
H141	0.4192(15)	0.1480(14)	0.2872(15)	0.288(6)	1.0000
H142	0.5078(15)	0.1832(14)	0.3661(15)	0.288(6)	1.0000
H143	0.4110(15)	0.2447(14)	0.3333(15)	0.288(6)	1.0000
H151	0.3109(8)	0.3336(8)	0.7604(8)	0.087(6)	1.0000
H152	0.3446(8)	0.3383(8)	0.6487(8)	0.087(6)	1.0000
H161	0.1513(9)	0.2734(9)	0.7062(9)	0.108(6)	1.0000
H162	0.1850(9)	0.2716(9)	0.5945(9)	0.108(6)	1.0000
H171	0.1469(11)	0.4301(10)	0.7036(11)	0.132(6)	1.0000
H172	0.1896(11)	0.4318(10)	0.5952(11)	0.132(6)	1.0000
H181	0.0123(11)	0.4592(11)	0.5845(11)	0.163(6)	1.0000
H182	-0.0075(11)	0.3671(11)	0.6376(11)	0.163(6)	1.0000
H183	0.0352(11)	0.3687(11)	0.5293(11)	0.163(6)	1.0000
O1	0.548(2)	0.5659(16)	1.481(2)	0.251(12)	0.5000
H1	0.540(2)	0.5412(16)	1.422(2)	0.291(12)	0.5000
H2	0.528(2)	0.5513(16)	1.540(2)	0.291(12)	0.5000

A2. 3 Fractional Atomic Coordinates and Equivalent Isotropic Thermal Parameters (U(iso) in $Å^2$) for $[Ni(terpy)_2][Hg(CN)_2Cl]_2$ (**2.4**).

Atom	**x**	**y**	**z**	**U(iso)($Å^2$)**
Hg1	0.32402(7)	0.55525(4)	0.54698(3)	0.0677
Hg2	0.22805(7)	1.55898(4)	0.96828(3)	0.0620

Ni1	0.04958(17)	1.09514(11)	0.75375(7)	0.0368
Cl1	0.4593(5)	0.5511(3)	0.40958(18)	0.0700
Cl2	-0.0515(4)	1.4020(3)	0.9100(2)	0.0818
N1	0.2808(11)	1.1221(7)	0.8007(4)	0.0421
N2	0.1427(11)	1.2664(7)	0.7638(4)	0.0408
N3	-0.1426(11)	1.1411(7)	0.7140(4)	0.0391
N4	0.1214(11)	1.0722(8)	0.6434(4)	0.0421
N5	-0.0379(10)	0.9259(8)	0.7368(5)	0.0418
N6	-0.0609(11)	1.0436(8)	0.8561(4)	0.0420
N11	0.0042(18)	0.3375(12)	0.5227(7)	0.0958
N12	0.503(2)	0.8036(13)	0.6227(8)	0.1366
N21	0.3553(18)	1.3957(14)	1.0639(10)	0.1286
N22	0.251(2)	1.7730(13)	0.8720(9)	0.1362
C11	0.1192(19)	0.4130(12)	0.5304(7)	0.0615
C12	0.443(2)	0.7165(14)	0.5956(8)	0.0867
C21	0.3063(18)	1.4503(13)	1.0273(9)	0.0819
C22	0.243(2)	1.6972(13)	0.9062(8)	0.0810
C1	0.3397(14)	1.0409(10)	0.8203(6)	0.046(3)
C2	0.4927(15)	1.0697(11)	0.8535(6)	0.058(4)
C3	0.5824(18)	1.1797(12)	0.8669(7)	0.073(4)
C4	0.5274(16)	1.2659(11)	0.8472(6)	0.059(4)
C5	0.3732(15)	1.2332(10)	0.8133(6)	0.046(3)
C6	0.2997(14)	1.3147(10)	0.7893(6)	0.042(3)
C7	0.3700(16)	1.4349(11)	0.7892(6)	0.058(3)
C8	0.2830(15)	1.4950(11)	0.7619(6)	0.055(3)
C9	0.1286(15)	1.4446(10)	0.7355(6)	0.056(3)
C10	0.0556(14)	1.3244(10)	0.7365(6)	0.043(3)
C13	-0.1072(14)	1.2551(10)	0.7093(6)	0.045(3)
C14	-0.2200(16)	1.2985(11)	0.6811(6)	0.061(4)
C15	-0.3690(17)	1.2206(12)	0.6564(7)	0.070(4)
C16	-0.4039(16)	1.1070(11)	0.6599(6)	0.061(4)

C17	-0.2874(14)	1.0704(10)	0.6903(6)	0.046(3)
C18	0.2055(15)	1.1556(11)	0.6000(6)	0.053(3)
C19	0.2589(16)	1.1333(12)	0.5309(7)	0.068(4)
C20	0.2289(17)	1.0220(12)	0.5089(8)	0.073(4)
C23	0.1436(16)	0.9340(12)	0.5517(7)	0.065(4)
C24	0.0872(13)	0.9636(10)	0.6207(6)	0.042(3)
C25	-0.0102(14)	0.8807(10)	0.6719(6)	0.048(3)
C26	-0.0773(17)	0.7633(13)	0.6560(8)	0.080(4)
C27	-0.168(2)	0.6965(15)	0.7088(9)	0.102(5)
C28	-0.1955(17)	0.7460(12)	0.7764(8)	0.074(4)
C29	-0.1274(15)	0.8637(10)	0.7890(6)	0.051(3)
C30	-0.1433(15)	0.9291(10)	0.8570(6)	0.049(3)
C31	-0.2345(17)	0.8819(13)	0.9167(8)	0.076(4)
C32	-0.2359(18)	0.9529(13)	0.9785(8)	0.077(4)
C33	-0.1533(16)	1.0643(12)	0.9797(7)	0.068(4)
C34	-0.0645(14)	1.1096(11)	0.9161(6)	0.053(3)
H1	0.2755(14)	0.9625(10)	0.8113(6)	0.085(10)
H2	0.5347(15)	1.0122(11)	0.8661(6)	0.105(10)
H3	0.6857(18)	1.1991(12)	0.8916(7)	0.113(10)
H4	0.5919(16)	1.3444(11)	0.8552(6)	0.101(10)
H7	0.4780(16)	1.4722(11)	0.8082(6)	0.095(10)
H8	0.3328(15)	1.5757(11)	0.7610(6)	0.093(10)
H9	0.0688(15)	1.4888(10)	0.7172(6)	0.096(10)
H14	-0.1945(16)	1.3785(11)	0.6780(6)	0.106(10)
H15	-0.4490(17)	1.2476(12)	0.6367(7)	0.111(10)
H16	-0.5059(16)	1.0540(11)	0.6423(6)	0.100(10)
H17	-0.3107(14)	0.9908(10)	0.6944(6)	0.083(10)
H18	0.2298(15)	1.2328(11)	0.6177(6)	0.091(10)
H19	0.3134(16)	1.1934(12)	0.4996(7)	0.114(10)
H20	0.2687(17)	1.0045(12)	0.4625(8)	0.118(10)
H23	0.1231(16)	0.8563(12)	0.5365(7)	0.106(10)

H26	-0.0594(17)	0.7303(13)	0.6095(8)	0.128(10)
H27	-0.214(2)	0.6161(15)	0.6994(9)	0.138(10)
H28	-0.2579(17)	0.7002(12)	0.8138(8)	0.116(10)
H31	-0.2961(17)	0.8025(13)	0.9149(8)	0.118(10)
H32	-0.2969(18)	0.9212(13)	1.0206(8)	0.121(10)
H33	-0.1515(16)	1.1125(12)	1.0228(7)	0.116(10)
H34	-0.0089(14)	1.1897(11)	0.9156(6)	0.096(10)

A2. 4 Fractional Atomic Coordinates and Equivalent Isotropic Thermal Parameters (U(iso) in $Å^2$) for $[Cu(en)_2][Hg(CN)_2Cl]_2$ (**2.5**).

Atom	**x**	**y**	**z**	**U(iso)($Å^2$)**
Hg1	0.67792(4)	0.19489(4)	-0.53351(3)	0.0503
Cu1	1.0000	0.5000	0.0000	0.0447
Cl1	0.8036(3)	-0.1731(2)	-0.46342(19)	0.0580
N1	0.6427(14)	0.2111(15)	-0.2189(9)	0.1049
N2	0.7010(12)	0.3104(11)	-0.8664(8)	0.0748
N3	1.0933(10)	0.5325(9)	0.1732(6)	0.0594
N4	0.7650(10)	0.7384(8)	-0.0233(8)	0.0672
C1	0.6532(12)	0.2048(13)	-0.3282(8)	0.0646
C2	0.6894(12)	0.2674(10)	-0.7535(8)	0.0525
C3	0.9088(15)	0.6707(14)	0.2096(10)	0.0794
C4	0.8229(14)	0.8211(11)	0.0746(12)	0.0860
H31	0.9613(15)	0.7157(14)	0.2731(10)	0.103(17)
H32	0.7944(15)	0.6184(14)	0.2531(10)	0.103(17)
H41	0.9338(14)	0.8796(11)	0.0347(12)	0.106(17)
H42	0.6948(14)	0.9077(11)	0.0925(12)	0.106(17)
H51	1.2197(10)	0.5722(9)	0.1551(6)	0.076(13)
H52	1.1235(10)	0.4226(9)	0.2481(6)	0.076(13)
H61	0.7608(10)	0.8160(8)	-0.1167(8)	0.079(13)
H62	0.6270(10)	0.7183(8)	-0.0013(8)	0.079(13)

A2. 5 Fractional Atomic Coordinates and Equivalent Isotropic Thermal Parameters (U(iso) in $Å^2$) for $[Co(en)_3][Hg(CN)_2Cl_2]\{[Hg(CN)_2]_2Cl\}$ (**2.6**).

Atom	x	y	z	U(iso)($Å^2$)
Hg1	0.07268(8)	-0.39110(5)	0.61631(5)	0.0477
Hg2	0.55088(7)	-0.34603(5)	0.63743(5)	0.0447
Hg3	-0.07827(8)	0.33136(5)	1.09401(5)	0.0480
Co1	0.3376(2)	0.14585(13)	0.79413(13)	0.0320
Cl1	0.2681(5)	-0.5055(4)	0.4816(4)	0.0715
Cl2	0.3355(5)	-0.2019(3)	0.7935(3)	0.0482
Cl3	-0.1502(5)	0.1426(3)	0.9291(3)	0.0580
N1	0.5558(16)	0.2583(10)	0.7919(10)	0.0549
N2	0.4155(16)	0.0371(10)	0.6907(10)	0.0534
N3	0.1228(17)	0.0246(10)	0.7845(11)	0.0636
N4	0.2321(18)	0.2073(11)	0.6926(11)	0.0672
N5	0.2742(17)	0.2596(10)	0.8984(10)	0.0538
N6	0.4177(18)	0.0811(10)	0.9025(10)	0.0618
N11	0.168(2)	-0.1616(14)	0.5241(11)	0.0751
N12	0.027(2)	-0.5921(16)	0.7433(15)	0.0983
N21	0.647(2)	-0.1458(12)	0.5104(10)	0.0704
N22	0.4484(18)	-0.5265(11)	0.7829(12)	0.0635
N31	-0.245(2)	0.4892(14)	0.9853(13)	0.0815
N32	0.148(2)	0.2330(14)	1.2201(13)	0.0754
C1	0.631(2)	0.2199(14)	0.6990(12)	0.0549
C2	0.5943(17)	0.0876(13)	0.6868(12)	0.0521
C3	0.019(2)	0.0279(17)	0.6965(14)	0.0767
C4	0.055(3)	0.145(2)	0.682(2)	0.1058
C5	0.362(2)	0.2584(14)	0.9927(12)	0.0577
C6	0.354(3)	0.1328(14)	0.9947(13)	0.0692
C11	0.124(2)	-0.2439(15)	0.5517(14)	0.0615
C12	0.035(2)	-0.5235(16)	0.7009(12)	0.0545
C21	0.611(2)	-0.2186(12)	0.5544(11)	0.0504

C22	0.4867(18)	-0.4621(12)	0.7333(10)	0.0386
C31	-0.192(2)	0.4322(14)	1.0252(13)	0.0536
C32	0.075(2)	0.2660(13)	1.1765(13)	0.0514
H11	0.747(2)	0.2578(14)	0.7039(12)	0.131(19)
H12	0.580(2)	0.2390(14)	0.6446(12)	0.131(19)
H21	0.6522(17)	0.0697(13)	0.7393(12)	0.127(19)
H22	0.6290(17)	0.0555(13)	0.6258(12)	0.127(19)
H31	-0.095(2)	-0.0023(17)	0.7059(14)	0.150(19)
H32	0.046(2)	-0.0195(17)	0.6400(14)	0.150(19)
H41	0.004(3)	0.188(2)	0.730(2)	0.185(19)
H42	0.010(3)	0.146(2)	0.618(2)	0.185(19)
H51	0.309(2)	0.2892(14)	1.0466(12)	0.137(19)
H52	0.474(2)	0.3056(14)	0.9963(12)	0.137(19)
H61	0.421(3)	0.1294(14)	1.0499(13)	0.147(19)
H62	0.242(3)	0.0883(14)	0.9989(13)	0.147(19)
H71	0.6242(16)	0.2581(10)	0.8458(10)	0.132(19)
H72	0.5447(16)	0.3347(10)	0.7946(10)	0.132(19)
H81	0.3933(16)	-0.0384(10)	0.7067(10)	0.132(19)
H82	0.3614(16)	0.0314(10)	0.6298(10)	0.132(19)
H91	0.0685(17)	0.0403(10)	0.8408(11)	0.141(19)
H92	0.1392(17)	-0.0507(10)	0.7787(11)	0.141(19)
H101	0.2516(18)	0.2895(11)	0.7115(11)	0.152(19)
H102	0.2762(18)	0.1905(11)	0.6326(11)	0.152(19)
H111	0.1599(17)	0.2356(10)	0.9029(10)	0.135(19)
H112	0.3054(17)	0.3358(10)	0.8835(10)	0.135(19)
H121	0.5332(18)	0.1033(10)	0.9082(10)	0.142(19)
H122	0.3772(18)	-0.0018(10)	0.8901(10)	0.142(19)

A2. 6 Fractional Atomic Coordinates and Equivalent Isotropic Thermal Parameters (U(iso) in $Å^2$) for $[Co(NH_3)_6]_2[Hg(CN)_2]_5Cl_6 \cdot 2\ H_2O$ (**2.7**).

Atom	x	y	z	U(iso)($Å^2$)	Occ
Hg1	1.0000	-0.34570(4)	0.0000	0.0446	1.0000
Hg2	1.5000	0.0000	0.0000	0.0516	1.0000
Hg3	1.5000	-0.31467(5)	0.0000	0.0471	1.0000
Co1	1.0628(2)	0.0000	0.18983(10)	0.0332	1.0000
Cl1	1.2283(3)	-0.15820(18)	-0.00522(16)	0.0473	1.0000
Cl2	0.7291(5)	-0.5000	0.0094(2)	0.0519	1.0000
O1	0.7473(15)	0.000000(7)	0.3146(7)	0.0723	1.0000
N1	1.0852(13)	-0.3447(8)	0.1666(7)	0.0626	1.0000
N2	1.4492(18)	0.0000	-0.1669(10)	0.0661	1.0000
N3	1.5076(15)	-0.2838(9)	0.1647(6)	0.0749	1.0000
N4	1.2235(10)	-0.1092(6)	0.1864(5)	0.0467	1.0000
N5	0.8978(10)	0.1099(7)	0.1925(5)	0.0469	1.0000
N6	1.0266(15)	0.000000(7)	0.0890(6)	0.0427	1.0000
N7	1.0991(15)	0.000000(7)	0.2942(6)	0.0413	1.0000
C1	1.0522(14)	-0.3457(8)	0.1068(6)	0.0455	1.0000
C2	1.468(2)	0.0000	-0.1076(9)	0.0473	1.0000
C3	1.5079(14)	-0.2987(8)	0.1067(6)	0.0465	1.0000
H1	0.6349(15)	0.000000(7)	0.2872(7)	0.04(3)	1.0000
H2	0.7362(15)	0.094090(7)	0.3241(7)	0.04(3)	0.5000
H41	1.2319(10)	-0.1258(6)	0.1394(5)	0.28(4)	0.5000
H42	1.3200(10)	-0.0853(6)	0.2081(5)	0.28(4)	0.5000
H43	1.1942(10)	-0.1679(6)	0.2100(5)	0.28(4)	0.5000
H44	1.2658(10)	-0.1266(6)	0.2323(5)	0.28(4)	0.5000
H45	1.3030(10)	-0.0849(6)	0.1615(5)	0.28(4)	0.5000
H46	1.1773(10)	-0.1675(6)	0.1637(5)	0.28(4)	0.5000
H51	0.8561(10)	0.1270(7)	0.1465(5)	0.28(4)	0.5000
H52	0.9427(10)	0.1686(7)	0.2152(5)	0.28(4)	0.5000
H53	0.8181(10)	0.0852(7)	0.2171(5)	0.28(4)	0.5000

H54	0.8888(10)	0.1270(7)	0.2394(5)	0.28(4)	0.5000
H55	0.9263(10)	0.1686(7)	0.1686(5)	0.28(4)	0.5000
H56	0.8018(10)	0.0852(7)	0.1708(5)	0.28(4)	0.5000
H61	0.9214(15)	0.000000(7)	0.0731(6)	0.28(4)	1.0000
H62	1.0744(15)	-0.058894(7)	0.0712(6)	0.28(4)	1.0000
H63	1.0744(15)	0.058894(7)	0.0712(6)	0.28(4)	1.0000
H71	1.0055(15)	0.000000(7)	0.3127(6)	0.28(4)	1.0000
H72	1.1581(15)	-0.058894(7)	0.3099(6)	0.28(4)	1.0000
H73	1.1581(15)	0.058894(7)	0.3099(6)	0.28(4)	1.0000

A2. 7 Fractional Atomic Coordinates and Equivalent Isotropic Thermal Parameters (U(iso) in $Å^2$) for $[Mn(bipy)_2(\mu\text{-}Cl)_2Hg(CN)_2]$ (**3.1**).

Atom	x	y	z	U(iso)($Å^2$)
Hg1	1.0000	0.762220(18)	0.7500	0.0425
Mn1	1.0000	0.33517(6)	0.7500	0.0314
Cl1	1.08193(5)	0.52382(8)	0.82801(6)	0.0446
N1	1.1192(3)	0.8076(5)	0.5975(3)	0.0928
N2	1.08574(15)	0.1535(3)	0.79850(15)	0.0359
N3	1.09800(16)	0.2951(3)	0.65492(16)	0.0380
C1	1.0769(3)	0.7927(4)	0.6521(3)	0.0566
C2	1.0752(2)	0.0831(4)	0.8702(2)	0.0498
C3	1.1269(3)	-0.0299(4)	0.8966(2)	0.0578
C4	1.1919(2)	-0.0718(4)	0.8474(2)	0.0579
C5	1.2041(2)	0.0005(4)	0.7743(2)	0.0474
C6	1.14986(17)	0.1137(3)	0.75077(18)	0.0345
C7	1.15880(18)	0.1964(3)	0.67234(19)	0.0353
C8	1.2263(2)	0.1766(4)	0.6205(2)	0.0462
C9	1.2313(2)	0.2588(4)	0.5490(2)	0.0539
C10	1.1689(2)	0.3580(4)	0.5306(2)	0.0532
C11	1.1036(2)	0.3731(4)	0.5852(2)	0.0475
H2	1.0303(2)	0.1135(4)	0.9042(2)	0.060(4)

H3	1.1177(3)	-0.0775(4)	0.9479(2)	0.068(4)
H4	1.2279(2)	-0.1502(4)	0.8637(2)	0.068(4)
H5	1.2492(2)	-0.0261(4)	0.7396(2)	0.056(4)
H8	1.2687(2)	0.1072(4)	0.6339(2)	0.055(4)
H9	1.2773(2)	0.2474(4)	0.5130(2)	0.064(4)
H10	1.1710(2)	0.4147(4)	0.4814(2)	0.064(4)
H11	1.0605(2)	0.4417(4)	0.5728(2)	0.057(4)

A2. 8 Fractional Atomic Coordinates and Equivalent Isotropic Thermal Parameters (U(iso) in $Å^2$) for $[Ni(bipy)_2(\mu\text{-}Cl)_2Hg(CN)_2]$ (**3.2**).

Atom	x	y	z	U(iso)($Å^2$)
Hg1	0.5000	-0.25086(9)	0.7500	0.0380
Ni1	0.5000	0.1824(3)	0.7500	0.0275
Cl1	0.41420(16)	-0.0098(3)	0.7341(2)	0.0367
N1	0.6157(9)	-0.3046(19)	1.0224(11)	0.0831
N2	0.5794(5)	0.3438(11)	0.7810(8)	0.0381
N3	0.5897(5)	0.1978(11)	0.9319(7)	0.0331
C1	0.5750(9)	-0.2864(14)	0.9260(12)	0.0512
C2	0.5715(7)	0.4165(15)	0.7004(11)	0.0445
C3	0.6230(8)	0.5284(16)	0.7250(12)	0.0567
C4	0.6901(8)	0.5701(15)	0.8432(12)	0.0507
C5	0.7013(7)	0.4982(14)	0.9285(12)	0.0439
C6	0.6455(6)	0.3820(12)	0.8961(9)	0.0344
C7	0.6522(6)	0.2971(12)	0.9788(9)	0.0284
C8	0.7191(7)	0.3139(17)	1.101(1)	0.0462
C9	0.7194(8)	0.2274(16)	1.173(1)	0.0543
C10	0.6551(7)	0.1278(15)	1.122(1)	0.0452
C11	0.5918(7)	0.1130(14)	1.0023(9)	0.0401
H2	0.5259(7)	0.3863(15)	0.6204(11)	0.055(13)
H3	0.6142(8)	0.5762(16)	0.6642(12)	0.060(13)
H4	0.7277(8)	0.6481(15)	0.8642(12)	0.058(13)

H5	0.7468(7)	0.5261(14)	1.0090(12)	0.050(13)
H8	0.7635(7)	0.3833(17)	1.134(1)	0.054(13)
H9	0.7643(8)	0.2361(16)	1.256(1)	0.054(13)
H10	0.6545(7)	0.0688(15)	1.170(1)	0.056(13)
H11	0.5478(7)	0.0420(14)	0.9681(9)	0.043(13)

A2. 9 Fractional Atomic Coordinates and Equivalent Isotropic Thermal Parameters (U(iso) in $Å^2$) for $[Mn(phen)_2(\mu\text{-}Cl)_2Hg(CN)_2]$ (**3.3**).

Atom	x	y	z	U(iso)($Å^2$)
Hg1	0.48530(5)	0.47346(7)	0.75152(4)	0.0531
Mn1	0.49462(14)	0.0433(2)	0.74857(13)	0.0412
Cl1	0.3859(3)	0.2283(4)	0.6758(2)	0.0537
Cl2	0.5898(2)	0.2360(4)	0.8324(2)	0.0532
N1	0.3509(12)	0.5379(18)	0.8427(9)	0.0950
N2	0.6200(11)	0.5130(17)	0.6584(9)	0.0860
N3	0.4277(8)	-0.0115(13)	0.8344(7)	0.0485
N4	0.5745(8)	-0.1443(13)	0.8198(7)	0.0514
N5	0.4318(7)	-0.1417(11)	0.6639(6)	0.0409
N6	0.5751(8)	0.0257(13)	0.6691(7)	0.0454
C1	0.3996(12)	0.5114(17)	0.8124(11)	0.0715
C2	0.5696(13)	0.5011(17)	0.6877(11)	0.0707
C3	0.356(1)	0.0564(17)	0.8415(9)	0.0595
C4	0.3233(12)	0.022(2)	0.9022(11)	0.0814
C5	0.3642(13)	-0.080(2)	0.955(1)	0.0742
C6	0.4403(11)	-0.1512(19)	0.950(1)	0.0603
C7	0.4872(13)	-0.258(2)	1.0023(11)	0.0771
C8	0.5566(15)	-0.325(2)	0.995(1)	0.0775
C9	0.5913(12)	-0.2909(18)	0.936(1)	0.0610
C10	0.6649(13)	-0.361(2)	0.9227(11)	0.0805
C11	0.6926(12)	-0.3226(16)	0.8644(12)	0.0802
C12	0.649(1)	-0.2121(15)	0.8162(9)	0.0555

C13	0.5485(9)	-0.1844(16)	0.8818(9)	0.0459
C14	0.469(1)	-0.1127(18)	0.8881(8)	0.0518
C15	0.359(1)	-0.2280(18)	0.6598(9)	0.0593
C16	0.3269(11)	-0.3370(18)	0.606(1)	0.0655
C17	0.3667(12)	-0.360(2)	0.552(1)	0.0746
C18	0.4418(11)	-0.2767(18)	0.554(1)	0.0621
C19	0.4875(14)	-0.294(2)	0.4993(11)	0.0745
C20	0.5574(13)	-0.213(2)	0.5006(11)	0.0757
C21	0.5889(11)	-0.103(2)	0.557(1)	0.0589
C22	0.6645(13)	-0.015(2)	0.564(1)	0.0794
C23	0.690(1)	0.093(2)	0.618(1)	0.0733
C24	0.6453(9)	0.1101(18)	0.6704(8)	0.0526
C25	0.548(1)	-0.0778(15)	0.6132(9)	0.0468
C26	0.471(1)	-0.1668(15)	0.6093(8)	0.0420
H3	0.324(1)	0.1229(17)	0.8031(9)	0.079(15)
H4	0.2742(12)	0.077(2)	0.9073(11)	0.096(15)
H5	0.3403(13)	-0.104(2)	0.994(1)	0.094(15)
H7	0.4679(13)	-0.283(2)	1.0440(11)	0.090(15)
H8	0.5852(15)	-0.399(2)	1.031(1)	0.097(15)
H10	0.6957(13)	-0.438(2)	0.9555(11)	0.108(15)
H11	0.7419(12)	-0.3702(16)	0.8559(12)	0.091(15)
H12	0.670(1)	-0.1802(15)	0.7770(9)	0.073(15)
H15	0.328(1)	-0.2108(18)	0.6951(9)	0.085(15)
H16	0.2778(11)	-0.3969(18)	0.606(1)	0.086(15)
H17	0.3434(12)	-0.432(2)	0.513(1)	0.100(15)
H19	0.4670(14)	-0.367(2)	0.4608(11)	0.098(15)
H20	0.5863(13)	-0.226(2)	0.4636(11)	0.091(15)
H22	0.6971(13)	-0.029(2)	0.529(1)	0.092(15)
H23	0.739(1)	0.156(2)	0.619(1)	0.084(15)
H24	0.6643(9)	0.1840(18)	0.7084(8)	0.075(15)

A2. 10 Fractional Atomic Coordinates and Equivalent Isotropic Thermal Parameters (U(iso) in $Å^2$) for $[Ni(phen)_2(\mu\text{-}Cl)_2Hg(CN)_2]$ (**3.4**).

Atom	x	y	z	U(iso)($Å^2$)
Hg1	0.2500	0.03940(5)	0.7500	0.0426
Ni1	0.2500	0.47462(18)	0.7500	0.0324
Cl1	0.3580(2)	0.28269(19)	0.6684(1)	0.0401
N1	-0.110(1)	-0.022(1)	0.6606(5)	0.0734
N2	0.1814(7)	0.6445(7)	0.8246(3)	0.0393
N3	0.4680(6)	0.4900(6)	0.8249(3)	0.0340
C1	0.0218(11)	-0.0004(9)	0.6915(5)	0.0522
C2	0.0381(9)	0.7184(8)	0.8226(5)	0.0449
C3	0.0091(12)	0.832(1)	0.8777(5)	0.0623
C4	0.1328(12)	0.8608(9)	0.9345(5)	0.0592
C5	0.2869(11)	0.7848(9)	0.9379(5)	0.0507
C6	0.4210(14)	0.811(1)	0.9954(5)	0.0653
C7	0.5651(13)	0.737(1)	0.9959(5)	0.0630
C8	0.5901(9)	0.6231(9)	0.9392(4)	0.0471
C9	0.7360(9)	0.5397(11)	0.9360(5)	0.0628
C10	0.7448(9)	0.4305(12)	0.8796(5)	0.0633
C11	0.6076(8)	0.4093(9)	0.8252(5)	0.0466
C12	0.3044(8)	0.6755(7)	0.8805(4)	0.0343
C13	0.4569(8)	0.5926(8)	0.8810(4)	0.0365
H2	-0.0498(9)	0.6922(8)	0.7842(5)	0.050(9)
H3	-0.0940(12)	0.885(1)	0.8750(5)	0.064(9)
H4	0.1163(12)	0.9344(9)	0.9722(5)	0.065(9)
H6	0.4086(14)	0.883(1)	1.0344(5)	0.075(9)
H7	0.6550(13)	0.758(1)	1.0341(5)	0.065(9)
H9	0.8300(9)	0.5589(11)	0.9724(5)	0.062(9)
H10	0.8432(9)	0.3718(12)	0.8781(5)	0.061(9)
H11	0.6131(8)	0.3353(9)	0.7864(5)	0.047(9)

A2. 11 Fractional Atomic Coordinates and Equivalent Isotropic Thermal Parameters (U(iso) in $Å^2$) for [Cu(terpy)Cl_2(μ-Hg$(CN)_2$)] (**3.5**).

Atom	x	y	z	U(iso)($Å^2$)
Hg1	-0.448120(19)	0.119658(14)	0.830296(10)	0.0425
Cu1	0.09470(6)	0.22654(4)	0.70468(3)	0.0346
Cl1	0.23434(13)	0.01880(9)	0.75075(7)	0.0433
Cl2	-0.19596(13)	0.13998(11)	0.65294(7)	0.0503
N1	-0.5793(6)	0.4386(4)	0.7969(3)	0.0636
N2	-0.3294(7)	-0.1802(5)	0.9226(3)	0.0816
N3	-0.0215(4)	0.2768(3)	0.8442(2)	0.0368
N4	0.0717(4)	0.4306(3)	0.6831(2)	0.0340
N5	0.2308(4)	0.2554(3)	0.5633(2)	0.0384
C1	-0.5331(5)	0.3263(4)	0.8099(3)	0.0458
C2	-0.3714(6)	-0.0753(4)	0.8891(3)	0.0503
C3	-0.0642(5)	0.1868(4)	0.9247(3)	0.0450
C4	-0.1657(6)	0.2292(5)	1.0131(3)	0.0530
C5	-0.2240(6)	0.3654(5)	1.0175(3)	0.0544
C6	-0.1799(5)	0.4616(4)	0.9356(3)	0.0484
C7	-0.0755(5)	0.4141(4)	0.8498(2)	0.0376
C8	-0.0106(5)	0.5042(4)	0.7583(3)	0.0382
C9	-0.0226(5)	0.6504(4)	0.7470(3)	0.0468
C10	0.0552(6)	0.7165(4)	0.6560(3)	0.0488
C11	0.1430(5)	0.6389(4)	0.5797(3)	0.0432
C12	0.1520(4)	0.4936(3)	0.5957(2)	0.0352
C13	0.2421(4)	0.3919(4)	0.5266(2)	0.0360
C14	0.3337(5)	0.4284(4)	0.4311(3)	0.0457
C15	0.4117(5)	0.3226(5)	0.3729(3)	0.0548
C16	0.3952(6)	0.1835(5)	0.4092(3)	0.0542
C17	0.3044(5)	0.1550(4)	0.5062(3)	0.0490
H3	-0.0227(5)	0.0912(4)	0.9210(3)	0.054(4)
H4	-0.1942(6)	0.1631(5)	1.0695(3)	0.063(4)

H5	-0.2964(6)	0.3954(5)	1.0768(3)	0.063(4)
H6	-0.2188(5)	0.5580(4)	0.9377(3)	0.057(4)
H9	-0.0815(5)	0.7034(4)	0.8002(3)	0.056(4)
H10	0.0472(6)	0.8165(4)	0.6458(3)	0.059(4)
H11	0.1976(5)	0.6840(4)	0.5177(3)	0.051(4)
H14	0.3421(5)	0.5247(4)	0.4067(3)	0.055(4)
H15	0.4770(5)	0.3459(5)	0.3079(3)	0.063(4)
H16	0.4456(6)	0.1095(5)	0.3692(3)	0.063(4)
H17	0.2999(5)	0.0550(4)	0.5109(3)	0.057(4)

A2. 12 Fractional Atomic Coordinates and Equivalent Isotropic Thermal Parameters (U(iso) in $Å^2$) for $\{[Cu(phen)_2Cl]_2Hg(CN)_2[Hg(CN)_2Cl]_2$ (**3.6**).

Atom	**x**	**y**	**z**	**U(iso)($Å^2$)**
Hg1	0.08138(3)	0.37269(3)	0.42962(2)	0.0507
Hg2	0.5000	0.5000	1.0000	0.0523
Cu1	0.70644(7)	0.02914(7)	1.22271(6)	0.0430
Cl1	0.15062(15)	0.46465(18)	0.58190(13)	0.0541
Cl2	0.57806(15)	0.18535(16)	1.10320(13)	0.0500
N1	-0.0603(8)	0.1271(8)	0.6076(6)	0.0918
N2	0.2846(5)	0.5049(6)	0.2001(5)	0.0566
N3	0.7069(7)	0.5814(7)	1.1083(6)	0.0793
N4	0.6860(5)	-0.0270(5)	1.4010(4)	0.0419
N5	0.5795(5)	-0.1106(5)	1.2671(4)	0.0419
N6	0.8706(4)	-0.0869(5)	1.1720(4)	0.0368
N7	0.8484(5)	0.1498(5)	1.1935(4)	0.0443
C1	-0.0143(7)	0.2112(7)	0.5460(6)	0.0560
C2	0.2090(6)	0.4638(6)	0.2822(5)	0.0468
C3	0.6342(7)	0.5520(7)	1.0701(6)	0.0571
C4	0.7408(6)	0.0152(6)	1.4670(6)	0.0481
C5	0.7221(6)	-0.0434(7)	1.5852(6)	0.0515
C6	0.6443(6)	-0.1465(7)	1.6371(5)	0.0492

C7	0.5849(6)	-0.1938(6)	1.5702(5)	0.0441
C8	0.5016(6)	-0.3016(6)	1.6168(5)	0.0499
C9	0.4447(6)	-0.3403(6)	1.5481(6)	0.0526
C10	0.4673(5)	-0.2786(6)	1.4284(5)	0.0435
C11	0.4129(6)	-0.3153(6)	1.3528(6)	0.0504
C12	0.4441(6)	-0.2525(7)	1.2397(6)	0.0566
C13	0.5266(6)	-0.1489(7)	1.1984(6)	0.0496
C14	0.6091(5)	-0.1304(5)	1.4531(5)	0.0375
C15	0.5510(5)	-0.1745(6)	1.3805(5)	0.0390
C16	0.8805(6)	-0.2059(6)	1.1637(5)	0.0459
C17	1.0012(7)	-0.2669(6)	1.1289(5)	0.0526
C18	1.1154(6)	-0.2062(6)	1.1059(5)	0.0499
C19	1.1103(5)	-0.0819(6)	1.1166(4)	0.0390
C20	1.2236(6)	-0.0091(7)	1.0953(5)	0.0479
C21	1.2125(6)	0.1090(7)	1.1085(5)	0.0490
C22	1.0864(6)	0.1694(6)	1.1415(5)	0.0454
C23	1.0659(7)	0.2919(7)	1.1547(6)	0.0571
C24	0.9404(7)	0.3415(7)	1.1857(7)	0.0668
C25	0.8336(7)	0.2665(7)	1.2035(7)	0.0649
C26	0.9856(5)	-0.0270(6)	1.1500(4)	0.0371
C27	0.9732(5)	0.1002(6)	1.1623(4)	0.0374
H4	0.7946(6)	0.0877(6)	1.4317(6)	0.060(5)
H5	0.7636(6)	-0.0105(7)	1.6288(6)	0.065(5)
H6	0.6306(6)	-0.1866(7)	1.7175(5)	0.062(5)
H8	0.4874(6)	-0.3469(6)	1.6965(5)	0.064(5)
H9	0.3868(6)	-0.4098(6)	1.5808(6)	0.062(5)
H11	0.3537(6)	-0.3835(6)	1.3816(6)	0.060(5)
H12	0.4092(6)	-0.2795(7)	1.1886(6)	0.067(5)
H13	0.5465(6)	-0.1043(7)	1.1188(6)	0.063(5)
H16	0.8016(6)	-0.2505(6)	1.1819(5)	0.055(5)
H17	1.0036(7)	-0.3512(6)	1.1219(5)	0.066(5)

H18	1.1983(6)	-0.2472(6)	1.0823(5)	0.063(5)
H20	1.3091(6)	-0.0452(7)	1.0712(5)	0.060(5)
H21	1.2902(6)	0.1534(7)	1.0960(5)	0.060(5)
H23	1.1399(7)	0.3418(7)	1.1413(6)	0.070(5)
H24	0.9263(7)	0.4247(7)	1.1962(7)	0.080(5)
H25	0.7462(7)	0.3014(7)	1.2235(7)	0.082(5)

A2. 13 Fractional Atomic Coordinates and Equivalent Isotropic Thermal Parameters (U(iso) in $Å^2$) for $[Cu(dien)Cl][Hg(CN)_2Cl]$ (**3.7**).

Atom	x	y	z	U(iso)($Å^2$)
Hg1	-0.127781(15)	-0.24765(3)	0.249227(12)	0.0326
Cu1	0.01434(5)	0.17739(10)	0.33640(4)	0.0270
Cl1	-0.00272(9)	0.04173(18)	0.23336(7)	0.0276
Cl2	-0.25406(10)	0.00201(19)	0.22444(9)	0.0354
N1	-0.1113(3)	0.2010(7)	0.3447(3)	0.0307
N4	0.0329(3)	0.2499(6)	0.4360(2)	0.0312
N7	0.1427(3)	0.2002(7)	0.3420(3)	0.0311
N11	-0.0875(4)	-0.1599(9)	0.4110(3)	0.0551
N12	-0.1403(5)	-0.3340(11)	0.0890(4)	0.0799
C2	-0.1205(4)	0.2351(8)	0.4188(3)	0.0387
C3	-0.0462(4)	0.3320(9)	0.4490(3)	0.0394
C5	0.1131(4)	0.3402(9)	0.4439(3)	0.0369
C6	0.1790(4)	0.2421(8)	0.4147(3)	0.0370
C11	-0.1010(5)	-0.1956(9)	0.3546(4)	0.0386
C12	-0.1360(5)	-0.2996(9)	0.1444(4)	0.0410
H11	-0.1342(3)	0.2824(7)	0.3164(3)	0.050(6)
H12	-0.1402(3)	0.1096(7)	0.3308(3)	0.050(6)
H41	0.0404(3)	0.1726(6)	0.4699(2)	0.050(6)
H71	0.1555(3)	0.2783(7)	0.3117(3)	0.050(6)
H72	0.1664(3)	0.1071(7)	0.3296(3)	0.050(6)
H21	-0.1726(4)	0.2895(8)	0.4213(3)	0.039(6)

H22	-0.1207(4)	0.1408(8)	0.4444(3)	0.039(6)
H31	-0.0464(4)	0.3456(9)	0.4979(3)	0.037(6)
H32	-0.0491(4)	0.4306(9)	0.4266(3)	0.037(6)
H51	0.1310(4)	0.3611(9)	0.4921(3)	0.050(6)
H52	0.1052(4)	0.4353(9)	0.4189(3)	0.050(6)
H61	0.1900(4)	0.1506(8)	0.4420(3)	0.050(6)
H62	0.2309(4)	0.2988(8)	0.4148(3)	0.050(6)

A2. 14 Fractional Atomic Coordinates and Equivalent Isotropic Thermal Parameters (U(iso) in $Å^2$) for $[Cu(tren)Hg(CN)_2Cl][HgX_2Cl]$ (**3.8**).

Atom	x	y	z	U(iso)($Å^2$)	Occ
Hg1	0.67322(6)	0.23413(2)	-0.42542(3)	0.0436	1.0000
Hg2	0.69855(6)	0.19990(3)	-0.10186(3)	0.0586	1.0000
Cu1	0.67620(16)	0.50723(7)	-0.29288(8)	0.0403	1.0000
Cl1	0.8968(3)	0.25125(16)	-0.56014(17)	0.0495	1.0000
Cl2	0.4437(4)	0.25728(18)	-0.21705(19)	0.0583	1.0000
N1	0.6841(14)	0.4308(5)	-0.1812(6)	0.0722	1.0000
N2	0.6665(10)	0.5913(4)	-0.1942(5)	0.0369	1.0000
N3	0.9176(11)	0.5575(6)	-0.3140(6)	0.0582	1.0000
N4	0.4817(12)	0.5691(5)	-0.3652(6)	0.0578	1.0000
N11	0.6906(14)	0.0499(6)	-0.4185(9)	0.0904	1.0000
N12	0.6755(11)	0.4157(5)	-0.3756(6)	0.0519	1.0000
C1	0.6928(16)	0.4753(6)	-0.0930(7)	0.0610	1.0000
C2	0.6088(15)	0.5527(6)	-0.1114(7)	0.0547	1.0000
C3	0.8419(14)	0.6248(6)	-0.1768(8)	0.0543	1.0000
C4	0.9272(14)	0.6328(6)	-0.2650(8)	0.0561	1.0000
C11	0.6794(13)	0.1160(7)	-0.4175(8)	0.0554	1.0000
C12	0.6765(13)	0.3513(6)	-0.3949(7)	0.0444	1.0000
C5	0.4032(14)	0.6141(7)	-0.2948(9)	0.0651	1.0000
C6	0.5388(14)	0.6504(6)	-0.2304(7)	0.0511	1.0000
Cl3	0.6779(15)	0.0648(4)	-0.1347(8)	0.0732	0.4717

Cl4	0.7724(16)	0.2919(6)	0.0117(6)	0.0761	0.5035
N10	0.663(3)	0.0254(5)	-0.1537(16)	0.070(5)	0.5283
C10	0.667(5)	0.0860(7)	-0.143(3)	0.062(6)	0.5283
N20	0.771(3)	0.3228(9)	0.0550(10)	0.072(5)	0.4965
C20	0.753(5)	0.2826(19)	0.000(2)	0.069(5)	0.4965
H11	0.8097	0.4834	-0.0707	0.081(7)	1.0000
H12	0.6374	0.4474	-0.0475	0.061(7)	1.0000
H21	0.6335	0.5857	-0.0589	0.070(7)	1.0000
H22	0.4884	0.5446	-0.1216	0.068(7)	1.0000
H31	0.8350	0.6746	-0.1479	0.049(6)	1.0000
H32	0.9097	0.5910	-0.1358	0.061(7)	1.0000
H41	1.0438	0.6480	-0.2510	0.057(6)	1.0000
H42	0.8684	0.6711	-0.3032	0.092(7)	1.0000
H51	0.3319	0.6534	-0.3243	0.061(7)	1.0000
H52	0.3367	0.5806	-0.2602	0.064(7)	1.0000
H61	0.5957	0.6892	-0.2629	0.073(7)	1.0000
H62	0.4897	0.6735	-0.1795	0.076(7)	1.0000
H71	0.7796	0.3989	-0.1814	0.106(7)	1.0000
H72	0.5852	0.4007	-0.1862	0.116(7)	1.0000
H81	0.9261	0.5649	-0.3775	0.058(7)	1.0000
H82	1.0059	0.5254	-0.2895	0.106(7)	1.0000
H91	0.5250	0.6019	-0.4085	0.087(7)	1.0000
H92	0.4021	0.5352	-0.3955	0.083(7)	1.0000

A2. 15 Fractional Atomic Coordinates and Equivalent Isotropic Thermal Parameters (U(iso) in $Å^2$) for $\{[Ni(en)_2]Hg(CN)_2]_3Cl_2\}_2$ (**3.9**).

Atom	x	y	z	U(iso)($Å^2$)
Hg1	1.16071(7)	-0.17604(12)	0.77808(5)	0.0373
Hg2	0.83496(7)	-0.12048(11)	0.74397(5)	0.0380
Hg3	1.02803(7)	0.08783(12)	0.74797(5)	0.0412
Hg4	0.84991(7)	0.31758(12)	0.69824(5)	0.0368

Hg5	1.16588(7)	0.36949(12)	0.73611(5)	0.0370
Hg6	0.99179(7)	0.58872(13)	0.78241(6)	0.0457
Ni1	1.2708(3)	0.3482(4)	0.97811(19)	0.0387
Ni2	0.8603(2)	0.1867(4)	0.46499(18)	0.0296
Cl1	1.0025(4)	-0.1664(8)	0.7655(4)	0.0565
Cl2	0.8657(4)	0.1027(6)	0.7518(3)	0.0402
Cl3	1.0052(4)	0.3334(7)	0.7548(4)	0.0475
Cl4	1.1395(4)	0.5952(7)	0.7318(3)	0.0451
N1	1.2072(18)	0.474(2)	1.0115(13)	0.0593
N2	1.1719(17)	0.262(3)	0.9858(12)	0.0777
N3	1.3702(18)	0.443(3)	0.9758(14)	0.0705
N4	1.344(2)	0.235(3)	0.9484(11)	0.0886
N5	0.7388(12)	0.162(2)	0.4637(11)	0.0444
N6	0.8634(14)	0.024(2)	0.4838(9)	0.0454
N7	0.8631(13)	0.3459(19)	0.4361(10)	0.0347
N8	0.9828(12)	0.1990(19)	0.4680(10)	0.0363
C1	1.140(3)	0.432(3)	1.0359(19)	0.0761
C2	1.108(2)	0.341(5)	0.9942(19)	0.1064
C3	1.435(2)	0.370(4)	0.969(2)	0.0882
C4	1.413(2)	0.289(4)	0.9231(18)	0.0875
C5	0.7262(13)	0.052(3)	0.4870(14)	0.0445
C6	0.7836(16)	-0.021(2)	0.4628(12)	0.0367
C7	0.9457(17)	0.387(3)	0.4494(19)	0.0615
N11	1.1580(14)	-0.146(2)	0.6318(11)	0.0394
N12	1.1883(17)	-0.184(2)	0.9277(10)	0.0537
N21	0.8340(19)	-0.124(2)	0.5976(14)	0.0622
N22	0.831(2)	-0.150(3)	0.8887(13)	0.0939
N31	1.0121(17)	0.055(3)	0.6004(11)	0.0725
N32	1.1022(19)	0.087(3)	0.8935(13)	0.0702
N41	0.8684(14)	0.239(2)	0.5603(11)	0.0492
N42	0.7825(18)	0.423(4)	0.813(2)	0.1135

N51	1.138(2)	0.306(3)	0.5919(16)	0.0996
N52	1.2238(13)	0.382(3)	0.8832(12)	0.0623
N61	0.870(2)	0.575(3)	0.6561(15)	0.0919
N62	1.0711(18)	0.599(3)	0.9239(14)	0.0727
C12	1.1781(17)	-0.184(3)	0.8737(11)	0.0540
C21	0.8317(16)	-0.126(3)	0.6492(12)	0.0404
C31	1.0178(17)	0.068(3)	0.6516(11)	0.0390
C32	1.0811(19)	0.084(3)	0.8419(16)	0.0540
C41	0.8619(16)	0.269(3)	0.6095(13)	0.0396
C42	0.803(3)	0.390(3)	0.7720(16)	0.0697
C51	1.148(2)	0.326(3)	0.6434(18)	0.0665
C52	1.2040(19)	0.373(3)	0.8302(13)	0.0549
C61	0.9143(19)	0.582(3)	0.6997(14)	0.0493
C62	1.0443(19)	0.592(4)	0.8745(15)	0.0634
C8	0.999(2)	0.300(3)	0.4388(16)	0.061(9)
C11	1.1652(17)	-0.153(3)	0.6833(15)	0.045(8)
C22	0.8279(19)	-0.143(3)	0.8344(16)	0.054(9)
H11	1.155(3)	0.408(3)	1.0780(19)	0.10(3)
H12	1.100(3)	0.486(3)	1.0348(19)	0.10(3)
H21	1.069(2)	0.305(5)	1.0133(19)	0.14(3)
H22	1.085(2)	0.368(5)	0.9542(19)	0.14(3)
H31	1.451(2)	0.335(4)	1.009(2)	0.12(3)
H32	1.479(2)	0.409(4)	0.958(2)	0.12(3)
H41	1.455(2)	0.240(4)	0.9204(18)	0.12(3)
H42	1.397(2)	0.321(4)	0.8830(18)	0.12(3)
H51	0.7357(13)	0.052(3)	0.5317(14)	0.07(3)
H52	0.6740(13)	0.029(3)	0.4726(14)	0.07(3)
H61	0.7798(16)	-0.092(2)	0.4786(12)	0.06(3)
H62	0.7733(16)	-0.022(2)	0.4180(12)	0.06(3)
H71	0.9570(17)	0.409(3)	0.4921(19)	0.09(3)
H72	0.9516(17)	0.446(3)	0.4225(19)	0.09(3)

H81	1.052(2)	0.321(3)	0.4551(16)	0.08(3)
H82	0.995(2)	0.289(3)	0.3946(16)	0.08(3)
H91	1.2394(18)	0.509(2)	1.0437(13)	0.08(3)
H92	1.1907(18)	0.522(2)	0.9789(13)	0.08(3)
H101	1.1815(17)	0.216(3)	1.0202(12)	0.10(3)
H102	1.1569(17)	0.222(3)	0.9493(12)	0.10(3)
H111	1.3817(18)	0.483(3)	1.0127(14)	0.09(3)
H112	1.3620(18)	0.490(3)	0.9415(14)	0.09(3)
H121	1.364(2)	0.191(3)	0.9820(11)	0.10(3)
H122	1.316(2)	0.194(3)	0.9164(11)	0.10(3)
H131	0.7196(12)	0.213(2)	0.4895(11)	0.06(3)
H132	0.7125(12)	0.169(2)	0.4227(11)	0.06(3)
H141	0.8774(14)	0.012(2)	0.5268(9)	0.06(3)
H142	0.9000(14)	-0.010(2)	0.4625(9)	0.06(3)
H151	0.8306(13)	0.3871(19)	0.4575(10)	0.05(3)
H152	0.8453(13)	0.3498(19)	0.3931(10)	0.05(3)
H161	1.0075(12)	0.1981(19)	0.5097(10)	0.06(3)
H162	1.0006(12)	0.1414(19)	0.4464(10)	0.06(3)

A2. 16 Fractional Atomic Coordinates and Equivalent Isotropic Thermal Parameters (U(iso) in $Å^2$) for $\{[Ni(tren)]_4[Hg(CN)_2]_8Cl_6\}HgCl_4$ (**3.10**).

Atom	**x**	**y**	**z**	**U(iso)($Å^2$)**
Hg1	-0.94722(3)	-0.42577(3)	-0.78868(11)	0.0421
Hg2	-0.78078(3)	-0.32488(3)	-1.19930(11)	0.0423
Hg3	-1.0000	0.0000	-1.0000	0.0485
Ni1	-0.72918(10)	-0.51136(10)	-0.8614(3)	0.0387
Cl1	-1.0000	-0.5000	-1.0310(9)	0.0600
Cl2	-0.87654(18)	-0.3254(2)	-0.9843(6)	0.0459
Cl3	-0.9505(2)	0.0692(2)	-0.8020(7)	0.0565
N5	-0.7075(7)	-0.4482(6)	-0.6777(19)	0.0497
N6	-0.6387(7)	-0.5326(7)	-0.910(2)	0.0527

N7	-0.7630(8)	-0.5853(6)	-0.987(2)	0.0615
N8	-0.7214(6)	-0.5720(6)	-0.6719(18)	0.0431
C5	-0.6937(9)	-0.4779(9)	-0.528(2)	0.0593
C6	-0.7285(9)	-0.5386(8)	-0.521(3)	0.0567
C7	-0.6299(8)	-0.5927(9)	-0.842(2)	0.0567
C8	-0.6604(8)	-0.5989(8)	-0.681(3)	0.0544
C9	-0.7712(10)	-0.6348(9)	-0.868(3)	0.0672
C10	-0.7676(10)	-0.6170(10)	-0.694(3)	0.0755
N1	-0.8207(6)	-0.4899(6)	-0.812(2)	0.048(4)
N2	-1.0663(8)	-0.3499(8)	-0.771(3)	0.088(6)
N3	-0.7352(6)	-0.4477(6)	-1.0450(17)	0.040(4)
N4	-0.7977(9)	-0.1923(9)	-1.295(3)	0.097(6)
C1	-0.8650(8)	-0.4666(7)	-0.796(3)	0.046(4)
C2	-1.0235(8)	-0.3734(8)	-0.772(3)	0.055(5)
C3	-0.7482(7)	-0.4038(8)	-1.111(2)	0.038(4)
C4	-0.7893(6)	-0.2336(7)	-1.2671(19)	0.026(4)
H11	-0.7408(7)	-0.4243(6)	-0.6587(19)	0.09(3)
H12	-0.6760(7)	-0.4246(6)	-0.7150(19)	0.09(3)
H21	-0.6308(7)	-0.5310(7)	-1.022(2)	0.07(3)
H22	-0.6134(7)	-0.5063(7)	-0.854(2)	0.07(3)
H31	-0.8003(8)	-0.5754(6)	-1.030(2)	0.10(3)
H32	-0.7377(8)	-0.5969(6)	-1.072(2)	0.10(3)
H51	-0.7052(9)	-0.4532(9)	-0.439(2)	0.063(18)
H52	-0.6516(9)	-0.4836(9)	-0.526(2)	0.063(18)
H61	-0.7694(9)	-0.5324(8)	-0.493(3)	0.065(18)
H62	-0.7101(9)	-0.5620(8)	-0.437(3)	0.065(18)
H71	-0.6485(8)	-0.6198(9)	-0.917(2)	0.072(18)
H72	-0.5885(8)	-0.6018(9)	-0.834(2)	0.072(18)
H81	-0.6644(8)	-0.6402(8)	-0.655(3)	0.052(18)
H82	-0.6356(8)	-0.5803(8)	-0.600(3)	0.052(18)
H91	-0.8090(10)	-0.6532(9)	-0.885(3)	0.072(18)

H92	-0.7403(10)	-0.6631(9)	-0.889(3)	0.072(18)
H101	-0.8053(10)	-0.6015(10)	-0.660(3)	0.092(18)
H102	-0.7579(10)	-0.6509(10)	-0.628(3)	0.092(18)

A2. 17 Fractional Atomic Coordinates and Equivalent Isotropic Thermal Parameters (U(iso) in $Å^2$) for $\{(tmeda)Cu[Hg(CN)_2]_2\}HgCl_4$ (**4.1**).

Atom	x	y	z	U(iso)($Å^2$)
Hg1	-0.22465(3)	-0.27535(3)	-0.46482(5)	0.0413
Hg2	0.0000	0.0000	-0.5000	0.0585
Cu1	0.0000	-0.5000	-0.84850(19)	0.0341
Cl1	-0.1889(2)	-0.0424(2)	-0.6300(3)	0.0528
N1	-0.0914(7)	-0.4086(7)	-0.7084(10)	0.0371
N2	-0.3372(7)	-0.1628(7)	-0.2003(12)	0.0507
N3	-0.0926(9)	-0.4074(9)	-0.9970(13)	0.0693
C1	-0.1379	-0.3621	-0.6219	0.0358
C2	-0.2972	-0.2028	-0.2948	0.0359
C3	-0.0707(13)	-0.2734(13)	-0.9897(14)	0.089(4)
C4	-0.0497(18)	-0.4503(18)	-1.111(3)	0.155(12)
H31	-0.1040	-0.2442	-0.9098	0.0879
H32	-0.1135	-0.2355	-1.0667	0.0879
H33	0.0123	-0.2568	-0.9985	0.0879
H41	-0.1116	-0.4885	-1.1771	0.1327
H42	-0.0115	-0.3884	-1.1771	0.1327

A2. 18 Fractional Atomic Coordinates and Equivalent Isotropic Thermal Parameters (U(iso) in $Å^2$) for $\{(tmeda)Cu[Hg(CN)_2]_2\}HgBr_4$ (**4.2**).

Atom	x	y	z	U(iso)($Å^2$)
Hg1	-0.72213(19)	-0.22213(19)	-1.0398(2)	0.0423
Hg2	-1.0000	0.0000	-1.0000	0.0538
Cu1	-0.5000	0.0000	-0.6607(10)	0.0343

Br1	-0.9538(5)	-0.1913(5)	-0.8569(4)	0.0516
N3	-0.592(4)	-0.092(4)	-0.515(6)	0.0742
C3	-0.716(5)	-0.071(4)	-0.513(5)	0.089(18)
C4	-0.540(6)	-0.040(6)	-0.404(9)	0.17(6)
N1	-0.591(3)	-0.091(3)	-0.806(4)	0.030(12)
N2	-0.841(4)	-0.341(4)	-1.297(5)	0.051(17)
C1	-0.636(4)	-0.136(4)	-0.883(5)	0.019(13)
C2	-0.798(4)	-0.298(4)	-1.216(5)	0.037(15)
H31	-0.730(5)	0.013(4)	-0.515(5)	0.07(7)
H32	-0.753(5)	-0.106(4)	-0.589(5)	0.07(7)
H33	-0.749(5)	-0.103(4)	-0.433(5)	0.07(7)
H41	-0.603(6)	-0.005(6)	-0.354(9)	0.22(7)
H42	-0.505(6)	-0.103(6)	-0.354(9)	0.22(7)

A2. 19 Fractional Atomic Coordinates and Equivalent Isotropic Thermal Parameters (U(iso) in $Å^2$) for $\{(tmeda)Cu[Hg(CN)_2]_2\}HgI_4$ (**4.3**).

Atom	x	y	z	U(iso)($Å^2$)
Hg1	0.77838(7)	0.72162(7)	-0.04223(13)	0.0514
Hg2	1.0000	1.0000	0.0000	0.0588
I1	0.80865(12)	0.95116(12)	0.15801(16)	0.0547
Cu1	1.0000	0.5000	0.3209(5)	0.0422
N1	0.9144(13)	0.5856(13)	0.182(3)	0.0447
N2	0.660(2)	0.840(2)	-0.283(4)	0.0746
C1	0.865(2)	0.635(2)	0.100(4)	0.0551
C2	0.6996(16)	0.8004(16)	-0.203(3)	0.0381
N3	0.9114	0.5886	0.4670	0.0625
C3	0.931(2)	0.712(2)	0.466(3)	0.082(8)
C4	0.954(3)	0.546(3)	0.588(6)	0.13(2)
H31	1.012(2)	0.728(2)	0.467(3)	0.10(5)
H32	0.896(2)	0.746(2)	0.541(3)	0.10(5)
H33	0.898(2)	0.744(2)	0.387(3)	0.10(5)

H41	0.9836	0.6112	0.6387	0.1474
H42	0.8888	0.5164	0.6387	0.1474

A2. 20 Fractional Atomic Coordinates and Equivalent Isotropic Thermal Parameters (U(iso) in $Å^2$) for $\{(tmeda)Ni[Hg(CN)_2]_2\}HgCl_4$ (**4.4**).

Atom	x	y	z	U(iso)($Å^2$)
Hg1	0.73078(4)	0.23078(4)	-0.05243(8)	0.0449
Hg2	1.0000	0.0000	0.0000	0.0605
Ni1	0.5000	0.0000	0.3338(3)	0.0278
Cl1	0.9614(3)	0.1891(3)	0.1321(4)	0.0586
N1	0.8623(9)	0.3623(9)	-0.2998(15)	0.0405
N2	0.5954(10)	0.0954(10)	0.1876(15)	0.0383
C1	0.8134(10)	0.3134(10)	-0.2170(18)	0.0357
C2	0.6438(12)	0.1438(12)	0.103(3)	0.0527
N3	0.5941(13)	0.0941(13)	0.4897(17)	0.0530
C3	0.7278(19)	0.073(2)	0.488(2)	0.088(5)
C4	0.548(3)	0.048(3)	0.612(4)	0.142(17)
H31	0.7462	-0.0109	0.4866	0.1057
H32	0.7648	0.1094	0.5677	0.1057
H33	0.7633	0.1110	0.4081	0.1057
H41	0.6151	0.0151	0.6598	0.1632
H42	0.5151	0.1151	0.6598	0.1632

A2. 21 Fractional Atomic Coordinates and Equivalent Isotropic Thermal Parameters (U(iso) in $Å^2$) for $\{(tmeda)Ni[Hg(CN)_2]_2\}HgBr_4$ (**4.5**).

Atom	x	y	z	U(iso)($Å^2$)
Hg1	1.22886(8)	0.27114(8)	0.05622(15)	0.0480
Hg2	1.5000	0.5000	0.0000	0.0573
Ni1	1.0000	0.5000	-0.3222(6)	0.0291
Br1	1.4578(2)	0.3101(2)	-0.1459(3)	0.0580
N1	1.0943(18)	0.4057(18)	-0.181(4)	0.0563

N2	1.3647(17)	0.1353(17)	0.293(2)	0.0382
C1	1.1428(18)	0.3572(18)	-0.094(3)	0.0335
C2	1.311(2)	0.189(2)	0.215(5)	0.0666
N3	1.0913(16)	0.4087(16)	-0.481(3)	0.0446
C3	1.218(2)	0.427(3)	-0.479(3)	0.084(9)
C4	1.043(3)	0.457(3)	-0.602(7)	0.13(2)
H31	1.234(2)	0.511(3)	-0.481(3)	0.07(4)
H32	1.254(2)	0.389(3)	-0.555(3)	0.07(4)
H33	1.250(2)	0.394(3)	-0.397(3)	0.07(4)
H41	1.1097	0.4885	-0.6578	0.1581
H42	1.0115	0.3903	-0.6578	0.1581

A2. 22 Fractional Atomic Coordinates and Equivalent Isotropic Thermal Parameters (U(iso) in $Å^2$) for $\{(tmeda)Ni[Hg(CN)_2]_2\}HgI_4$ (**4.6**).

Atom	x	y	z	U(iso)($Å^2$)
Hg1	0.2704(2)	-0.2296(2)	1.0574(4)	0.0376
Hg2	0.5000	-0.5000	1.0000	0.0386
I1	0.5426(4)	-0.3081(4)	1.1620(3)	0.0389
Ni1	0.5000	0.0000	0.6965(16)	0.009(4)
N1	0.413(5)	-0.087(5)	0.819(7)	0.029(17)
C1	0.359(6)	-0.141(6)	0.902(10)	0.04(3)
N2	0.130(4)	-0.370(4)	1.285(6)	0.026(17)
C2	0.198(5)	-0.302(5)	1.196(8)	0.017(19)
N3	0.410(5)	-0.090(5)	0.541(8)	0.05(2)
C3	0.437(6)	-0.220(6)	0.551(6)	0.041(17)
C4	0.459(6)	-0.041(6)	0.420(10)	0.06(3)
H31	0.5187	-0.2324	0.5433	0.0503
H32	0.4108	-0.2500	0.6327	0.0503
H33	0.4000	-0.2609	0.4795	0.0503
H41	0.4913	-0.1035	0.3717	0.0672
H42	0.3965	-0.0087	0.3717	0.0672

A2. 23 Fractional Atomic Coordinates and Equivalent Isotropic Thermal Parameters (U(iso) in $Å^2$) for $[Cu(bipy)_2(\mu\text{-}Cl)_2Hg(CN)_2]$ (**5.1**).

Atom	x	y	z	U(iso)($Å^2$)
Hg1	1.25473(3)	0.249628(16)	0.239532(18)	0.0490
Cu1	0.81088(7)	0.24916(4)	0.25595(4)	0.0382
Cl1	0.93271(15)	0.2660(1)	0.4018(1)	0.0504
Cl2	1.11484(18)	0.23662(11)	0.07859(11)	0.0576
N1	0.7020(5)	0.4264(3)	0.2587(3)	0.0401
N2	0.5615(5)	0.2760(3)	0.3897(3)	0.0430
N3	0.8941(5)	0.0717(3)	0.2522(3)	0.0401
N4	0.7349(5)	0.2227(3)	0.1201(3)	0.0418
N11	1.4253(8)	-0.0238(5)	0.2863(6)	0.0923
N12	1.1940(9)	0.5233(5)	0.2080(6)	0.0901
C1	0.7803(6)	0.4980(4)	0.1940(4)	0.0489
C2	0.7045(8)	0.6197(4)	0.1998(4)	0.0582
C3	0.5427(7)	0.6699(4)	0.2763(4)	0.0559
C4	0.4593(7)	0.5969(4)	0.3436(4)	0.0492
C5	0.5394(6)	0.4752(4)	0.3335(3)	0.0406
C6	0.4604(6)	0.3913(4)	0.4030(4)	0.0428
C7	0.2918(6)	0.4261(5)	0.4782(4)	0.0537
C8	0.2291(8)	0.3399(6)	0.5387(4)	0.0654
C9	0.3339(9)	0.2232(6)	0.5270(5)	0.0706
C10	0.4978(7)	0.1959(4)	0.4508(5)	0.0589
C11	1.3667(7)	0.0715(5)	0.2683(5)	0.0581
C12	1.2138(7)	0.4280(4)	0.2209(5)	0.0551
C13	0.9815(6)	-0.0001(4)	0.3180(4)	0.0509
C14	1.0339(7)	-0.1213(4)	0.3105(4)	0.0581
C15	0.9996(7)	-0.1723(4)	0.2318(5)	0.0593
C16	0.9078(7)	-0.0995(4)	0.1638(4)	0.0518
C17	0.8572(5)	0.0226(4)	0.1742(3)	0.0386
C18	0.7629(6)	0.1073(4)	0.1036(4)	0.0434

C19	0.7067(7)	0.0738(5)	0.0249(4)	0.0539
C20	0.6199(8)	0.1619(5)	-0.0379(5)	0.0644
C21	0.5964(8)	0.2772(5)	-0.0232(5)	0.0665
C22	0.6541(7)	0.3054(4)	0.0572(4)	0.0580
H1	0.8918(6)	0.4627(4)	0.1400(4)	0.055(4)
H2	0.7646(8)	0.6687(4)	0.1538(4)	0.067(4)
H3	0.4872(7)	0.7538(4)	0.2821(4)	0.060(4)
H4	0.3467(7)	0.6303(4)	0.3968(4)	0.053(4)
H7	0.2197(6)	0.5074(5)	0.4854(4)	0.057(4)
H8	0.1145(8)	0.3617(6)	0.5898(4)	0.077(4)
H9	0.2948(9)	0.1630(6)	0.5703(5)	0.077(4)
H10	0.5700(7)	0.1146(4)	0.4397(5)	0.066(4)
H13	1.0078(6)	0.0345(4)	0.3717(4)	0.052(4)
H14	1.0938(7)	-0.1700(4)	0.3599(4)	0.058(4)
H15	1.0394(7)	-0.2564(4)	0.2237(5)	0.058(4)
H16	0.8782(7)	-0.1323(4)	0.1107(4)	0.055(4)
H19	0.7295(7)	-0.0080(5)	0.0135(4)	0.056(4)
H20	0.5757(8)	0.1414(5)	-0.0900(5)	0.072(4)
H21	0.5406(8)	0.3379(5)	-0.0676(5)	0.071(4)
H22	0.6381(7)	0.3859(4)	0.0683(4)	0.060(4)

A2. 24 Fractional Atomic Coordinates and Equivalent Isotropic Thermal Parameters (U(iso) in $Å^2$) for $[Cu(bipy)_2Hg_2Cl_6]_2$ (**5.2**).

Atom	**x**	**y**	**z**	**U(iso)($Å^2$)**
Hg1	0.59815(11)	0.35134(8)	0.55093(9)	0.0561
Hg2	0.49031(11)	0.14547(9)	0.85507(9)	0.0611
Cu1	0.1804(3)	0.2559(2)	1.1326(2)	0.0479
Cl2	0.3908(7)	0.2177(5)	0.6619(6)	0.0601
Cl5	0.5538(8)	0.5372(5)	0.6156(6)	0.0722
Cl6	0.7805(7)	0.2397(6)	0.4289(6)	0.0714
Cl1	0.7038(7)	0.2434(6)	0.7538(6)	0.0688

Cl4	0.3270(9)	-0.0004(7)	0.9546(7)	0.1006
Cl3	0.3689(7)	0.3283(5)	0.9748(5)	0.0580
N1	0.0299(19)	0.3054(15)	1.0597(17)	0.0538
N2	0.0768(18)	0.4010(14)	1.2186(15)	0.0431
N3	0.3087(17)	0.1950(15)	1.2226(14)	0.0449
N4	0.0739(17)	0.1080(15)	1.2168(15)	0.0471
C1	0.023(3)	0.252(2)	0.973(2)	0.072(8)
C2	-0.101(3)	0.270(2)	0.931(2)	0.068(7)
C3	-0.201(3)	0.345(2)	0.985(2)	0.064(7)
C4	-0.195(3)	0.401(2)	1.071(2)	0.055(7)
C5	-0.076(2)	0.3829(18)	1.1110(18)	0.039(5)
C6	-0.048(3)	0.435(2)	1.200(2)	0.056(7)
C7	-0.136(2)	0.5220(19)	1.2528(19)	0.052(6)
C8	-0.102(2)	0.575(2)	1.331(2)	0.060(7)
C9	0.025(3)	0.539(2)	1.354(2)	0.064(7)
C10	0.114(2)	0.4486(19)	1.2962(19)	0.052(6)
C11	0.433(2)	0.244(2)	1.2144(19)	0.052(6)
C12	0.518(3)	0.197(2)	1.278(2)	0.067(7)
C13	0.473(3)	0.102(2)	1.354(2)	0.069(7)
C14	0.348(3)	0.048(2)	1.364(2)	0.064(7)
C15	0.264(2)	0.0977(19)	1.298(2)	0.044(6)
C16	0.129(2)	0.0532(18)	1.2960(18)	0.045(6)
C17	0.066(3)	-0.046(2)	1.369(2)	0.063(7)
C18	-0.062(3)	-0.078(2)	1.357(2)	0.070(7)
C19	-0.117(3)	-0.028(2)	1.279(2)	0.072(8)
C20	-0.049(3)	0.070(2)	1.211(2)	0.066(7)
H1	0.100(3)	0.202(2)	0.936(2)	0.11(2)
H2	-0.111(3)	0.232(2)	0.872(2)	0.12(2)
H3	-0.285(3)	0.358(2)	0.962(2)	0.10(2)
H4	-0.269(3)	0.456(2)	1.102(2)	0.09(2)
H7	-0.224(2)	0.5446(19)	1.2376(19)	0.09(2)

H8	-0.161(2)	0.638(2)	1.366(2)	0.11(2)
H9	0.051(3)	0.573(2)	1.410(2)	0.11(2)
H10	0.200(2)	0.4222(19)	1.3128(19)	0.09(2)
H11	0.462(2)	0.313(2)	1.1632(19)	0.09(2)
H12	0.607(3)	0.231(2)	1.269(2)	0.11(2)
H13	0.528(3)	0.072(2)	1.403(2)	0.11(2)
H14	0.319(3)	-0.021(2)	1.415(2)	0.11(2)
H17	0.108(3)	-0.088(2)	1.422(2)	0.10(2)
H18	-0.114(3)	-0.139(2)	1.410(2)	0.11(2)
H19	-0.197(3)	-0.061(2)	1.268(2)	0.11(2)
H20	-0.094(3)	0.113(2)	1.160(2)	0.11(2)

A2. 25 Fractional Atomic Coordinates and Equivalent Isotropic Thermal Parameters (U(iso) in $Å^2$) for $\{[Cu(bipy)Cl]_2Hg(CN)_2[Hg(CN)_2Cl]_2\}$ (**5.3**).

Atom	**x**	**y**	**z**	**U(iso)($Å^2$)**
Hg1	0.02796(4)	0.83861(3)	0.854502(19)	0.0457
Hg2	0.5000	0.5000	1.0000	0.0541
Cu1	0.14669(9)	0.40562(9)	0.77095(5)	0.0368
Cl1	0.3349(2)	0.5851(2)	0.80875(12)	0.0449
Cl2	-0.1317(2)	0.58637(19)	0.80633(13)	0.0454
N1	0.2006(6)	0.4628(6)	0.6189(4)	0.0359
N2	0.3523(6)	0.2159(6)	0.7252(4)	0.0393
N11	0.1007(9)	1.0335(8)	0.6355(5)	0.0695
N12	-0.0811(8)	0.7020(7)	1.0886(4)	0.0533
N21	0.672(1)	0.1280(9)	0.9577(6)	0.0803
C1	0.3357(8)	0.3541(7)	0.5627(5)	0.0381
C2	0.3837(9)	0.3793(9)	0.4554(5)	0.0482
C3	0.295(1)	0.5156(9)	0.4068(5)	0.0550
C4	0.163(1)	0.6251(9)	0.4649(5)	0.0544
C5	0.1168(9)	0.5961(8)	0.5708(5)	0.0456
C6	0.4236(8)	0.2154(7)	0.6223(5)	0.0373

C7	0.5693(9)	0.0941(9)	0.5806(6)	0.0540
C8	0.642(1)	-0.0295(9)	0.6446(7)	0.0636
C9	0.570(1)	-0.0318(8)	0.7487(7)	0.0658
C10	0.4248(9)	0.0939(8)	0.7877(6)	0.0539
C11	0.0732(9)	0.9695(8)	0.7134(5)	0.0472
C12	-0.0423(9)	0.7575(8)	1.0071(5)	0.0500
C21	0.607(1)	0.2626(9)	0.9725(6)	0.0567
H2	0.4777(9)	0.3010(9)	0.4162(5)	0.068(8)
H3	0.326(1)	0.5323(9)	0.3337(5)	0.078(8)
H4	0.102(1)	0.7216(9)	0.4323(5)	0.075(8)
H5	0.0241(9)	0.6741(8)	0.6110(5)	0.064(8)
H7	0.6194(9)	0.0962(9)	0.5081(6)	0.073(8)
H8	0.742(1)	-0.1139(9)	0.6164(7)	0.085(8)
H9	0.620(1)	-0.1163(8)	0.7939(7)	0.087(8)
H10	0.3733(9)	0.0937(8)	0.8601(6)	0.071(8)

A2. 26 Fractional Atomic Coordinates and Equivalent Isotropic Thermal Parameters (U(iso) in $Å^2$) for $\{[Cu(bipy)(OH)Cl]_2Hg(CN)_2\} \cdot 2\ H_2O$ (**5.4**).

Atom	x	y	z	U(iso)($Å^2$)
Hg1	0.0000	0.0000	1.0000	0.0359
Cu1	0.48238(7)	0.01075(5)	0.86467(4)	0.0288
Cl2	0.33056(17)	0.17661(12)	1.2485(1)	0.0378
O1	0.3030(6)	0.5697(4)	0.8163(4)	0.0554
O2	0.6728(4)	0.1164(3)	1.0388(3)	0.0305
N1	0.2739(5)	-0.0866(4)	0.6900(3)	0.0292
N2	0.5804(5)	0.1852(4)	0.7870(3)	0.0301
N11	0.2135(7)	0.2810(5)	0.8964(4)	0.0563
C1	0.1279(6)	-0.2329(5)	0.6443(4)	0.0373
C2	0.0067(7)	-0.2968(5)	0.5160(4)	0.0383
C3	0.0374(7)	-0.2091(5)	0.4310(4)	0.0369
C4	0.1887(6)	-0.0585(5)	0.4769(4)	0.0332

C5	0.3032(6)	-0.0001(4)	0.6069(4)	0.0264
C6	0.4665(6)	0.1587(4)	0.6670(4)	0.0283
C7	0.4986(7)	0.2749(5)	0.6073(4)	0.0355
C8	0.6532(7)	0.4212(5)	0.6734(5)	0.0417
C9	0.7709(7)	0.4471(5)	0.7939(5)	0.0440
C10	0.7320(7)	0.3271(5)	0.8481(4)	0.0382
C11	0.1401(6)	0.1822(5)	0.9283(4)	0.0315
H1	0.1077(6)	-0.2938(5)	0.7026(4)	0.048(5)
H2	-0.0962(7)	-0.4005(5)	0.4863(4)	0.045(5)
H3	-0.0445(7)	-0.2513(5)	0.3422(4)	0.045(5)
H4	0.2137(6)	0.0042(5)	0.4202(4)	0.040(5)
H7	0.4148(7)	0.2535(5)	0.5229(4)	0.045(5)
H8	0.6777(7)	0.5032(5)	0.6352(5)	0.052(5)
H9	0.8792(7)	0.5466(5)	0.8400(5)	0.054(5)
H10	0.8149(7)	0.3455(5)	0.9319(4)	0.048(5)
H11	0.325(9)	0.516(7)	0.853(6)	0.076(13)
H12	0.385(9)	0.623(7)	0.797(6)	0.076(13)
H21	0.687(9)	0.196(7)	1.070(6)	0.076(13)

REFERENCES

(1) Caulder, D. L.; Raymond, K. N. *Acc. Chem . Res.* **1999**, *32*, 975-982.

(2) Fujita, M. *Chem. Soc. Rev.* **1998**, *27*, 417-425.

(3) Jones, C. J. *Chem. Soc. Rev.* **1998**, *27*, 289-299.

(4) Janiak, C. *J. Chem. Soc. Dalton Trans.* **2003**, 2781-2804.

(5) Chen, C. T.; Suslick, K. S. *Coord. Chem. Rev.* **1993**, *128*, 293-322.

(6) Yaghi, O. M.; O'Keeffe, M.; Ockwig, N. W.; Chae, H. K.; Eddaoudi, M.; Kim, J. *Nature* **2003**, *423*, 705-714.

(7) Mitzi, D. B. *J. Chem. Soc., Dalton Trans.* **2001**, 1-12.

(8) Holliday, B. J.; Mirkin, C. A. *Angew. Chem. Int. Ed.* **2001**, *40*, 2022-2043.

(9) Moulton, B.; Zaworotko, M. J. *Chem. Rev.* **2001**, *101*, 1629-1658.

(10) Braga, D. *Crystal Engineering : From Molecules and Crystals to Materials* Kluwer Academic, 1999.

(11) Braga, D.; Grepioni, F.; Desiraju, G. R. *Chem. Rev.* **1998**, *98*, 1375-1405.

(12) Decurtins, S.; Pellaux, R.; Antorrena, G.; Palacio, F. *Coord. Chem. Rev.* **1999**, *192*, 841-854.

(13) Roundhill, D. M.; Fackler, J. P. *Optoelectronic Properties of Inorganic Compounds*; Plenum Press: New York, 1999.

(14) Marks, T. J.; Ratner, M. A. *Angew. Chem. Int. Ed.* **1995**, *34*, 155-173.

(15) Skotheim, T. A. *Handbook of Conducting Polymers*; M. Dekker: New York, 1986.

(16) Marguerettaz, X.; Redmond, G.; Rao, S. N.; Fitzmaurice, D. *Chem. Eur. J.* **1996**, *2*, 420-428.

(17) Cassoux, P.; Valade, L.; Kobayashi, H.; Kobayashi, A.; Clark, R. A.; Underhill, A. E. *Coord. Chem. Rev.* **1991**, *110*, 115-160.

(18) Imakubo, T.; Tajima, N.; Tamura, M.; Kato, R.; Nishio, Y.; Kajita, K. *J. Mater. Chem.* **2002**, *12*, 159-161.

(19) Zaworotko, M. J. *Angew. Chem. Int. Ed.* **2000**, *39*, 3052-3054.

(20) Day, P. *J. Chem. Soc., Dalton Trans.* **1997**, 701-705.

(21) Eddaoudi, M.; Moler, D. B.; Li, H. L.; Chen, B. L.; Reineke, T. M.; O'Keeffe, M.; Yaghi, O. M. *Acc. Chem . Res.* **2001**, *34*, 319-330.

(22) Ouahab, L. *Chem. Mater.* **1997**, *9*, 1909-1926.

(23) Guloy, A. M.; Tang, Z. J.; Miranda, P. B.; Srdanov, V. I. *Adv. Mater.* **2001**, *13*, 833-837.

(24) Desiraju, G. R. *Crystal Design : Structure and Function*; Wiley: London, 2003.

(25) Steed, J. W.; Atwood, J. L. *Supramolecular Chemistry*; John Wiley: Chichester ; New York, 2000.

(26) Ciurtin, D. M.; Smith, M. D.; zur Loye, H. C. *J. Chem. Soc. Dalton Trans.* **2003**, 1245-1250.

(27) Hoskins, B. F.; Robson, R. *J. Am. Chem. Soc.* **1990**, *112*, 1546-1554.

(28) Gardner, G. B.; Venkataraman, D.; Moore, J. S.; Lee, S. *Nature* **1995**, *374*, 792-795.

(29) Keller, S. W. *Angew. Chem. Int. Ed.* **1997**, *36*, 247-248.

(30) Xu, Z. M.; White, S.; Thompson, L. K.; Miller, D. O.; Ohba, M.; Ōkawa, H.; Wilson, C.; Howard, J. A. K. *J. Chem. Soc., Dalton Trans.* **2000**, *11*, 1751-1757.

(31) Orr, G. W.; Barbour, L. J.; Atwood, J. L. *Science* **1999**, *285*, 1049-1052.

(32) Yaghi, O. M.; Li, H. L.; Davis, C.; Richardson, D.; Groy, T. L. *Acc. Chem . Res.* **1998**, *31*, 474-484.

(33) Chesnut, D. J.; Hagrman, D.; Zapf, P. J.; Hammond, R. P.; LaDuca, R.; Haushalter, R. C.; Zubieta, J. *Coord. Chem. Rev.* **1999**, *192*, 737-769.

(34) Iwamoto, T.; In *Comprehensive Supramolecular Chemistry*; Atwood, J. L., Lehn, J. M., Eds.; Pergamon: New York, 1996; Vol. 7, pp 643-690.

(35) Černák, J.; Orendáč, M.; Potočňák, I.; Chomič, J.; Orendáčová, A.; Skoršepa, J.; Feher, A. *Coord. Chem. Rev.* **2002**, *224*, 51-66.

(36) Sharpe, A. G. *The Chemistry of Cyano Complexes of the Transition Metals*; Academic Press: London ; New York, 1976.

(37) Dunbar, K. R.; Heintz, R. A. *Prog. Inorg. Chem.* **1997**, *45*, 283-391.

(38) Chadwidwick, B. M.; Sharpe, A. G.; In *Advances in Inorganic Chemistry and Radiochemistry*; Emelâeus, H. J., Sharpe, A. G., Eds.; Academic Press.: New York, 1966; Vol. 8, pp pp 83-176.

(39) Britton, D.; In *Perspectives in Structural Chemistry*; Dunitz, J. D., Ibers, J. A. Eds.; J. Wiley: New York, 1967; Vol. 1, pp 109-171.

(40) Griffith, W. P.; In *Comprehensive Inorganic Chemistry*; Trotman-Dickenson, A. F., Bailar, J. C., Eds.; Pergamon Press: Oxford, 1973; Vol. 4, pp 105-180.

(41) Hanusa, T. P.; Burkey, D. J.; In *Encyclopedia of Inorganic Chemistry*; King, R. B., Ed.; Wiley: Chichester ; New York, 1994; Vol. 2, pp 558-949.

(42) Gill, J. B.; Gans, P.; Dougal, J. C.; Johnson, L. H. *Rev. Inorg. Chem.* **1990**, *11*, 155-194.

(43) Griffith, W. P. *Coord. Chem. Rev.* **1975**, *17*, 177-247.

(44) Ludi, A.; Gedel, H. U. *Structure and Bonding (Berlin, Germany)* **1973**, *14*, 1-21.

(45) Rigo, P.; Turco, A. *Coord. Chem. Rev.* **1974**, *13*, 133-172.

(46) Ohba, M.; Ōkawa, H. *Coord. Chem. Rev.* **2000**, *198*, 313-328.

(47) Verdaguer, M.; Bleuzen, A.; Marvaud, V.; Vaissermann, J.; Seuleiman, M.; Desplanches, C.; Scuiller, A.; Train, C.; Garde, R.; Gelly, G.; Lomenech, C.; Rosenman, I.; Veillet, P.; Cartier, C.; Villain, F. *Coord. Chem. Rev.* **1999**, *192*, 1023-1047.

(48) Vahrenkamp, H.; Geiss, A.; Richardson, G. N. *J. Chem. Soc., Dalton Trans.* **1997**, 3643-3651.

(49) Kahn, O.; Larionova, J.; Ouahab, L. *Chem. Commun.* **1999**, 945-952.

(50) Mallah, T.; Thiébaut, S.; Verdaguer, M.; Veillet, P. *Science* **1993**, *262*, 1554-1557.

(51) Ferlay, S.; Mallah, T.; Ouahes, R.; Veillet, P.; Verdaguer, M. *Nature* **1995**, *378*, 701-703.

(52) Kaemper, M.; Wagner, M.; Weiss, A. *Angew. Chem. Int. Ed.* **1979**, *91*, 517-518.

(53) Kondo, M.; Okubo, T.; Asami, A.; Noro, S.; Yoshitomi, T.; Kitagawa, S.; Ishii, T.; Matsuzaka, H.; Seki, K. *Angew. Chem. Int. Ed.* **1999**, *38*, 140-143.

(54) Kondo, M.; Shimamura, M.; Noro, S.; Minakoshi, S.; Asami, A.; Seki, K.; Kitagawa, S. *Chem. Mater.* **2000**, *12*, 1288-1299.

(55) Seki, K.; Mori, W. *J. Phys. Chem. B* **2002**, *106*, 1380-1385.

(56) Iwamoto, T.; In *Inclusion Compounds*; Atwood, J. L., Davies, J. E. D., MacNicol, D. D., Eds.; Academic Press: London ; Orlando, 1984; Vol. 5, pp 177-208.

(57) Kuroda, R. *Inorg. Nucl. Chem. Lett.* **1973**, *9*, 13-18.

(58) Sertbakan, T. R.; Kantarci, Z.; Kasap, E. *ARI* **1998**, *50*, 211-213.

(59) Miyasaka, H.; Matsumoto, N. *Chem. Lett.* **1997**, 427-428.

(60) Mahon, C. *Inorg. Chem.* **1971**, *10*, 1813-1816.

(61) Britton, D.; Mahon, C. *Inorg. Chem.* **1971**, *10*, 586-589.

(62) Holub, A. M.; Köhler, H.; Skopenko, V. V. *Chemistry of Pseudohalides*; Elsevier: Amsterdam ; New York, 1986.

(63) Rosenzweig, A.; Cromer, D. T. *Acta Cryst.* **1959**, *12*, 709-712.

(64) Corden, B. J.; Cunningham, J. A.; Eisenberg, R. *Inorg. Chem.* **1970**, *9*, 356-362.

(65) Bok, L. D. C.; Leipoldt, J. G.; Basson, S. S. *Acta Crystallogr., Sect. B* **1970**, *26*, 684-692.

(66) Turnbull, M. M.; Landee, C. P.; Soesbe, T. C.; Willett, R. D. *Mol. Cryst. Liq. Cryst.* **1993**, *A 233*, 269-276.

(67) Willett, R. D.; Wang, Z.; Molnar, S.; Brewer, K.; Landee, C. P.; Turnbull, m. M.; Zhang, W. *Mol. Cryst. Liq. Cryst.* **1993**, *A 233*, 277-282.

(68) Kahn, O. *Molecular Magnetism*; VCH: New York, NY, 1993.

(69) Miller, J. S.; Epstein, A. J. *Angew. Chem. Int. Ed.* **1994**, *33*, 385-415.

(70) Kollmar, C.; Kahn, O. *Acc. Chem . Res.* **1993**, *26*, 259-265.

(71) Buser, H. J.; Ludi, A.; Petter, W.; Schwarzenbach, D. *J. Chem. Soc., Chem. Commun.* **1972**, 1299.

(72) Gatteschi, D.; In *NATO ASI Series E Applied Sciences*; Kahn, O.; Miller, J.; Palacio, F.; Eds.; Kluwer Academic Publishers: Dordrecht ; Boston, 1991; Vol. 198, pp 411-442.

(73) Batten, S. R.; Hoskins, B. F.; Robson, R. *J. Am. Chem. Soc.* **1995**, *117*, 5385-5386.

(74) Batten, S. R.; Robson, R. *Angew. Chem. Int. Ed.* **1998**, *37*, 1461-1494.

(75) Iwamoto, T. *J. Mol. Struct.* **1981**, *75*, 51-65.

(76) Iwamoto, T. *Gendai Kagaku* **1981**, *123*, 14-22.

(77) Powell, H. M.; Rayner, J. H. *Nature* **1949**, *163*, 566-567.

(78) Rayner, J. H.; Powell, H. M. *J. Chem. Soc., Abs.* **1952**, 319-328.

(79) Leznoff, D. B.; Xue, B. Y.; Batchelor, R. J.; Einstein, F. W. B.; Patrick, B. O. *Inorg.Chem.* **2001**, *40*, 6026-6034.

(80) Leznoff, D. B.; Xue, B. Y.; Patrick, B. O.; Sanchez, V.; Thompson, R. C. *Chem. Commun.* **2001**, 259-260.

(81) Leznoff, D. B.; Xue, B. Y.; Stevens, C. L.; Storr, A.; Thompson, R. C.; Patrick, B. O. *Polyhedron* **2001**, *20*, 1247-1254.

(82) Shorrock, C. J.; Xue, B. Y.; Kim, P. B.; Batchelor, R. J.; Patrick, B. O.; Leznoff, D. B. *Inorg. Chem.* **2002**, *41*, 6743-6753.

(83) Pyykkö, P. *Chem. Rev.* **1997**, *97*, 597-636.

(84) Pyykkö, P.; Straka, M. *Phys. Chem. Chem. Phys.* **2000**, *2*, 2489-2493.

(85) King, J. B.; Haneline, M. R.; Tsunoda, M.; Gabbaï, F. P. *J. Am. Chem. Soc.* **2002**, *124*, 9350-9351.

(86) Brodersen, K.; Hummel, H.-U.; In *Comprehensive Coordination Chemistry*; Wilkinson, G., Gillard, R. D., McCleverty, J. A. Eds.; 1st ed.; Pergamon Press: Oxford, England ; New York, 1987; Vol. 5; pp 1048-1088.

(87) Breitinger, D. K.; In *Comprehensive Coordination Chemistry II : From Biology to Nanotechnology*; McCleverty, J. A., Meyer, T. J., Eds.; Boston : Elsevier Pergamon: Amsterdam, 2004; Vol. 6, pp 1253-1292.

(88) Grdenić, D. *Quart. Rev.* **1965**, *19*, 303-328.

(89) Cotton, F. A. *Advanced Inorganic Chemistry*; 6th ed.; Wiley: New York, 1999.

(90) Seidel, N.; Jacob, K.; Fischer, A. K.; Merzweiler, K.; Wagner, C.; Fontani, M.; Zanello, P. *J. Organomet. Chem.* **2001**, *630*, 149-156.

(91) Popović, Z.; Roje, V.; Pavlović, G.; Matković-Čalogović, D.; Rajić, M.; Giester, G. *Inorg. Chim. Acta* **2001**, *322*, 65-73.

(92) Hu, N. H.; Aoki, K.; Adeyemo, A. O.; Williams, G. N. *Inorg. Chim. Acta* **2002**, *333*, 63-71.

(93) Patra, G. K.; Goldberg, I. *Polyhedron* **2002**, *21*, 2195-2199.

(94) Bebout, D. C.; Garland, M. M.; Murphy, G. S.; Bowers, E. V.; Abelt, C. J.; Butcher, R. J. *J. Chem. Soc. Dalton Trans.* **2003**, 2578-2584.

(95) Graddon, D. P. *Rev. Inorg. Chem.* **1982**, *4*, 211-283.

(96) House, D. A.; Robinson, W. T.; Mckee, V. *Coord. Chem. Rev.* **1994**, *135*, 533-586.

(97) Fenn, R. H.; Oldham, J. W. H.; Phillips, D. C. *Nature* **1963**, *198*, 381-382.

(98) Alcock, N. W.; Curson, E. H.; Herron, N.; Moore, P. *J. Chem. Soc., Dalton Trans.* **1979**, 1987-1993.

(99) Šćavničar, S. *Z. Kristallogr.* **1963**, *118*, 248-256.

(100) Bradley, D. C.; Kunchur, N. R. *Chem. Ind.* **1962**, 1240-1241.

(101) Bradley, D. C.; Kunchur, N. R. *J. Chem. Phys.* **1964**, *40*, 2258-2261.

(102) Kruse, F. H. *Acta Cryst.* **1963**, *16*, 105-109.

(103) Gade, L. H. *Angew. Chem. Int. Ed.* **1993**, *32*, 24-40.

(104) Vogler, A.; Kunkely, H. *J. Organomet. Chem.* **1988**, *355*, 1-6.

(105) Pan, L.; Noll, B. C.; Wang, X. T. *Chem. Commun.* **1999**, 157-158.

(106) Dong, Y. B.; Cheng, J. Y.; Ma, J. P.; Wang, H. Y.; Huang, R. Q.; Guo, D. S.; Smith, M. D. *Solid State Sci.* **2003**, *5*, 1177-1186.

(107) Dong, Y. B.; Smith, M. D.; zur Loye, H. C. *Angew. Chem. Int. Ed.* **2000**, *39*, 4271-4273.

(108) Dong, Y. B.; Smith, M. D.; zur Loye, H. C. *Solid State Sci.* **2000**, *2*, 861-870.

(109) Batten, S. R.; Hoskins, B. F.; Robson, R. *Angew. Chem. Int. Ed.* **1995**, *34*, 820-822.

(110) Batten, S. R.; Harris, A. R.; Murray, K. S.; Smith, J. P. *Cryst. Growth Des.* **2002**, *2*, 87-89.

(111) Rais, D.; Mingos, D. M. P.; Vilar, R.; White, A. J. P.; Williams, D. J. *Organometallics* **2000**, *19*, 5209-5217.

(112) Burini, A.; Fackler, J. P.; Galassi, R.; Grant, T. A.; Omary, M. A.; Rawashdeh-Omary, M. A.; Pietroni, B. R.; Staples, R. J. *J. Am. Chem. Soc.* **2000**, *122*, 11264-11265.

(113) Abrahams, B. F.; Hoskins, B. F.; Michail, D. M.; Robson, R. *Nature* **1994**, *369*, 727-729.

(114) Hagrman, D.; Hagrman, P. J.; Zubieta, J. *Angew. Chem. Int. Ed.* **1999**, *38*, 3165-3168.

(115) Qin, J. G.; Liu, D. Y.; Dai, C. Y.; Chen, C. T.; Wu, B. C.; Yang, C. L.; Zhan, C. M. *Coord. Chem. Rev.* **1999**, *188*, 23-34.

(116) Niu, Y. Y.; Song, Y. L.; Chen, T. N.; Xue, Z. L.; Xin, X. Q. *Cryst. Eng. Comm.* **2001**, 1-3.

(117) Ciurtin, D. M.; Pschirer, N. G.; Smith, M. D.; Bunz, U. H. F.; zur Loye, H. C. *Chem. Mater.* **2001**, *13*, 2743-2745.

(118) Seccombe, R. C.; Kennard, C. H. L. *J. Organomet. Chem.* **1969**, *18*, 243-247.

(119) Penneman, R. A.; Jones, L. H. *J. Inorg. Nucl. Chem.* **1961**, *20*, 19-31.

(120) Ashurst, K. G.; Finkelstein, N. P.; Goold, L. A. *J. Chem. Soc. (A)* **1971**, 1899-1902.

(121) Thiele, G.; Hilfrich, P. *Z. Anorg. Allg. Chem.* **1980**, *461*, 109-124.

(122) Thiele, G.; Brodersen, K.; Frohring, H. *Z. Naturforsch. Teil B* **1981**, *36B*, 180-187.

(123) Thiele, G.; Grossmann, J.; Pürzer, A. W. *Z. Naturforsch. Sect. B* **1986**, *41*, 1346-1350.

(124) Brodersen, K.; Hummel, H. U. *Z. Anorg. Allg. Chem.* **1983**, *500*, 171-180.

(125) Wang, S. N.; Trepanier, S. J.; Zheng, J. C.; Pang, Z.; Wagner, M. J. *Inorg. Chem.* **1992**, *31*, 2118-2127.

(126) Exarchos, G.; Robinson, S. D.; Steed, J. W. *Polyhedron* **2001**, *20*, 2951-2963.

(127) Li, D. F.; Gao, S.; Zheng, L. M.; Sun, W. Y.; Okamura, T.; Ueyama, N.; Tang, W. X. *New J. Chem.* **2002**, *26*, 485-489.

(128) Ferlay, S.; Bulach, V.; Félix, O.; Hosseini, M. W.; Planeix, J. M.; Kyritsakas, N. *Cryst. Eng. Comm.* **2002**, 447-453.

(129) Orendáč, M.; Orendáčová, A.; Černák, J.; Feher, A. *Solid State Comm.* **1995**, *94*, 833-835.

(130) Černák, J.; Chomič, J.; Gravereau, P.; Orendáčová, A.; Orendáč, M.; Kovač, J.; Feher, A.; Kappenstein, C. *Inorg. Chim. Acta* **1998**, *281*, 134-140.

(131) Porzsolt, E. C.; Mohai, B.; Beck, M. T. *Magy. Kem. Foly.* **1974**, *80*, 254-259.

(132) Nakamoto, K. *Infrared and Raman spectra of inorganic and coordination compounds*; 5th ed.; John Wiley & Sons: New York ; Chichester, England, 1997.

(133) Dows, D. A.; Haim, A.; Wilmarth, W. K. *J. Inorg. Nucl. Chem.* **1961**, *21*, 33-37.

(134) Shriver, D. F.; Shriver, S. A.; Anderson, S. E. *Inorg. Chem.* **1965**, *4*, 725-730.

(135) Swanson, B. I. *Inorg. Chem.* **1976**, *15*, 253-259.

(136) Wuest, J. D. *Acc. Chem . Res.* **1999**, *32*, 81-89.

(137) Xie, Y. S.; Ni, J.; Jiang, H.; Liu, Q. L. *J. Mol. Struct.* **2004**, *687*, 73-78.

(138) Strömholm, D. *Z. Anorg. Allgem. Chem.* **1923**, *126*, 129-140.

(139) Reedijk, J.; Groeneveld, W. L. *Recueil des Travaux Chimiques des Pays-Bas* **1969**, *88*, 655-666.

(140) Aurivillius, K.; Stalhandske, C. *Acta Chem. Scand.* **1976**, *A30*, 735-739.

(141) Putzas, D.; Rotter, H. W.; Thiele, G.; Brodersen, K.; Pezzei, G. *Z. Anorg. Allg. Chem.* **1991**, *595*, 193-202.

(142) Cramer, R. E.; Carrie, M. J. J. *Inorg. Chem.* **1990**, *29*, 3902-3904.

(143) Xie, Y. S.; Liu, X. T.; Ni, J.; Jiang, H.; Liu, Q. L. *Appl. Organomet. Chem.* **2003**, *17*, 800-800.

(144) Zouari, R.; Bensalah, A.; Daoud, A.; Rothammel, W.; Burzlaff, H. *Acta Crystallogr., Sect. C* **1993**, *49*, 1596-1598.

(145) Mitzi, D. B. *Inorg. Chem.* **2000**, *39*, 6107-6113.

(146) Larock, R. C.; Burns, L. D.; Varaprath, S.; Russell, C. E.; Richardson, J. W.; Janakiraman, M. N.; Jacobson, R. A. *Organometallics* **1987**, *6*, 1780-1789.

(147) Goggin, P. L.; King, P.; McEwan, D. M.; Taylor, G. E.; Woodward, P.; Sandstroem, M. *J. Chem. Soc., Dalton Trans.* **1982**, 875-882.

(148) Chaari, P. S.; Bensalah, A.; Jouini, T.; Daoud, A. *Acta Crystallogr., Sect. C* **1989**, *45*, 1495-1497.

(149) Bondi, A. *J. Phys. Chem.* **1964**, *68*, 441-451.

(150) Bell, N. A.; Goldstein, M.; Jones, T.; Nowell, I. W. *Inorg. Chim. Acta* **1978**, *28*, L169-L170.

(151) Bell, N. A.; Goldstein, M.; Jones, T.; Nowell, I. W. *Inorg. Chim. Acta* **1981**, *48*, 185-189.

(152) Schunk, A.; Thewalt, U. *Z. Anorg. Allg. Chem.* **2001**, *627*, 797-802.

(153) Zhan, S. Z.; Chen, X. Y.; Vij, A.; Guo, D.; Meng, Q. J. *Inorg. Chim. Acta* **1999**, *292*, 157-162.

(154) Koolhaas, G. J. A. A.; vanBerkel, P. M.; vanderSlot, S. C.; MendozaDiaz, G.; Driessen, W. L.; Reedijk, J.; Kooijman, H.; Veldman, N.; Spek, A. L. *Inorg. Chem.* **1996**, *35*, 3525-3532.

(155) Milburn, G. H. W.; Truter, M. R. *J. Chem. Soc. (A)* **1966**, 1609-1616.

(156) Yap, G. P. A.; Rheingold, A. L.; Das, P.; Crabtree, R. H. *Inorg. Chem.* **1995**, *34*, 3474-3476.

(157) Gillon, A. L.; Orpen, A. G.; Starbuck, J.; Wang, X. M.; Rodríguez-Martín, Y.; Ruiz-Pérez, C. *Chem. Commun.* **1999**, 2287-2288.

(158) Gillon, A. L.; Lewis, G. R.; Orpen, A. G.; Rotter, S.; Starbuck, J.; Wang, X. M.; Rodríguez-Martín, Y.; Ruiz-Pérez, C. *J. Chem. Soc., Dalton Trans.* **2000**, 3897-3905.

(159) Mitzi, D. B.; Brock, P. *Inorg. Chem.* **2001**, *40*, 2096-2104.

(160) Wen, H.; Miller, S. E.; House, D. A.; Mckee, V.; Robinson, W. T. *Inorg. Chim. Acta* **1992**, *193*, 77-85.

(161) Verweel, H. J.; Bijvoet, J. M. *Z. Kristallogr.* **1931**, *77*, 122-139.

(162) Rüdorff, W.; Brodersen, K. *Z. Anorg. Allg. Chem.* **1952**, *270*, 145-159.

(163) Brodersen, K.; Rüdorff, W. *Z. Naturforsch.* **1954**, *9b*, 164.

(164) Lipscomb, W. N. *Acta Cryst.* **1951**, *4*, 266-268.

(165) Nijssen, L.; Lipscomb, W. N. *Acta Cryst.* **1952**, *5*, 604-605.

(166) Harmsen, E. J. *Z. Kristallogr.* **1938**, *100*, 208-211.

(167) Herlinger, A. W.; Brown, J. N.; Dwyer, M. A.; Pavkovic, S. F. *Inorg. Chem.* **1981**, *20*, 2366-2371.

(168) Clegg, W. *J. Chem. Soc., Dalton Trans.* **1982**, 593-595.

(169) Draper, N. D.; Batchelor, R. J.; Leznoff, D. B., Submitted to *Inorg. Chem.*

(170) Desiraju, G. R. *Acc. Chem . Res.* **2002**, *35*, 565-573.

(171) Gardinier, J. R.; Gabbaï, F. P. *J. Chem. Soc., Dalton Trans.* **2000**, 2861-2865.

(172) Delaigue, X.; Hosseini, M. W.; Kyritsakas, N.; Decian, A.; Fischer, J. *J. Chem. Soc., Chem. Commun.* **1995**, 609-610.

(173) Martin, J. D.; Greenwood, K. B. *Angew. Chem. Int. Ed.* **1997**, *36*, 2072-2075.

(174) Chesnut, D. J.; Haushalter, R. C.; Zubieta, J. *Inorg. Chim. Acta* **1999**, *292*, 41-51.

(175) Corradi, A. B.; Cramarossa, M. R.; Saladini, M. *Inorg. Chim. Acta* **1997**, *257*, 19-26.

(176) Corradi, A. B.; Ferrari, A. M.; Pellacani, G. C. *Inorg. Chim. Acta* **1998**, *272*, 252-260.

(177) Martin, J. D.; Dattelbaum, A. M.; Thornton, T. A.; Sullivan, R. M.; Yang, J. C.; Peachey, M. T. *Chem. Mater.* **1998**, *10*, 2699-2713.

(178) Gabe, E. J.; White, P. S.; Enright, G. D.: DIFRAC: A Fortran 77 Control routine for 4-Circle Diffractometers, N.R.C., Ottawa, 1995.

(179) Gabe, E. J.; Lepage, Y.; Charland, J. P.; Lee, F. L.; White, P. S. *J. Appl. Cryst.* **1989**, *22*, 384-387.

(180) Watkin, D. J.; Prout, C. K.; Carruthers, J. R.; Betteridge, P. W.; Cooper, R. I.: CRYSTALS Issue 12.16, Chemical Crystallography Laboratory, University of Oxford, Oxford, England, 2001.

(181) Farrugia, L. J. *J. Appl. Cryst.* **1997**, *30*, 565.

(182) Bruno, I. J.; Cole, J. C.; Edgington, P. R.; Kessler, M.; Macrae, C. F.; McCabe, P.; Pearson, J.; Taylor, R. *Acta Crystallogr., Sect. B* **2002**, *58*, 389-397.

(183) International Union of Crystallography. *International tables for X-ray crystallography*; Kynoch Press: Birmingham, Eng., 1952.

(184) Ahmed, F. R.; Hall, S. R.; Huber, C. P.; International Union of Crystallography. Commission on Crystallographic Computing.; Carleton University. *Crystallographic computing;*; Munksgaard: Copenhagen, 1970.

(185) Carlin, R. L. *Magnetochemistry*; Springer-Verlag: Berlin ; New York, 1986.

(186) Hummel, R. E. *Electronic Properties of Materials*; 3rd ed.; Springer: New York, 2001.

(187) Bleaney, B.; Bowers, K. D. *Proc. Roy. Soc. (London)* **1952**, *A214*, 451-465.

(188) Bonner, J. C.; Fischer, M. E. *Phys. Rev. A.* **1964**, *135*, 646.

(189) Estes, W. E.; Gavel, D. P.; Hatfield, W. E.; Hodgson, D. J. *Inorg. Chem.* **1978**, *17*, 1415-1421.

(190) Hall, J. W.; Marsh, W. E.; Weller, R. R.; Hatfield, W. E. *Inorg. Chem.* **1981**, *20*, 1033-1037.

(191) Fontaine, F. G. *Acta Crystallogr., Sect. E* **2001**, *57*, m270-m271.

(192) McCann, S.; McCann, M.; Casey, M. T.; Jackman, M.; Devereux, M.; McKee, V. *Inorg. Chim. Acta* **1998**, *279*, 24-29.

(193) Lumme, P. O.; Lindell, E. *Acta Crystallogr., Sect. C* **1988**, *44*, 463-465.

(194) Song, J. L.; Mao, J. G.; Zeng, H. Y.; Dong, Z. C. *Eur. J. Inorg. Chem.* **2004**, 538-543.

(195) Leznoff, D. B.; Draper, N. D.; Batchelor, R. J. *Polyhedron* **2003**, *22*, 1735-1743.

(196) Dance, I.; Scudder, M. *J. Chem. Soc., Dalton Trans.* **1998**, 1341-1350.

(197) Russell, V.; Scudder, M.; Dance, I. *J. Chem. Soc., Dalton Trans.* **2001**, 789-799.

(198) Podberezskaya, N. V.; Belyaev, A. V.; Bakakin, V. V.; Baidina, I. A. *Zhur. Strukt. Khim.* **1981**, *22*, 32-36.

(199) Rojo, T.; Vlasse, M.; Beltran-Porter, D. *Acta Crystallogr., Sect. C* **1983**, *C39*, 194-198.

(200) Anderson, O. P.; Packard, A. B.; Wicholas, M. *Inorg. Chem.* **1976**, *15*, 1613-1618.

(201) Addison, A. W.; Rao, T. N.; Reedijk, J.; Van Rijn, J.; Verschoor, G. C. *J. Chem. Soc., Dalton Trans.* **1984**, 1349-1356.

(202) Shorrock, C. J.; Jong, H.; Batchelor, R. J.; Leznoff, D. B. *Inorg. Chem.* **2003**, *42*, 3917-3924.

(203) Urtiaga, M. K.; Arriortua, M. I.; Cortés, R.; Rojo, T. *Acta Crystallogr., Sect. C* **1996**, *52*, 3007-3009.

(204) Rojo, T.; Arriortua, M. I.; Ruiz, J.; Darriet, J.; Villeneuve, G.; Beltranporter, D. *J. Chem. Soc., Dalton Trans.* **1987**, 285-291.

(205) Draper, N. D.; Batchelor, R. J.; Sih, B. C.; Ye, Z. G.; Leznoff, D. B. *Chem. Mater.* **2003**, *15*, 1612-1616.

(206) Zhang, H.; Cai, J. W.; Feng, X. L.; Sang, H. Y.; Liu, J. Z.; Li, X. Y.; Ji, L. N. *Polyhedron* **2002**, *21*, 721-728.

(207) Zhong, Z. J.; Matsumoto, N.; Ōkawa, H.; Kida, S. *Chem. Lett.* **1990**, 87-90.

(208) Chu, I. K.; Shek, I. P. Y.; Siu, K. W. M.; Wong, W. T.; Zuo, J. L.; Lau, T. C. *New J. Chem.* **2000**, *24*, 765-769.

(209) Březina, F.; Trávníček, Z.; Šindelář, Z.; Pastorek, R.; Marek, J. *Trans. Met. Chem.* **1999**, *24*, 459-462.

(210) Rodríguez, M.; Llobet, A.; Corbella, M.; Martell, A. E.; Reibenspies, J. *Inorg. Chem.* **1999**, *38*, 2328-2334.

(211) Llobet, A.; Martell, A. E.; Martinez, M. A. *J. Mol. Catal.* **1998**, *129*, 19-26.

(212) Rodríguez, M.; Llobet, A.; Corbella, M. *Polyhedron* **2000**, *19*, 2483-2491.

(213) Draper, N. D.; Batchelor, R. J.; Leznoff, D. B. *Cryst. Growth Des.* **2004**, *4*, 621-632.

(214) Higashi, T.; Rigaku Corporation: Tokyo, Japan, 1999.

(215) Rapid Process-Auto Control Routine for Rigaku MSC Diffractometer; 3.0 ed.: Tokyo, Japan, 1999.

(216) Ehlert, M. K.; Rettig, S. J.; Storr, A.; Thompson, R. C.; Trotter, J. *Can. J. Chem.* **1989**, *67*, 1970-1974.

(217) Desiraju, G. R. *Crystal Engineering : The Design of Organic Solids*; Elsevier: Amsterdam ; New York, 1989.

(218) West, A. R. *Basic Solid State Chemistry*; 2nd ed.; John Wiley & Sons: New York, 1999.

(219) Newnham, R. E. *Structure-Property Relations*; Springer-Verlag: New York, 1975.

(220) Ladd, M. F. C.; Palmer, R. A. *Structure Determination by X-ray Crystallography*; 4th ed.; Kluwer Academic/Plenum Publishers: New York, 2003.

(221) Fromm, K. M.; Gueneau, E. D.; Rivera, J. P.; Bernardinelli, G. *Z. Anorg. Allg. Chem.* **2002**, *628*, 171-178.

(222) Fishbane, P. M.; Gasiorowicz, S.; Thornton, S. T. *Physics for Scientists and Engineers*; 2nd. ed.; Prentice-Hall Inc.: Upper Saddle River, New Jersey, 1996.

(223) Lide, D. R. E. *CRC Handbook of Chemistry and Physics.*; 71st ed.; Chemical Rubber Publishing Company: Boston, 1991; **12**-27.

(224) Rao, C. N. R.; Ranganathan, A.; Pedireddi, V. R.; Raju, A. R. *Chem. Commun.* **2000**, 39-40.

(225) Coleman, J. S.; Penneman, R. A.; Jones, L. H.; Kressin, I. K. *Inorg. Chem.* **1968**, *7*, 1174-1178.

(226) Falk, M.; Knop, O. *Can. J. Chem.* **1977**, *55*, 1736-1744.

(227) Hagrman, P. J.; Hagrman, D.; Zubieta, J. *Angew. Chem. Int. Ed.* **1999**, *38*, 2639-2684.

(228) Vicente, R.; Escuer, A.; Penalba, E.; Solans, X.; FontBardia, M. *Inorg. Chim. Acta* **1997**, *255*, 7-12.

(229) Janiak, C.; Scharmann, T. G.; Albrecht, P.; Marlow, F.; Macdonald, R. *J. Am. Chem. Soc.* **1996**, *118*, 6307-6308.

(230) Bergmann, L.; Schaefer, C.; Niedrig, H. *Optics of Waves and Particles*; W. de Gruyter: Berlin ; New York, 1999.

(231) Nye, J. F. *Physical Properties of Crystals, their Representation by Tensors and Matrices*; Clarendon Press: Oxford, 1964.

(232) CrystalClear Control Routine for Rigaku MSC Diffractometer; 1.3.5 SP2 ed.: The Woodlands, TX, 2003.

(233) Černák, J.; Abboud, K. A. *Acta Crystallogr., Sect. C* **2000**, *56*, 783-785.

(234) Falvello, L. R.; Tomas, M. *Chem. Commun.* **1999**, 273-274.

(235) Weiss, A.; Damn, K. *Z. Naturforsch.* **1954**, *9b*, 82.

(236) Castro, I.; Faus, J.; Julve, M.; Bois, C.; Real, J. A.; Lloret, F. *J. Chem. Soc., Dalton Trans.* **1992**, 47-52.

(237) Demunno, G.; Julve, M.; Lloret, F.; Faus, J.; Verdaguer, M.; Caneschi, A. *Inorg. Chem.* **1995**, *34*, 157-165.

(238) Grasa, G.; Tuna, F.; Gheorghe, R.; Leznoff, D. B.; Rettig, S. J.; Andruh, M. *New J. Chem.* **2000**, *24*, 615-618.

(239) White, C. A.; Yap, G. P. A.; Raju, N. P.; Greedan, J. E.; Crutchley, R. J. *Inorg. Chem.* **1999**, *38*, 2548-2549.

(240) Miller, J. S. *Extended Linear Chain Compounds*; Plenum Press: New York, 1982.

(241) Oshio, H.; Watanabe, T.; Ohto, A.; Ito, T.; Nagashima, U. *Angew. Chem. Int. Ed.* **1994**, *33*, 670-671.

(242) Oshio, H.; Watanabe, T.; Ohto, A.; Ito, T. *Inorg. Chem.* **1997**, *36*, 1608-1610.

(243) Ruiz, E.; Alemany, P.; Alvarez, S.; Cano, J. *Inorg. Chem.* **1997**, *36*, 3683-3688.

(244) Ruiz, E.; Alemany, P.; Alvarez, S.; Cano, J. *J. Am. Chem. Soc.* **1997**, *119*, 1297-1303.

(245) McGregor, K. T.; Watkins, N. T.; Lewis, D. L.; Drake, R. F.; Hodgson, D. J.; Hatfield, W. E. *Inorg. Nucl. Chem. Lett.* **1973**, *9*, 423-428.

(246) Crawford, V. H.; Richardson, H. W.; Wasson, J. R.; Hodgson, D. J.; Hatfield, W. E. *Inorg. Chem.* **1976**, *15*, 2107-2110.

(247) van Albada, G. A.; Mutikainen, I.; Turpeinen, U.; Reedijk, J. *Inorg. Chim. Acta* **2001**, *324*, 273-277.

(248) Borrasalmenar, J. J.; Coronado, E.; Curely, J.; Georges, R.; Gianduzzo, J. C. *Inorg. Chem.* **1994**, *33*, 5171-5175.